COMMON SENSE APPROACH TO THERMAL IMAGING

Gerald C. Holst

BRITISH LIBRARY
DOCUMENT SUPPLY CENTRE

22 NOV 2000

m00/.45433

Copublished by

JCD Publishing
Winter Park, Florida USA

and



SPIE OPTICAL ENGINEERING PRESS
A Publication of SPIE – The International Society for Optical Engineering
Bellingham, Washington USA

Library of Congress Cataloging-in-Publication Data

Holst, Gerald C.
Common sense approach to thermal imaging / Gerald C. Holst
p. cm.
Includes bibliographical references and index.
ISBN 0-8194-3722-0 – ISBN 0-9640000-7-5-
1. Infrared imaging. 2. Thermography. 3. Imaging systems. I. Title

TA1570.H63 2000
621.36'72–dc21

00-036561

Copublished by

JCD Publishing
2932 Cove Trail
Winter Park, FL 32789
ISBN: 0-9640000-7-5
Phone: 407-629-5370
Fax: 407-629-5370
email: jcdgch@aol.com

SPIE – The International Society for Optical Engineering
P.O. Box 10
Bellingham, WA 98227-0010
SPIE Volume PM-86
ISBN: 0-8194-3722-0
Phone: 360-676-3290
Fax: 360-647-1445
WWW: http://www.spie.org

COVER: Mid-wave infrared image of the Great Pyramid of Cheops and the Sphinx. Scene temperatures are represented by pseudo-colors. The sky is cold and appears black. The sun is overhead so that the top of the Sphinx and the ground behind the Sphinx are hot. They appear white. Intermediate temperatures are represented by yellows and reds (By courtesy of Stan Laband).

Notice:
Reasonable efforts have been made to publish reliable data and information, but the Author and Publishers cannot assume responsibility for the validity of all materials or the consequences of their use.

Copyright ©2000 Gerald C. Holst

All rights reserved. No part of this book may be reproduced in any form by any means without written permission from the copyright owner.

This book is dedicated to

Mom and Dad

They provide continual guidance

PREFACE

Objects are characterized by a variety of physical parameters such as size, shape, and weight. However, the most frequently measured physical property is temperature. Heat is a byproduct of all work whether it is from electrical, mechanical, or chemical activity. We generate, contain, and transfer heat to run our industries and make our everyday lives comfortable. Unexpected temperature variations may indicate design flaws, poor workmanship, or damaged components. A temperature variation can also be used to recognize an intruder, locate a buried object, or to identify geological events.

Thermal imaging systems are used by the military to detect, recognize, and identify enemy personnel, equipment, and buildings. Police patrol border crossings and use thermal imaging systems for search and rescue. The systems are particularly useful for evaluating the condition of power lines, transformers, circuit breakers, and motors. Simply put, they can be used to evaluate the "health" of any electrical or mechanical component.

Several texts that describe the applications of thermal imaging systems are:

Nondestructive Evaluation of Materials by Infrared Thermography, X.P.V. Maldague, Springer-Verlag, New York (1992).

Applications of Thermal Imaging, S. G. Burney, T. L. Williams, and C.H.N. Jones, Adam Hilger, Philadelphia, PA (1988).

Practical Applications on Infrared Thermal Sensing and Imaging Equipment, second edition, H. Kaplan, SPIE Press Vol. TT34, Bellingham WA (1999).

SPIE has assembled two compendiums:

Selected SPIE papers on Thermal Sensing and Imaging 1980-1999, SPIE CD-ROM, Volume 7, J. Snell and D. Burleigh, eds. (1999).

Selected Papers on Temperature Sensing: Optical Methods, R.D. Lucier, ed., SPIE Milestone Series Vol. MS 1164, Bellingham WA (1995).

The first compendium is a collection of papers from the proceedings of the SPIE conference *Thermosense*. Since this is an important contribution to the literature, Appendix C of this book contains the Table of Contents of the CD-ROM. The second contains reprints of articles that appeared in professional journals.

This book differs from those texts by clearly describing the phenomenology of heat transfer and providing numerous thermograms to support the concepts. It also covers a diverse set of applications. This book is divided into two parts. The first part (Chapters 1-9) provides the physics background that is necessary to interpret thermo-

grams. The second part (Chapters 10-20) discusses various applications. Except for Chapter 19, *Nondestructive Testing*, minimal math is used in the second part. Heat transfer during nondestructive testing is a complex phenomenon and therefore requires more math. The researcher and scientist will read the first part in detail whereas the thermographer performing inspections will concentrate on the second part.

Heat transfer (Chapter 2), radiation theory (Chapter 3), and emissivity (Chapter 4) form the backbone of all thermal imaging system applications. The atmosphere (Chapter 5) may attenuate the received signal. This becomes an issue over long path lengths - typical of military applications. Camera design, performance parameters, and camera selection are contained in Chapters 6 through 8. It is can not be understated that each camera has specific design features and unique performance parameters. As a result, it is somewhat of a challenge to find a system that is *best* for a specific application. Interpretation of thermograms requires training (Chapter 9). This training must include the material provided in Chapters 2 through 5.

Part 2 begins with an introduction to applications (Chapter 10). Chapter 11 discusses the influence of the environment of target signatures. With this knowledge, it is possible to perform quantitative temperature measurements. For some tests, qualitative results are adequate. These include building envelope inspections (Chapter 13), roof inspections (Chapter 14), and the location of buried objects (Chapter 17). Electrical and mechanical inspections often require quantitative results (Chapters 15 and 16). Here, the temperature of a component is compared to a standard or guideline. If the temperature is too high, then the component must be repaired or replaced. Although surveillance refers to the observation of a person, this definition is extended to include the detection, recognition, and identification of both people and objects (Chapter 18). It includes search and rescue, endangered species monitoring, border patrol, law enforcement, and military applications. Nondestructive testing (Chapter 19) can locate disbonding, delamination, and corrosion. These are of prime concern of our aging commercial aircraft. Chapter 20 briefly discusses applications in six different industries. Chapter 21 lists the steps necessary for a successful test or inspection.

The physics is described by three equations. The first is the "easy" approach to describe the phenomenology. For example, the output of a detector is given by

$$V_{DETECTOR} = kR_D M$$

where R_D is the detector's responsivity, M is the radiation from the target, and k is a constant. The effect of R_D and M on $V_{DETECTOR}$ is described and supported by numerous examples. Then the concept of wavelength, λ, is introduced with the second equation. The radiant intensity also depends upon the target's temperature, T. The sum of all the outputs at the various wavelengths must be added together.

This is represented by an integral (third equation):

$$V_{CAMERA} = \int_{\lambda_1}^{\lambda_2} V_{DETECTOR}(\lambda)\, d\lambda .$$

Long-wave infrared (LWIR) and mid-wave infrared (MWIR) systems have different wavelength intervals [λ_1, λ_2]. The reader who is less interested in the math complexities will use the first equation. But he will fully understand the phenomenology. If detailed calculations are necessary, the reader will use the third equation. This last equation provides the guidance in selecting an appropriate camera for a specific application (i.e., MWIR or LWIR camera).

By using both simple and complex math, this book is intended for all that work with thermal imaging systems. This includes the researcher, system designer, test engineer, salesman, and end user. Since civilian and military applications are discussed, this book is useful to both communities.

The scientific community and many industries around the world use the metric system and it is used in this book. However, some industries in the U.S. and other countries still use English units. The conversion from miles per hour (mph) to meters per second (m/s) and degrees Fahrenheit (°F) to degrees Celsius (°C) are straightforward. While the reader can easily make the conversion, it takes time and it interrupts reading comprehension. Therefore, the English equivalent is always provided parenthetically.

I extend my deepest gratitude to all my coworkers and students who have contributed to the ideas in this book. They are too many to mention by name. I especially thank all those who read draft copies of the manuscript: Mary Lee Cassetta, consultant; Arnold Daniels, Optics-1; Dennis Hewins, Academy of Infrared Thermography; A. J. Holst, American Credit; Chris Johnston, IRcameras.com; Ron Newport, Academy of Infrared Thermography; Harold Orlando, Northrup Grumman; Jim Porter, Raytheon Systems; Dr. Austin Richards, Indigo; Elliot Rittenberg, EFR Associates; John Snell, Snell Infrared; and Gary Weil, EnTech Engineering. Although these reviewers provided valuable comments, the accuracy of the text is solely my responsibility. Douglas F. Marks provided the graphics and manuscript layout.

The thermograms were obtained from a number of sources. However, some images have been so widely distributed that the original owner is not known to many. If I missed a credit or gave credit to the wrong person, I apologize. Every attempt has been made to authenticate the owners. I hope that you find the title accurate: That this book **IS** the common sense approach to thermal imaging.

Gerald C. Holst *Winter Park, FL*

Table of Contents

1. INTRODUCTION 1
1.1. Heat 3
1.2. Temperature measuring devices 4
1.2.1. Contact devices 5
1.2.2. Non-contact devices 7
1.3. Temperature scales 9
1.4. The electromagnetic spectrum 11
1.5. Brief history of thermography 15
1.6. System development 16
1.7. Applications overview 18
1.8. Units 19
1.9. References 20

2. HEAT 21
2.1. Heat capacity and specific heat capacity 23
2.2. Phase change 24
2.3. Heat transfer 27
2.3.1. Conduction 27
2.3.2. Convection 32
2.3.3. Radiation 34
2.4. Heat sources 35
2.4.1. Sun 35
2.4.2. Combustion 36
2.4.3. Chemical reaction 38
2.4.4. Nuclear power plant 38
2.4.5. Energy conversion 39
2.4.6. Mass transport 45
2.4.7. Man-made 45
2.5. Useful conversions and constants 46
2.6. References 47

3. DETECTION OF RADIATION 48
3.1. Stefan-Boltzmann law 48
3.1.1. General response 49
3.1.2. The background 49
3.2. Planck's blackbody law 52
3.2.1. General response 56
3.2.2. The background 58

4. EMISSIVITY 60
4.1. Conservation of energy 60
4.2. Target emissivity 61
4.3. Surface conditions 63
4.4. Environmental effects 63
4.5. Geometric factors 65
4.6. Spectral dependence 68
4.7. References 73

5. ATMOSPHERIC TRANSMITTANCE 74
5.1. Extinction 75
5.2. Path length dependence 76
5.3. Atmospheric constituents 79
5.3.1. Water vapor 80
5.3.2. Aerosols 81
5.4. Path radiance 83
5.5. Modeling the atmosphere 84
5.6. Back-of-the-envelope modeling 85
5.6.1. "Average" weather conditions 86
5.6.2. Range predictions 87
5.7. References 89

6. CAMERA DESIGN 90
6.1. Camera output 92
6.2. System designs 93
6.2.1. Military systems 93
6.2.2. Civilian systems 94
6.3. Optics 94
6.4. Scanners 95
6.5. Detectors and coolers 97
6.5.1. Detector operation 97
6.5.2. Specific detectors 99
6.5.3. Detector responsivity 100
6.5.4. Fixed pattern noise 102
6.5.5. AC coupling 102
6.5.6. Fill factor 103
6.6. Digitization 104
6.7. Image processing 105
6.8. Reconstruction 107
6.9. Monitors 108
6.10. MWIR versus LWIR 108
6.11. References 109

7. PERFORMANCE PARAMETERS 110
7.1. Spatial frequency 113
7.2. Sensitivity (NEDT) 114
7.2.1. NEDT measurement 114
7.2.2. NEDT theory 114
7.3. Spatial resolution 117
7.3.1. Airy disk 117
7.3.2. Instantaneous-field-of-view 118
7.3.3. Pixel-angular-subtense 119
7.3.4. Slit response function 119
7.3.5. Measuring IFOV 121
7.3.6. Nyquist frequency 122
7.3.7. Optical zoom/electronic magnification 123
7.4. Observer response 125
7.5. MRT and MDT 127
7.6. References 129

8. CAMERA SELECTION 130
8.1. Environment 132
8.1.1. Harsh environment 132
8.1.2. Ambient temperature 133
8.1.3. Viewing geometry 133
8.2. Camera 139
8.2.1. Physical attributes 139
8.2.2. Dynamic range 139
8.2.3. Frame rate 143
8.2.4. Image processing 144
8.2.5. Calibration 145
8.3. Storage and output 145
8.4. Other issues 146
8.5. References 146

9. OBSERVER TRAINING 147
9.1. Certification 148
9.2. Military users 149
9.3. MRT observers 149
9.4. References 150

10. INTRODUCTION TO APPLICATIONS 151
10.1. Condition monitoring 153
10.2. Process control/quality control 155

11. TARGET SIGNATURES 157
11.1. Thermal anomaly identification 157
11.2. The environment 159
11.3. Passive targets 163
11.3.1. Solar heating 163
11.3.2. Clouds 168
11.3.3. Wind 168
11.3.4. Rain and snow 169
11.3.5. The scanning window 169
11.3.6. Outdoor considerations 172
11.4. Emissivity variations 173
11.5. Active targets 176
11.5.1. Vehicles 177
11.5.2. Small targets 178
11.5.3. Estimate of the scanning window 178
11.6. Limited access components 181
11.7. References 182

12. TEMPERATURE MEASUREMENTS 183
12.1. Apparent temperature 183
12.2. Temperature calibration 185
12.3. Emissivity 187
12.3.1. Emissivity correction 187
12.3.2. Angle of incidence 188
12.3.3. Emissivity uncertainty 190
12.3.4. Increasing the emissivity 194
12.4. Measurement of T_S 196
12.5. Atmospheric correction 197
12.6. Dual band measurements 197
12.7. Signal averaging 198
12.8. References 199

13. BUILDING ENVELOPE INSPECTION 200
13.1. Building science 201
13.1.1. Historic buildings 201
13.1.2. 1880 to 1940 construction 203
13.1.3. 1940 to 1960 construction 203
13.1.4. 1960 to 1990 construction 204
13.1.5. Modern construction 204
13.1.6. Windows 204
13.2. Heat transfer 206

13.2.1. Conductivity 207
13.2.2. Evaporation 209
13.2.3. Mass transport 210
13.3. Building inspection 212
13.4. References 212

14. ROOF INSPECTION 213
14.1. Roof construction 215
14.2. Temperature differential 216
14.2.1. Solar loading 216
14.2.2. Clouds 219
14.2.3. Wind 220
14.2.4. Surface moisture 220
14.2.5. High relative humidity 220
14.2.6. Phase change 221
14.2.7. Reflections 221
14.2.8. Interior effects 221
14.3 Inspections 222
14.4. References 224

15. POWER DISTRIBUTION 225
15.1. Resistance 226
15.2. Temperature 230
15.2.1. Radiation 231
15.2.2. Conduction 232
15.2.3. Convection 233
15.3. Power distribution inspection 235
15.4. References 238

16. ELECTRICAL/MECHANICAL INSPECTION 239
16.1. Baseline thermogram 240
16.2. Electrical connections 240
16.3. Motors: electrical components 243
16.4. Motors: mechanical components 244
16.5. Machinery 246
16.6. Emissivity 250
16.7. Temperature guidelines 251
16.7.1. Electrical circuits 251
16.7.2. Mechanical systems 254
16.8. References 255

17. BURIED OBJECTS 256
17.1. Heat transfer 257
17.2. Environment 260
17.3. Underground objects 260
17.3.1. Hot fluids 260
17.3.2. Voids 264
17.4. References 264

18. SURVEILLANCE 265
18.1. Surveillance applications 266
18.1.1. Law enforcement 267
18.1.2. Search and rescue 270
18.1.3. Air/space surveillance 270
18.1.4. Animal monitoring 273
18.1.5. Military 274
18.2. Minimum resolvable temperature (MRT) 276
18.2.1. Perceived signal-to-noise ratio 276
18.2.2. Three-dimensional noise model 278
18.2.3. Two-dimensional MRT 280
18.3. Range predictions 281
18.3.1. Target ΔT 282
18.3.2. Johnson criteria 283
18.3.3. Discrimination 283
18.3.4. Target transfer probability function 284
18.3.5. Range prediction methodology 286
18.4. References 290

19. NONDESTRUCTIVE TESTING 291
19.1. Applications 293
19.2. Heat transfer 295
19.2.1. Flash pulse (impulse or Dirac pulse) 296
19.2.2. Step and square pulse irradiation 298
19.2.3. Modulated irradiation 300
19.3. Test methodology 301
19.3.1. Heat injection methods 302
19.3.2. Data analysis 305
19.3.3. Temperature/time guidelines 307
19.4. References 309

20. PROCESS/QUALITY CONTROL 310
20.1. Automotive 311
20.2. Petrochemical 311

20.3. Die castings and molding 313
20.4. Printed circuit boards 313
20.5. Metals 315
20.5.1. Aluminum 316
20.5.2. Steel 317
20.6. Paper industry 317
20.7. References 318

21. INSPECTION PROCEDURES 319
21.1. Preliminary work 320
21.1.1. Who 320
21.1.2. What 321
21.1.3. When 321
21.1.4. Where 322
21.1.5. Why 322
21.1.6. How 322
21.2. Safety 323
21.3. Standards and guidelines 323
21.4. Test procedure 324
21.4.1. Test plan 324
21.4.2. Good engineering practices 327
21.5. Exit conference 328
21.6. Final report 328
21.7. References 330

APPENDIX A: TEMPERATURE CONVERSION 331

APPENDIX B: EMISSIVITY 336

APPENDIX C: T HERMAL SENSING AND IMAGING 1980-1999 . 343

INDEX 370

1
INTRODUCTION

Objects are characterized by a variety of physical parameters such as size, shape, and weight. However, the most frequently measured physical property is temperature. Heat is a byproduct of all work whether it is from electrical, mechanical, or chemical activity. We generate, contain, and transfer heat to run our industries and make our every day lives comfortable. Unexpected temperature variations may indicate design flaws, poor workmanship, or damaged components. Excessive temperatures often exist just before failure.

Your internal temperature is 98.6°F (37°C) and a fever suggests that a disease may be present. Localized elevated temperatures may indicate a local abnormality. Since cancer cells have a high metabolic rate, a localized elevated temperature may warrant further tests for the presence of cancer.

An internal-combustion engine converts the potential energy contained in the fuel into mechanical energy. Heat is a byproduct. As the efficiency decreases, more heat is exhausted. Thus, the exhaust temperature is an indicator of the "health" of an engine. The brakes convert forward motion (kinetic energy) into heat. Defective brakes may create excessive localized heating that may lead to failure with disastrous results.

Energized electric motors, transformers, and electronic components create heat. Operational efficiency degrades as the temperature increases. As a result, components are routinely measured and the temperature dictates a course of action (Table 1-1).

Temperatures may be measured with either a contact or non-contact device. Contact devices include the common liquid-in-glass thermometer, resistance thermometer, and thermocouple. Non-contact devices may be either non-imaging or imaging systems. A non-imaging system (such as a radiometer) simply measures the radiation. The system's calibration converts the output voltage to a temperature. Imaging systems, discussed in this book, create a two-dimensional electronic image of the object. As with the radiometer, the imaging system measures the radiation that appears to emanate from the object. Here, calibration provides a two-dimensional representation of the surface temperature.

Table 1-1
REPRESENTATIVE REPAIR PRIORITY
Precise values depend upon specific equipment

Temperature rise above ambient	**Situation**	**Repair priority**
Greater than 50°C (Greater than 90°F)	Acute overheating	Immediate repairs required
30°C to 50°C (54°F to 90°F)	Excessive overheating	Repair as soon as possible
10°C to 30°C (18°F to 54°F)	Second stage of overheating	Should be attended to at the first opportunity
5°C to 10°C (9°F to 18°F)	First stage of overheating	Should be monitored and repaired during next scheduled maintenance
Less than 5°C (Less than 9°F)	Normal operation	None

Measurements can be either qualitative or quantitative. Qualitative measurements compare the thermal signature of one component to that of an identical (or at least similar) under the same (or at least similar) operating conditions. The object (or anomaly) is identified by the intensity variations between the two similar objects without assigning temperature values. This technique is easy and does not usually require any adjustment to the thermal imaging system to compensate for atmospheric conditions or surface emissivity (discussed in Chapter 12, *Temperature Measurements*). Qualitative measurements are appropriate for surveillance (detection of intruders, illegal border crossing, and endangered animal location), location of buried objects, roof inspections, and building inspections.

Quantitative measurements provide the true temperature of the object. Accurate values are required for condition monitoring. The condition of a component (as determined by its true temperature or temperature increase above ambient) is compared to a baseline (e.g., a predetermined value). If the temperature is above the baseline, then a course of action is taken (e.g., Table 1-1).

The maintenance industry[1] generally uses *preventive maintenance* to mean planned activities to maintain equipment to assure that the design life of equipment can be achieved. *Predictive maintenance* is the periodic testing and monitoring of equipment. That is, the results of the tests (predictive maintenance) determine when preventive maintenance should take place.

1.1. HEAT

Heat is the transfer of energy from one object to another. We monitor this transfer by measuring the temperature of the object. Heat flows from a hot object to a cool object. After a period of time, they eventually reach a common temperature called thermal equilibrium. Once heat is lost, it can never be recovered. It must be replaced.

On earth, the sun constantly replenishes the heat. Without the sun, the surface of the earth will eventually cool to the temperature of space – which is near absolute zero. The rate of heating and cooling depends upon the insulating properties of the atmosphere and cloud cover. The insulating effects of these two tend to minimize surface temperature variations and this permits life to exist.

Heat is created when the internal energy of a body is released. We harnessed the heat to perform mechanical work (Figure 1-1). For example, burning fossil fuel creates most electricity. The "internal" energy of the gas, oil, or coal is released upon combustion. The heat is used to create steam, which in turn, makes a generator rotate.

Within an automobile engine, combustion creates a heated gas that pushes the cylinders. The crankshaft converts this linear motion into circular motion to propel the car. But no process is 100% efficient. Some heat is lost. A significant amount of heat is lost through the cooling radiator and exhaust (Figure 1-2).



Figure 1-1. Heat provides the transfer of energy from one system to another.

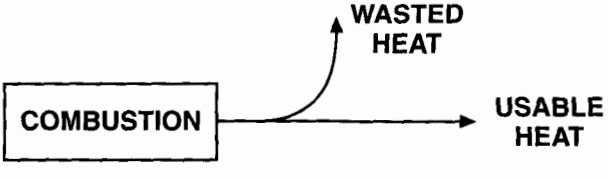


Figure 1-2. All processes lose heat.

The car's forward motion is limited by friction – friction caused by the air, tires, and gear train. This friction heats the air, tires, and gears. If it were not for this friction, then we would have a perpetual motion machine. Energy must be continually supplied to overcome the loss to friction (Figure 1-3). By applying the brakes, the car stops. Here, the useful mechanical energy is transformed into heat and the brakes dissipate the heat.

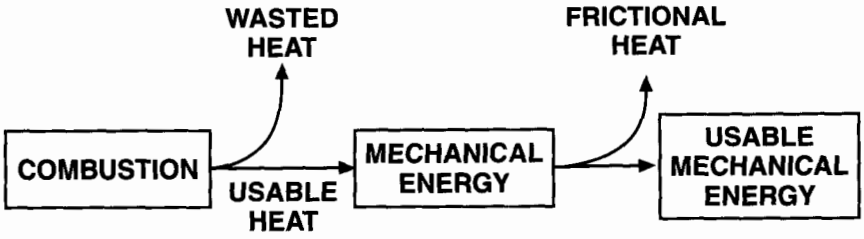


Figure 1-3. Friction always creates heat. As the frictional losses are reduced, the fuel consumption goes down. Economy cars (in terms of miles per gallon) have an aerodynamic design and are lightweight. The lower weight reduces frictional loss in bearings and tires.

1.2. TEMPERATURE MEASURING DEVICES

Heat is an intangible energy. Its presence is monitored by the temperature of an object. Temperature measuring devices may either be contact or non-contact devices. Contact devices rely upon heat conduction and convection. Non-contact devices rely upon the radiation emitted by the object.

Contact devices generally are inexpensive whereas non-contact (notably the thermal imaging system) can be quite expensive. The selection of one over the other depends upon the application. When measuring the temperature with contact devices, data is obtained only at those regions where the devices are placed. Table 1-2 lists those applications where a thermal imaging system is an appropriate measuring device.

Table 1-2
THERMAL IMAGING SYSTEM APPLICATIONS

Reason	Example
Object is inaccessible	Distant power lines
Object is moving	Motor shaft or brake rotor
Safety is an issue	Dangerous to place contact on electrically "hot" equipment
Contact method may damage object	Delicate materials
Harsh environment that would destroy a contact device	Inside a furnace
Object is so small that it would be difficult to attach a contact device	Component on a printed circuit board
Two-dimensional temperature distribution required	Determine defect size

1.2.1. CONTACT DEVICES

A thermometer contains a material that changes its physical characteristics as its temperature changes. It could be the change in the length of a rod, the volume of a liquid, or the electrical resistance of a wire.

LIQUID-IN-GLASS THERMOMETER

The common liquid-in-glass thermometer contains a liquid that expands as it heats up. The liquid could be colored alcohol or mercury. As illustrated in Figure 1-4, the expanding liquid moves up a narrow bore.

When a thermometer is placed inside an object, heat flows from the object (if warmer) to the thermometer. The temperature recorded is that of the thermometer. If it in thermal equilibrium with the object, then the measured temperature is the same as the object. Ideally, the thermal mass of the thermometer is much less that of the object. Then as the thermometer heats up, the amount of heat transferred is very small, and then the temperature of the object is not significantly affected. Simply stated, it is difficult to accurately measure the temperature of small objects with a liquid-in-glass thermometer.

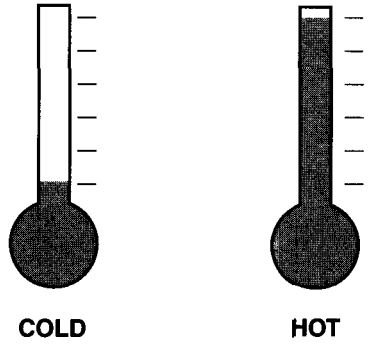


Figure 1-4. Liquid-in-glass thermometer. As the reservoir heats up, the expanding liquid moves up the narrow bore. The calibration marks on the bore represent temperature.

RESISTANCE THERMOMETER

The resistance thermometer consists of a material whose resistance increases as the temperature increases. An external circuit (Figure 1-5) measures the resistance change. Platinum is used most often to create the PRT (platinum resistance thermometer). Platinum has excellent mechanical and electrical properties from -270°C to 700°C (-450°F to 1300°F). This thermometer can be immersed in non-reactive liquids. To ensure accurate measurements of solids, a heat conducting grease (thermal grease) is used to ensure good thermal contact.

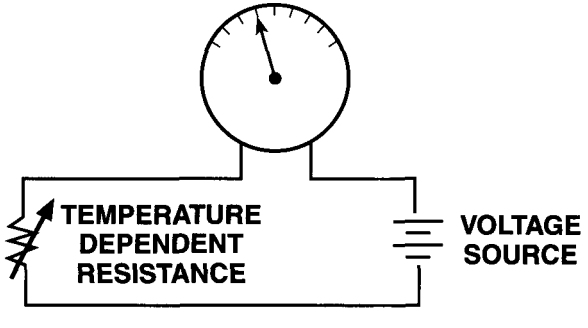


Figure 1-5. Resistance thermometer. An external circuit measures the change in current [(current = (voltage)/(resistance)]. The analog meter (shown here) has marks that represent temperature. Usually a digital meter is used.

THERMOCOUPLE

A thermocouple is composed of two dissimilar metals that create an electromotive force (EMF). As illustrated in Figure 1-6, the EMF is usually measured with a voltmeter. To avoid creating an EMF at the input to the voltmeter, two thermocouples are used. The reference is held at a well-known temperature (e.g., an ice-water bath). It is one of the cheapest methods to measure temperature. The thermocouple can be immersed in non-reactive liquids. To ensure accurate measurements of solids, a heat conducting grease (thermal grease) is used to ensure good thermal contact.

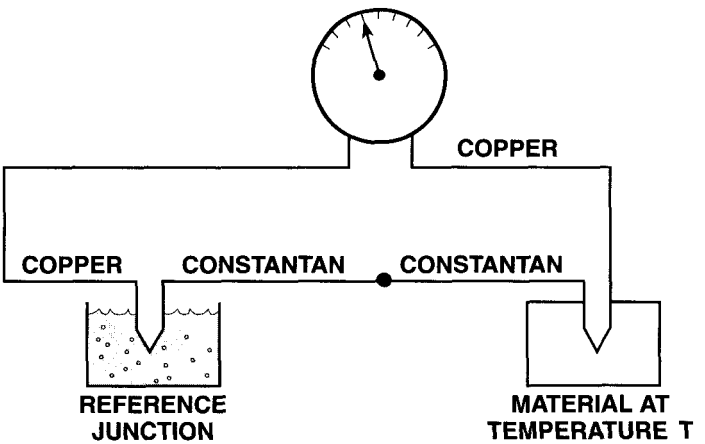


Figure 1-6. Copper-constantan thermocouple. A variety of dissimilar materials may be used. The small differential EMF is monitored by a voltmeter. The analog meter (shown here) has marks that represent temperature. Usually a digital meter is used.

1.2.2. NON-CONTACT DEVICES

Non-contact devices may be used for quantitative or qualitative measurements. The most popular devices are the pyroelectric detector, optical pyrometer, and the thermal imaging system.

MOTION SENSOR

Motion sensors are used as a qualitative method to locate individuals. Most sensors contain very low cost pyroelectric detectors. This detector senses

temperature changes only. The sensor output is simply a voltage that activates an alarm. It indicates that a warm object (assumed to be an intruder) has moved within the field-of-view. It is carefully adjusted to prevent false alarms created by pets. Since the pyroelectric detector only measures temperature changes, very slowly moving objects will not be detected.

OPTICAL PYROMETER

The optical pyrometer consists of a calibrated lamp whose filament voltage is adjustable. As the voltage changes, the filament brightness (color) changes. The filament brightness is simply matched to the target brightness (Figure 1-7). Since colors are matched in the visible part of the spectrum, the object must be heated to incandescence (greater than 600K or greater than 620°F). Optical pyrometers can measure temperatures up to 10,000K (17,500°F). These high temperatures could melt contact devices.

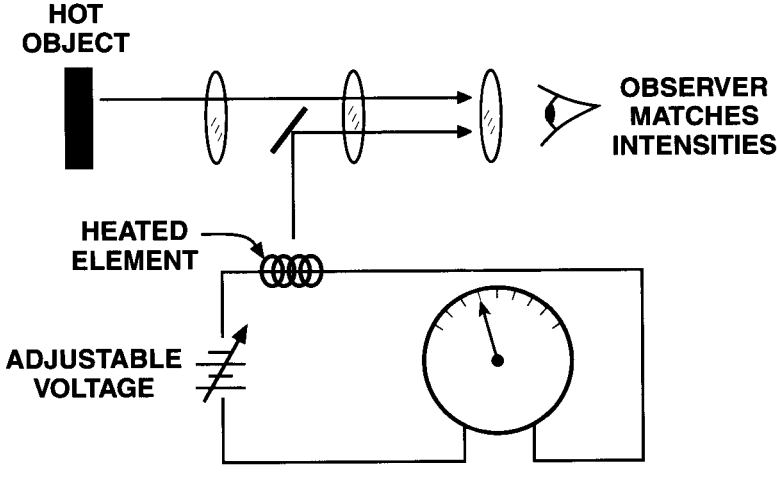


Figure 1-7. Optical pyrometer. The filament current is measured with an ammeter. The analog meter (shown here) has marks that represent temperature.

THERMAL IMAGING SYSTEM

The thermal imaging system (Figure 1-8) creates an electronic picture of the scene. The picture may be converted to color (pseudo color or false color) where reds indicate hot areas and blues represent cool objects.

When presented in black-and-white, the brightness (more white) indicates hotter objects. When the electronic picture is printed, it becomes a thermogram. A thermogram is simply a map of thermal energy where shades of gray or colors represent different levels of radiant energy. Many of the original images in this book were in color. The conversion back to black-and-white does not provide the original gray scale.

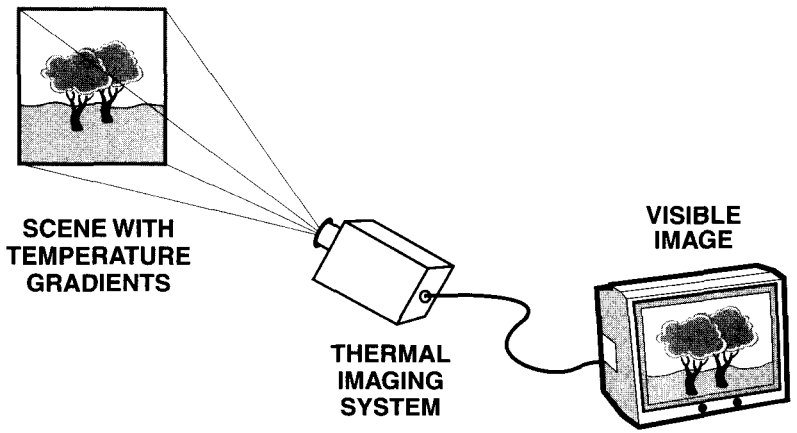


Figure 1-8. Thermal imaging system. A variety of detectors can be used in the thermal imaging system (discussed in Section 6.5, *Detectors and Coolers*). Each has its own advantages and disadvantages. All convert an infrared scene into a visible image.

1.3. TEMPERATURE SCALES

Both contact and non-contact devices are calibrated by recording the output at known temperatures. The two most common temperatures are the freezing point and boiling point of water. These two points are scribed onto the thermometer (Figure 1-9). Then the space between these marks is uniformly divided by more scribe marks.

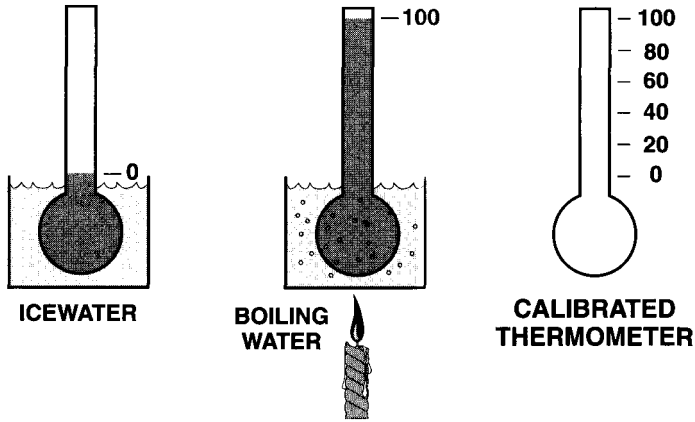


Figure 1-9. Calibrating a liquid-in-glass thermometer (Celsius scale).

Four temperature scales exist: Fahrenheit, Celsius (originally called centigrade), Kelvin, and Rankine. Both the Fahrenheit and Celsius scales are referenced to the freezing and boiling of water. The Kelvin and Rankine scales use absolute zero as their zero point (Table 1-3). Absolute zero is that temperature where all molecular motion stops. It is the lowest theoretically possible temperature. The symbols are °F, °C, K, °R for Fahrenheit, Celsius, Kelvin, and Rankine, respectively. Note that on the Kelvin scale, the units are *Kelvin* and not *degrees Kelvin*.

Table 1-3
TEMPERATURE SCALES

	Kelvin K	**Celsius °C**	**Fahrenheit °F**	**Rankine °R**
Absolute zero	0	-273.15	-459.7	0
Freezing point of water	273.15	0	32	491.7
Boiling point of water	373.15	100	212	671.7

The mathematical relationships between these scales are

$$T_{FAHRENHEIT} = \frac{9}{5} T_{CELSIUS} + 32 \quad , \tag{1-1}$$

$$T_{CELSIUS} = \frac{5}{9}(T_{FAHRENHEIT} - 32) \quad , \tag{1-2}$$

$$T_{KELVIN} = T_{CELSIUS} + 273.15 \quad , \tag{1-3}$$

$$T_{CELSIUS} = T_{KELVIN} - 273.15 \quad , \tag{1-4}$$

$$T_{RANKINE} = T_{FAHRENHEIT} + 459.7 \quad , \tag{1-5}$$

and

$$T_{FAHRENHEIT} = T_{RANKINE} - 459.7 \quad . \tag{1-6}$$

Temperature difference is relative to a baseline. For example, many devices are rated by the temperature rise above ambient rather than the absolute temperature. This rise is labeled as ΔT (pronounced *delta T* and is sometimes shortened to *delta*):

$$\Delta T_{FAHRENHEIT} = \frac{9}{5} \Delta T_{CELSIUS} \quad , \tag{1-7}$$

$$\Delta T_{CELSIUS} = \frac{5}{9} \Delta T_{FAHRENHEIT} \quad , \tag{1-8}$$

$$\Delta T_{KELVIN} = \Delta T_{CELSIUS} \quad , \tag{1-9}$$

and

$$\Delta T_{RANKINE} = \Delta T_{FAHRENHEIT} \quad . \tag{1-10}$$

Appendix A contains an easy look-up table for conversion between Fahrenheit and Celsius.

1.4. THE ELECTROMAGNETIC SPECTRUM

Non-contact devices detect electromagnetic radiation (discussed in Chapter 3, *Detection of radiation*). Radiation is characterized by its wavelength. Wavelength is defined as the distance between two peaks (Figure 1-10). Speed is the movement of the peaks. Electromagnetic energy travels at the speed on light. In a vacuum this is approximately 3×10^8 m/s. Since the wave is moving, the distance between the peaks can also be measured in time and the inverse is the frequency (measured in Hertz).

The wavelength is

$$\lambda = cT = \frac{c}{\nu} \quad , \tag{1-11}$$

where c is the speed of light, T is the period, and ν is the frequency. Shorter wavelength light has a higher frequency. A wavelength is usually measured in micrometers (also called microns) and is represented by the symbol μm. It is one-millionth (1/1,000,000) of a meter. For the longwave infrared region, the average wavelength is $\lambda = 10$ μm and the frequency is 3×10^{13} Hz. For the mid-wave infrared region, the average wavelength is $\lambda = 5$ μm resulting in a frequency of 6×10^{13} Hz. For the visible region, average wavelength is $\lambda = 0.5$ μm resulting in a frequency of 6×10^{14} Hz. These frequencies cannot be measured directly. As a result, we measure the average power (averaged over many cycles).

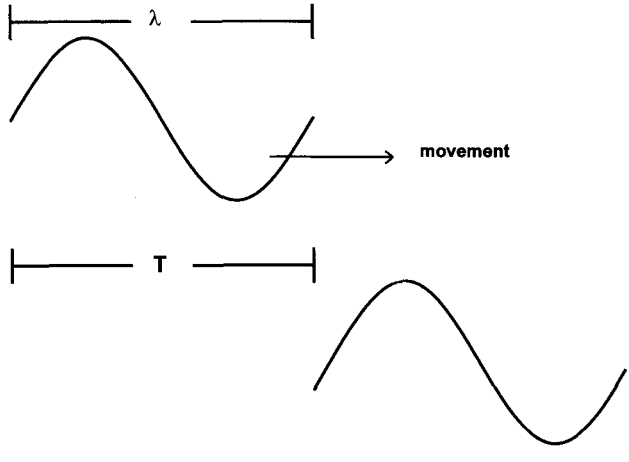


Figure 1-10. Definition of wavelength and period. At time T, the wave moved the distance of one wavelength.

In 1905, Einstein postulated that light is composed of particles of energy. The energy associated with each particle is

$$E = h\nu = h\frac{c}{\lambda} \quad , \tag{1-12}$$

where h is Planck's constant ($h = 6.626\times10^{-34}$ J-s). These particles were later called photons (Figure 1-11).

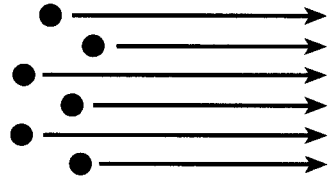


Figure 1-11. Photons are considered particles. Radiation exhibits both wave-like properties and particle-like properties.

Due to the atmospheric spectral transmittance, electronic imaging system design is partitioned into seven generic spectral regions (Figure 1-12) of which four are associated with thermal imaging systems. The ultraviolet (UV) region ranges in wavelength from 0.2 to 0.4 μm. The visible spectral region ranges in wavelength from 0.4 to 0.7 μm. Televisions, electronic still cameras, and most solid state cameras* operate in this region. The near infrared imaging spectral region (NIR) spans approximately 0.7 to 1.1 μm. Low light level television (LLLTV), image intensifiers, star light scopes, and night vision goggles operate in this region. For historical reasons, the UV, visible, and NIR technologies have developed their own terminologies.

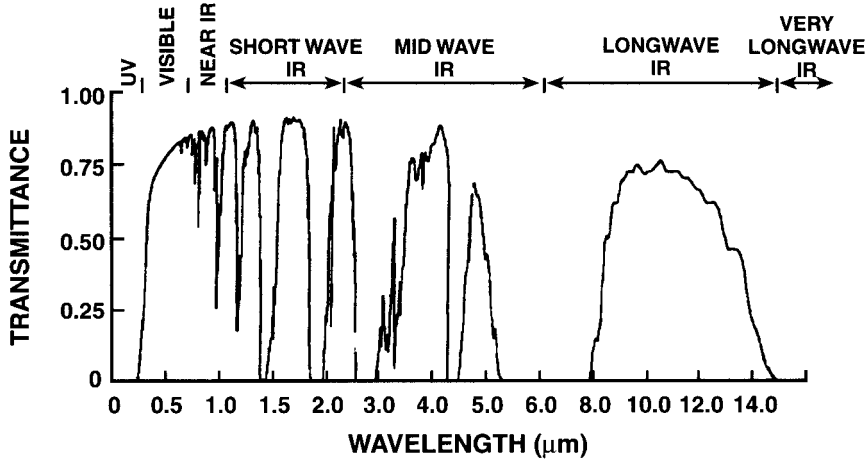


Figure 1-12. Representative atmospheric transmittance over a 1-km path length. The transmittance varies with temperature, relative humidity, and airborne particulates (e.g., fog, dust, pollution, and haze).

**Solid state cameras are popularly called CCD cameras because most contain charge-coupled device detector arrays.*

For this book, the first infrared imaging band is the short wavelength infrared imaging band (SWIR) which approximately covers 1.1 to 2.5 μm. The second infrared band is the mid-wavelength infrared (MWIR) spectral region that covers approximately 2.5 to 7.0 μm. In older literature, the MWIR band was labeled as SWIR, The third infrared band is the long wavelength infrared (LWIR) spectral band. It covers the spectral region from approximately 7 to 15 μm. The fourth infrared band is the far infrared (FIR) or very long wave infrared (VLWIR) region. It applies to all systems whose spectral response extends past 15 μm. The MWIR and LWIR regions are sometimes called the first and second thermal imaging bands respectively.

The word *infrared* has a different definition that depends upon the technology. For example, film was invented to reproduce visible images. If the film is sensitive to longer wavelengths, it is called infrared film. Infrared film is sensitive out to about 0.85 μm. Imaging systems were also created to reproduce visible images. If the spectral response was past 0.7 μm, it was called an infrared device. Most of these systems used photosensitive detectors whose spectral response went to about 1 μm. A variety of labels were attached to these devices. This includes thermal imaging systems, snooper scopes, and night vision devices.

Table 1-4 lists the wavelengths associated with specific systems. The precise spectral response for any system depends upon the design. To say a system is a LWIR system only means its response is somewhere in the LWIR region. For example, a LWIR system may have a spectral response from 7.7 to 11 μm or 8 to 12 μm. The atmospheric carbon dioxide (CO_2) absorption band will completely attenuate all target information at 4.2 μm. As a result, a MWIR system may have a spectral response from 3 to 4.2 or 4.3 to 5.5 μm.

Table 1-4
SPECTRAL NOMENCLATURE

Spectral band	Wavelength range (μm)
Vacuum ultraviolet	0.05 to 0.20
Short ultraviolet (UV-C)	0.20 to 0.29
Mid-wave ultraviolet (UV-B)	0.29 to 0.32
Long-wave ultraviolet (UV-A)	0.32 to 0.40
Visible	0.40 to 0.70
Violet	0.40 to 0.46
Blue	0.46 to 0.49
Green	0.49 to 0.55
Yellow	0.55 to 0.58
Orange	0.58 to 0.60
Red	0.60 to 0.70
Near infrared (NIR)	0.7 to 1.1
Short wavelength infrared (SWIR)	1.1 to 2.5
Mid-wavelength infrared (MWIR)	2.5 to 7.0
Note: labeled as SWIR in older literature	
First thermal imaging band	3.0 to 5.5
Blue spike plume	4.1 to 4.3
Red spike plume	4.3 to 4.6
Long wavelength infrared (LWIR)	7.0 to 15.0
Second thermal imaging band	8 to 14
Very long wavelength infrared (VLWIR)	> 15.0
Extreme infrared	15 to 100
Near millimeter	100 to 1000
Millimeter	1000 to 10,000

1.5. BRIEF HISTORY OF THERMOGRAPHY

As with most technologies, thermal imaging systems are based on phenomena discovered nearly 200 years ago. In 1800, William Herschel discovered infrared rays. Later, John Herschel (1840) produced the first infrared image using a method that he called evaporography. By evaporating alcohol from a carbon-coated surface, a visible image was produced. This was the first thermogram. It took another 89 years (1929) before Czerny provided an improvement to image creation.

In 1946, the military developed the first infrared line scanner. By putting many lines together, a two-dimensional image was created. A thermogram took one hour to produce. By adding a scanner (1954), the system could directly create a two-

dimensional image. Even with this improvement, it still took 45 minutes to create an image. By 1960, image-creation time was reduced to 5 minutes.

In 1966, the first commercial real-time imager, producing 20 images per second, was introduced. 1966 could be considered the year that thermal imaging systems, as we know them today, were created. Rapid advances in technology, spurred on by expanding applications, occurred in the '70s, '80s, and '90s. Perhaps the greatest advances in system design occurred in the '90s: The introduction of high-resolution focal plane arrays (FPAs) and uncooled FPAs. Imaging systems can now produce hundreds of images per second and high-speed electronics provide real-time image processing. The imaging system of tomorrow is limited only by man's imagination.

1.6. SYSTEM DEVELOPMENT

This section provides a very brief overview of system development. Chapter 6, *Camera Design*, provides more detail.

The very first system was a line scanner. The militarized system was mounted on an aircraft and looked straight down. A scanner moved the line-of-sight perpendicular to the aircraft motion. Only a single detector was used. The two dimensional image was created by the aircraft forward motion.

In the late 1960s, Texas Instruments designed a system that could look at other angles: namely forward. It had two moving mirrors to create a raster pattern. This was called a *Forward Looking Infrared* system or FLIR. The acronym still exists today even though no system is built like the initial FLIR. This design was the start of the common module design. This LWIR system used mercury-cadmium-telluride (HgCdTe) detectors. MWIR systems were introduced using lead tin telluride (PbSnTe) and indium antimonide (InSb) detectors. InSb is used extensively today whereas PbSnTe experienced technological problems and has fallen out of favor.

Only one person could view the image produced by the early common module systems. In mid 1975, the electro-optically multiplexed (EOMUX) system was developed. This allowed the image to be routed to a monitor for multiple viewers to appreciate. The electronically multiplexed (EMUX) system, developed in the early 1980s, improved reliability and overcame some image defects. It was very clear to all that a focal plane array had numerous advantages over a scanning system. However, technology in the '70s limited FPA development. To bridge the gap between linear arrays and staring arrays, the time-delay-and-integrate (TDI)

array way developed. It had an improved signal-to-noise ratio but still required a scanner. Dr. Tom Elliott introduced a HgCdTe filament detector that has an inherent TDI capability in the United Kingdom. Originally called TED (Tom Elliott's device), it is now known as the SPRITE (signal processing in the element) detector. EMUX, SPRITE and TDI systems are still manufactured today.

The 1980s saw the introduction of the MWIR platinum silicide (Pt:Si) and quantum well infrared photodetectors (QWIP). Then in the 1990s uncooled arrays became commercially viable. Since no cooler is required, power consumption dropped significantly leading to small, hand-held systems. High-speed digital electronics permitted image storage on credit-card-sized memory disks. This revolutionized the commercialization of thermal imaging systems.

The early commercial versions were derivative of military designs. Today, with the wide range of applications, military and commercial designs are different (Table 1-5). The table also lists the chapters were the topics are discussed in detail.

Table 1-5
DIFFERENCES in DESIGN REQUIREMENTS

Design areas	**Military**	**Commercial**	**Chapters**
Image processing algorithms	Application specific (e.g., target detection or automatic target recognition)	Menu-driven multiple options	Chapter 6, *Camera Design* Chapter 8, *Camera Selection*
Resolution	High resolution (resolve targets at long distances)	Typically not an issue because the image can be magnified by moving closer	Chapter 7, *Performance Parameters*
Target signature	Usually just perceptible	Usually high contrast target	Chapter 11, *Target Signatures*
Sensitivity	Low noise (i.e., high sensitivity)	Noise not necessarily a dominant design factor	Chapter 7, *Performance Parameters*

1.7. APPLICATIONS OVERVIEW

In 1969, Hudson[2] listed over 100 separate applications for thermal imaging systems. He divided the list into four major categories: military, industrial, medical and scientific. Each category was then subdivided into (1) search, track and range, (2) radiometry, (3) spectroradiometry. (4) thermal imaging, (5) reflected flux, and (6) cooperative source. The list is surprisingly complete. Today, two broad categories are in use: military and commercial. Table 1-6 highlights a few applications in each category. Military and commercial systems are similar in basic design, but each system is built for a specific purpose. Consequently, military and commercial systems tend to be described by different performance parameters.

Table 1-6
REPRESENTATIVE THERMAL IMAGING SYSTEM APPLICATIONS

Community	**Applications**	
Military	Reconnaissance, target acquisition, fire control, and navigation	
Commercial	Civil	Law enforcement, firefighting, and building integrity
	Environmental	Earth resources, pollution control, and energy conservation
	Industrial	Predictive maintenance, manufacturing, and nondestructive testing
	Medical	Mammography, soft tissue injury, and arterial constriction

With so many commercial applications, various terminologies appeared. Nondestructive testing (NDT), nondestructive inspection (NDI) and nondestructive evaluation (NDE) are names to describe methods of testing without causing damage to the object being tested (discussed in Chapter 19, *Nondestructive testing*). These terms all mean much the same and attempts to assign different meanings has not been fully accepted. In 1996, Vavilov[3] offered the following definitions:

THERMOGRAPHY

Method of determining the spatial distribution of heat in objects.

NONDESTRUCTIVE TESTING

Material inspection by monitoring heat flux disturbances caused by defects. Generally, the object is at ambient temperature. Therefore, heat must be supplied to the object by an external source.

THERMAL WAVE NONDESTRUCTIVE TESTING

Nondestructive testing where heat is applied in a periodic fashion.

Since 1976, SPIE has hosted the internationally acclaimed conference *Thermosense*. This conference concentrates on the civil and industrial applications. Selected papers appear[4] in *Thermal Sensing and Imaging* and its Table of Contents are provided in Appendix C. Papers on other topics appear in *Infrared Technology*[5] and *Infrared Imaging Systems: Design, Analysis, Modeling, and Testing*.[6]

1.8. UNITS

Each equation must be dimensionally correct. That is, each quantity must have the correct units before using an equation to calculate a value. The scientific community uses SI (Systeme International d'Unites) units. It is also known as the mks (meter-kilogram-second) system. Numerous attempts have been made to get worldwide acceptance of these units. Unfortunately, some nations and industries still use the English system.

To facilitate understanding, both sets of units are provided when appropriate (Table 1-7). Since thermal imaging systems are calibrated in temperature both degrees Celsius (°C) and degrees Fahrenheit (°F) are given throughout. Chapter 3, *Detection of radiation*, is a "scientific" chapter and exclusively uses SI units. While Chapter 2, *Heat*, has scientific underpinnings, the values are used by various industries and therefor both units are used. Section 2.5 provides numerous conversion factors.

Table 1-7
SI and ENGLISH UNITS

Physical quantity	**SI /mks**	**English**
Energy	J (or cal)	BTU
Weight	g (or kg)	pounds
Distance	m (or km)	feet (or miles)
Speed	m/s (or kph)	ft/s (or mph or knots)
Power	kW (or kcal/hr)	BTU/hr
Temperature	K (or °C)	°F

A word of caution. The conversion from English to SI units is exact. But the meaning is sometimes distorted. For example, a distance may be about 35 feet. A precise conversion provides 10.67 meters. The use of four significant figures suggests something about accuracy. A better statement is that 35 feet is about 10 meters. In this chapter it was stated: *Optical pyrometers can measure temperatures up to 10,000K (17,500°F)*. The temperature, 17,500°F, is an approximate value. A precise conversion would provide 17,540.33°F. The value, 17,500°F, provides an equivalent estimate on the Fahrenheit scale. Exact conversions are not always required.

1.9. REFERENCES

1. R. D. Lucier, "Predictive Maintenance for the 90's - An Overview" in *Thermosense XIV*, J. K. Eklund, ed., SPIE Proceedings Vol. 1682, pp. 35-42 (1992).
2. R. D. Hudson Jr., *Infrared System Engineering*, Chapters 16 to 19, John Wiley and Sons, New York (1969).
3. V. P. Vavilov, "Subjective Remarks on the Terminology used in Thermal/Infrared Nondestructive Testing," in *Thermosense XVIII*, D. D. Burleigh and J. W. M. Spicer, eds., SPIE Proceeding Vol. 2766, pp. 276-281, (1996).
4. *Thermal Sensing and Imaging 1980-1999*, J. Snell and D. Burleigh, Eds., Selected SPIE papers on CD-ROM, Volume 7, Bellingham, WA (1999).
5. SPIE has hosted *Infrared Technology* since 1975. The proceeding for each conference is available from SPIE, Bellingham, WA. These are available at www.spie.org.
6. SPIE has hosted *Infrared Imaging Systems: Design, Analysis, Modeling, and Testing* since 1990. The proceeding for each conference is available from SPIE, Bellingham, WA. These are available at www.spie.org

2
HEAT

Heat is the transfer of energy from one object to another. It travels from a hot object to a cool object. This energy comes from the internal molecular vibrational energy of the hot object. The object's temperature is a direct measure of the internal vibrational energy. The greater the internal energy, in general, the higher the temperature.

We commonly misuse use the word *heat*. It is incorrect to say an object contains heat. While we set the oven *heat* at 350°F, we are really setting the temperature. Likewise, if a room is cold, we turn on the *heat*. We are, in fact, transferring heat from a source (the furnace) to a room. We control the *heat* by a thermostat that actually controls the temperature.

Our body can sense temperature changes. Whether something *feels* hot or cold depends upon our environment. For example if we were outside when the temperature is 20°F (-6.7°C) and enter a room that is 65°F (18.3°C), the room would feel warm. On the other hand, if it were 100°F (37.8°C) outside and we entered that same room, it would appear cold. Regardless of the outside temperature, after a while we will become acclimated to the room temperature. Whether it feels hot or cold now depends upon our clothing and amount of activity. It also depends upon our long-term conditioning. People from the arctic would always think that the room is quite warm whereas those from the desert would think it was excessively cold. When we touch objects and heat flows into the hand, the object feels hot. If heat flow is from our hand into the object, the object feels cold. Nerves respond to the arrival or departure of heat. The brain's interpretation of the nerve impulses identifies the object as hot or cold.

Heat is an intangible thing. We cannot directly measure heat. We can only measure the effects of heat: namely by a temperature change. The amount of heat necessary to change the temperature of an object depends on the object's heat capacity.

The three common units of heat are the gram-calorie (cal or g-cal), kilogram-calorie (kcal or kg-cal), and the British thermal unit (BTU). One kilogram-calorie is the quantity of heat that must be supplied to one kilogram of water to raise its temperature one degree Celsius. Likewise, the calorie is the quantity of heat that must be supplied to one gram of water to raise its temperature one degree Celsius (1 kcal = 1000 cal). The BTU has the same meaning but in English units: one BTU is the

quantity of heat that must be supplied to one pound of water to raise its temperature one Fahrenheit degree (Figure 2-1).

The gram-calorie should not be confused with the nutritionist's definition of Calorie. The energy in food is specified by the Calorie. That Calorie is equal to our kilogram-calorie. The mechanical equivalent of heat equates one kcal to 4186 joules (J) of energy (conversion is 4186 J/kcal). The SI unit of heat is the joule. Other units are used are various industries. Additional conversion factors are provided in section 2.5.

Heat transfer can be by conduction, convection, or radiation. Since we measure the temperature, we must understand the relationship between temperature and heat flow. The temperature of the object depends upon the physical properties of the material. These include the heat capacity and specific heat. These quantities vary with the material phase (solid, liquid, or gas).

Because heat transfer and resultant temperature is based upon several interrelated factors, it is difficult to predict the influence of each component. This chapter highlights the major heat transfer mechanisms that form the basis for understanding the final temperature of an object.

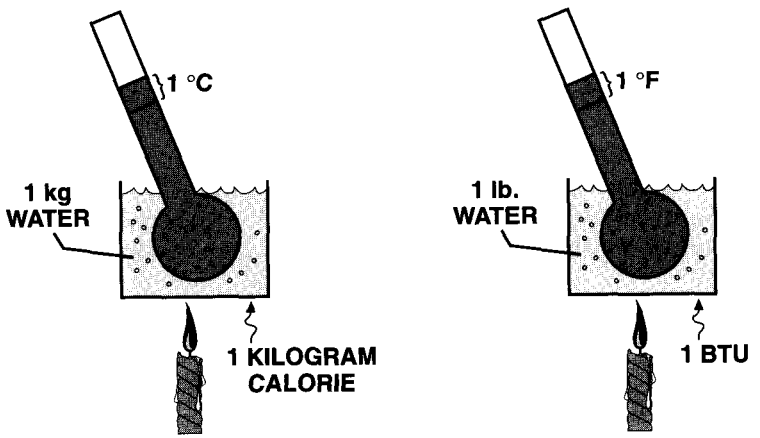


Figure 2-1. Definition of kilogram-calorie and BTU. One BTU equals 0.252 kcal.

2.1. HEAT CAPACITY AND SPECIFIC HEAT CAPACITY

Materials differ in the quantity of heat required to produce an elevation of temperature. This heat quantity is related to the heat capacity by

$$\textit{heat capacity} = \frac{Q}{T_2 - T_1} \quad , \tag{2-1}$$

where Q is the quantity of heat supplied and T_2-T_1 is the temperature increase. The specific heat capacity (often simply called the specific heat) is defined as the heat capacity per unit mass:

$$c = \frac{\textit{heat capacity}}{\textit{mass}} = \frac{Q}{m\left(T_2 - T_1\right)} \quad . \tag{2-2}$$

The specific heat capacity is the amount of heat that must be supplied to a unit mass of material to increase its temperature through one degree. The value, c, is unique to each material (Table 2-1). The amount of heat that must be supplied to raise the temperature from T_1 to T_2 is

$$Q = mc\left(T_2 - T_1\right) \quad . \tag{2-3}$$

High specific heat objects (high c) require more heat than objects with a lower specific heat. For example, one kilogram of aluminum requires more heat than one kilogram of silver to raise its temperature by one degree. Equivalently, materials with high heat capacity can store large amounts of heat energy. If warmer than ambient, these materials will take a relatively long time to cool. Outside, the temperature of water will lag changing air temperature. Large bodies of water create a local microclimate where the temperature does not fluctuate as much as over dry land.

The term "heat capacity" should not be confused with the "capacity" of a bucket. A bucket can hold only so much water and no more. Heat can be supplied indefinitely to a material (with a corresponding rise in temperature). Of course, if the material temperature rises significantly, the material may change phase (solid to liquid or liquid to vapor). The heat capacity of the new phase may be substantially different from the original phase.

Table 2-1
SPECIFIC HEAT CAPACITY of
SOME COMMON MATERIALS
(Varies with composition and impurities)

Material	Specific heat capacity	
	J/(kg-K)	kcal/(kg-K)*
Water	4186	1.000
Ice	2302	0.550
Wood	1394	0.333
Brick	1005	0.240
Aluminum	908	0.217
Iron	473	0.113
Brass	393	0.094
Copper	389	0.093
Silver	234	0.056
Lead	130	0.031

*The values in this column are the same in units of cal/(g-K) and BTU/(lb-°F). Note that °C could be used as units.

2.2. PHASE CHANGE

Nearly all materials exhibit three phases: solid, liquid, and gas. A transition from one phase to another is accompanied by the absorption or liberation of heat (Table 2-2) and usually a change in volume. During the phase change, the temperature of the material remains constant. For example, the temperature of boiling water remains constant even though heat is continually added to create more vapor.

The pressure plays a big role in determining the boiling temperature. At sea level water boils at 212°F (100°C). As the elevation increases, the pressure decreases. For every 500 feet of elevation, the boiling point drops about 0.9°F (0.5°C). In Denver (altitude = 5000 feet), water boils at about 203°F (95°C). Your car radiator is pressurized so that the boiling temperature increases to about 240°F (116°C). This higher temperature provides a safety margin to your cooling system. The engine can still be water-cooled as it reaches 240°F (116°C).

Consider a pot full of ice that is placed upon a stove to which heat is constantly added. Initially, the ice temperature will increase (Figure 2-2). At 32°F (0°C), all the heat supplied will be used to convert the ice into water. Once in the liquid state, the temperature will again increase. At 212°F (100°C), the heat will be used to create vapor (steam). The temperature of the steam depends upon the

overall vessel. If open to the air, the steam will diffuse away and be absorbed by the air. This increases the relative humidity of the air. If the vessel is closed, the steam temperature can increase to produce super heated steam. This also increases the pressure and it increases the temperature at which the water boils.

Table 2-2
PHASE CHANGE

Phase change	Heat transfer	Quantity of transformation
Solid to liquid	Requires heat	Heat of fusion
Liquid to gas	Requires heat	Heat of vaporization
Gas to liquid	Heat liberated	Heat of condensation
Liquid to solid	Heat liberated	Heat of solidification

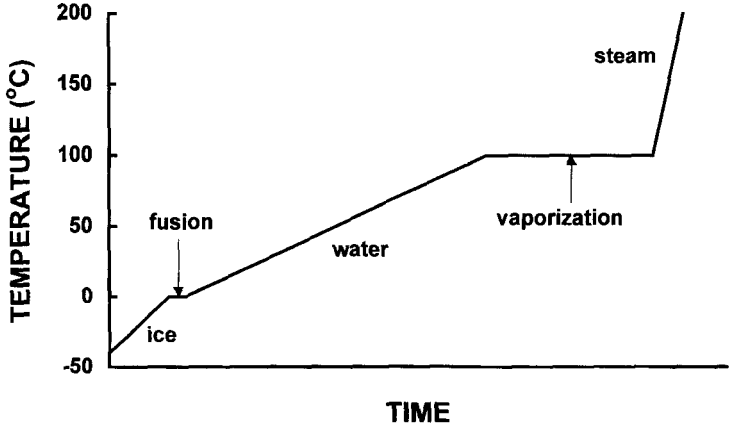


Figure 2-2. Temperature as a function of time as ice is converted into vapor. Since the specific heat capacity of ice is less than water, it will warm up faster. The heat of vaporization (539 kcal/kg) is greater than the heat of fusion is (79.7 kcal/kg). Therefore, the time to create steam is about 6.7 times longer than the time to create water.

Evaporative cooling is widely used to reduce the temperature of a liquid or solid. The heat required for vaporization comes from the remaining liquid or the solid. Air-conditioners transfer heat from the inside to an outside unit. The outside unit must then expel the heat into the environment. Water towers are

sometimes used to cool the outside units. As water evaporates, the temperature of the unit decreases. However, the water must be constantly replenished.

The identical process is used to keep drinking water cool in hot environments. The water is placed in a porous container. As the water seeps out, it evaporates and cools the water. It, of course, must be shielded from the sun. Each gram, as it evaporates, removes 539 cal of heat. The temperature drop is calculated from Equation 2-2. Evaporating surface water, whether from porous surfaces, dew, or rain, significantly affects the object's temperature (Figures 2-3 and 2-4).

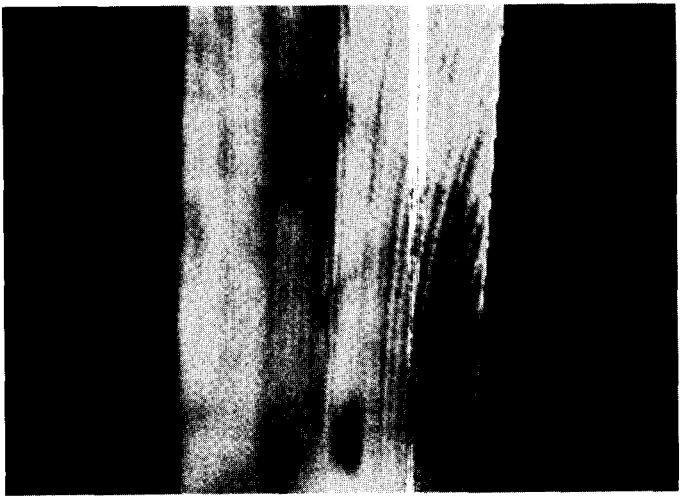


Figure 2-3. Wood porosity depends upon the grain structure. Wet wood dries (and cools) unevenly. (By courtesy of the Academy of Infrared Thermography).

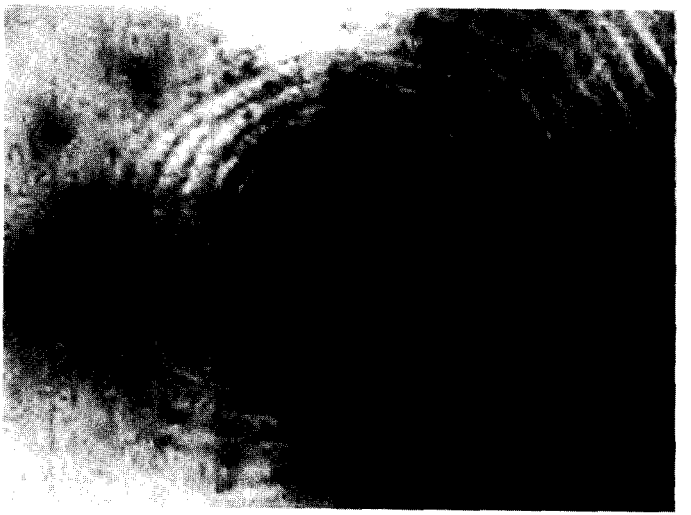


Figure 2-4. The sweat glands on this fingertip become detectable due to evaporative cooling. (By courtesy of Indigo Systems).

2.3. HEAT TRANSFER

Heat travels by conduction, convection, and radiation. Each process is different, but the result is the same: heat travels from the hotter object to the cooler object. It is convenient to discuss the amount of heat transferred per unit time.

2.3.1. CONDUCTION

The conduction process is straightforward. The heat source directly excites atoms (increases their internal vibrations). These atoms collide with their neighbors and transfer some of the energy to the neighbor. The neighbors then collide it its neighbors and again pass on some energy. Thus, the energy of thermal motion is passed along from one atom to the next. How quickly if flows depends upon the material's thermal conductivity. Metals have high thermal conductivity and insulators have low thermal conductivity.

If one end of a metal rod is placed in a flame and the other end is held in the hand, the held part will become hotter and hotter. This occurs even though the handheld part is not in direct contact with the flame. The heat has reached the cooler end through conduction. On the other hand, if a same-sized ceramic rod is used, the held part will very slowly increase in temperature because of its poor thermal conductivity.

If the surfaces of an object are held at two different temperatures, there will be a temperature gradient within the object. The temperature decreases uniformly from the hot surface to the cold surface. The direction of heat flow is always from the point with higher temperature to the point with lower temperature. The heat flowing through a flat plate per unit time is

$$\frac{Q}{t} = \frac{k A(T_2 - T_1)}{L} \quad , \tag{2-4}$$

where k is the coefficient of thermal conductivity (or simply the thermal conductivity), A is the cross-sectional area, and L is the material thickness in the direction of the heat flow. In the older literature, the symbol λ was used for the coefficient of thermal conductivity. Do not confuse this with our λ, which is wavelength.

Figure 2-5 illustrates heat conduction through a flat plate, rod, and cooling fin. The flat plate has a very large surface area and therefore heat flow is high. On the other hand, the fin has a very small edge area and heat conduction is very small (edge to edge) compared to a flat plate. A single cooling fin will not have a large temperature gradient compared to a flat plate of equal length. Clearly, a single fin is very inefficient for moving heat. Therefore thousands are often employed (e.g. car radiator). Heat flow through a rod depends upon its diameter. Thin wires do not transfer much heat.

For continuous heat flow, heat must be continually added to the hot side (T_2). Likewise, the cool side (T_1) must be attached to a heat sink. Otherwise, the flat plate or rod will reach thermal equilibrium with the environment. That is, the both reach the same temperature.

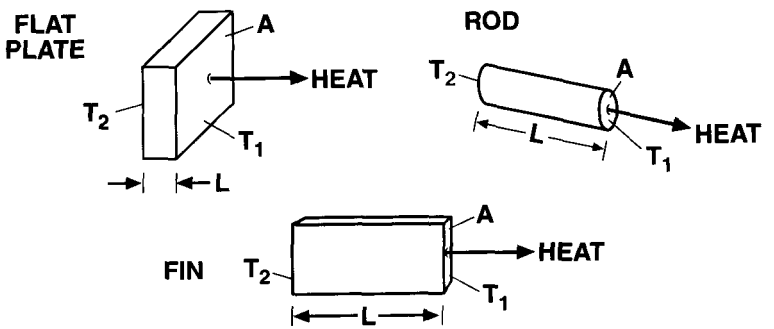


Figure 2-5. The arrow indicates the direction of heat flow. The hot side is labeled as T_2 and the cool side as T_1.

The thermal conductivity is an inherent property of the material (Table 2-3). If ***k*** is high, it is a good conductor of heat. If ***k*** is small, the material is a good insulator (does not conduct heat). A wooden building will exhibit fairly good insulation properties. On the other hand, stone structures transmit heat and therefore are very expensive to heat. To keep heating and air-conditioning bill to a minimum, it pays to use good thermal insulation. Scanning Table 2-3 suggests that air is an excellent insulator. In fact, most building insulation rely upon trapped air. Note that water has a relatively high thermal conductivity. Therefore, if the insulation gets wet, the thermal conductivity may increase 25-fold.

Table 2-3
REPRESENTATIVE THERMAL CONDUCTIVITIES
of some COMMON MATERIALS
(Values vary with composition and impurities)

	k		
Material	**kcal/(s-m-K)**	**W/(m-K)**	**BTU/(hr-ft-°F)**
Silver	0.097	406.	234.
Copper	0.092	385.	222.
Aluminum	0.049	205	118.
Brass	0.026	109.	62.9
Steel	0.012	50.2	29.0
Granite	0.00089	3.73	2.15
Ice	0.00045	1.88	1.09
Glass	0.00018	0.753	0.435
Water	0.00014	0.586	0.339
Building brick	0.00014	0.586	0.338
Oak wood	0.000043	0.181	0.105
Pine wood	0.000033	0.138	0.08
Rock wool	0.0000089	0.037	0.0215
Air	0.0000056	0.023	0.0135
Styrofoam	0.000002	0.0083	0.00483
Vacuum	"zero"	"zero"	"zero"

Styrofoam, goose down, and wool contain very many small pockets of trapped air. We take advantage of the trapped air by placing hot liquids in Styrofoam cups, using goose down comforters, and dressing "in layers."

For good insulation, we want ***Q/t*** to be small. This requires a small ***k*** and a large thickness (***L***). Construction engineers rewrite Equation 2-4 as

$$\frac{Q}{t} = \frac{(T_2 - T_1)A}{L/k} \quad . \tag{2-5}$$

The ratio L/k is the thermal resistance. When Q, t, T_2-T_1, A, and L are expressed in BTU, hours, °F, feet^2, and feet respectively, then L/k is the ***R-value***. The ***R-value*** is convenient because it expresses both thermal conductivity and thickness as a single number:

$$R-value = \frac{L}{k} = \frac{(T_2 - T_1)A}{Q/t} \quad \frac{ft^2 - hr-{}^oF}{BTU} \quad . \tag{2-6}$$

The key to insulation is to use low k value material. As k decreases, we can use thinner insulation to obtain the same ***R-value***. Table 2-4 provides the ***R-value*** for one-inch thickness materials. Commercially available products may not have the values listed in Table 2-4. Table 2-5 lists the ***R-value*** of two products used for residential insulation. Loose rock wool and fiberglass insulation are similar materials, so they both have approximately the same ***R-value*** per inch of insulation. Commercial Styrofoam insulation is clearly different than the Styrofoam listed in Table 2-4. The thermal resistance depends upon the cell size; nevertheless, trapped air provides good insulation. Figure 2-6 illustrates the effectiveness of a double-glazed window. Using the data in Table 2-4, a 1/4-inch thick glass has an ***R-value*** of 0.048. With a 1/2-inch air separation, double glazed windows increase the ***R-value*** to 4.04. A vacuum between the glass sheets would increase the ***R-value*** substantially.

Table 2-4
R-VALUE PER INCH of MATERIAL
(Calculated from data in Table 2-3)

Material	R-value/inch
Ice	0.0764
Glass	0.192
Water	0.246
Building brick	0.247
Oak wood	0.794
Pine wood	1.04
Rock wool	3.88
Air	6.17
Styrofoam	17.3
Vacuum	"infinite"

Table 2-5
TYPICAL VALUES of RESIDENTIAL INSULATION

Product	**Manufacturer**	**Standard thickness (inches)**	**Nominal *R-value***	***R-value*/ inch**
Fiberglass	Owens Corning	3.5	13	3.71
Fiberglass	Owens Corning	6.25	19	3.03
Fiberglass	Owens Corning	9.5	30	3.16
Styrofoam	Dow Chemical	0.75	3.8	5.1
Styrofoam	Dow Chemical	1.0	5.0	5.0
Styrofoam	Dow Chemical	1.5	7.5	5.0
Styrofoam	Dow Chemical	2.0	10.0	5.0

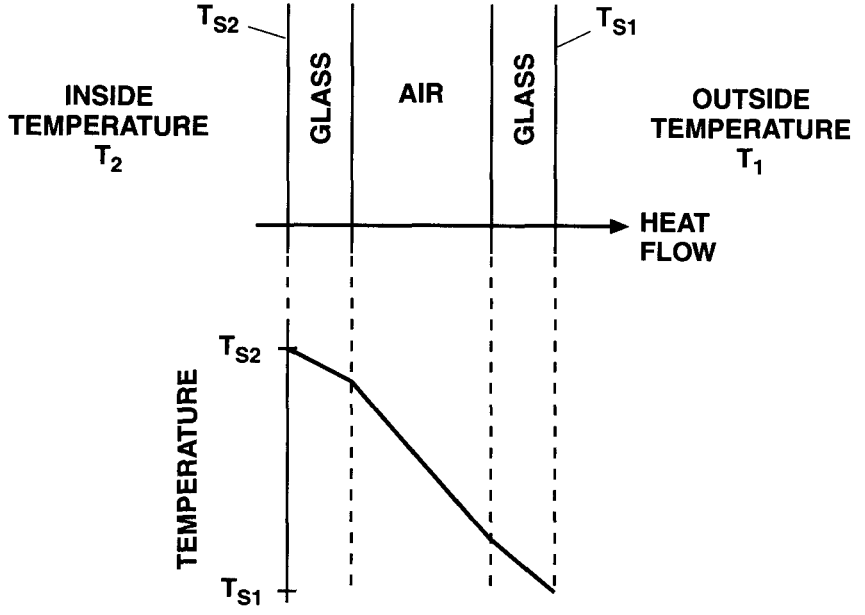


Figure 2-6. Glass has a relatively high thermal conductivity and therefore acts a poor insulator. On the other hand, air has a low thermal conductivity. If the separation between the panes is small so that convective currents are small, the heat loss through the double set of glass will be small. The glass surface temperatures, T_{S1} and T_{S2}, depend upon both convective and conductive considerations. With an ideal insulator, they will be equal to T_1 and T_2, respectively.

2.3.2. CONVECTION

Convection is the transfer of heat from one place to another by the motion of a fluid (Figures 2-7 and 2-8). The hot-air furnace and hot-water heating system are examples. If the heated fluid is forced to move by a pump or blower, the process is called forced convection. Figure 2-9 shows convective currents within a pot of water.

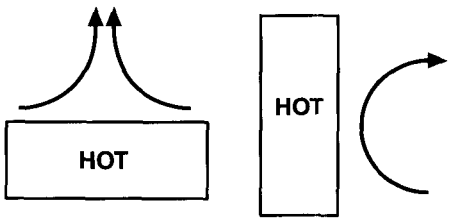


Figure 2-7. Conduction heats the air in the immediate vicinity of the hot object. Because hot air has a lower density, it will rise. This heated air is then replaced with cool air. This causes a constant motion until the heated object comes into equilibrium with the surroundings. The arrows indicate the direction of air movement.

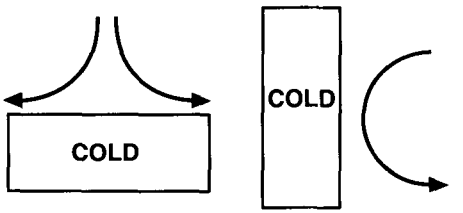


Figure 2-8. Cool air has a higher density and then drops to the ground. The arrows indicate the direction of air movement.

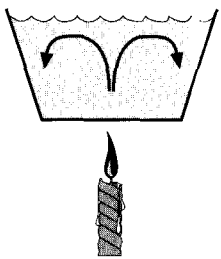


Figure 2-9. Heating water. Although convective currents are shown, conduction also occurs.

There is no simple equation for convective losses. An approximation provides

$$Q = h\,A\left(T_S - T_{AMBIENT}\right) \quad , \tag{2-7}$$

where T_S is the surface temperature and $T_{AMBIENT}$ is the fluid temperature. The value, h, is an empirical factor that depends upon a variety of factors such as the surface orientation (horizontal or vertical), fluid used, fluid speed, and surface type (e.g., plate or pipe). The variable h is also called the convective heat-transfer coefficient.

Air (indoors and outdoors), water (in cooling pipes) and oil (in transformers) are fluids that produce convective cooling. Forced cooling provides greater cooling (higher h) than static fluids. Outdoors, the wind creates forced convection. As the wind speed increases, its cooling effect increases. In cold climates, the weather bureau calls this cooling effect the wind-chill factor. Wind dramatically affects an object's temperature. This is further discussed in Section 11.3.3, *Wind*.

Kaplan[1] provides a correction factor (Table 2-6) for a temperature differential as a function of wind speed for a large vertical plate. For example, if the measured ΔT is 10°C and the wind speed is 5 m/s, the estimated temperature without wind is $\Delta T = (2.06)(10°C) = 20.6°C$. These factors are illustrated in Figure 2-10. The conversion is 1 m/s = 1.94 knots = 2.237 mph.

It should be noted that nearly all heat transfer devices eventually rely on convection. This includes automobile radiators, fins on transformers, refrigerators, and air conditioners.

Table 2-6
CORRECTION FACTORS for a VERTICAL PLATE
(From reference 1)

Wind speed				Correction factor
m/s	kph	knots	mph	
<1	<3.6	<1.9	<2.24	1.00
2	7.2	3.9	4.48	1.36
3	10.8	5.8	6.72	1.64
4	14.4	7.7	8.96	1.86
5	18.0	9.7	11.2	2.06
6	21.6	11.6	13.4	2.23
7	25.2	13.6	15.7	2.40
8	28.8	15.5	17.9	2.50

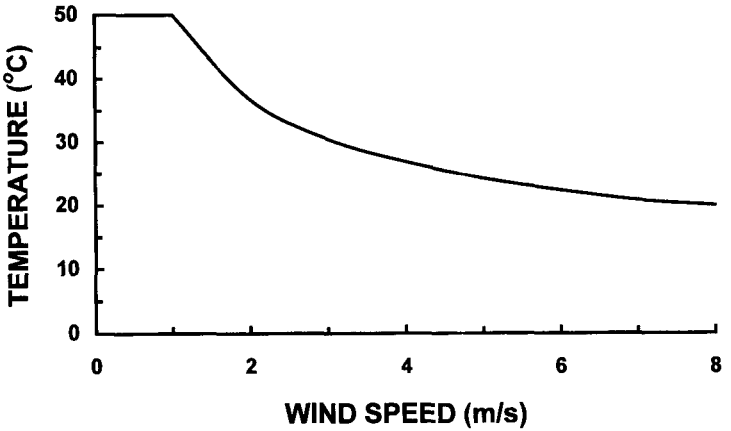


Figure 2-10. Typical decrease in temperature differential as a function of wind speed. Without wind, the ΔT of the vertical plate is 50°C. Different shaped objects (e.g., power lines) will exhibit different wind dependencies.

2.3.3. RADIATION

All objects radiate heat. The amount of heat depends upon the object's temperature and surface condition. As the object's temperature increases, the theoretical maximum radiant energy also increases.

While contact thermometers rely upon conduction, non-contact devices (e.g., optical pyrometers and thermal imaging systems) measure the radiation that appears to emanate from the object. Since radiation theory is so important in thermal imaging system operation, the following two chapters are dedicated to the subject.

Heat transfer by radiation occurs at the speed of light whereas conduction and convection depend upon the specific material involved. Radiation takes place across a vacuum whereas conduction and convection cannot. This is apparent with the sun. Space is nearly a vacuum yet we can feel the sun's heat. Similarly, the sun's radiation can pass through a glass window and we can feel the heat independent of the actual air temperature.

A thermos bottle (called a dewar in the laboratory) is an excellent example of a device that minimizes conductive, convective, and radiative losses. As illustrated in Figure 2-11, the thermos usually consists of a double-walled glass vessel. The space between the walls is evacuated to reduce both conduction and convective heat

transfer. The walls are silvered to reflect most of the radiant energy that would otherwise enter or leave the bottle. As a result, liquids will maintain their temperature for a very long time.

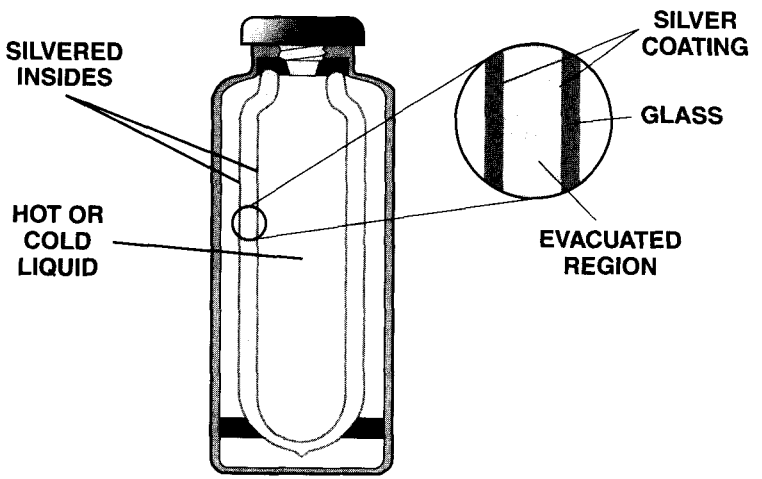


Figure 2-11. A thermos bottle (dewar).

2.4. HEAT SOURCES

Some sources are easy to quantify. The solar spectrum, energy content of fossil fuels, and calibrated blackbodies have known outputs. Other sources can only be described in qualitative terms. The heat source injects heat into an object and this raises the object's temperature. The temperature distribution determines whether an object is "healthy." Specific temperature distributions are discussed in Chapters 10 through 20.

2.4.1. SUN

The sun provides heat to the earth on a diurnal basis. The amount of heat depends upon the cloud cover and atmospheric constituents. The temperature rise of an object depends upon absorption, conduction to surrounding objects, convection (significantly increases with wind speed), and reradiation. A thermal imaging system can sense the resultant temperature created by the sun. The thermal imaging system is used to locate defective roofing (Figure 2-12), buried objects, and virtually any outdoor object.



Figure 2-12. A nighttime image of a water-laden roof. The heat capacity of water is much higher than good roofing. As a result, the water-laden areas will remain warmer (shown in white). (By courtesy of the Academy of Infrared Thermography).

2.4.2. COMBUSTION

Controlled combustion is used for heating dwellings, creating power (fossil fuel power plants), and powering engines. Since we buy energy, power plants use fuels that have a high heat of combustion (Table 2-7). Car engines combust fossil fuel to create motion. Efficient operation requires a controlled engine temperature (Figure 2-13). Proper cooling by the radiator prevents overheating that can lead to catastrophic results. Controlled heating makes our lives comfortable. Uncontrolled heating can be disastrous (Figure 2-14).

Table 2-7
APPROXIMATE HEATS OF COMBUSTION
Depends upon composition and impurities

Fuel	Approximate heat of combustion	
	MJ/m^3	BTU/ft^3
Natural gas	40-95*	1,000 - 2,500
Coal	400-500	11,000 - 14,000
Ethyl alcohol	500	14,000
Fuel oil	700	20,000

*MJ = 10^6 J

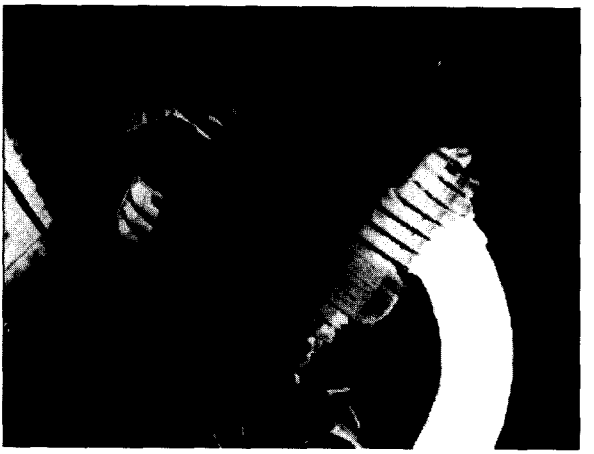


Figure 2-13. Heat is a byproduct of combustion. The exhaust pipe of this motorcycle is very hot. The cooling fins keep the cylinder much cooler than the pipe (By courtesy of the Academy of Infrared Thermography).



Figure 2-14. A forest fire. The heated smoke also radiates energy. (By courtesy of the Academy of Infrared Thermography).

2.4.3. CHEMICAL REACTION

The human body creates heat through metabolic activity. This is the basic chemical reaction of life. Figure 2-15 illustrates the surface temperature of legs. Numerous chemical reactions are used by industries to create a wide variety of products.

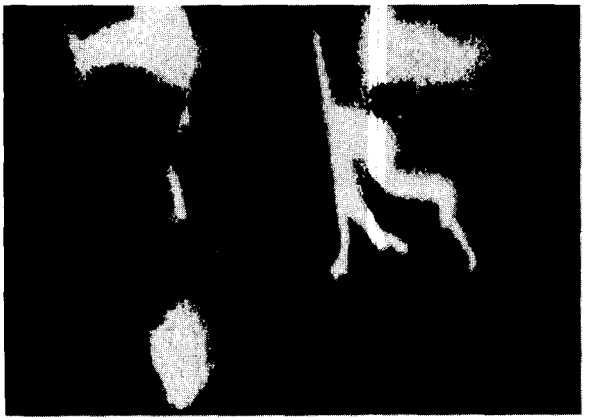


Figure 2-15. Human legs with varicose veins. The blood in the near-surface veins heats the surface more so than normal veins and arteries. Localized elevated temperatures are easier to discern when the person has been in a cool room for at least 20 minutes (By courtesy of the Academy of Infrared Thermography).

2.4.4. NUCLEAR POWER PLANT

In a nuclear power plant, the reaction creates the heat that produces steam. The steam turns the turbines that create electricity. Generally, too much heat is created and it must be dissipated to avoid melt down. A heat exchanger (forced convection) moves the heat from the reactor to cooling towers. Here evaporative cooling is used to move the heat into the atmosphere. Additional heat is removed by running cool water over a heat exchanger. A naturally occurring river typically supplies this water. This heats the river and changes the local ecosystem (Figure 2-16). The temperature distribution indicates the physical extent of the ecosystem imbalance.

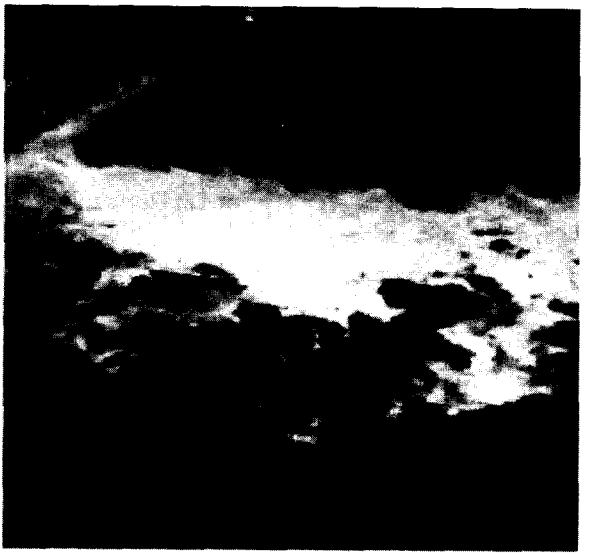


Figure 2-16. The effect of a leaking sluice gate. Heated discharge water (106°F), leaking through a sluice gate just to the right of the thermogram, is heating up the intake (cooling) water from 82°F to 88°F. (By courtesy of Richard Wurzbach).

2.4.5. ENERGY CONVERSION

HEAT TO MECHANICAL

The internal combustion engine converts heat into mechanical energy. With combustion, there is rapid expansion of gases accompanied with the release of heat. The hot gases force the cylinder to move (conversion of heat into mechanical energy) and are expelled (Figure 2-17). Excess heat is often removed from the engines by circulating water (forced convection). (See Figure 2-13 for an air-cooled engine). The hot water loses it heat to the atmosphere in the radiator – again by forced convection. The forward motion of the car and the fan creates this forced convection. Generally, the fan typically simulates forward motion of about 48 kph (30 mph). Above 48 kph, the fan looses its effectiveness.

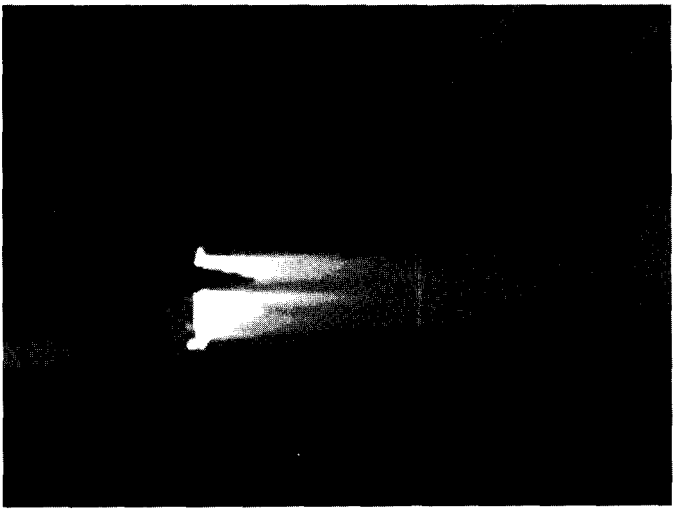


Figure 2-17. All engines have hot exhaust gases. In a jet engine, the gases force a turbine to rotate. (By courtesy of the Academy of Infrared Thermography).

FRICTIONAL HEAT

Frictional heat converts mechanical energy into heat. Bearings, gear trains, air resistance, or brakes may create it. Figures 2-18 and 2-19 illustrate two disk brakes. Abnormal heating can lead to glazing of pads, reducing the rotor alloy strength, and boiling of the brake fluid. All these can lead to brake failure.

GAS EXPANSION

Expanding gases cool the orifice through which the gas is escaping. This technique (called the Joule-Thompson effect) is used to cool the detector in some thermal imaging systems. It can also be noted with handheld propane tanks such as those used for small blowtorches. If the torch is used for an extended period, the tank will become quite cool.



Figure 2-18. Brake rotor. With a warped rotor, the brake pads only come in contact with a small portion of the rotor. This provides very localized local heating (shown in white). The air vents are easily discerned. A reflective gold mirror, placed behind the rotor, provides an image of the backside (image on left). (By courtesy of Ralph Dinwiddie).

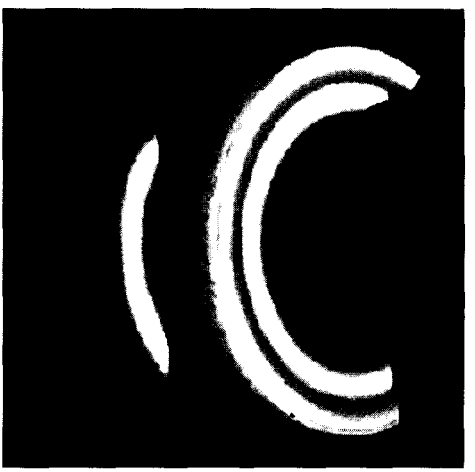


Figure 2-19. Brake rotor. Rotors often have circular gouges caused by dirt and sand. The brake pads can only contact the high areas (shown in white). (By courtesy of Ralph Dinwiddie).

MECHANICAL TO HEAT

No device is 100% efficient and heat is the usual byproduct of this inefficiency. As air is compressed, its temperature increases. This can be noted with mechanical compressors (Figure 2-20) and simple manually operated bicycle pumps.



Figure 2-20. Heat created by a compressor. Large compressors have cooling fins to dissipate the heat. (By courtesy of the Academy of Infrared Thermography).

DISSIPATION OF ELECTRICAL ENERGY

Since all electrical circuits, transformers, and components have resistance, they dissipate power:

$$P = I^2 R \text{ watts} \quad , \tag{2-8}$$

where I is the current flowing through the resistance R. Using the mechanical equivalence of heat (one watt equals 2.39×10^{-4} kcal/s) with Equation 2-2, provides the temperature rise after one second:

$$\Delta T = \frac{Q_{ELECTRICAL}}{m\,c} = 2.39 \times 10^{-4} \frac{I^2 R}{m\,c} \quad . \tag{2-9}$$

By knowing the heat capacity, mass, resistance, and current, the temperature increase can be calculated. This approach neglects all heat losses. The actual temperature will be much lower due to conduction, convection and radiation. Excessive heat buildup would indicate unexpected resistance. Excessive resistance may be due to poor connections (Figures 2-21 and 2-22), broken wires, or defective components.



Figure 2-21. A closed circuit breaker box. A defective breaker, partially broken wire, or a poor connection is dissipating electrical energy. The wire on top is heated by conduction and cools by convection. As illustrated, the wire temperature decreases from the hot defective component to ambient temperature. The defective component, which cannot be seen since the box is closed, also heats the side of the box. This image was in pseudo colors. The conversion back to black-and-white does not provide the original gray scale. The dark band around the hot (white) area is an elevated temperature. (By courtesy of the Academy of Infrared Thermography).



Figure 2-22. High resistance electrical connection between three transformers located on a pole. This is representative of a defective crimp connection. The temperature of the defect is outside the dynamic range of the camera; it is saturated. (By courtesy of the Academy of Infrared Thermography).

INDUCTION HEATING

When an electric current flows through a conductor, it creates a magnetic field. If the conductor (wire) is wound into a coil with *N* loops, the magnetic field increases *N*-fold. If the magnetic field is changing, then a current can be created in nearby components. This current is called an induced current. This is precisely the mechanism by which a transformer works (Figure 2-23). The changing current in the primary coil creates a changing magnetic field in the iron core. This changing magnetic field induces a changing current in the secondary coil.

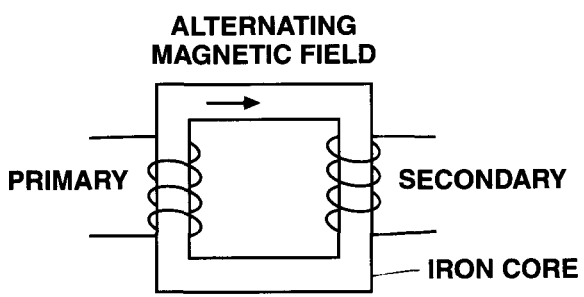


Figure 2-23. Transformer. Although most transformers have iron cores, some may have air cores. Transformer operation requires a changing magnetic field (AC circuits only).

Any ferrous metal near the magnetic field will have an induced current. Since all metals have some resistance, they will heat up. In motors, where there are a large number of loops, magnetic fields can be quite large. With this knowledge, motors are appropriately designed to minimize heat buildup. If there is a short or open in one of the windings, the magnetic field distribution changes and then motor components can heat up significantly.

2.4.6. MASS TRANSPORT

Mass transport is not a direct source of heat. Rather, it is heat transported by the movement of hot air. It is typically seen when the heated interior air seeps though cracks in the building envelope. The heated air heats the outside of the structure. We see do not see the air leakage but the effect of the air leakage (mass transport) on the surface temperature (Figure 2-24). The magnitude of the temperature seen depends upon the nature and size of the leak, pressure differential, and temperature differential.

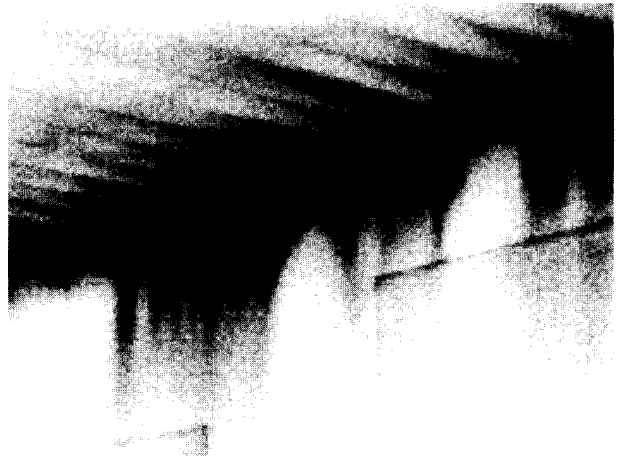


Figure 2-24. Air infiltration. The cool outside air seeped though numerous cracks at the wall-ceiling joint. The cool surfaces appear black. Heating/cooling energy costs can increase substantially with building envelope leaks. (By courtesy of the Academy of Infrared Thermography).

2.4.7. MAN-MADE

Nondestructive testing analysis often requires the injection of a known amount of heat (discussed in Chapter 19). A laser, xenon flash lamps, heat guns, or incandescent

lamps may supply this heat. Most of these sources can be well controlled and are easily characterized.

Calibrated blackbodies are used for characterizing the performance parameters of thermal imaging systems (discussed in Chapter 7). These devices can be set to a precise temperature. The radiation emanating is estimated by Planck's blackbody radiation law (discussed in next chapter).

2.5. USEFUL CONVERSIONS AND CONSTANTS

Table 2-8
CONVERSION FACTORS

Physics	Convert		Multiply by
	from	To	
Heat (*Q*)	J	Kcal	2.389×10^{-4}
	J	BTU	9.472×10^{-4}
	kcal	BTU	3.968
Specific heat (*c*)	J/(kg-K)	kcal/(kg-K)	2.389×10^{-4}
	kcal/(kg-K)	cal/(g-K)	1
	kcal/(kg-K)	BTU/(lb-°F)	1
Distance (*R*)	m	in	39.37
	m	ft	3.28
	km	mi	0.621
	km	nmi	0.54
Speed (*v*)	m/s	kph	3.6
	m/s	knots	1.94
	m/s	mph	2.237
Power (*P*)	kW	BTU/hr	3409
	kW	kcal/hr	859
	kcal/hr	BTU/hr	3.969
Conductivity (*k*)	W/(m-K)	BTU/(ft-hr-°F)	0.5778
	W/(m-K)	kcal/(m-s-K)	2.389×10^{-4}
	kcal/(s-m-K)	BTU/(ft-hr-°F)	2419
Thermal resistance (*L/k*)	$(m^2$-K)/w	$(ft^2$-hr-°F)/BTU (R-value)	5.678
	$(m^2$-K)/w	$(m^2$-s-K)/kcal	4186
	$(m^2$-s-K)/kcal	$(ft^2$-hr-°F)/BTU (R-value)	1.356×10^{-3}

If you want to convert a quantity in the **"to"** column to a quantity in the **"from"** column, then you **divide** by the constant given. For example, to convert from kcal to joules **divide** by 2.389×10^{-4}. Equivalently, multiply by $1/2.389\times10^{-4} = 4186$.

Note that 1 J = 1 w-s and 1000 cal = 1 kcal. Kelvin (K) is the SI unit of temperature. In many texts, it is replaced with degrees Celsius (°C). This does not change the conversion factors since all quantities are based on temperature change: if T_2-T_1 = 1K, then T_2-T_1 = 1°C.

CONSTANTS

Heat of vaporization for water: 539 kcal/kg
Heat of fusion for water: 79.7 kcal/kg

2.6. REFERENCES

1. H. Kaplan, *Practical Applications on Infrared Thermal Sensing and Imaging Equipment*, page 91, SPIE Press Vol. TT13, Bellingham WA (1993).

3
DETECTION OF RADIATION

The term *radiation* refers to the continual emission of energy from a surface. Since thermal imaging systems are non-contact measuring devices, they sense the radiation that appears to emanate from the surface. The emitted energy depends upon the surface temperature and surface characteristics. The camera formula describes the amount of flux impinging upon a detector. By knowing the detector's spectral responsivity, the electrical signal is determined. The electrical signal is amplified to create a visible image.

The Stefan-Boltzmann law describes the total maximum radiation that can be released from a surface. Since thermal imaging systems only respond to a small portion of the spectrum, it is necessary to introduce Planck's blackbody law. This chapter assumes that the target and its background are ideal blackbodies. Real materials are not ideal blackbodies. Their surface quality is described by their emissivities (described in the Chapter 4, *Emissivity*).

3.1. STEFAN-BOLTZMANN LAW

Agitated atoms release their energy through a radiative process. The Stefan-Boltzmann law describes the total rate of emission per unit surface area:

$$M = \sigma T^4 \quad \frac{W}{m^2} \quad , \tag{3-1}$$

where T is the absolute temperature (measured in Kelvin) and the Stefan-Boltzmann constant, σ, is 5.67×10^{-8} W/(m^2-K^4). As the energy is released, the temperature decreases. This process continues until the target reaches thermal equilibrium with its environment. At 300K (approximately 80°F) the total power is 459 W/m^2. An object at 98.6°F (310K) with 2 m^2 of surface area would radiate 2.8 kW if the environmental temperature were absolute zero (0K). The human body (at 98.6°F with 2 m^2 of skin) cannot provide 2.8 kW. It only has to provide the difference between the local environment and 98.6°F. Since our bodies only have limited resources to provide heat, we wear additional clothing as the ambient temperature drops. The effects of the environment are further described in Chapter 4, *Emissivity*.

3.1.1. GENERAL RESPONSE

In its simplest form, the detector's output voltage is

$$V_{DETECTOR} = kR_D M \tag{3-2}$$

or

$$V_{DETECTOR} = kR_D \sigma T^4 \quad , \tag{3-3}$$

where k is a constant that depends upon the specific design and R_D is the detector responsivity. Although k is used for thermal conductivity, the context is always clear when to use it as a constant. Sufficient electronic gain, G, is added to create the camera's output. The complete camera formula is provided in Chapter 6, *Camera Design*.

3.1.2. THE BACKGROUND

The environment is also radiating power. When the target reaches the same temperature as the environment, no heat transfer occurs. At thermal equilibrium, both the target and the environment are radiating the same amount of power. Targets can be "seen" only when its emitted power, M_T is different that the background power, M_B (Figure 3-1).

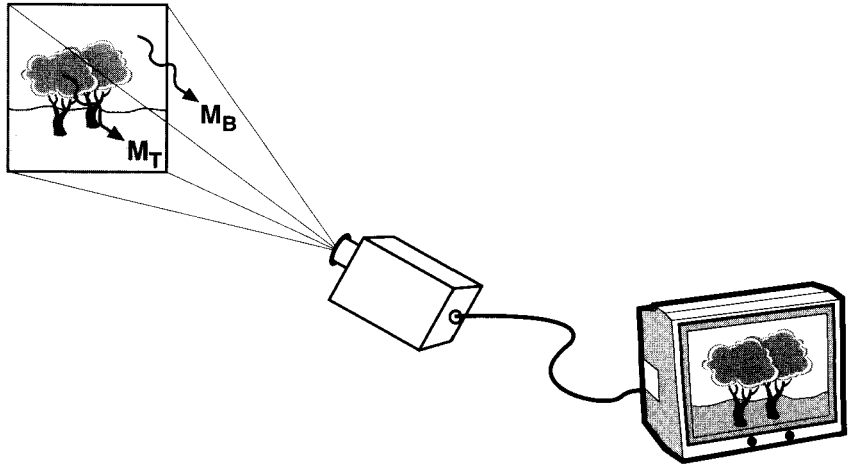


Figure 3-1. M_T must different from M_B for target detection.

If a target is warmer than its background, the power difference is

$$\Delta M = M_T - M_B \tag{3-4}$$

or

$$\Delta M = \sigma(T_T^4 - T_B^4) \quad , \tag{3-5}$$

where T_T and T_B are the target and background temperatures, respectively. While σT^4 can be large, ΔM can be quite small. A target can only be detected if the system has sufficient sensitivity to detect ΔM.

Rather than specify the target by its absolute temperature, it is convenient to specify it by its target-background difference or ΔT (pronounced *delta-T*) where $\Delta T = T_T - T_B$. Replacing T_T with $T_B + \Delta T$ provides:

$$\Delta M = \sigma\left[(T_B + \Delta T)^4 - T_B^4 \right] \quad . \tag{3-6}$$

Expanding the bracketed term provides

$$\Delta M = \sigma\left[4T_B^3 \Delta T + 6T_B^2 \Delta T^2 + 4T_B \Delta T^3 + \Delta T^4 \right] \quad . \tag{3-7}$$

If ΔT is small, then we can neglect all terms except the first one:

$$\Delta M \approx 4\sigma T_B^3 \Delta T \quad . \tag{3-8}$$

Figure 3-2 illustrates ΔM as a function of T_B for a target whose ΔT is one degree. Note that ΔM is proportional to the cube of T_B. When specifying a target by its ΔT, it is necessary to specify the background temperature. Although ΔT is fixed, ΔM depends upon where ΔT is defined (Figure 3-3 and Table 3-1).

When viewing a target against a background, the differential detector voltage is

$$\Delta V_{DETECTOR} = kR_D \Delta M \approx 4kR_D \sigma T_B^3 \Delta T \quad . \tag{3-9}$$

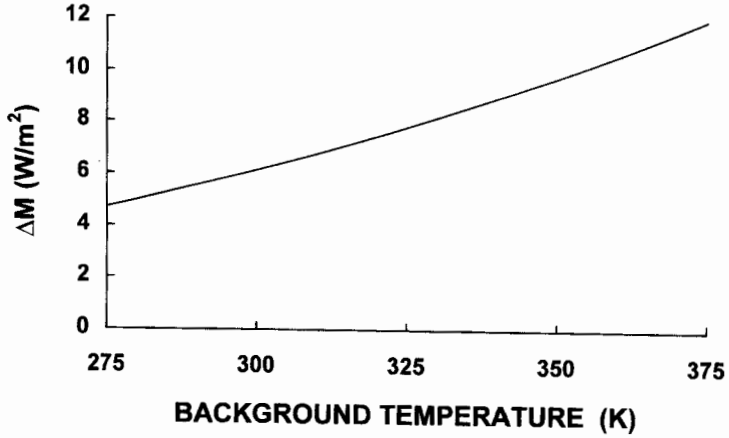


Figure 3-2. ΔM as a function of T_B. The target ΔT is one degree.

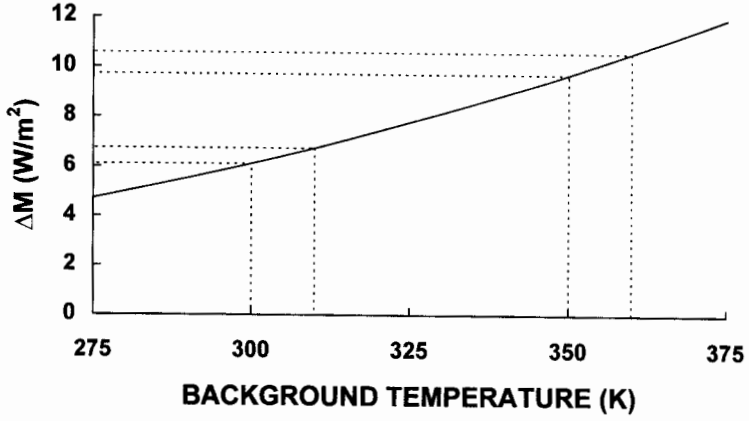


Figure 3-3. ΔM as a function of T_B. As the background temperature changes (fixed ΔT), ΔM changes. The differences in ΔM are shown for $\Delta T = 10$K.

Table 3-1
ΔM for various background temperatures ($\Delta T = 10$K)

Temperature range	ΔM (W/m²)
280-290	0.553
300-310	0.633
320-330	0.719
340-350	0.810

3.2. PLANCK'S BLACKBODY LAW

The spectral radiant exitance of an ideal blackbody can be described by Planck's blackbody radiation law:

$$M(\lambda,T) = \frac{c_1}{\lambda^5}\left(\frac{1}{e^{(c_2/\lambda T)} - 1}\right) \quad \frac{W}{m^2 - \mu m} \quad , \qquad (3\text{-}10)$$

where the first radiation constant, c_1, is 3.7411×10^8 W-μm^4/m^2, the second radiation constant, c_2, is 1.4388×10^4 μm-K, and λ is the wavelength expressed in micrometers. The value $M(\lambda,T)$ is the power density at wavelength λ. As the temperature increases, $M(\lambda,T)$ increases. The value T is also called the color temperature. Figure 3-4 illustrates Planck's spectral exitance in logarithmic coordinates. Each curve has a maximum at λ_{PEAK}. Wien's displacement law provides $\lambda_{PEAK} = 2898/T$ μm. Since a photodetector responds linearly to the available power, linear coordinates may provide an easier representation to interpret (Figure 3-5).

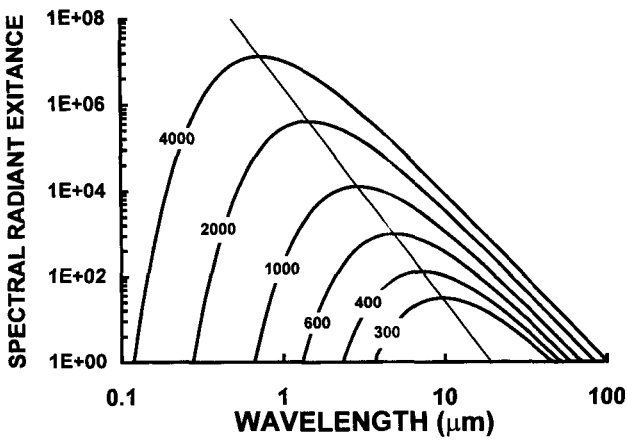


Figure 3-4. Planck's spectral exitance plotted in logarithmic coordinates for various absolute temperatures. The units of spectral radiant exitance are W/(m^2-μm). The light line is Wien's law.

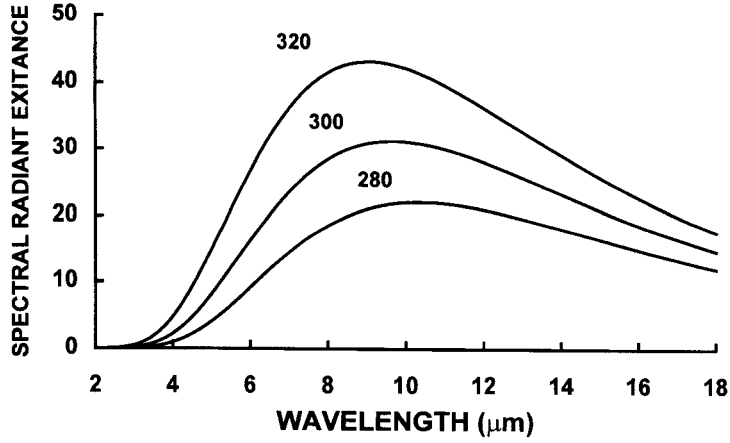


Figure 3-5. Planck's spectral exitance plotted in linear coordinates for three different absolute temperatures. The units of the spectral radiant exitance are W/(m^2-μm).

Another feature of blackbody radiation is that the curves do not cross. If we monitor the light intensity of at a specific wavelength, then we can uniquely determine the temperature. This fact is used in optical pyrometers.

As the temperature increases, the rate of emission increases very rapidly. At 300K, nearly all the radiation is in the infrared. When the temperature reaches approximately 600K, the target starts to glow (visibly discernible). We call this heated to incandescence. As the temperature increases even more, more visible light is present. Consider an incandescent lamp that is attached to a dimmer switch. When the switch is off, the light appears "off" to our eyes even though it is radiating at approximately 300K. Our eyes are not sensitive to infrared radiation. When the dimmer is set low, the bulb barely glows: It appears as a dull red. As the dimmer voltage is increased, the color changes to an orange and then a yellow. At higher voltages, the filament produces more blue and the light *appears* white (Figure 3-6).

Since our eyes are photon detectors, the photon flux is plotted rather than the power. The photon flux is related to the power by λ/hc, where h is Planck's constant (6.626×10^{-34} J-s) and c is the speed of light (3×10^{8} m/s). Although c is also used for the specific heat, the context always is clear when it means the speed of light.

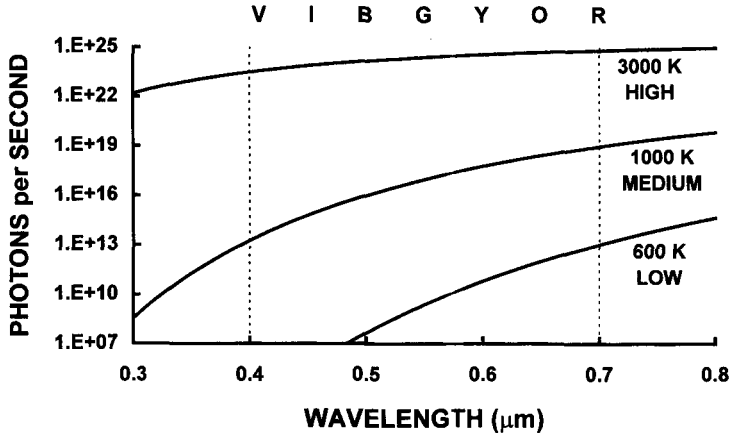


Figure 3-6. Spectral output of an ideal incandescent bulb. A typical, fully powered, 100-watt incandescent bulb has a color temperature of 3000K. At low voltages, the bulb appears to be dull red (T = 600K). At moderate voltages, the bulb is yellow (T = 1000K). Our eyes are sensitive to radiation whose wavelengths fall between 0.4 and 0.7 μm. The letters refer to violet, indigo, blue, green, yellow, orange, and red.

Another example of changing color temperature exists when we heat a metal nail with a propane torch. Initially, the nail appears as a piece of metal even though it is radiating at 300K. The nail color is due to the reflection of room lights. Our ability to see the nail requires a different reflectivity between the nail and its background. The nail must be held with pliers, remembering that metal is a good conductor of heat. Since the propane torch reaches about 2200K, the nail can only be heated to 2200K.

Referring to Planck's curves, we see that a 2200K-blackbody source does not have much blue and therefore, the heated portion will appear orange. Due to conduction, heat flows down the nail and into the pliers (the pliers get hot also). Since the pliers are relatively cool, a temperature gradient exists within the nail. Careful examination reveals a changing color temperature from orange to dull red as you view the nail portion within the flame down to the pliers. When the temperature drops to 600K, the nail no longer glows. Just because it is not glowing does not mean that you cannot get a nasty burn.

When $M(\lambda,T)$ is summed over all wavelengths, the Stefan-Boltzmann law is obtained. Summing is written symbolically as an integral:

$$M = \int_0^\infty M(\lambda, T)\, d\lambda = \sigma T^4 . \qquad (3\text{-}11)$$

It is simply the area under the curve as illustrated in Figure 3-7. Most detectors sense radiation from a specific wavelength region. The total power density in an interval from λ_1 to λ_2 is the area under the curve (Figure 3-8). It is represented mathematically by

$$M(\Delta\lambda, T) = \int_{\lambda_1}^{\lambda_2} M(\lambda, T)\, d\lambda \quad , \tag{3-12}$$

where $\Delta\lambda = \lambda_2 - \lambda_1$. For many applications, the target temperature is near ambient ($T \approx 300$K). As illustrated in Figure 3-8, more power is available in the LWIR region when $T \approx 300$K. This would initially suggest that a LWIR system is ideal. However, what is important is the signal-to-noise ratio. By lowering the noise, the MWIR systems can provide excellent imagery. As the temperature increases (see Figure 3-4), the power in the MWIR region increases rapidly. This suggests that a MWIR system is desirable when viewing hot sources. Regardless of the target temperature, the signal-to-noise ratio must be high to create good imagery.

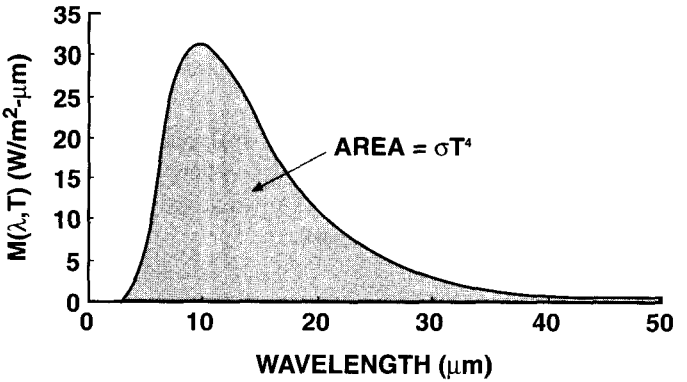


Figure 3-7. The area under Planck's radiation law is equal to the Stefan-Boltzmann relationship. The target temperature is 300K.

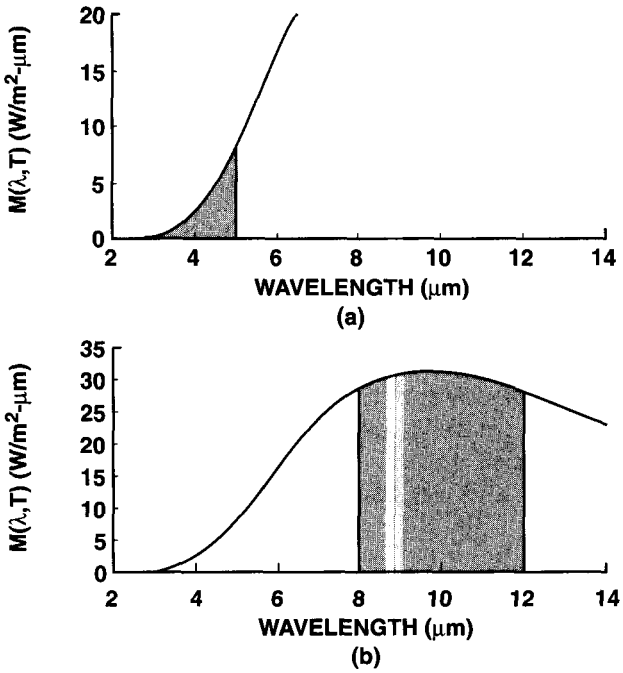


Figure 3-8. Detectors respond to only a small portion of the total power available (shaded area). (a) MWIR system (3 to 5 μm) and (b) LWIR system (8 to 12 μm). The target temperature is 300K. Note the difference in vertical scales.

3.2.1. GENERAL RESPONSE

Since detectors are sensitive to only certain wavelengths, Planck's blackbody radiation law is used in conjunction with the detector spectral responsivity. The output voltage at a specific wavelength is

$$V_{DETECTOR}(\lambda) = kR_D(\lambda)M(\lambda, T) \quad . \tag{3-13}$$

Finally, the sum of all the outputs due to the various wavelengths must be added together. This is represented by an integral:

$$V_{DETECTOR} = \int_{\lambda_1}^{\lambda_2} V_{DETECTOR}(\lambda)\, d\lambda \tag{3-14}$$

and it is the area under the curve in the wavelength interval from λ_1 to λ_2. This integral is illustrated in Figure 3-9.

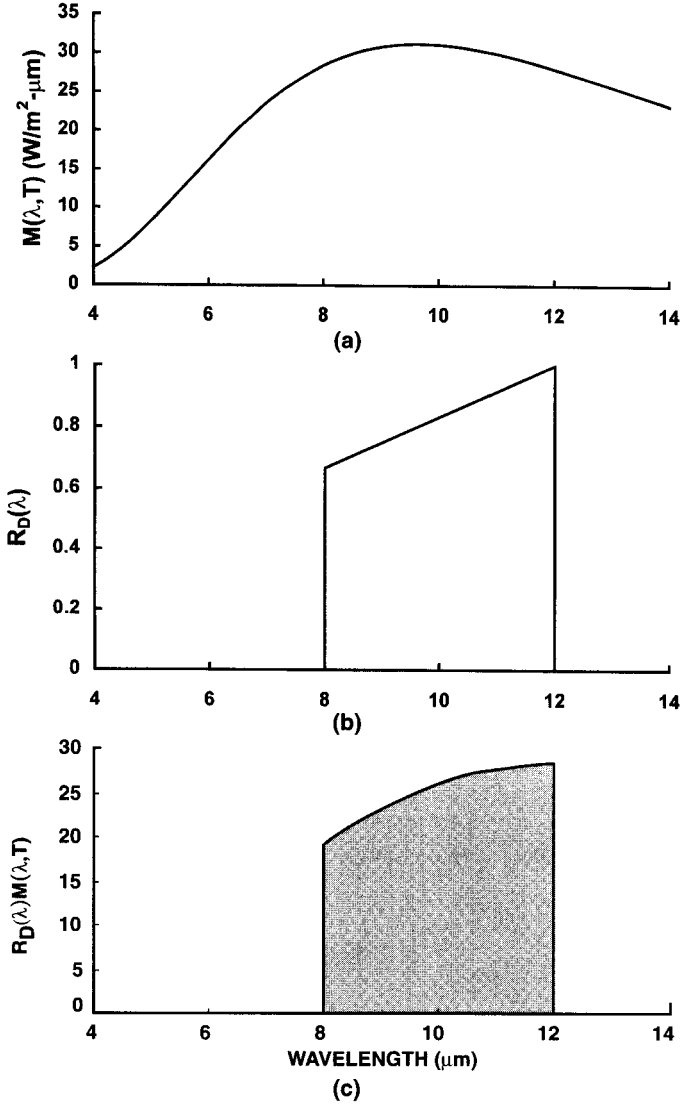


Figure 3-9. Graphical representation of Equation 3-14. (a) Available power $M(\lambda,T)$ when T = 300K. (b) Typical spectral response of a LWIR detector. (c) Product of $M(\lambda,T)$ and $R_D(\lambda)$. The detector output is proportional to the area under this curve.

3.2.2. THE BACKGROUND

Detectors are sensitive to a limited spectral range. The spectral difference between a target and its background is

$$\Delta M(\lambda,\Delta T) = M(\lambda, T_T) - M(\lambda, T_B) \tag{3-15}$$

or

$$\Delta M(\lambda,\Delta T) = \frac{c_1}{\lambda^5}\left(\frac{1}{e^{c_2/\lambda T_T}-1}\right) - \frac{c_1}{\lambda^5}\left(\frac{1}{e^{c_2/\lambda T_B}-1}\right) . \tag{3-16}$$

The total power over a limited spectral range is

$$\Delta M(\lambda,\Delta T) = \int_{\lambda_1}^{\lambda_2}\frac{c_1}{\lambda^5}\left(\frac{1}{e^{c_2/\lambda T_T}-1}\right) d\lambda - \int_{\lambda_1}^{\lambda_2}\frac{c_1}{\lambda^5}\left(\frac{1}{e^{c_2/\lambda T_B}-1}\right) d\lambda \tag{3-17}$$

For small ΔTs, we express the target as a small increment above the background or

$$\Delta M(\lambda,\Delta T) = M(\lambda, T_B+\Delta T) - M(\lambda, T_B) . \tag{3-18}$$

For small ΔTs, we can expand the right side of the equation into a Taylor's series. If ΔT is sufficiently small, we keep only the first term of the series:

$$\Delta M(\lambda,\Delta T) \approx \left[\frac{\partial M(\lambda, T_B)}{\partial T}\right]\Delta T . \tag{3-19}$$

The bracketed term is called the thermal derivative. It is the partial derivative of Planck's law with respect to temperature:

$$\frac{\partial M(\lambda, T_B)}{\partial T} = M(\lambda, T_B)\ \frac{c_2 e^{c_2/\lambda T_B}}{\lambda T_B^2 (e^{c_2/\lambda T_B}-1)} . \tag{3-20}$$

Note that the thermal derivative must be evaluated at the background temperature (Figure 3-10). This again illustrates that if a target is specified by a temperature differential, then the background temperature must be stated. Instead of using Equation 3-17, the total power is approximately

$$\Delta M(\lambda,\Delta T) \approx \left[\int_{\lambda_1}^{\lambda_2}\frac{\partial M(\lambda, T_B)}{\partial T} d\lambda\right]\Delta T . \tag{3-21}$$

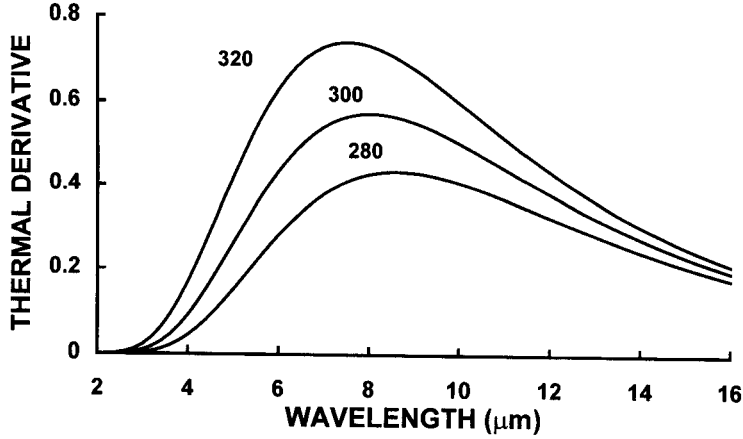


Figure 3-10. Thermal derivative of Planck's blackbody radiation law for three different background temperatures. It is a function of wavelength and background temperature. The thermal derivative has units of W/(m^2-μm-K).

For small ΔTs, the differential detector output is

$$\Delta V_{DETECTOR} = k \int_{\lambda_1}^{\lambda_2} R_D(\lambda)\, \Delta M(\lambda, \Delta T)\, d\lambda \qquad (3\text{-}22)$$

or

$$\Delta V_{DETECTOR} = \left[k \int_{\lambda_1}^{\lambda_2} R_D(\lambda) \frac{\partial M(\lambda, T_B)}{\partial T}\, d\lambda \right] \Delta T \quad . \qquad (3\text{-}23)$$

Since the thermal derivative is a function of the background (ambient) temperature, the differential output voltage also depends upon the background temperature.

Since $M(\lambda, \Delta T)$ can be quite small, the camera must provide sufficient gain so that $\Delta V_{DETECTOR}$ is measurable. This is the fundamental limit of the camera. When $\Delta V_{DETECTOR}$ is below the camera's noise level, then ΔT cannot be measured. This limit on ΔT is called the noise equivalent temperature difference or NEDT. The NEDT is discussed in Chapter 7, *Performance Parameters*.

4

EMISSIVITY

Most objects do not emit all the radiation described by Planck's law. They only emit a fraction of it. This fraction is called the emissivity:

$$\varepsilon = \frac{M_{ACTUAL}}{M_{BLACKBODY}} \quad . \tag{4-1}$$

The emissivity may vary with wavelength, the object's shape, temperature, surface quality, and viewing angle. While it is instructive to study the emissivity of specific targets, the radiation measured depends upon the target and its environment. Target signatures are affected by the environment (described in Chapter 11, *Target Signatures*). When the emissivity is not known, it is convenient to assign an apparent temperature to the target (described in Chapter 18, *Surveillance*).

4.1. CONSERVATION OF ENERGY

When radiation is incident on an object, some of it is transmitted, some absorbed, and some is reflected. Energy conservation requires that the total flux (measured in watts) be constant:

$$\Phi_{TRANSMITTED} + \Phi_{ABSORBED} + \Phi_{REFLECTED} = \Phi_{INCIDENT} \quad . \tag{4-2}$$

Expressed as a ratio,

$$\tau + \alpha + \rho = 1 \quad , \tag{4-3}$$

where τ, α, and ρ are the transmittance, absorptance, and reflectance, respectively (Figure 4-1). Each value can vary between zero and one but the sum must be unity. Most targets are opaque and the transmittance is zero ($\tau = 0$). Then

$$\alpha + \rho = 1 \quad . \tag{4-4}$$

The emiss*ivity*, reflect*ivity*, and absorpt*ivity* are properties of ideal materials. Real world materials have defects, surface irregularities, and may contain a variety of trace materials. Real materials are characterized by emitt*ance*, reflect*ance*, and absorpt*ance*. Unfortunately, the infrared community indiscriminately mixes emissivity

with emittance. Since emissivity is used more often, this book will use emissivity for real materials.

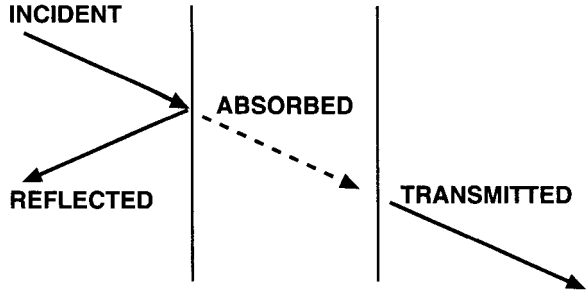


Figure 4-1. Conservation of energy

4.2. TARGET EMISSIVITY

When averaged over all wavelengths, the total power density is

$$M = \varepsilon \sigma T^4 \quad . \tag{4-5}$$

However, a target cannot be studied in isolation. The environment is also emitting radiation (Figure 4-2). When an object is in thermal equilibrium with its environment, the amount of energy absorbed must equal the amount radiated. Otherwise, the object would either heat up or cool down. Thus, the absorptance must be equal to the emissivity

$$\alpha = \varepsilon \quad . \tag{4-6}$$

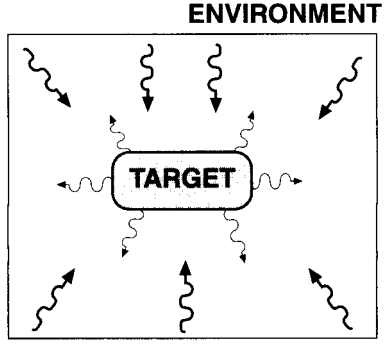


Figure 4-2. An object's temperature is influenced its environment.

This leads to the popular saying "Good absorbers are good emitters." Similarly, a poor absorber is a poor emitter. For opaque objects ($\tau = 0$),

$$\varepsilon + \rho = 1 \quad . \tag{4-7}$$

A poor absorber must be a good reflector.

The best emitter will be that surface which is the best absorber. Such a surface will not reflect any radiation and appear black in color (provided that its temperature is not so high that it is self-luminous). In general, the emissivity is higher for rough surfaces and smaller for smooth polished surfaces. The emissivity for ideal blackbodies is unity and zero for perfectly reflective surfaces. Figure 4-3 illustrates the emissivities of some common materials.

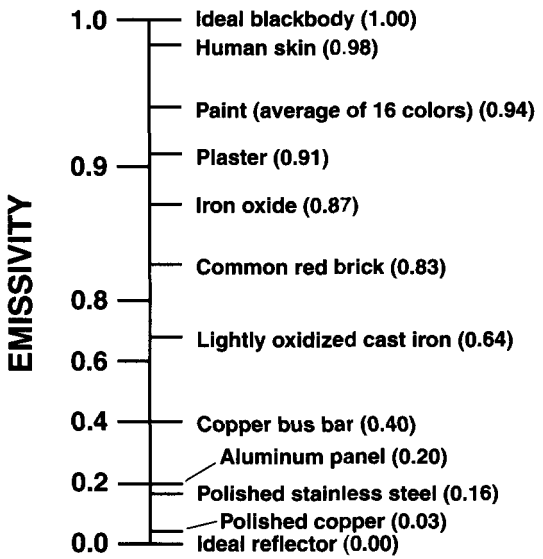


Figure 4-3. Representative emissivities. Note the expanded scale from 0.8 to 1.0. Reflectors have emissivities less than 0.2 and absorbers have emissivities greater than 0.8.

Unfortunately, the reflectance (and hence emissivity) is a function of viewing angle. In general, as the viewing angle increases from normality, the reflectance increases. This can be experienced while driving. When looking at the road at a grazing angle (viewing angle near 90°), the road appears reflective even if it is made of asphalt. As an example, Figure 4-4 illustrates the reflectance of glass as a function of viewing angle.

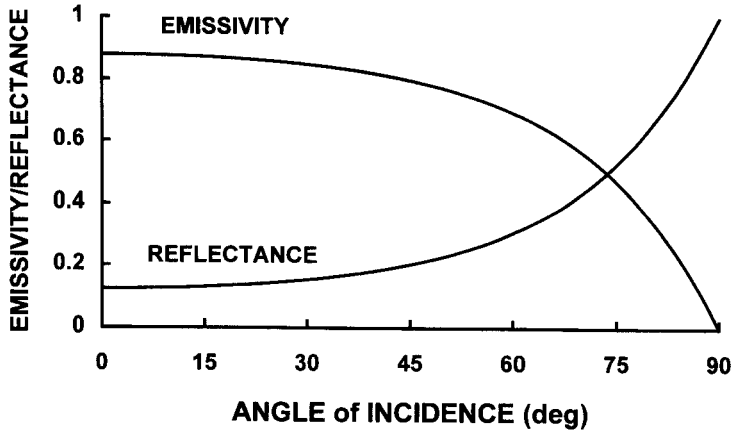


Figure 4-4. Average LWIR reflectance and emissivity of glass as a function of viewing angle. The glass transmittance is assumed to be zero (valid for the LWIR region).

4.3. SURFACE CONDITIONS

The emissivity depends upon surface properties, geometrical shape, and environmental factors. These include age of paint, type of paint, dust, dirt, and condensation. For example, the emissivity of copper varies from 0.03 for a clean polished surface to 0.80 for a heavily oxidized surface. Similar variations are seen with other metals like cast iron, aluminum, and steel. Although typical emissivity values are tabulated (see Appendix B), the material being tested should be measured.

4.4. ENVIRONMENTAL EFFECTS

As a non-contact measuring device, the thermal imaging system cannot separate the emitted radiation from the reflected radiation. The radiation that appears to emanate from the surface must include the power reflected from the surroundings (Figure 4-5).

Using the Stefan-Boltzmann law, the total power emanating from an opaque object is

$$M = \varepsilon\sigma T_T^4 + \rho\sigma T_S^4 \quad , \tag{4-8}$$

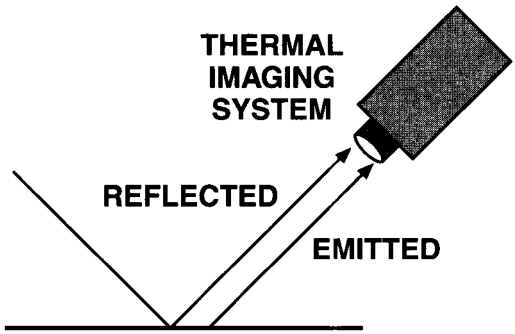


Figure 4-5. A thermal imaging system can only measure radiation. The system cannot separate emitted radiation from the reflected radiation.

where T_S is the effective temperature of the surroundings. This, of course, could be written as

$$M = \varepsilon\sigma T_T^4 + (1-\varepsilon)\sigma T_S^4 \quad . \tag{4-9}$$

It is impossible to measure the ambient radiation that comes from all the surrounding objects. Each is different in shape, distance, orientation, emissivity, and temperature. Rather all the radiation is lumped together and regarded as an equivalent radiation from a blackbody at temperature T_S. The effect of the changing environment is described in Chapter 12, *Temperature Measurements*.

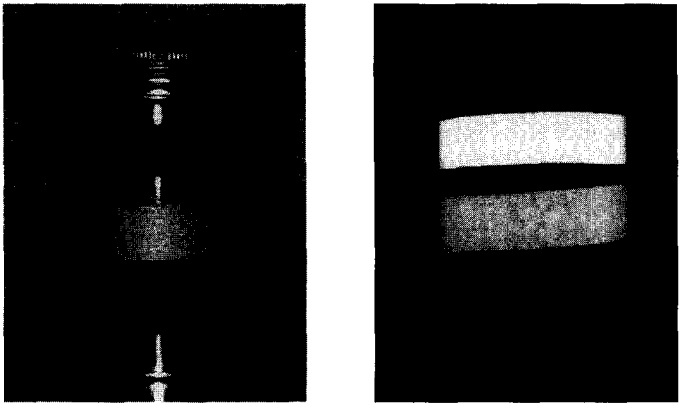
The total radiation can be equated to an apparent temperature

$$M = \sigma T_{APPARENT}^4 = \varepsilon\sigma T_T^4 + \rho\sigma T_S^4 \quad , \tag{4-10}$$

and then

$$T_{APPARENT} = \left(\varepsilon T_T^4 + \rho T_S^4\right)^{1/4} \quad . \tag{4-11}$$

As $\varepsilon \rightarrow 1$, $T_{APPARENT} \rightarrow T_T$. As $\varepsilon \rightarrow 0$, $T_{APPARENT} \rightarrow T_S$. Figure 4-6 illustrates the effect of various emissivities. The can appears to have the same temperature as the surroundings since ε_{CAN} is small (equivalently, ρ_{CAN} is large).



VISIBLE **THERMOGRAM**
(a) **(b)**

Figure 4-6. Thermogram illustrating the effects of different emissivities. (a) Visual image of a bare-metal can filled with warm water. The top tape is black electrician's tape, the middle is masking tape, and the bottom is Mylar packaging tape. Each tape has a different emissivity. (b) Since the can has high reflectivity, its apparent temperature is influenced by the surroundings. The black electrician's tape has near unity emissivity and its apparent temperature is nearly equal to the water temperature. It is difficult to obtain precisely the same view of an object with two, significantly different, cameras. (By courtesy of IRcameras.com)

4.5. GEOMETRIC FACTORS

Each time a light beam is reflected, its intensity is reduced by the surface reflectance. If the beam is reflected N times, the resultant intensity is

$$I = I_o \rho^N \quad , \tag{4-12}$$

where I_o is the initial intensity. Multiple reflections have a dramatic effect on the reflected intensity. If $\rho = 0.9$ (a highly reflective surface) and the beam is reflected 10 times, the intensity is reduced to 0.349. If the number of reflections increases to 50, the intensity becomes 0.0052. Equivalently, the effective emissivity approached unity. If a highly emissive paint is used ($\varepsilon = 0.9$ or equivalently $\rho = 0.1$) then after 10 reflections, the reflected power is reduced to an infinitesimal 10^{-10}.

This fact is used in the design of blackbody calibration sources. Years ago, all blackbodies were cone-shaped (Figure 4-7). The cone angle was selected to increase the number of reflections. This insures a uniform temperature within the cone and the cone appears to have an effective emissivity of unity (ideal blackbody). Today, many calibration sources have a flat surface. They are painted with high emissivity paint. Many paints have embedded filaments that upon drying, produce a very diffuse surface. Diffuse surfaces may be considered to consist of numerous, randomly located, microcavities.

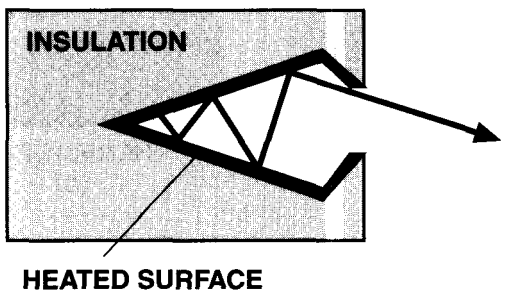


Figure 4-7. A traditional blackbody. The cavity is cone-shaped to increase multiple reflections.

To illustrate this effect, consider a polished aluminum box ($\varepsilon = 0.1$). If viewing the surface, both the target and surroundings contribute to the measured radiation (Figure 4-8a). When the emissivity is low, the reflected radiation can easily exceed the emitted radiation. Now remove one side and view the same surface. The wall temperature becomes part of the surrounding temperature (Figure 4-8b). Finally consider the same box but with a hole drilled in the side (Figure 4-8c). Now the local surrounding temperature is identical to the wall temperature and the measured radiation appears as if it came from an ideal blackbody. The threads of the screw top on the can illustrated in Figure 4-6 form a wedge that acts like a cavity. As a result, the threaded area appears warmer than the rest of the top.

Equivalently, the received radiation is

$$M = \varepsilon\sigma T_T^4 + (1-\varepsilon)\sigma T_S^4 \quad . \tag{4-13}$$

As the number of reflections increase, it simply means that the surrounding temperature is slowly reaching the target temperature. As $T_S \rightarrow T_T$,

$$M \rightarrow \sigma T_T^4 \quad . \tag{4-14}$$

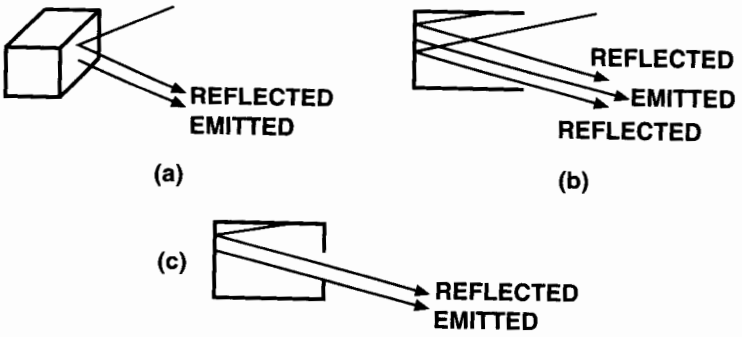


Figure 4-8. The apparent emissivity depends upon the target geometry. (a) Polished aluminum box. (b) Top view of box with one side removed, and (c) the same surface viewed though a small hole.

The same effect can be seen visually when viewing a stack of razor blades. When viewed from the side, they appear shiny and reflect light. When the edges are viewed, the area appears nearly black because of the multiple reflections (Figure 4-9).

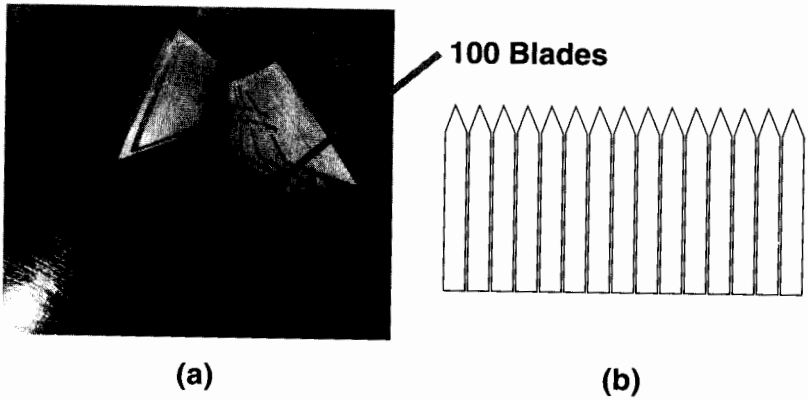


Figure 4-9. A stack of 100 utility knife blades. (a) Photograph and (b) cross sectional view. Adjoining edges create a cavity similar to that shown in Figure 4-7. As a result, the edges appear black. Careful examination reveals reflections from dust particles and damaged edges.

4.6. SPECTRAL DEPENDENCE

It was tacitly assumed in the above equations that the transmittance, absorptance, and reflectance are a constant value for all wavelengths. Objects that have a constant emissivity are called gray bodies. This may not always be the case. Selective radiators will have an emissivity that varies with wavelength (Figure 4-10). At each wavelength,

$$\tau(\lambda) + \alpha(\lambda) + \rho(\lambda) = 1 \quad . \tag{4-15}$$

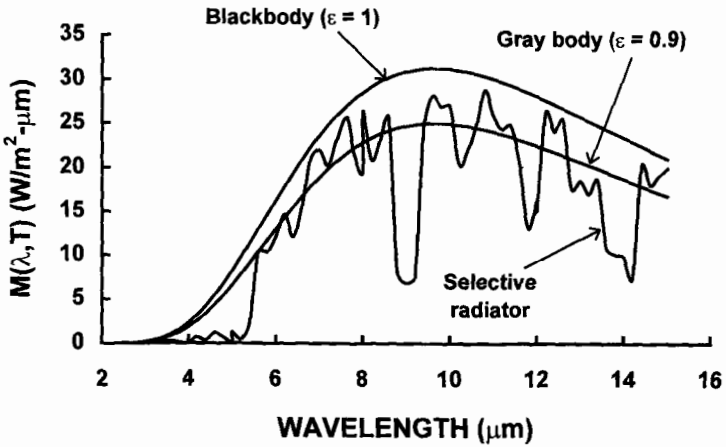


Figure 4-10. The emitted power density depends upon the emissivity.

Many materials, such as glass, are transparent in the visible but opaque in the infrared. Other objects that appear opaque in the visible may be quite transparent in the infrared. Black plastic is an example. It is quite easy to see the contents of a black plastic shopping bag with a thermal imaging system. To further illustrate spectral properties, many infrared lens materials are opaque in the visible. Germanium, which is used almost exclusively as LWIR optics, is opaque in the visible spectrum.

With semi-transparent materials, measurements are further complicated because the objects behind the material also contribute to the measured radiation. To measure the temperature (discussed in Chapter 12, *Temperature Measurements*) of these materials it is necessary to select a wavelength when the transmittance is zero. This requires filtering the thermal imaging systems so that it is responsive only in the region where the transmittance is zero.

Figure 4-11 illustrates the spectral transmittance of glass. The thickness of typical household bulbs is about 0.025 inch (0.625 mm). If attempting to measure the envelope of a household light bulb, it is necessary to select a system whose spectral response is greater than about 4.8 μm.[1] Below this wavelength, the heated filament will become visible. It would appear that a LWIR system would work well. However, the reflectance increases in the LWIR (Figure 4-12). While the LWIR could be used for temperature measurements, the reflectance means that a correction factor must be used to make an accurate temperature measurement. To avoid correction factors, it would be best to use an imaging system whose spectral response lies between 4.8 and 5.5 μm. For thick glass, the emissivity is unity in this region.

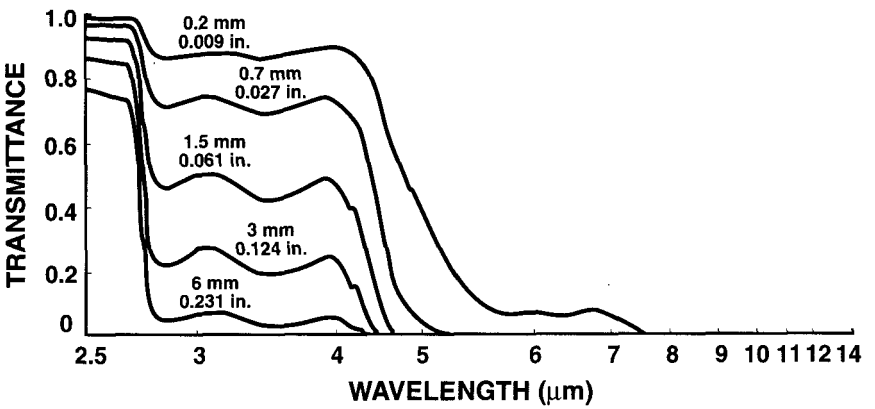


Figure 4-11. Spectral transmittance of glass. Note the nonlinear wavelength scale (From reference 1).

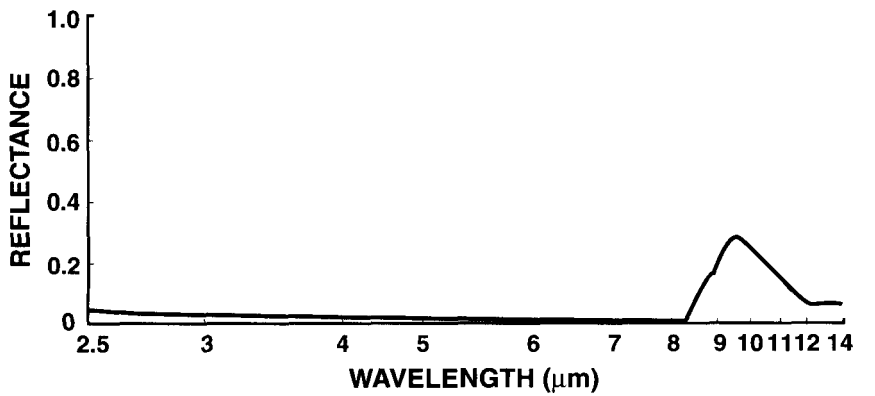


Figure 4-12. Spectral reflectance of glass. Note the nonlinear wavelength scale (From reference 1).

The military has been using LWIR systems routinely. Since glass is opaque in this region, occupants of vehicles cannot be seen. However, if the military used a MWIR system whose response was below 4 μm, then occupants could be detected. Figures 4-11 and 4-12 also explain why eyeglasses appear dark when viewed with a LWIR system. They are radiating at ambient temperature (typically 70°F or 21°C) while the face is emitting at 98.6°F (37°C).

Many semi-transparent materials have a spectrally varying emissivity. While measurements could be at any wavelength band, the energy transmitted through the material confounds temperature measurements. Therefore, if a spectral region can be found where the transmittance is zero, it is possible to make accurate temperature measurements. Figure 4-13 illustrates the transmittance of a 0.75-mil thick Mylar polyester film. When the transmittance is zero (at 7.9 μm), the measured radiation is due to emitted and reflected radiation only. At 7.9 μm, the emissivity is about 0.96 so that the reflected radiation is minimal. Thus, a filtered infrared imaging system whose spectral response is limited to a small spectral band about 5.8, 7.9, or 9.0 μm can accurately measure the Mylar temperature. Other plastics exhibit spectrally varying transmittances. For example, polyethylene has a strong absorption at 3.45 μm. Careful selection of filters can lead to accurate temperature measurements.

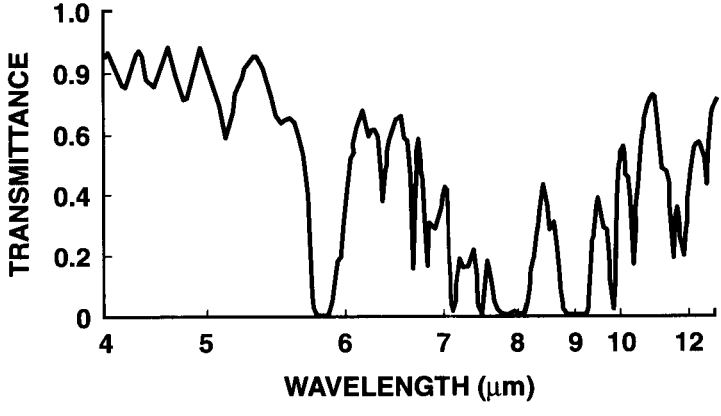


Figure 4-13. Spectral transmittance of a Mylar polyester film. The film thickness is 0.75 mil (0.00075 inches). Temperature measurements can be made at various spectral bands. The most popular band is centered at 7.9 μm. Note the nonlinear wavelength scale.

At times, it may be necessary to look though an obscurant to measure the temperature of an object. This is the case with furnaces where the flame blocks the wall of the furnace. With clean combustion (as with natural gas fuel), the byproducts are water vapor (H_2O) and carbon dioxide (CO_2). These very hot combustion products emit significant radiation. Each byproduct has its own spectrally varying transmittance. Fortunately, the combination is nearly transparent at 3.9 μm (Figure 4-14). By using a flame filter, it is possible to accurately measure the furnace walls. This filter limits the infrared imaging system spectral response to a small band around 3.9 μm. Although called a *flame filter*, it allows you to look through the flame and see the walls.

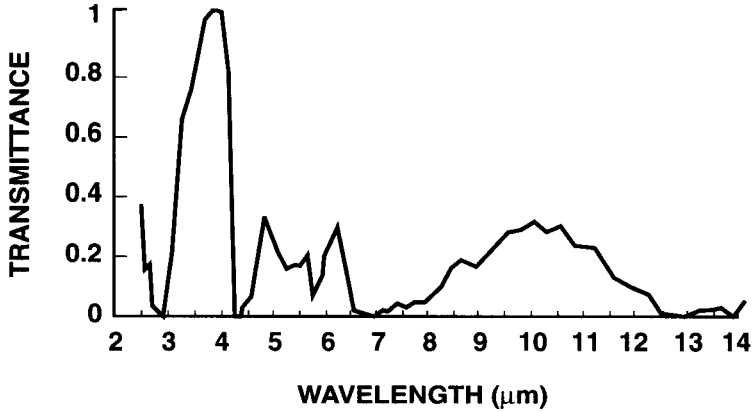


Figure 4-14. Spectral transmittance of a gas flame.

By examining the spectral absorptance, it is possible to test for the presence of a variety of gas plumes. For example, exhaled air is rich with CO_2. Carbon dioxide has a highly absorbent (and hence has a high emissivity) at 4.3 μm. By selecting a narrow band filter about 4.3 μm, it is possible to detect heated breath. Note that the atmospheric transmittance must be high at the selected wavelengths (described in Chapter 5, *Atmospheric Transmittance*). The atmosphere also contains CO_2 and attenuates all radiation centered about 4.3 μm. Therefore heated breath can only be seen over a few meters of path length. With any longer distances, the atmosphere significantly attenuates the signal.

Engines also emit significant amounts of heated carbon dioxide. In fact, the thermal signature of a missile and jet engine exhaust is dominated by heated carbon dioxide. Figure 4-15 illustrates the remaining signal after propagating a long path length. This is the signal available for target detection in IRST (infrared search and

track) scenarios. IRST systems have narrow band filters centered on the "blue" and "red" spikes to maximize the signal-to-noise ratio.

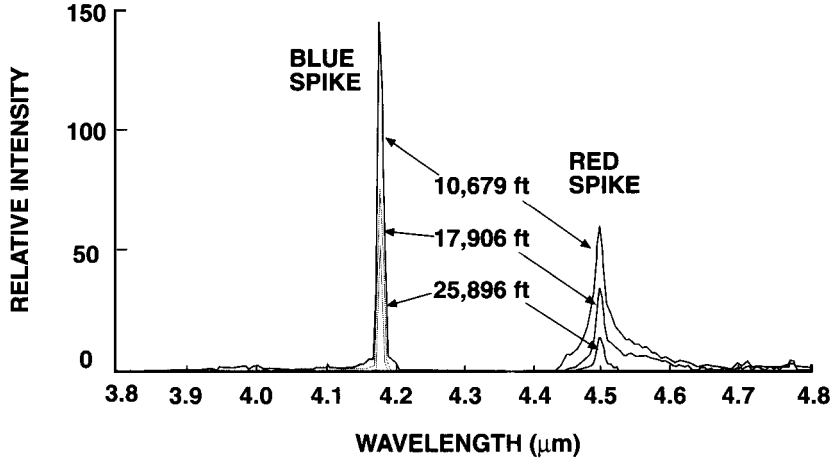


Figure 4-15. The "blue" and "red" signals of a jet engine exhaust as a function of path length (From reference 2).

Our eyes are sensitive from 0.4 to 0.7 μm. When pigments reflect light in this region, we perceive colors. These pigments, which can be paint, ink, or dye, may be semi-transparent in the infrared region. As a result, it is possible to detect changes in the original work by comparing a visible image to an infrared image. For example, art forgeries and counterfeiting are often detectable with an infrared imaging system. Figures 4-16 and 4-17 illustrate two different detectable alterations in original documents. Photocopies have the same ink (toner) on the entire page and therefore alterations cannot be detected on photocopies.

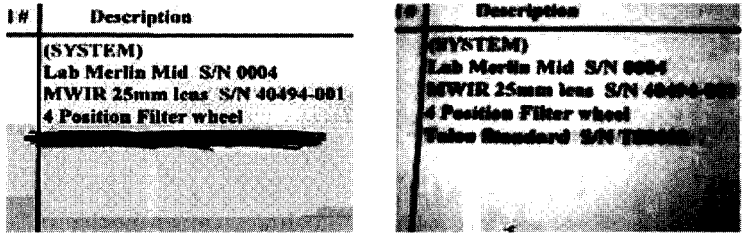


Figure 4-16. Printed words under a line obliterated with black ink are easily readable in the MWIR region. (By courtesy of Indigo Systems).

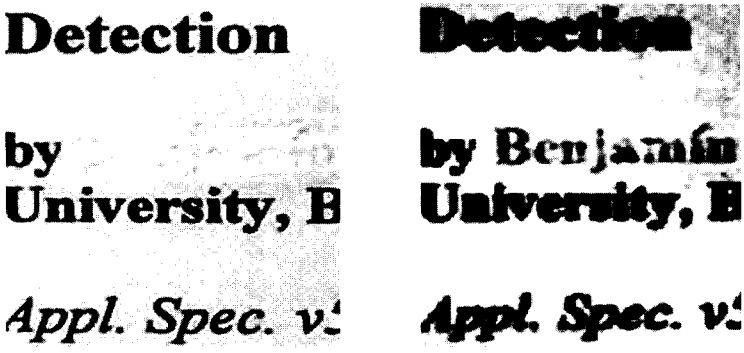


Figure 4-17. White correction fluid (a form of paint) is widely used to correct typing errors. It is semi-transparent in the MWIR region. (By courtesy of Indigo Systems).

4.7. REFERENCES

1. B. Wallin, "Temperature Measurement On and Inside Lamps," in *Thermosense XVI*, J. R. Snell, ed., SPIE Proceeding Vol. 2245, pp. 241-251 (1994).

2. D. E. Schmieder and G. W. Walker, "Camouflage, Suppression, and Screening Systems," in *Countermeasure Systems*, D. H. Pollack, ed., page 166. This is Volume 7 of *The Infrared and Electro-Optical Systems Handbook*, J. S. Accetta and D. L. Shumaker, eds., copublished by Environmental Research Institute of Michigan, Ann Arbor, MI and SPIE Press, Bellingham, WA (1993).

5

ATMOSPHERIC TRANSMITTANCE

The atmosphere is composed of numerous gases and aerosols. These constituents both absorb and scatter radiation as it travels from the target to the thermal imaging system. This reduction in radiation is the atmospheric transmittance. Because these same constituents are at ambient temperature, they also radiate energy. The radiation accumulated along the line-of-sight is called path radiance. In the visible, path radiance is caused by the scattering of ambient light into the line-of-sight. It prevents us from seeing far-away objects on a hazy or foggy day. The net effect is the same in both the visible and infrared: It reduces target contrast.

When atmospheric effects are considered, the detector output becomes

$$V_{DETECTOR} = kR_D(T_A M_T + M_A) \quad , \tag{5-1}$$

where T_A is the atmospheric transmittance and M_A is the path radiance. Note that the radiation reaching the imaging system is the sum of the attenuated target radiation and the path radiance. Figure 5-1 illustrates the two atmospheric effects.

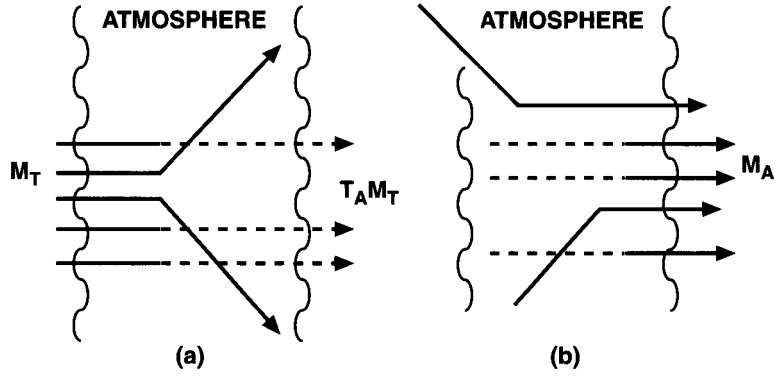


Figure 5-1. Atmospheric effects. For illustrative purposes, the atmosphere is shown with a finite width. In fact, the target and thermal imaging system are embedded in the atmosphere. (a) Transmittance and (b) path radiance. Absorption and scattering of scene radiation out of line-of-sight reduce target signature. Scattering into line-of-sight and self-emission reduce target contrast.

It would appear that the camera electronic gain could be increased to offset the loss in signal. This is true up to a point. If the signal is below the system's noise level, the signal is lost. No amount of gain can pull a signal out of the noise.

The magnitude of the transmittance and path radiance depends upon the atmospheric constituents, path length, and spectral response of the thermal imaging system. However, the atmosphere is constantly changing. The constituents vary hourly, daily, seasonally, and by location (e.g., urban, maritime, or arctic).

It is impossible to assign a single number to the transmittance or path radiance. These values must be measured (or at least estimated) when performing a specific measurement. For system performance studies, values that are considered representative of certain locations (typical for military scenarios) are used. Therefore, these studies only provide an average performance value.

5.1. EXTINCTION

Using the Beer-Lambert law, the atmospheric transmittance is:

$$T_A = e^{-\gamma R} \quad , \tag{5-2}$$

where R is the path length and γ is the extinction coefficient. Because scattering and absorption are independent, the extinction coefficient can be separated into its scattering component, σ_A, and its the absorptive component k_A. This allows us to study the two phenomena separately and then to combine the results:

$$\gamma = \sigma_A + k_A \quad . \tag{5-3}$$

The military adopted an *unusual* attenuation coefficient:

$$\tau_A = e^{-\gamma} \quad .. \tag{5-4}$$

Then

$$T_A = \tau_A^R = e^{-\gamma R} \quad . \tag{5-5}$$

Unfortunately, the terminology used to describe the reduction of radiation is author dependent. Both τ_A and γ have units of 1/km. Generally, γ will have low values (between 0.001 and 0.4) and τ_A will have high values (between 0.65 and 0.95). In a transparent atmosphere, $\gamma = 0$, $\tau_A = 1$, and $T_A = 1$.

Because each gas and aerosol has a unique spectral transmission, the extinction coefficient becomes

$$\gamma(\lambda) = \sigma_A(\lambda) + k_A(\lambda) \tag{5-6}$$

and

$$T_A(\lambda) = e^{\gamma(\lambda)R} \quad . \tag{5-7}$$

Figure 5-2 portrays a typical atmospheric transmittance curve that accounts only for absorption only. The dominant absorber in the 3 to 5 μm region is carbon dioxide (CO_2) which absorbs at 4.3 μm. This absorption band is obvious after a few meters of path length. Water vapor determines the upper and lower wavelength limits for both MWIR and LWIR spectral regions. Water vapor is also the dominant absorber in the LWIR region. As the water vapor increases, the LWIR transmittance decreases more quickly than the MWIR transmittance. This implies that a MWIR system may be better in a tropical or maritime environment.

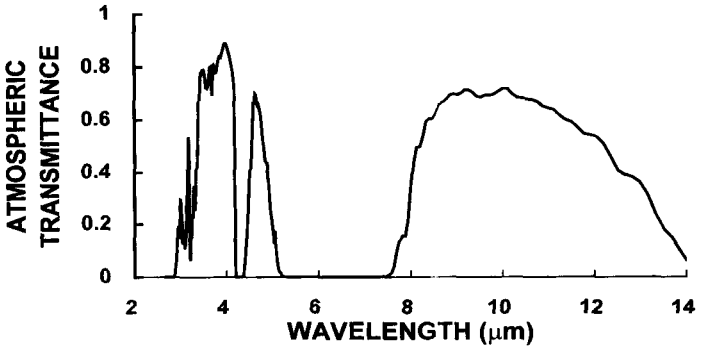


Figure 5-2. Representative atmospheric transmittance over a 1-km (3280 ft) path length. The actual transmittance depend upon the aerosols present (haze), and gases (including water vapor). These change with meteorological range, temperature, season, and location.

5.2. PATH LENGTH DEPENDENCE

Referring to Equation 5-7, it is evident that the transmittance is a function of path length. Figure 5-2 provided the transmittance over a 1-km (3280 ft) path length. At shorter path lengths, the atmospheric transmittance is higher (Figure 5-3). At longer path lengths, the atmospheric transmittance is lower (Figure 5-4). The short path lengths

are representative of those encountered for condition monitoring and predictive maintenance whereas long path lengths primarily affect surveillance activities.

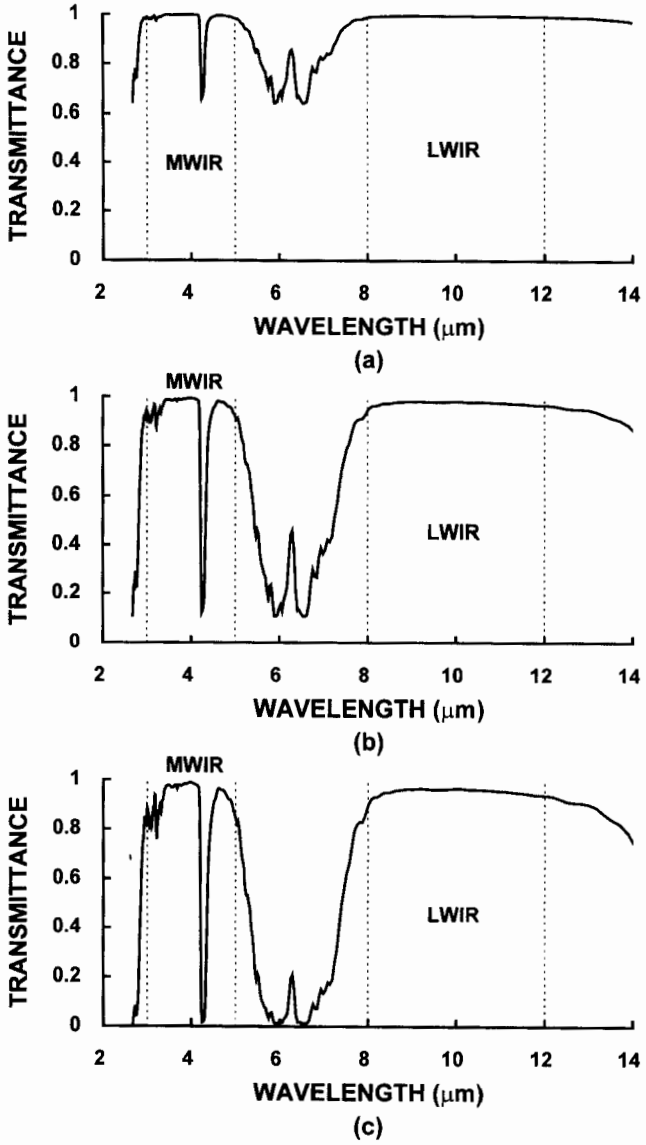


Figure 5-3. Representative atmospheric transmittance for (a) 10 m (32.8 ft), (b), 50 m (164 ft), and (c) 100 m (328 ft) path lengths. The vertical lines are representative of the MWIR (3 to 5 μm) and LWIR (8 to 12 μm) regions.

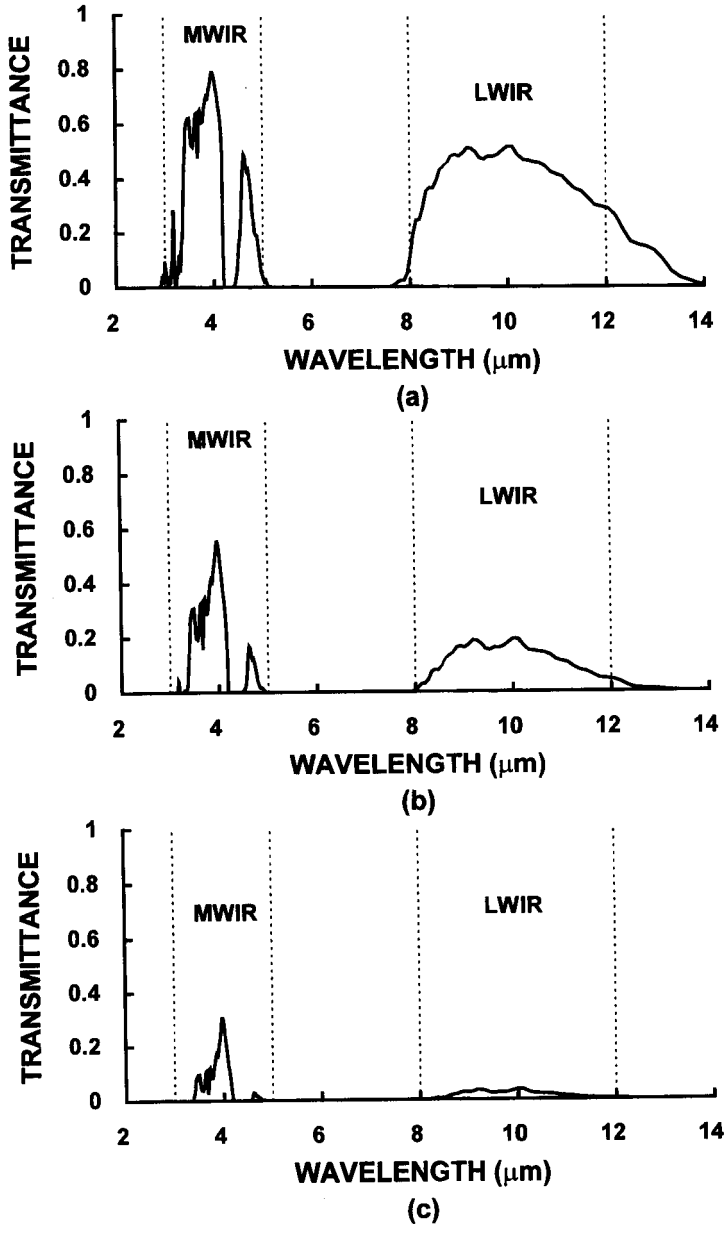


Figure 5-4. Representative atmospheric transmittance for (a) 2 km (1.26 mi), (b) 5 km (3.15 mi), and (c) 10 km (6.3 mi) path lengths.

Since the atmospheric transmittance is a function of the wavelength, it is necessary to describe its effect mathematically by an integral. Recall that, the integral just calculates the area under a curve. The attenuated target radiation produces

$$V_{DETECTOR} = k \int_{\lambda_1}^{\lambda_2} R_D(\lambda)\, T_A(\lambda) M(\lambda, T_T)\, d\lambda \quad . \tag{5-8}$$

The output depends upon the specific detector used. A LWIR system using a HgCdTe detector will provide a different output than an uncooled system using a microbolometer detector. Likewise, a Pt:Si MWIR detector will provide a different output than an InSb detector. Scanning the transmittances in Figures 5-3 and 5-4 reveal that the atmosphere affects MWIR differently than the LWIR. Short path lengths are not affected as much as long path lengths, and the output depends upon the target temperature as well as the detector spectral response. For very short path lengths (10 m or 32.8 ft), the atmospheric transmittance may be considered as unity in the MWIR and LWIR regions.

5.3. ATMOSPHERIC CONSTITUENTS

In order of concentration (by percent of volume), the gases in a dry atmosphere are nitrogen, oxygen, argon, neon, helium, krypton, xenon, hydrogen, and nitrous oxide. These tend to have a constant concentration. On the other hand, the concentrations of ozone, water vapor, carbon dioxide, and carbon monoxide are quite variable.

High humidity reduces transmittance by causing aerosol particulate growth, particularly with salt spray in maritime environments. Though the atmosphere may be quite clear visually, system performance may be degraded considerably because of the molecular absorption by the water vapor.

Aerosols, which are suspended particulates, include dust, dirt, carbon, minute organisms, sea salt, water droplets (haze or fog), smokes and artificial aerosols (pollutants). The relative concentrations of the atmospheric constituents can be different at different locales. For example, dense foliage and vehicular exhaust influence carbon monoxide and carbon dioxide concentrations. Urban areas produce more carbon monoxide. Pollutants vary according to population density and factory locations.

While gases absorb radiation, aerosols absorb and scatter the radiation. Scattering is quite dominant in the visible range and is the major contributor to path radiance. The meteorological range is a measure of this scattering.

5.3.1. WATER VAPOR

Water vapor or absolute humidity is a major absorber in the infrared region. Unfortunately, transmittance is not linearly related to absolute humidity. The absolute humidity is not normally a measured quantity but is calculated from standard meteorological observables[1] (e.g., temperature and relative humidity). Figure 5-5 illustrates the relationship between relative humidity (as a percentage) and the absolute humidity (g/m^3),

Although absolute humidity does not uniquely specify extinction, it can be used as a guide. Water vapor concentration may range from a few tenths of a g/m^3 in the desert to 40 to 50 g/m^3 in a tropical jungle or near the sea surface. As the absolute humidity increases, the transmittance decreases. Absolute humidity changes both daily and seasonally (Figure 5-6).

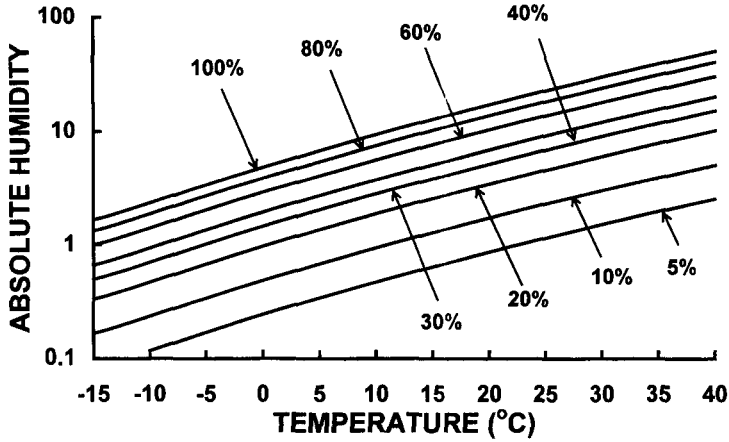


Figure 5-5. Absolute humidity (g/m^3) as a function of temperature and percent relative humidity. Tropical areas (high relative humidity and high temperatures) will have high absolute humidity. Arctic areas (cold with low relative humidity) will not. Water vapor (absolute humidity) attenuates both MWIR and LWIR radiation. As the water vapor increases, transmittance decreases.

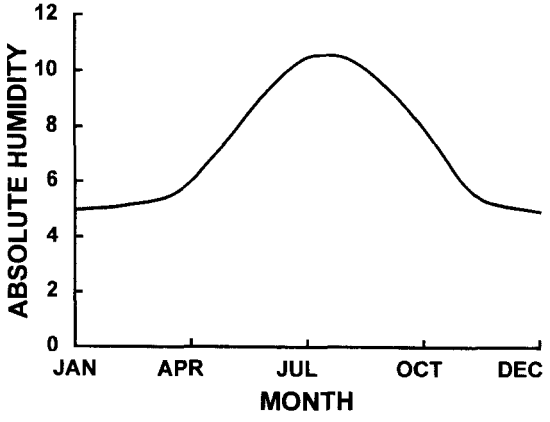


Figure 5-6. Typical absolute humidity variation for central Europe. Coastline areas may exhibit very large changes as the wind direction shifts from land-to-sea to sea-to-land.

5.3.2. AEROSOLS

Aerosols attenuate radiation primarily by scattering the radiation out of the line-of-sight. The magnitude of the scattering depends upon the ratio of the particle diameter to the wavelength. When the ratio is large (large diameter compared to the wavelength), scattering is significant. When the ratio is small, scattering is minimal. The aerosol diameter for light hazes is about 1 μm. This means that when the wavelength is less than 1 μm (i.e., the visible) there is significant scattering. The meteorological range, R_{MET}, is a visual estimate of the aerosol concentration (Table 5-1).

Table 5-1
INTERNATIONAL VISIBILITY CODE

DESIGNATION	VISIBILITY, R_{MET}	
Dense fog	0 - 50 m	0 - 164 ft
Thick fog	50 – 200 m	164 - 656 ft
Moderate fog	200 – 500 m	656 - 1640 ft
Light fog	500 - 1000 m	1640 - 3280 ft
Thin fog	1 - 2 km	0.63 - 1.26 mi
Haze	2 - 4 km	1.26 - 2.52 mi
Light haze	4 - 10 km	2.52 - 6.3 mi
Clear	10 - 20 km	6.3 - 12.6 mi
Very clear	20 - 50 km	12.6 - 31.5 mi
Exceptionally clear	> 50 km	> 31.5 mi

As particles grow in size, the scattering coefficient increases at all wavelengths and the transmittance decreases. Simultaneously, the spectral region that has a constant coefficient increases. In Figure 5-7, the particle size grows as the meteorological range decreases. Meteorological range is a visual method to estimate the aerosol concentration and particle size, Light hazes have small particles and therefore affect the visible and near infrared. As the particles grow in size, the region of maximum scattering moves out to the infrared.

Because thermal imaging systems operate at wavelengths that are five to 20 times the visible wavelengths, infrared imagery is less bothered by light-haze particles. Consequently, we say that thermal imaging systems can detect targets with minimal loss in range when light haze is present (meteorological ranges of 4 to 10 km). When moderate-sized particles are present (meteorological ranges of 2 to 4 km), scattering affects the MWIR region more so than the LWIR region. This leads to the statement that an LWIR system can provide better range performance in moderate haze than an MWIR system. When the particle size becomes very large (meteorological ranges less than 500 m), as with heavy fogs and raindrops, the visible, MWIR, and LWIR regions are affected equally.

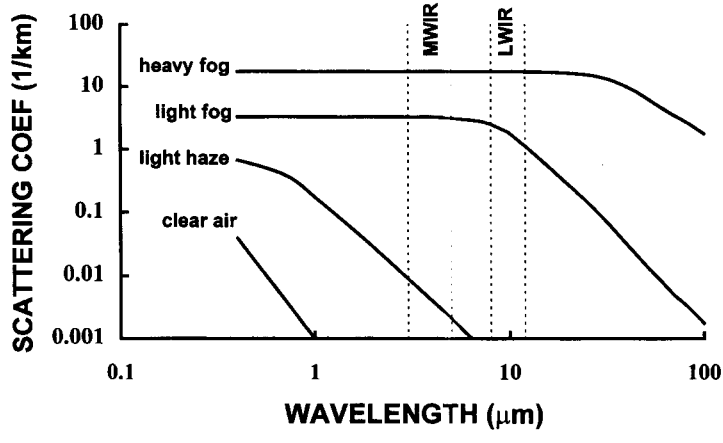


Figure 5-7. Scattering coefficient as a function of wavelength. As the particles grow in size, the scattering increases and they begin to affect the infrared region. For small particles compared to the wavelength, scattering is proportional to λ^{-4} (Raleigh scattering). For large particles (diameter much greater than the wavelength), scattering is independent of wavelength. The mean particle diameter of most tactical screening smokes and smoke from fires is about 1 μm (similar to light haze). They appear opaque in the visible because the concentration is very high. These smokes can be transparent in the LWIR region. (From reference 2).

5.4. PATH RADIANCE

Infrared path radiance is primarily due to atmospheric self-emission. It is independent of the target temperature and is seen even if the target is not present. The magnitude of this background radiation can vary with direction of observation, altitude, location, time of day, and meteorological conditions.

The path radiance depends upon the average atmospheric temperature. It represents a mean temperature that is obtained from averaging along the line-of-sight. The average temperature varies with elevation angle. When looking straight up, the sky appears very cold. As the elevation level decreases, more gases and aerosols are encountered. Near the surface of the earth (very small elevation angles), these aerosols will have a temperature that is near the earth's surface temperature (Figure 5-8).

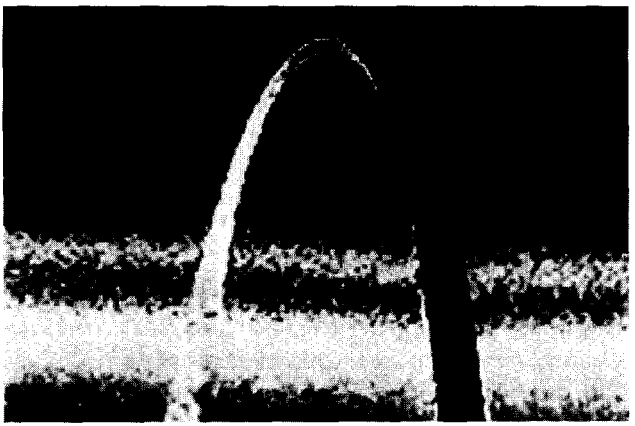


Figure 5-8. The St. Louis Gateway Arch. Inversions can create atmospheric layers of different (but constant) temperatures. The horizontal bands are created by the self-emission (path radiance) of the aerosol layers. (By courtesy of Gary J. Weil, president, Entech Engineering)

Since the path radiance does not contain any target information, it can be considered as noise. The signal-to-noise ratio may be approximated by

$$SNR = \frac{T_A \Delta T}{\sqrt{M_A}} \quad . \tag{5-9}$$

From the conservation of energy (Section 4.1), a semi-transparent medium provides

$$\alpha + \tau = 1 \quad . \tag{5-10}$$

At thermal equilibrium, $\alpha = \varepsilon$. Therefore, as the transmittance decreases, the emittance increases. Since path radiance is related to the emittance, as the transmittance decreases, the path radiance increases. As the numerator decreases in Equation 5-9, the denominator increases. Thus, the SNR decreases faster than predicted when only transmission is considered. The system gain can be increased to overcome the loss in target signal. But only up to a point. If the received SNR is too low, the target cannot be detected. Gain does not affect the SNR.

Path radiance complicates target temperature measurements. Fortunately, its effect only becomes a problem over very long path lengths when the transmittance is low (see Figures 5-3 and 5-4).

5.5. MODELING THE ATMOSPHERE

Numerous computer codes[3,4] such as LOWTRAN and MODTRAN are available to estimate the atmospheric transmittance. These codes provide the spectral extinction coefficient $\gamma(\lambda)$.

LOWTRAN (Low resolution transmission) has recently been replaced by MODTRAN (Moderate resolution transmission). The code contains representative (geographical and seasonal) atmospheric models and aerosol models (Table 5-2). In addition, the user can input radiosonde data as an environmental model or his aerosol model. The models provide radiance and transmittance for any slant path geometry.

Table 5-2
MODTRAN CHOICES

Environmental models	**Aerosol models**
Tropical	Rural
Mid-latitude summer	Maritime
Mid-latitude winter	Urban
Sub-arctic summer	Desert
Sub-arctic winter	Troposphere
1962 Standard	Navy Aerosol Model

Figure 5-9 illustrates the calculated LWIR attenuation as a function of absolute humidity and meteorological range. The absolute humidity is obtained from Figure 5-5. The finite extinction (less than unity) when there is no water vapor present is due to aerosol scattering and molecular absorption.

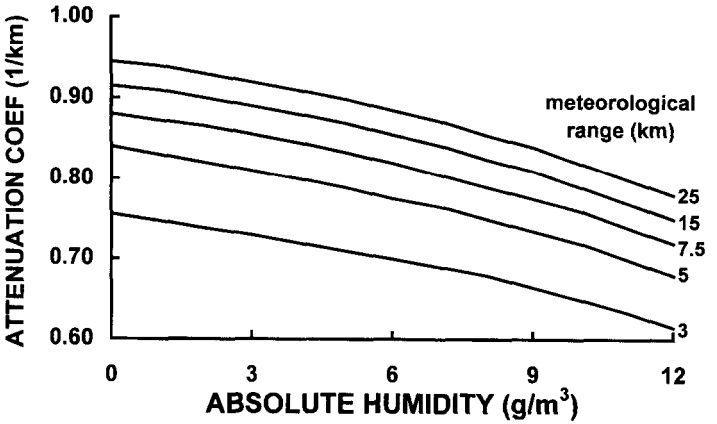


Figure 5-9. Representative attenuation as a function of absolute humidity and visibility. The attenuation coefficient has been spectrally averaged over the LWIR range. The aerosol concentration and particle size are embedded in the meteorological range. Both aerosol scattering (as specified by the meteorological range) and water vapor affect attenuation. Calculated from LOWTRAN using a mid-latitude summer aerosol model and a rural haze model.

5.6. BACK-OF-THE-ENVELOPE MODELING

To simply the mathematics, it is convenient to express $\gamma(\lambda)$ as a spectrally averaged value:

$$\gamma_{AVE} = \frac{1}{\lambda_2 - \lambda_1} \int_{\lambda_1}^{\lambda_2} \gamma(\lambda)\, d\lambda \quad . \tag{5-11}$$

Then

$$T_{AVE} = e^{\gamma_{AVE} R} = \tau_{AVE}^{R} \quad . \tag{5-12}$$

While mathematically convenient, T_{AVE} depends on path length, target temperature, and system spectral response.[5] Even with these disclaimers, a spectrally

averaged extinction coefficient permits extremely simple back-of-the-envelope calculations.

5.6.1. "AVERAGE" WEATHER CONDITIONS

Actual performance can have wide variations from that calculated due to the uncertainty of the atmosphere and the inability to accurately characterize it over the specific path length. While reasonable characterization is possible for ground systems, it is difficult to accurately characterize the atmosphere for systems on an airborne platform.

Atmospheric variations are a function of the season, location (continental, maritime or arctic environment, and latitude), time of the day, local meteorological conditions, naturally occurring aerosols, artificial aerosols, and pollutants. Local weather conditions measured at a nearby airport are not necessarily indicative of conditions at the test site. For back-of-the-envelope calculations, it is convenient to use a spectrally averaged attenuation value. Table 5-3 provides some approximate values.

Table 5-3
AVERAGE ATTENUATION VALUES
These approximate values can be used for back-of-the-envelope calculations.

Weather quality	**Average attenuation, τ_{AVE}**	**Approximate percentage of time with better weather**
Poor	0.70/km	80%
Fair	0.80/km	65%
Average	0.85/km	50%
Good	0.90/km	25%
Excellent	0.95/km	2%

The weather is typically either very good or very bad (Figure 5-10). Rarely is there an "average" day as suggested by Table 5-3. Every day exhibits large variations and the "average" value is a mathematical construct to make calculations easy and to allow system performance comparisons for different weather conditions. Actual values may be significantly different at any particular time. Casual observers tend to remember either very good or very bad weather and therefore are not good estimators of average conditions. Averages are based upon data collected over five to 10 years.[6]

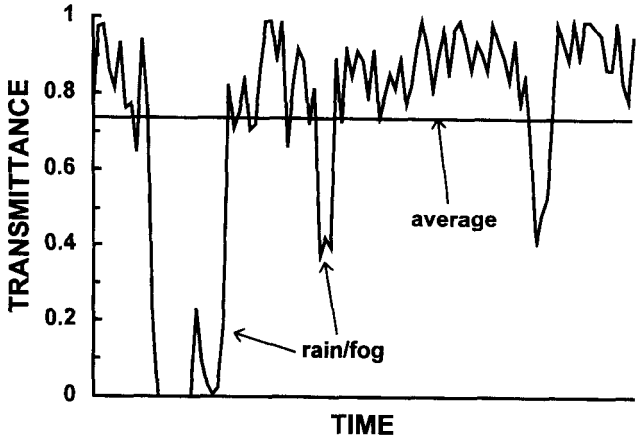


Figure 5-10. Typical atmospheric transmittance. Generally, the weather is either very good or very poor. Although it is convenient to discuss average values, it is rare to have an "average" day.

5.6.2. RANGE PREDICTIONS

A simple, back-of-the-envelope calculation can provide an average range at which a target can just be detected. This approach is based upon the signal-to-noise ratio only. The received signal-to-noise-ratio is

$$SNR \approx \frac{\tau_{AVE}^{R} \Delta T}{NEDT} , \qquad (5\text{-}13)$$

where ***NEDT*** is the noise equivalent differential temperature and ΔT is the target background temperature differential. The NEDT (discussed in Chapter 7, *Performance Parameters*) is a function of background temperature. When viewing objects against the sky, the background temperature becomes the effective aerosol temperature (path radiance temperature). Then Equation 5-13 is equivalent to Equation 5-9.

An average attenuation coefficient is selected from Table 5-3. A minimum ***SNR*** is then selected and the range is calculated. As an optimistic approach, let ***SNR*** = 1. Then

$$R = \frac{\log\left(\frac{NEDT}{\Delta T}\right)}{\log \tau_{AVE}} . \qquad (5\text{-}14)$$

To illustrate some trends, let the baseline values be $\tau_o = 0.85/\text{km}$, $R_o = 5$ km, $\Delta T_o = 10^o$ C and $NEDT_o = 0.2^o$ C. This provides $SNR = 22$. Suppose we can redesign the system such that the $NEDT$ is reduced to $NEDT = 0.15$. This allows one of three performance improvement choices. Depending upon the system application, one and only one choice is selected. For a fixed SNR:

CHOICE 1: For a fixed ΔT and τ, the range increases to

$$R = \frac{\log\left(\frac{\tau_{AVE}^{R_o} NEDT}{NEDT_o}\right)}{\log(\tau_{AVE})} = 6.77 \text{ km} \tag{5-15}$$

CHOICE 2: For a fixed range and τ, we can acquire cooler targets

$$\Delta T = \frac{NEDT_o}{NEDT} \Delta T_o = 7.5^o \tag{5-16}$$

CHOICE 3: For fixed range and ΔT, we can detect the same target in poorer weather

$$\tau_A = \tau_o \left(\frac{NEDT}{NEDT_o}\right)^{\frac{1}{R}} = 0.80/\text{km} \tag{5-17}$$

The spectrally averaged attenuation τ_{ave} should only be used for back-of-the-envelope calculations. It also can provide trends. For range performance predictions, the atmospheric transmittance should be calculated for each range of interest.

5.7. REFERENCES

1. G. C. Holst, *Electro-Optical Imaging System Performance*, page 275, JCD Publishing, Winter Park, FL (1995).
2. N. S. Kopeika and J. Bordegna, "Background Noise in Optical Communication Systems," *Proceedings IEEE*, Vol. 58(10), pp. 1571-1577 (1970).
3. LOWTRAN, MODTRAN, and HITRAN are discussed in many texts. See, for example, M. E. Thomas and L. D. Duncan, "Atmospheric Transmission," in *Atmospheric Propagation of Radiation*, F. G. Smith, ed. This is Volume 2 of *The Infrared & Electro-Optical Systems Handbook*, J. S. Accetta and D. L. Shumaker, eds., copublished by Environmental Research Institute of Michigan, Ann Arbor, MI and SPIE Press, Bellingham, WA (1993).
4. The ONTAR Corporation, 129 University Road, Brookline, MA 02146-4532, offers a variety of atmospheric transmittance codes and sensor performance models.
5. G. C. Holst, *Electro-Optical Imaging System Performance*, page 287, JCD Publishing, Winter Park, FL (1995).
6. See, for example, L. H. Janssen and J. van Schie, "Frequency of Occurrence of Transmittance in Several Wavelength Regions During a 3-year Period," *Applied Optics*, 21(12), pp. 2215-2223 (1982) or L. M. Biberman, R. E. Roberts, and L. N. Seekamp, "A Comparison of Electrooptical Technologies for Target Acquisition and Guidance; Part 2: Analysis of the Grafenwöhr Atmospheric Transmission Data," Paper P-1218, Institute for Defense Analysis, Arlington, VA (January 1977).

6
CAMERA DESIGN

The functional electro-optical block diagram shown in Figure 6-1 illustrates five major subsystems of an infrared camera: optics and scanner, detector and detector electronics, digitization, image processing, and image reconstruction. Figure 6-1 applies to scanning and staring systems. Not all components are present in all cameras. The specific design depends upon the number of detector elements and the required output format.

The detector is the heart of an imaging system because it converts infrared radiation into a measurable electrical signal and converts target spatial information into electrical temporal information. Amplification and signal processing create an electronic image in which voltage differences represent scene intensity differences. The detector electronics are matched to the detector characteristics and required output. Many systems digitize signals because of the relative ease of creating an image. In addition, many digital image enhancement algorithms are available. Machine vision systems typically operate in the digital domain.

It may be necessary to format the data into signals and timing that are consistent with monitor requirements. The monitor may or may not be an integral part of the infrared imaging system.

For convenience, targets are labeled as either hot or cold. *Hot* refers to a target that appears warmer than its immediate background and *cold* means the target appears cooler than its immediate background. The choice of hot objects appearing white and cold objects appearing black is arbitrary. With electronic polarity reversal available, either "white hot" or "black hot" targets can be created. With "black hot," *hot* objects appear dark gray against a neutral background. As the object becomes *hotter*, its representation on a monitor becomes blacker. The reverse is true for "white hot." With "white hot," the target becomes "whiter" as its apparent temperature increases relative to the background. All the images in this book are in "white hot."

The detector output is simply a voltage. This voltage can be mapped into pseudo-colors (There is no color information associated with the image). As is often done with human feelings, *cold* objects are often represented as blue and *hot* objects as red. Whether the output is displayed in a gray scale or pseudo-colors is a matter of personal preference. Note that these colors are used only to highlight features. These colors should not be confused with the color temperature of the object.

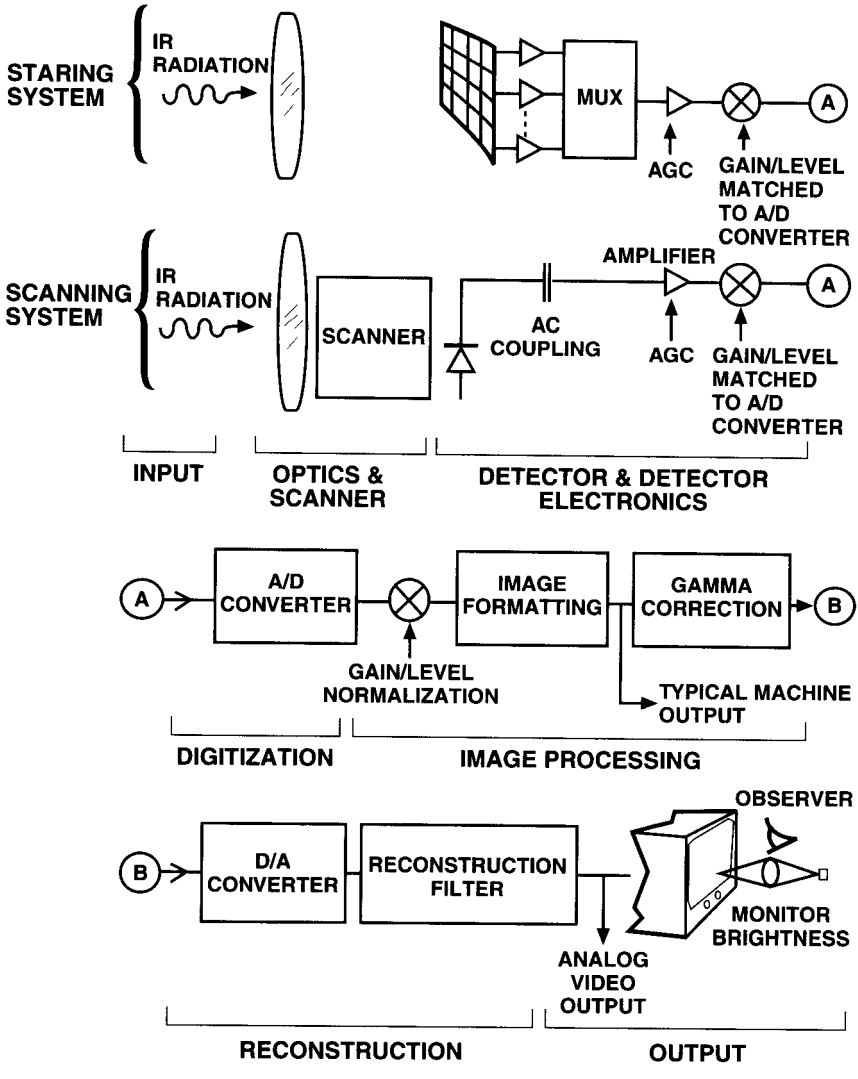


Figure 6-1. Generic functional block diagram. Not all components exist in every camera. The gamma correction circuitry is appropriate when the video is to be viewed on a CRT-based display. Analog cameras will not have an internal A/D converter.

6.1. CAMERA OUTPUT

It was shown in Section 3.1.1, *General response*, that the detector output is

$$V_{DETECTOR} = kR_D M \quad , \tag{6-1}$$

where R_D is the detector's responsivity, M is the radiation from the target, and k is a constant. The camera formula provides

$$k = \frac{A_D T_{OPTICS}}{4F^2} \quad , \tag{6-2}$$

where T_{OPTICS} is the transmittance of the optics, A_D is the active area of a detector, and F is the lens f-number. The f-number is

$$F = \frac{fl}{D} = \frac{focal\ length}{optical\ diameter} \quad . \tag{6-3}$$

Combining terms yields

$$V_{DETECTOR} = \frac{A_D T_{OPTICS}}{4F^2} R_D M \quad . \tag{6-4}$$

The detector output should be as large as possible so that small ΔT targets can be detected. Reducing the f-number increases the detector output. However, practical lenses are about F = 1 with the theoretical minimum of 0.5.

Often, lower f-number lens systems have more optical elements and therefore may have lower transmittance. The value T_{OPTICS}/F^2 must increase to increase the detector output. Lens systems may be described by the T-number:

$$T_{\#} = \frac{F}{\sqrt{T_{OPTICS}}} \quad . \tag{6-5}$$

Then

$$V_{DETECTOR} = \frac{A_D}{4T_{\#}^2} R_D M \quad . \tag{6-6}$$

The responsivity, R_D, is a characteristic of the detector selected. The f-number depends upon the desired field of view and aperture diameter. The lens material selected dictates the optical transmittance.

6.2. SYSTEM DESIGNS

This section provides a brief overview of common designs.

6.2.1. MILITARY SYSTEMS

Militarized systems evolved in the following chronological order:

LINE SCANNERS

A line scanner requires platform motion to create a two-dimensional image. It usually has a very wide field-of-view in the scan direction. Typically used for reconnaissance, it relies on aircraft or spacecraft motion to provide the cross-scan dimension. The very early infrared systems were downward looking line scanners. When designed to look out the front of an aircraft, they were called forward-looking infrared (FLIR) systems. The acronym FLIR is used generically to denote an infrared imaging system.

COMMON MODULE

All detectors, scanners, and amplifiers were built to the same specifications. Commonly designed components were called modules. The term now loosely refers to any LWIR system with bi-directional scan. Based upon blackbody curves, terrestrial objects emit more radiation in the LWIR region compared to the MWIR region. Further, for a fixed target-background temperature difference, the radiance difference (as specified by the thermal derivative) is about 10 times larger in the LWIR region than the MWIR region. This single fact prompted the design of LWIR common modules.

EOMUX

Only one person could view the common module display. By electro-optically multiplexing (EOMUX) the output, a common module FLIR can have a standard video output (e.g., RS 170, NTSC. PAL, or SECAM).

EMUX

As digital electronics matured, the EOMUX system was replaced with the electronically multiplexed (EMUX) design to create a standard output. This is the most prevalent "common module" design today.

SECOND GENERATION

As staring array technology improved, it was thought that the common module would be replaced by a staring array. However, low-noise LWIR staring arrays are difficult to build. As a result, second generation now refers to an array that has 480 detectors in the vertical direction and 4 time-delay-and-integrate detectors in the scan direction. It is loosely called a "480 by 4" array.

6.2.2. CIVILIAN SYSTEMS

For many years, civilian systems were derivatives of the militarized systems. However, military systems are usually designed for maximum sensitivity (very low noise). For many civilian applications, there is a strong signal (large temperature difference) so that low noise is not a major design concern. Cost, weight, ease of use, and power consumption now drive civilian system design.

While the military used LWIR exclusively, civilians had no restrictions. For many years, civilian systems contained a staring array operating in the MWIR. Newer systems are uncooled, meaning that the detector does not have to be cryogenically cooled. The uncooled systems can be designed to operate either in the MWIR or LWIR region. The LWIR region is the most popular since LWIR imagery is not affected by sun glints. Sun glints are a momentary sparkle or reflection. They occur from moving objects - such as waves on the sea. Solar reflections are continuous reflections.

6.3. OPTICS

The optics images the radiation onto the detector(s). Numerous computer codes assist the engineer in selecting a good optical design. There is nothing magical about infrared lens design. The challenge is to find materials that transmit infrared radiation, are strong, and are not affected by the environment. If the system will be used in a harsh environment, then an addition window may be necessary to protect the optics. Filters may be added to increase the dynamic range or change the spectral response.

Germanium (Ge) is widely used as a lens material for the LWIR. Although transparent in the infrared, it is opaque for wavelengths less than 2 μm and therefore visually appears black. Zinc sulfide (ZnS) and zinc selenide (ZnSe) are also used for LWIR lenses. They partially transmit visible light and objects appear yellow-orange. MWIR systems may use silicon, sapphire, quartz, or magnesium as lens material. Of these, only silicon is opaque in the visible.

6.4. SCANNERS

The function of the scanner is to dissect the image sequentially and completely. That is, the scanner moves the detector instantaneous-field-of-view (IFOV) around the system field-of-view (FOV) in a way that is consistent with the monitor requirements. A large variety of scanning schemes is available. There is nothing inherently good or bad with any particular scanning scheme: each has its own advantages and disadvantages. The most common scanners are rotating drums, polygons, refractive prisms, and oscillating mirrors. The detector output creates the image during the active scan time and during the inactive scan time the detector output is ignored. The inactive time provides the time necessary for the scanner to come into the appropriate position for the next frame or scan line.

Detector characteristics may dictate the scan direction. Figure 6-2 illustrates a system with a single detector with unidirectional (raster) scan. SPRITE (signal processing in the element) detectors require a unidirectional scan. Figure 6-3 illustrates a linear array that uses bi-directional scanning (parallel scan). U.S. common module systems employ bi-directional scanners. Figure 6-4 illustrates a series of detectors whose outputs are summed together to provide time-delay-and-integration (TDI). Systems with TDI usually require unidirectional scan. A full staring array does not have a scanner.

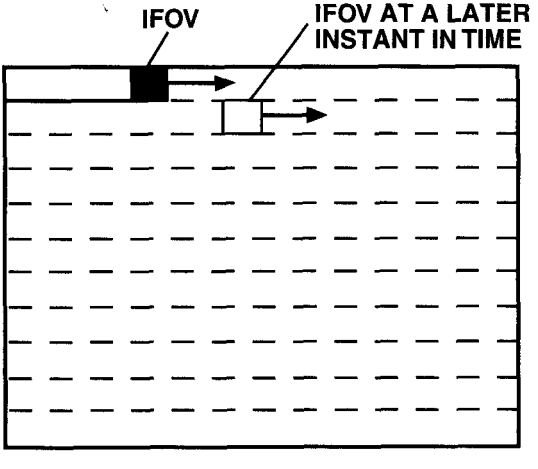


Figure 6-2. Single detector scan pattern employing unidirectional (raster) scanning.

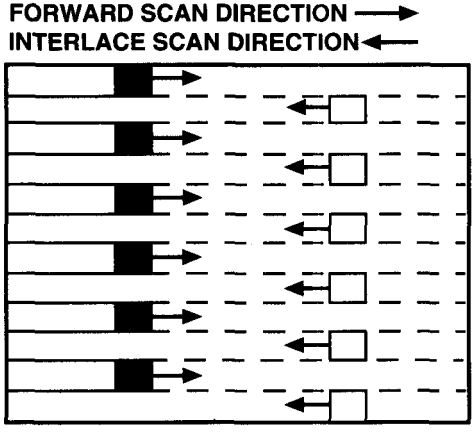


Figure 6-3. Linear array employing bi-directional scan and 2:1 interlace.

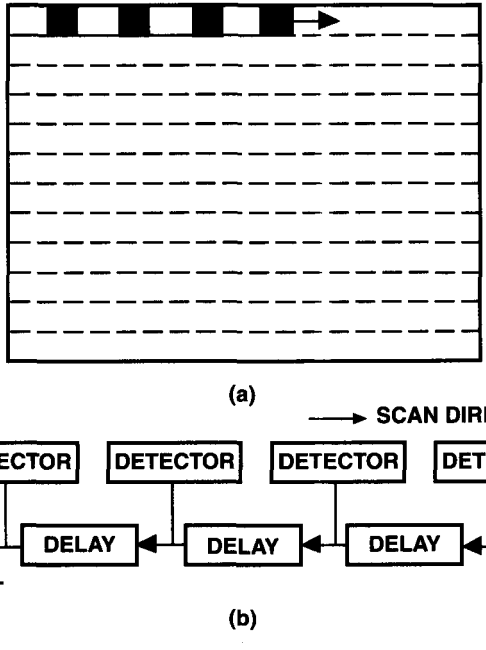


Figure 6-4. Multiple detectors operating in a pure serial scan mode. (a) Detector movement across the FOV. (b) The right-hand detector is the first to move across the target. After a suitable time delay for each succeeding detector, the outputs are added (TDI). If N detectors are present, the signal-to-noise ratio increases by $\sqrt{N}$.

6.5. DETECTORS AND COOLERS

Current detector terminology lists detectors as cooled or uncooled. These are only generic categories. Within each category, there are many different types of detectors.

COOLED DETECTORS

LWIR photon detectors have to be cooled below 100K with 77K considered a typical temperature. In the early days of thermal imaging systems, cryogenic cooling was achieved with liquid nitrogen (LN_2) whose boiling point is 77K. This temperature is still advocated today even though many systems have a mechanical cooler with an adjustable temperature range. Many MWIR detectors can operate at 200 K and this temperature can be easily achieved with a thermoelectric cooler (TEC). TECs appear to have an infinite lifetime whereas mechanical coolers degrade over time. Mechanical coolers add cost, bulk, and consume power.

UNCOOLED DETECTORS

Thermal detectors can operate at room temperature and therefore are called uncooled devices. Although called uncooled, these devices require a cooler to stabilize the detector temperature. Usually a thermoelectric cooler is used. Uncooled devices are lightweight, small in size, and easy to use. Because they use very low power, they lend themselves to hand-held, battery-operated, devices.

6.5.1. DETECTOR OPERATION

Detectors are classified as classical semi-conductors, novel semi-conductors, and thermal detectors. Detector performance parameters and therefore system performance parameters were developed for the classical semi-conductor and thermal detectors. More recently, novel semi-conductors such as the Schottky barrier photodiode and quantum well have been introduced. Classical theory is no longer appropriate and new measures of performance have been developed.

There are many different types of infrared detectors. The following lists the most popular types and some of their features.

CLASSICAL SEMICONDUCTORS

Photoconductive

The photoconductive detector requires a constant bias voltage. An absorbed photon changes the bulk resistivity, which, in turn, changes the current. The current change is monitored in an external circuit. Since current is constantly flowing, the detector dissipates heat. As a result, very large arrays are difficult to cool.

Photovoltaic

The photovoltaic detector is actually a p-n junction in a semiconductor. An absorbed photon produces a voltage change that is sensed in an external circuit. It does not dissipate heat and therefore can be built into very large arrays. Since minimal current flows, it is easy to couple the detector to a low noise amplifier.

NOVEL SEMICONDUCTORS

Schottky barrier photodiode (SBD)

The SBD is a photoemissive device that produces a voltage. These detectors are compatible with silicon fabrication technology. Therefore, it is easy to fabricate monolithic devices where the detector and readout are fabricated at the same time. SBDs can be built into very large (5000×5000) arrays.

Bandgap engineered photodetectors (quantum well)

The spectral response of quantum well detectors can be engineered (tuned) to any wavelength. Unfortunately, it has a very narrow spectral response. Its current limitation is that it requires significant cooling (below 60K).

THERMAL DETECTORS

Bolometer

As a bolometer absorbs heat, its resistance changes. It requires an external bias and the change in current (due to the change in resistance) is monitored in the external circuit. It is somewhat difficult to dissipate the heat in large arrays.

Pyroelectric

The pyroelectric detector can only sense a changing temperature. The thermal changes alter the electrical polarization that appears as a voltage difference. These AC devices create halos around high ΔT targets. These systems typically have a chopper (to produce a changing scene) between the lens system and detector. The chopper is synchronized with the frame rate of the camera so that the displayed image appears uniform.

6.5.2. SPECIFIC DETECTORS

PHOTON DETECTORS

Silicide Schottky-barrier devices

The most popular is Pt:Si (platinum silicide) which is sensitive in the 1.0 to 5.5 μm region. It requires a filter to limit the spectral response (e.g., to create a 3 to 5.5 μm system). Because of the low quantum efficiency, Pt:Si has poor performance when the background temperature is less than 0°C. Silicon technology is mature and very large arrays can be fabricated very cheaply. The device is often cooled to 70K to reduce the dark current.

InSb (Indium antimonide)

InSb is a high quantum efficiency MWIR detector. It has generally replaced PtSi in those systems using modest sized arrays (e.g., standard video format with approximately 640×480 elements). It peak response is near 5 μm. A filter is used to limit the spectral response to the MWIR region.

HgCdTe (Mercury cadmium telluride)

Mercury cadmium telluride is also called merc-cad or MCT. Although generally labeled as HgCdTe, it is a mixture ($Hg_{1-X}Cd_XTe$). By varying the ratio, the spectral response can be tailored to the MWIR or LWIR region. The most popular is the LWIR with a peak response near 12 μm. A filter is used to limit the response to the LWIR region. HgCdTe detectors are used in all common module systems.

SPRITE (Signal processing in the element)

The SPRITE detector is a stretched HgCdTe filament that provides inherent time-delay-and-integration (TDI). It was developed in England and has become the English common module detector.

QWIP (Quantum well infrared photodetector)

The QWIP is based upon mature GaAs growth technology. The wells are created by layers of GaAs/AlGaAs and the response can be tailored from 3 to 19 μm. The LWIR version typically has a spectral responsivity from 8.3 to 10 μm. The responsivity and noise are temperature sensitive so that QWIP devices are cooled to less than 60K.

THERMAL DETECTORS

As temperature sensors, thermal detectors can sense all wavelengths and therefore filters are used to limit the spectral response. The LWIR is usually

selected to overcome sun glints. Thermal detectors generally have much lower sensitivity than photon detectors. As a result, they probably will not replace photon detectors in critical, low signal-to-noise applications. A large variety of materials can be used as bolometer and pyroelectric detectors.

6.5.3. DETECTOR RESPONSIVITY

The early detector performance parameters were created for the classical photoconductive semiconductor. The responsivity is the output voltage per unit input radiant power:

$$R_D = \frac{V}{Power} \quad \frac{volts}{watt}. \tag{6-7}$$

The noise equivalent power is simply the rms noise divided by the responsivity:

$$NEP = \frac{V_{RMS}}{R_D} \quad watts. \tag{6-8}$$

There is a constantly increasing effort to reduce detector noise (reduce the ***NEP***). Since our society prefers big numbers rather than small numbers, the detectivity is defined as

$$D = \frac{1}{NEP} \quad . \tag{6-9}$$

Now, large ***D*** is desired. The normalized detectivity or ***D**** (pronounced dee-star) is a measure of detector performance. It includes the detector active area, the electronic bandwidth, and the noise equivalent power:

$$D^* = \frac{\sqrt{A_D \Delta f}}{NEP} = \frac{R_D \sqrt{A_D \Delta f}}{V_{RMS}} \quad \frac{cm - \sqrt{Hz}}{watt} \ (Jones) \ , \tag{6-10}$$

where Δf is the electronic bandwidth. The concept of ***D**** is attributed to Jones and his name often appears parenthetically. Photon detectors have a high ***D**** and therefore are low noise devices. These are the detectors of choice for research and military applications.

Figure 6-5 illustrates the D^* of a variety of detectors. Several points are of interest. Photon detectors have a responsivity that is of the functional form:

$$R_D(\lambda) = \left(\frac{q\lambda}{hc} \eta \right) R_{EXT} \quad , \tag{6-11}$$

where q is the electronic charge (1×10^{-19} coulombs), h is Planck's constant, c is the speed of light, and η is the quantum efficiency. The bracketed term is the detector's current responsivity with units of amps/watt. The external resistor, R_{EXT}, converts the amps into a measurable voltage. Quantum efficiencies can reach 90% for InSb and HgCdTe detectors.

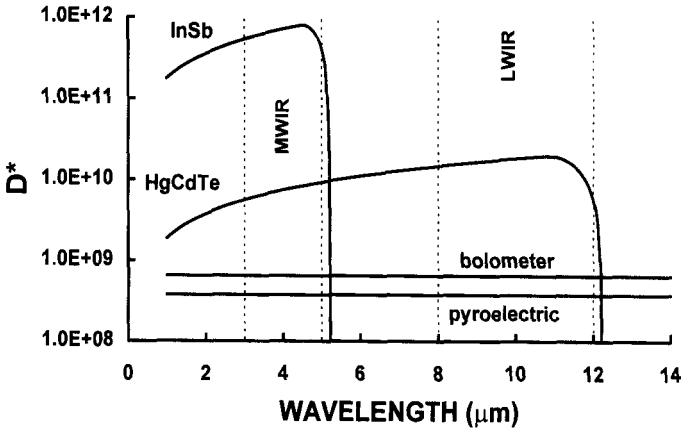


Figure 6-5. D^* for a variety of detectors. Filters are used to limit the spectral response.

As illustrated in Figure 6-5, D^* has the same functional form as the responsivity. It is convenient to characterize classical photon detectors by a peak D^* and cutoff wavelength:

$$D^*(\lambda) = \frac{\lambda}{\lambda_p} D_p^* \quad . \tag{6-12}$$

Thermal detectors are not photon detectors and therefore have no spectral features. Thermal detectors have a low D^* with a commensurate increase in noise. These detectors are very useful in situations where the ΔT is high. They work quite well for most condition monitoring and predictive maintenance applications.

Theoretically, photoconductive detectors have more noise than photovoltaic detectors. As a result, photovoltaic detectors will have a higher D^* by $\sqrt{2}$. Pt:Si operates on a different principle and therefore is not described by D^*. The quantum efficiency of a Pt:Si array is less than 1% at 4 μm and drops to zero at 5.5 μm.

With staring arrays, the photoelectrons are measured. The number of photoelectrons generated depends upon the photon flux, $M_q(\lambda,T)$, and the detector quantum efficiency:

$$n_e = k\,\eta\,M_q(\lambda,T)\,t_{INT} \quad , \tag{6-13}$$

where t_{INT} is the integration time. The maximum integration time is limited by the frame rate: t_{INT} = 1/(frame rate). For standard video operating at 30 Hz, t_{INT} becomes 33 ms (max). The integration time can be shortened to prevent saturation. As the frame rate increases, the integration time must decrease and, simultaneously, the signal level decreases. These electrons are converted to a voltage by the readout capacitor:

$$V = \frac{n_e\,q}{C} \quad . \tag{6-14}$$

6.5.4. FIXED PATTERN NOISE

In scanning systems, each detector usually has its own amplifier. Each detector/amplifier combination will have a different gain and level. These variations produce fixed pattern noise (FPN). For a linear array of elements, each line may have a different gain and offset. This produces FPN in the vertical direction only and will appear as horizontal streaks. For staring arrays, each detector will have a different response resulting in a two-dimensional FPN. Electronic gain/level normalization removes most FPN. FPN may be noticeable when the gain is maximized. This occurs when the target-background contrast is very low.

6.5.5. AC COUPLING

AC coupling is used in scanning systems to suppress a large uninformative background so that the small variations about ambient temperature can be amplified. The average level of each detector output is held constant such that the displayed image no longer is radiometrically correct. The same object can appear as either light gray or dark gray depending upon the immediate surroundings. Figure 6-6a illustrates a temperature-controlled board. The radiometric levels are shown in Figure 6-6b but after AC coupling, the video lines appear as that shown in Figure 6-6c. Figure 6-6d illustrates the resultant image. Very large uniform areas will appear as the same intensity

on the monitor independent of the absolute temperature. AC coupling affects only the line that is AC coupled. DC restoration is a process that adds signal to an AC coupled image so that it appears radiometrically correct.

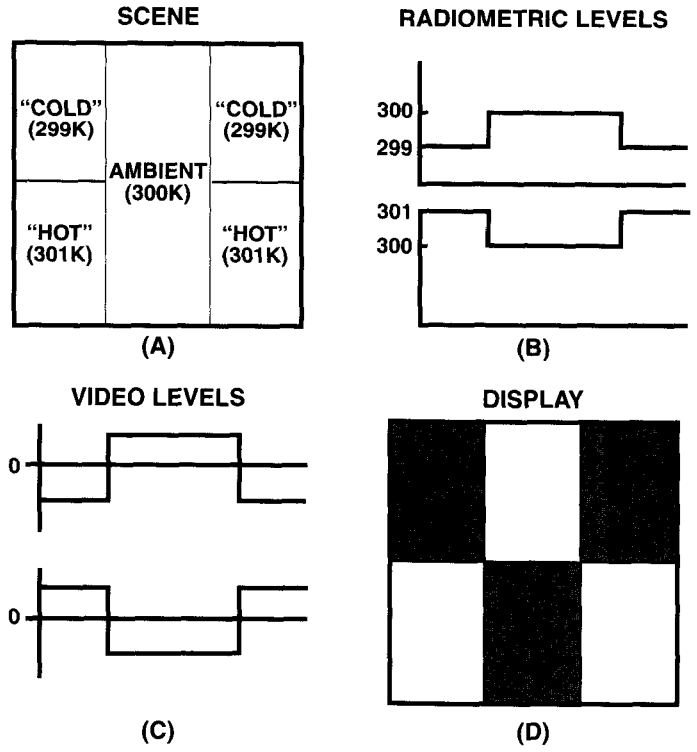


Figure 6-6. The AC coupling problem. (a) A calibrated target board with three different temperatures, (b) the radiometric values, (c) the output after AC coupling, and (d) the appearance on a monitor.

6.5.6. FILL FACTOR

Figure 6-7a illustrates a full focal plane array (no scanner) where the detectors are contiguous. With many detector arrays, the detector does not completely fill the cell area (Figure 6-7b). The ratio of active detector element area to the cell area is the fill factor. If a small object is imaged onto one of these dead areas between the detectors, there will be no output. A low fill factor becomes noticeable when viewing very small objects. As the small object moves, its image will move on and off the active detector element resulting in a twinkling of the object.

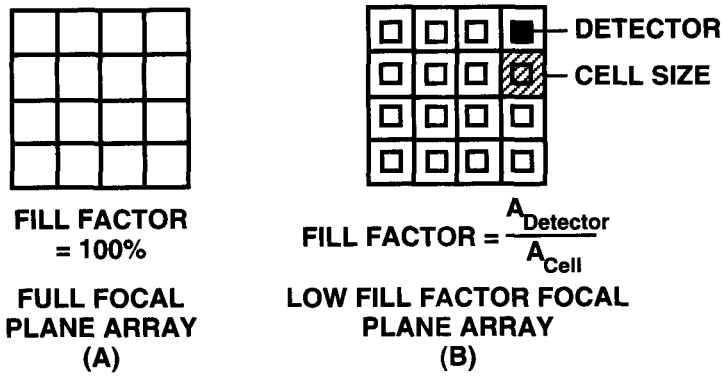


Figure 6-7. Fill factor definition. (a) 100% fill factor and (b) finite fill factor.

6.6. DIGITIZATION

Infrared systems spatially sample the scene because of the discrete location of the detectors. Staring systems, because of detector location symmetry, tend to have equal sampling rates in both the horizontal and vertical directions. With scanning systems, the detector output in the scan direction can be electronically digitized at any rate whereas in the cross scan direction, the detector locations define the sampling rate. Therefore, in a scanning system, the sampling rate may be different in the horizontal and vertical directions.

Sampling effects are obvious when viewing periodic targets such as those used for system characterization.[1] Sampling creates moiré patterns (Figure 6-8). Diagonal lines appear to have jagged edges or "jaggies." Sampling effects are not obvious when viewing complex scenery and, as such, are rarely reported during actual system usage although they are always present.

Sampling creates an uncertainty in target size. It is difficult to determine precisely where a target edge is located. This uncertainty is one detector width. It would initially appear that a target that completely fills a detector could be measured with accuracy. If a target is small, then the system must be carefully aligned so that the target is centered on one detector (Figure 6-9). While this is possible in the laboratory, it is extremely difficult to achieve in the field. Although the instantaneous-field-of-view (IFOV) is used as a measure of resolution, the smallest target that can be measured without critical alignment is probably 3 times the IFOV. This is further discussed in Section 7.3.5, *Measuring IFOV.*

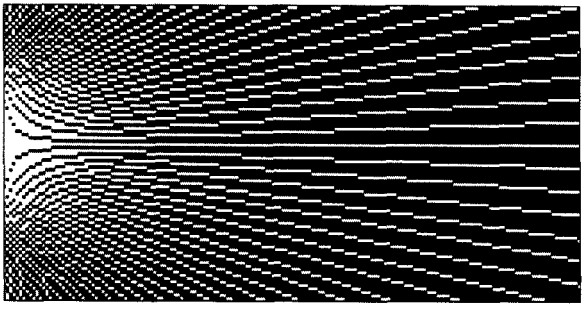


Figure 6-8. Moiré pattern. A raster scan system creates moiré patterns when viewing wedges or star bursts.

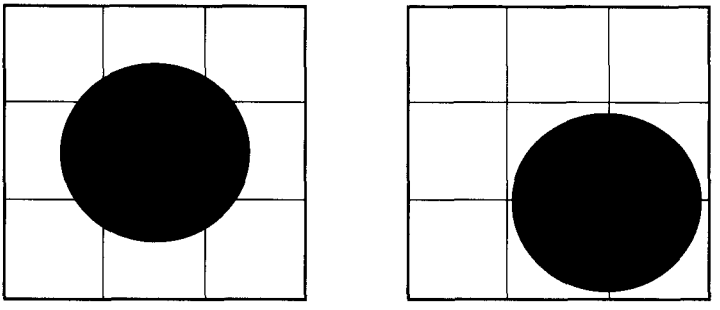


Figure 6-9. Sampling effects. (a) Small target centered on a target. The center detector can accurately measure the target's temperature. (b) Small target moved off center. In this case, no detector can accurately measure the temperature.

6.7. IMAGE PROCESSING

Image processing algorithms are used to enhance images, suppress noise, and put the image data into a format consistent with monitor requirements. Digital algorithms can provide boost and interpolation. Boost increases the signal amplitude at specific spatial frequencies but it does not affect the signal-to-noise ratio. For systems that are not noise limited, boost may improve image quality. However, for noisy images, the advantages of boost are less obvious.

Every detector/amplifier combination will have a different gain (responsivity) and offset. These variations result in fixed pattern noise or spatial noise. If large

deviations in responsivity exist, the image may be unrecognizable. As a result, systems employing more than one detector may require gain/level normalization or nonuniformity correction (NUC) to produce an acceptable image. Although most literature discusses NUC for staring systems, it also applies to scanning systems that have more than one detector in the cross scan direction. For good imagery, the individual detector outputs are normalized (made equal) for several discrete input intensities. These normalization intensities are also called calibration points, temperature references, or simply points.

With single point correction, the fixed pattern noise will be a minimum at the reference temperature. With perfect correction, there will be no fixed pattern noise at the reference temperature (Figure 6-10). Truncation errors in the normalization algorithm and different spectral response detectors produce residual FPN. As the background temperature deviates from the reference calibration temperatures, fixed pattern noise will increase. The increase depends upon how far the detector responsivity curves deviates from linearity.

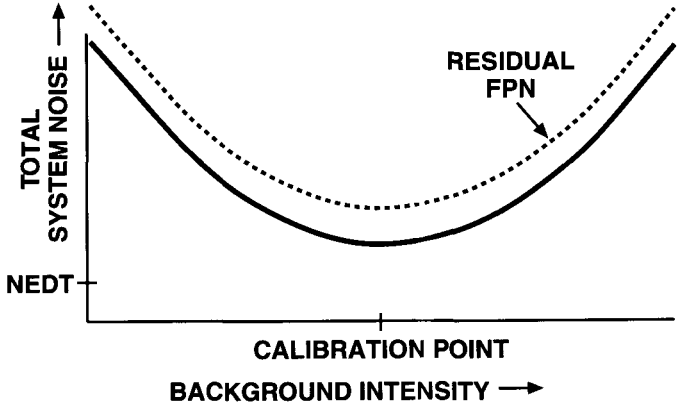


Figure 6-10. Fixed pattern noise after single point correction. Noise will be a minimum at the correction temperature (calibration point).

For two-point correction, the spatial noise will be at a minimum at two reference intensities. For any other intensity, the spatial noise increases. However, in the region between the two references (Figure 6-11), the spatial noise is less compared to the spatial noise outside the two references. This curve is often simply called the w-curve.

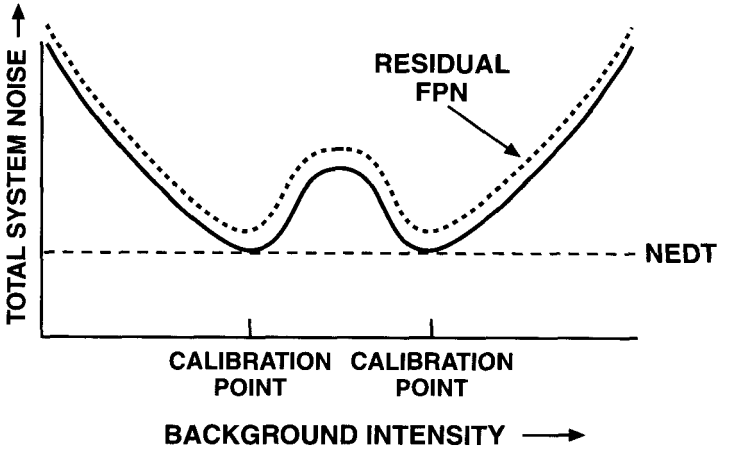


Figure 6-11. Fixed pattern noise after two-point correction. The amount of noise between the two correction points depends upon the system spectral response, detector responsivities, and the correction algorithm.

Thermal correction should be performed periodically. With scanning systems, the references can be placed at either end of the scan. During the inactive scan time, the detector views the internal blackbody references. The detector output due to the references is stored in memory and used in every frame for nonuniformity correction. One advantage of this method is that the thermal reference temperature can vary according to the scene dynamic range (called scene-based correction). If the overall scene ΔT is small, then the differences in the reference temperatures are small.

In some cases, it is not possible to include the blackbodies into the optical path for mechanical or optical reasons (notably staring arrays). With these systems, corrections are placed in firmware. Their success relies on detector stability; it assumes that the detector gain and offset does not change over time and this is true for many staring arrays. Staring arrays must be recalibrated periodically to ensure that the FPN corrections are correct.

6.8. RECONSTRUCTION

The D/A converter provides an output that typically has a stair step appearance. The reconstruction filter smoothes the data and removes the stair step. The output of the reconstruction filter is the analog video.

6.9. MONITORS

The monitor may be an integral part of the infrared system or stand-alone. If the monitor is separate from the infrared system, it is important to use a high quality monitor that does not degrade image quality.

6.10. MWIR versus LWIR

Since the advent of thermal imaging systems, many studies and arguments have resulted over whether MWIR is a better imaging band than the LWIR region. The detector output is a complex relationship among many factors. Assuming a perfect blackbody ($\varepsilon = 1$), The detector output is

$$V_{DETECTOR} = \frac{A_D}{4F^2} \int_{\lambda_1}^{\lambda_2} M(\lambda, T_T)\, R_D(\lambda)\, T_{OPTICS}(\lambda)\, T_A(\lambda)\, d\lambda \ . \quad (6\text{-}15)$$

Because so many quantities are involved, there is no "best" system. Comparing systems built to different designs is nearly impossible. Each design has its advantages and disadvantages. Comparing MWIR with LWIR automatically includes different detectors with different quantum efficiencies. The "best" system is the one that meets the needs of your application. Atmospheric conditions have the largest influence on MWIR/LWIR selection.

The atmospheric transmittance depends upon the amount of water vapor present, aerosols, and the molecular species present. As the aerosol concentration increases, the particle sizes grow and the MWIR region is affected more than the LWIR region (Figure 5-7). Water vapor affects the LWIR region more than the MWIR region. Whether MWIR transmittance is better than the LWIR depends upon the relationship between the visibility and the water vapor concentration. MWIR transmittance is higher only when the water vapor concentration is high and the aerosol concentration is low (long meteorological ranges). Even when this is true, the MWIR transmittance is better for path lengths greater than 10 km (6.3 mi). The MWIR system must be designed to exploit the increased transmittance. If the task was to detect targets at 5 km (3.1 mi), then the LWIR should be selected even in a high humidity environment.

Solar reflections are most troublesome in the MWIR region. Some cameras have a "sun filter" which blocks radiation below about 3.4 μm. This filter reduces sensitivity and increases the NEDT. For those applications that require very low NEDT, the sun filter will adversely affect performance. Clearly, solar reflections occur only

outdoors during daylight and with no clouds in the sky. This is not an issue indoors or if the measurements are made at nighttime.

Table 6-1 compares the solar radiation at ground level to that of a blackbody at 290K. If the target's emissivity is high, then the sun's effect is minimal. If the emissivity is low, then sun glints can occur. In the MWIR, the solar radiation is 6 times higher than the blackbody radiation, indicating that sun glints can be a problem in the MWIR. In the LWIR, sun glints are almost negligible. The magnitude of the solar glint depends upon the reflectivity and it depends upon the viewing angle (see Figure 4-4).

Table 6-1
COMPARISON of SUN and BLACKBODY EMISSION

Spectral region	**Solar radiation at Ground level**	**Self-emission of 290K blackbody**
MWIR	24.0 W/m^2	4.1 W/m^2
LWIR	1.5 W/m^2	127.0 W/m^2

Note that the terms "MWIR" and "LWIR" are used in a generic sense. To call a system MWIR only denotes that its spectral response is within the MWIR region. It says nothing about the precise response. For example, both PtSi and InSb are labeled as MWIR detectors but the spectral responses are very different and therefore their performances are very different. The atmospheric transmittance is only one parameter in range performance equation and as such should not be used exclusively to select MWIR or LWIR. Trade studies must include the specific sensor designs to determine which will perform better in the various scenarios and environments.

Cost, ease of use, reliability, and maintainability are additional factors that do not fit into a mathematical trade-off analysis. These factors are discussed in Chapter 8, *Camera Selection*. The system you select will depend upon your particular application. This chapter only provides the background information on why cameras are built the way they are.

6.11. REFERENCES

1. G. C. Holst, *Testing and Evaluation of Infrared Imaging Systems*, second edition, pp. 43-49 and pg. 348, JCD Publishing, Winter Park, FL (1998)

7
PERFORMANCE PARAMETERS

System characteristics, observer experience, scene content, atmospheric transmittance, monitor settings, and a variety of miscellaneous factors affect the perceived image quality (Figure 7-1). The cause of poor imagery cannot be discerned simply by examining the image. The purpose of laboratory testing is to be able to quantify the most important variables that support good image quality (Table 7-1). Optimal image quality cannot be determined by simply viewing an image. To determine if optimum quality has been achieved, it is necessary to verify focus, adjust gain, adjust level, tune the monitor, measure the response to different sized targets, and measure the response to different target intensities (i.e., quantify the parameters in Table 7-1). Although the parameters in Table 7-1 are often treated as independent quantities, they are not. The MRT depends upon both the NEDT and spatial resolution. Performance parameters should not be confused with features. Features are discussed in Chapter 8, *Camera Selection.*

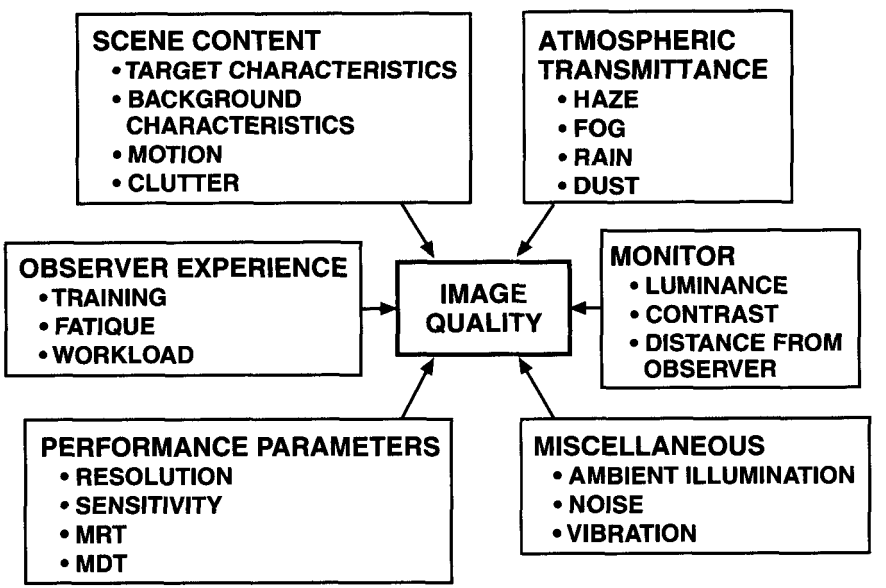


Figure 7-1. Various image quality contributors that affect perceived quality.

Table 7-1
PERFORMANCE PARAMETERS

Thermal sensitivity (NEDT)
Spatial resolution
Minimum resolvable temperature (MRT)
Minimum detectable temperature (MDT)

An overwhelming majority of imaging quality discussions center on spatial resolution or thermal sensitivity. The term *resolution* has been in use so long that it is thought to be something fundamental that uniquely determines image quality. It is the smallest detail that can be perceived. Spatial resolution may be specified by a variety of, sometimes unrelated, metrics such as the Airy disk diameter or the instantaneous-field-of-view. The appropriate metric depends upon the intended system application. Resolution does not include the effects of target contrast nor system noise. There is a clear distinction between resolution (the ability to see detail) and detection (the ability to see something).

Thermal sensitivity refers to the smallest temperature differential that can be detected. It depends upon the light-gathering properties of the optical system, the responsivity of the detector, and the noise of the system. A laboratory measure of thermal sensitivity is the noise equivalent differential temperature (NEDT). It is also called the noise equivalent temperature difference (NETD) and noise equivalent temperature (NET). Thermal sensitivity is independent of spatial resolution.

System performance depends on both sensitivity and resolution. As shown in Figure 7-2, the minimum resolvable temperature (MRT) is constrained by sensitivity and resolution considerations. Different systems (Figure 7-3) may have different MRTs. System A has a better thermal sensitivity because it has a lower MRT at low spatial frequencies. In this case, System A has a lower NEDT. Large targets consist of low spatial frequencies. At mid-range spatial frequencies, the systems are approximately equivalent and it can be said they provide equivalent performance. System B has better spatial resolution and can display finer detail than System A (fine detail is associated with high spatial frequency). Figure 7-3 illustrates that neither thermal sensitivity, spatial resolution, nor any other single parameter can be used to compare systems. Rather, all the quantities listed in Table 7-1 must be specified for system-to-system comparison.

This chapter highlights the most common performance parameters. Detailed measurement techniques can be found in *Testing and Evaluation of Infrared Imaging Systems*, second edition, G. C. Holst, JCD Publishing, Winter Park, FL 32779 (1998).

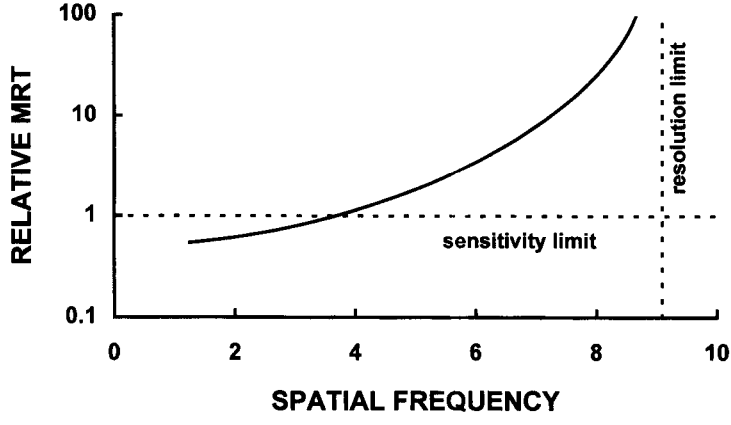


Figure 7-2. MRT is constrained by the system's resolution and sensitivity. The sensitivity limit is defined as the NEDT. Because of the eye's incredible spatial and temporal integration properties, the MRT is less than the NEDT at low spatial frequencies.

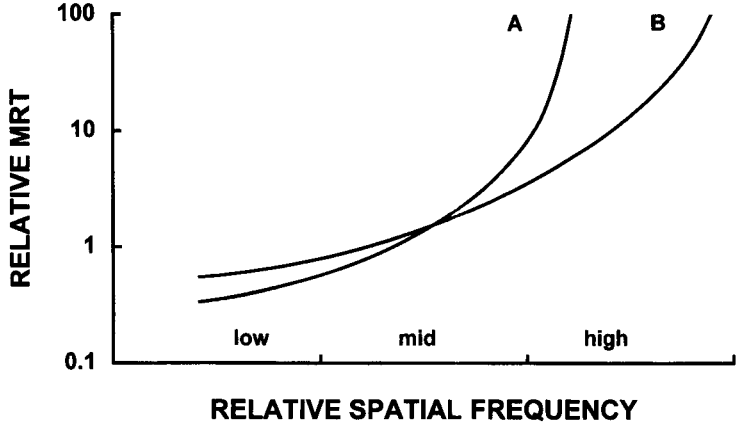


Figure 7-3. Two systems with different MRTs. Whether system A is better than B depends upon the specific application.

7.1. SPATIAL FREQUENCY

Object-space spatial frequency (Figure 7-4) is used to characterize system response. Using the small angle approximation, the angle subtended by one cycle (one bar and one space) is d/R where d is the spatial extent of one cycle and R is the distance from the infrared system entrance aperture to the target. When using a collimator, the collimator focal length, fl_{COL}, replaces R so that targets placed in the collimator's focal plane can be described in object space. The small angle approximation is valid when $d << R$ or $d << fl_{COL}$.

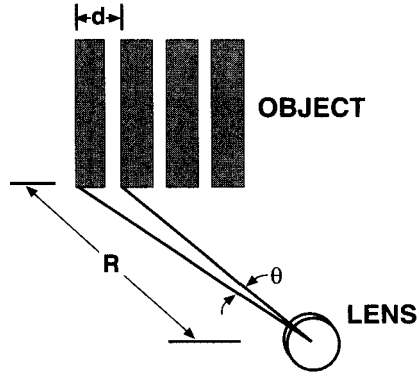


Figure 7-4. Object-space spatial frequency.

The horizontal object-space spatial frequency, f_x, is the inverse of the horizontal target angular subtense and is usually expressed in cycles/mrad:

$$f_x = \frac{1}{1000}\left(\frac{R}{d}\right) \quad \frac{cycles}{mrad} \tag{7-1}$$

or

$$f_x = \frac{1}{1000}\left(\frac{fl_{COL}}{d}\right) \quad \frac{cycles}{mrad} \; . \tag{7-2}$$

7.2. SENSITIVITY (NEDT)

Repeating Equation 5-13, the NEDT is used for a back-of-the-envelope estimation of the signal-to-noise ratio

$$SNR \approx \frac{(\tau_{AVE})^{R}\ \Delta T}{NEDT} \quad . \tag{7-3}$$

When $SNR = 1$ and $\tau_{AVE} = 1$, the minimum ΔT is the $NEDT$. The $NEDT$ represents an uncertainty in measuring a temperature. For a given a signal-to-noise ratio, the range can be determined. The minimum SNR is one. Solving for R provides

$$R \approx \frac{\log\left(\frac{NEDT}{\Delta T}\right)}{\log(\tau_{AVE})} \quad . \tag{7-4}$$

7.2.1. NEDT MEASUREMENT

The measurement is straightforward. The camera views a blackbody source. The blackbody temperature is changed and compared to a reference. This creates different ΔTs. For each ΔT, the differential output voltage, ΔV, is measured. The ΔTs and ΔVs are recorded and plotted. The slope, $\Delta V/\Delta T$, is the signal transfer function ($SiTF$). Then

$$NEDT = \frac{V_{RMS}}{SiTF} = \frac{V_{RMS}}{\Delta V / \Delta T} \quad , \tag{7-5}$$

where V_{RMS} is the rms (root-mean-square) value of the noise.

7.2.2. NEDT THEORY

Placing Equation 3-23 into a generic form (without wavelength dependence) provides

$$\Delta V_{DETECTOR} = k\, R_D \left[\frac{\Delta M}{\Delta T}\right] \Delta T \quad , \tag{7-6}$$

where the bracketed term is the thermal derivative. Since the ***NEDT*** is that input ΔT that produces a signal-to-noise ratio of one

$$\frac{\Delta V_{DETECTOR}}{V_{RMS}} = 1 \quad . \tag{7-7}$$

Solving the above equations for ΔT, and calling ΔT the ***NEDT*** provides

$$\Delta T = NEDT = \frac{V_{RMS}}{k R_D \left[\frac{\Delta M}{\Delta T}\right]} \quad . \tag{7-8}$$

Bringing in the definition of D^* (Equation 6-10), k from the camera formula yields

$$NEDT = \frac{4F^2\sqrt{\Delta f}}{\sqrt{A_D}\left[\frac{\Delta M}{\Delta T}\right] T_{OPTICS} D^*} \quad . \tag{7-9}$$

The thermal derivative is evaluated for a specific background temperature, T_B. As such, the NEDT is a function of the background temperature. As the background temperature increases the NEDT decreases (Figure 7-5). Since target detectability requires that ***SNR*** = 1, as the background temperature increases, the minimum detectable ΔT decreases.

As a system specification, the variation of NEDT with temperature is not a major problem. Suppose the NEDT is specified at a 20°C background. If the NEDT is measured at, say, 25°C then Equation 7-9 is used to scale the NEDT to a 20°C background. As the ambient temperature drops, the NEDT increases and the uncertainty in temperature measurements increases. This variation depends upon the system spectral response. Note that the NEDT is a function of the lens f-number and optical transmittance. Changing lenses can change the NEDT.

Since detectors have a limited spectral response, it is necessary to include the wave-length dependence in Equation 7-6:

$$\Delta V_{DETECTOR} = \left[k \int_{\lambda_1}^{\lambda_2} R_D(\lambda) \frac{\partial M(\lambda, T_B)}{\partial T} \, d\lambda \right] \Delta T \quad . \tag{7-10}$$

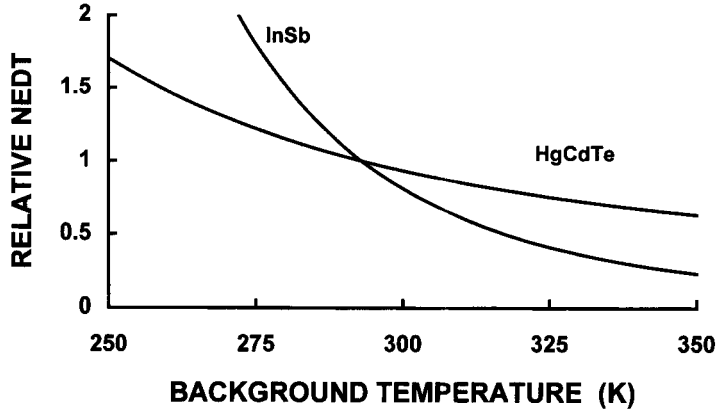


Figure 7-5. Relative NEDT as a function of background temperature. The NEDTs are normalized at 293K. The spectral response of the HgCdTe is 8 to 12 μm and 3 to 5 μm for the InSb detector. This graph is unique to the detectors and spectral response selected. It should not be construed to mean that a LWIR detector is better than a MWIR detector. Generally, the NEDT becomes excessively high in the MWIR region when the background temperature drops below 273K (0°C).

Equation 7-8 becomes

$$NEDT = \frac{V_{NOISE}}{k \int_{\lambda_1}^{\lambda_2} R_D(\lambda) \frac{\partial M(\lambda, T_B)}{\partial T} d\lambda} \quad . \tag{7-11}$$

Bringing in the definition of $D^*(\lambda)$ provides the full NEDT equation:

$$NEDT = \frac{4F^2 \sqrt{\Delta f}}{\sqrt{A_D} \int_{\lambda_1}^{\lambda_2} T_{OPTICS}(\lambda) \frac{\partial M(\lambda, T_B)}{\partial T} D^*(\lambda) d\lambda} \quad . \tag{7-12}$$

7.3. SPATIAL RESOLUTION

Spatial resolution provides valuable information regarding the finest detail that can be discerned. It does not include the effects of system noise nor is it directly related to thermal sensitivity. Spatial resolution may be specified by a variety of, sometimes, unrelated metrics such as the Airy disk size, the instantaneous-field-of-view (IFOV), imaging resolution, measurement resolution, measuring IFOV, or the Nyquist frequency associated with the detector pitch. The Airy disk, IFOV, and Nyquist frequency are calculated values.

The attractiveness of resolution is that it permits us to estimate the smallest discernible target size. A back-of-the-envelope approximation provides:

$$\textit{Target size} = \theta_{RESOLUTION} R \quad , \tag{7-13}$$

where $\theta_{RESOLUTION}$ is camera's angular resolution. Equivalently, when the target size is known, the maximum distance that the target that can be resolved is determined:

$$R = \frac{\textit{Target size}}{\theta_{RESOLUTION}} \quad , \tag{7-14}$$

Equations 7-13 and 7-14 are valid when the distance to the target is 10 times the system's focal length. Note that this range may be different than that calculated by Equation 7-4. The reported range should be the smaller of that calculated by thermal sensitivity and spatial resolution considerations.

7.3.1. AIRY DISK

Perhaps the most popular measure of optical resolution is Airy disk size. It is the bright center of the diffraction pattern produced by an ideal optical system. When expressed as an angle, the Airy disk diameter is

$$\theta_{AIRY} = 2.44 \frac{\lambda_{AVE}}{D} \quad , \tag{7-15}$$

where λ_{AVE} is the average wavelength and $\boldsymbol{D}$ is the lens diameter. For example, for a MWIR system operating from 3 to 5 μm, λ_{AVE} is 4 μm. For a LWIR system operating from 8 to 12 μm, λ_{AVE} is 10 μm. Using the Airy disk provides

$$\textit{Target size} = \theta_{AIRY}\textit{Range} = \left(\frac{2.44\lambda}{D}\right)\textit{Range} \quad . \tag{7-16}$$

7.3.2. INSTANTANEOUS-FIELD-OF-VIEW

Detector arrays are specified by the number of pixels, detector size, and detector pitch. These are not meaningful until an optical system is placed in front of the array. Using the small angle approximation, the detector-angular-subtense (DAS) is

$$\theta_{DAS} = \frac{d}{fl} \quad , \tag{7-17}$$

where $\boldsymbol{d}$ is the width of the detector's active area and $\boldsymbol{fl}$ is the optics focal length. The instantaneous-field-of-view (IFOV) is the angle over which the detector senses radiation. For most systems, the IFOV and DAS are equal:

$$\theta_{IFOV} = \theta_{DAS} \quad . \tag{7-18}$$

Using the IFOV, the minimum target size is

$$\textit{Target size} = \theta_{IFOV}\textit{Range} = \frac{d}{fl}\textit{Range} \quad . \tag{7-19}$$

Although the Airy disk and IFOV are treated independently, the system resolution is a composite of the two. The transition from the detector-limited to optics-limited region is gradual (Figure 7-6). Here,

$$\theta_{COMPOSITE} = \sqrt{\theta_{AIRY}^2 + \theta_{IFOV}^2} \quad . \tag{7-20}$$

A word of caution. Detectors are not necessarily square. Consequently the vertical and horizontal resolutions may be different. As an approximation, let the average resolution be

$$\theta_{AVE} = \sqrt{\theta_{IFOV-H}\theta_{IFOV-V}} \quad , \tag{7-21}$$

where $\theta_{IFOV\text{-}H}$ and $\theta_{IFOV\text{-}V}$ are the horizontal and vertical IFOVs, respectively. The value θ_{AVE} is the IFOV of a square detector whose area is the same as your rectangular detector.

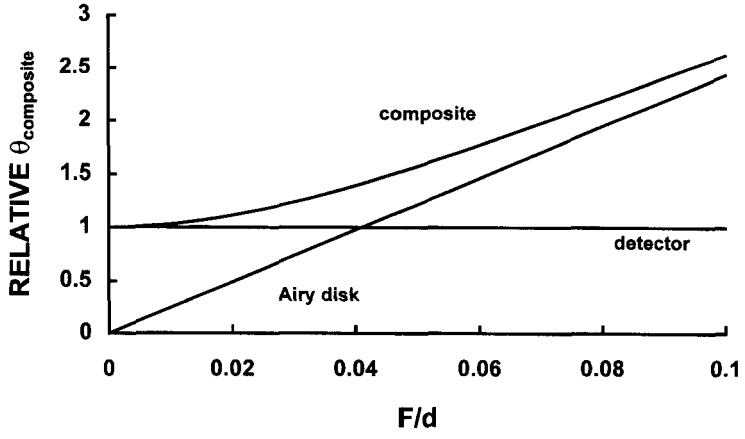


Figure 7-6. Relative composite resolution of a LWIR imaging system as a function of F/d. $\lambda_{AVE} = 10\,\mu m$. For small values of F/d, the system resolution is limited by the detector. For large values of F/d, resolution is limited by the optics. For most LWIR systems, F/d ranges from 0.02 to 0.04.

7.3.3. PIXEL-ANGULAR-SUBTENSE

With staring arrays, the pixel is often used to denote the full cell (see Figure 6-7). The pixel-angular-subtense (PAS) is the angle subtended by the cell:

$$\theta_{PAS} = \frac{d_{CC}}{fl} \quad , \tag{7-22}$$

where d_{CC} is the center-to-center spacing (detector pitch). For 100% fill-factor arrays, $\theta_{DAS} = \theta_{PAS}$.

7.3.4. SLIT RESPONSE FUNCTION

The slit response function (SRF) was developed many years ago when all thermal imaging systems had scanners. The SRF incorporated the response of

the optics, detector, and subsequent electronics. The SRF provides both the imaging resolution and measurement resolution. While commercial systems were characterized by these metrics, military systems always used the IFOV. These resolution metrics are rarely used for staring arrays. The DAS or PAS usually specifies staring array spatial resolution.

The imaging resolution is that target-angular-subtense that produces a 50% response in the slit response function (SRF) (Figure 7-7). For an ideal system, the DAS is twice the imaging resolution. The measurement resolution is approximately the smallest sized target that will be faithfully reproduced in intensity. Although no industry standard exists, it occurs when $0.90 < SRF < 0.99$. It is the absolute minimum size that can be used for accurate temperature measurements.

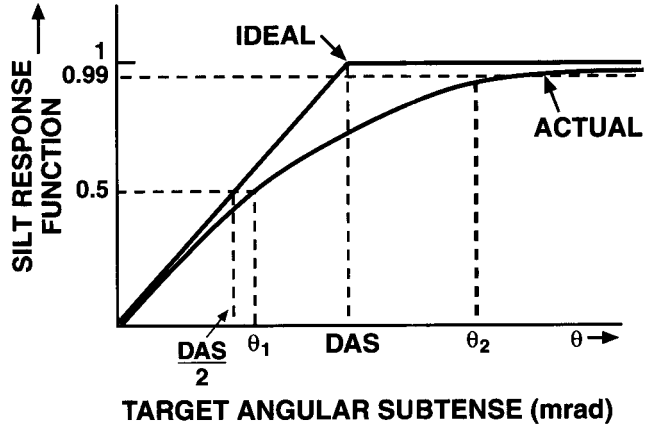


Figure 7-7. Slit response function. The value θ_1 is the imaging resolution and the value θ_2 is the measurement resolution. The measurement resolution occurs when the SRF is greater than 90%.

The test configuration for the SRF is shown in Figure 7-8a. The peak output is recorded for each target size as shown in Figure 7-8b. The SRF depends upon the lens system used. It should be measured with each lens system available. With the advent of staring arrays, the SRF has virtually disappeared.

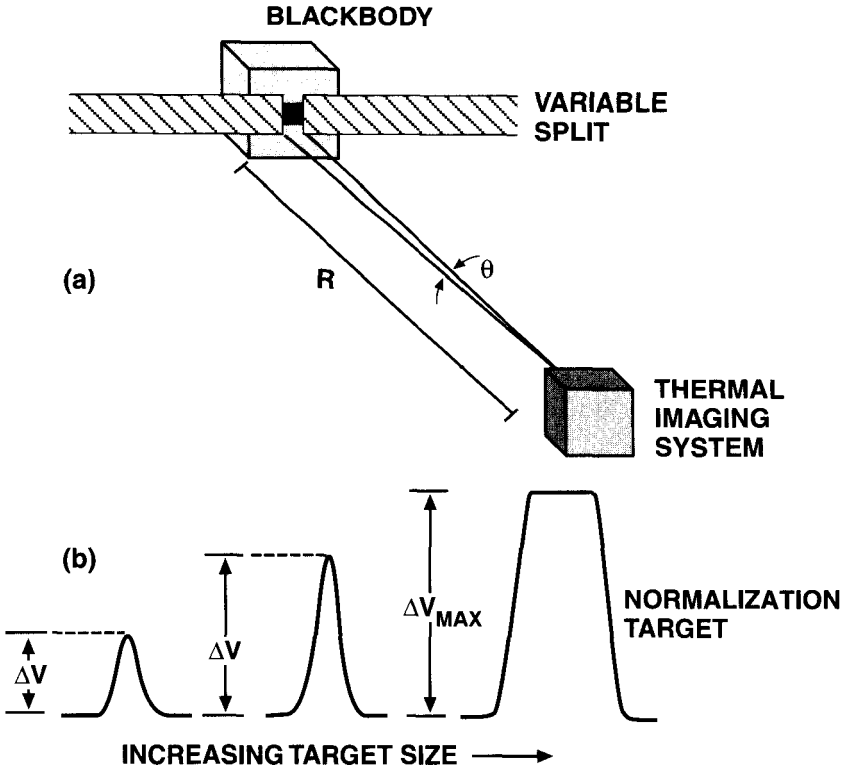


Figure 7-8. (a) Generic test configuration to obtain the SRF and (b) output signal as a function of target size. The distance R_1 should be at least 10 times the system's focal length. Ideally, the variable slit is place in the focal plane of a collimator.

7.3.5. MEASURING IFOV

The measuring IFOV (MIFOV) is similar to the measurement resolution. The MIFOV is the smallest target whose temperature can be accurately measured. It is now the metric of choice for staring systems.

The smallest target that can be accurately measured depends upon the application. In the laboratory, the camera can be carefully aligned to the target. Under these conditions, the MIFOV can be equal to the IFOV. In the field, alignment is more difficult. If placed on a rugged tripod, phasing effects limit the

smallest size that can be easily measured (see Figure 6-9). Conservatively, the target should subtend at least three pixels or

$$\theta_{MIFOV} = 3\theta_{PAS} \quad . \tag{7-23}$$

Phasing effects suggest that the minimum target size should be

$$\textit{Target size} = \theta_{MIFOV}\textit{Range} = 3\theta_{PAS}\textit{Range} \quad . \tag{7-24}$$

However, if handheld, involuntary motion during one frame will blur the image. This can significantly increase the MIFOV to some unknown value. If the image moves by 1/2DAS, the system MTF drops significantly.[1] Suppose the DAS is 2 mrad and a frame is collected every 1/30 second. Then the blurring motion is 1/2 (2)(30)=30 mrad/s. This is equivalent to doing a complete 360° turn in 3.5 minutes or moving 3.5 times *slower* than the second hand on a clock. Clearly, this motion can easily occur with handheld devices.

The MIFOV is a function of the lens system. Generally, but not always, zoom lenses (longer focal length) provide a smaller MIFOV. However, it should be verified for each lens system.

7.3.6. NYQUIST FREQUENCY

Because of sampling effects, the highest spatial frequency that can be faithfully reproduced is limited by the Nyquist frequency. The Nyquist frequency limit applies to periodic patterns. Periodic patterns are rarely seen in nature but are the pattern of choice for laboratory measurements.

The discrete location of detectors in an array act as a sampling lattice whose sampling rate is

$$f_S = \frac{fl}{d_{CC}} \quad . \tag{7-25}$$

The sampling frequency is simply the inverse of the PAS: f_S=1/PAS. The detector pitch may be different in the vertical and horizontal directions. The Nyquist frequency is one-half of the sampling frequency:

$$f_N = \frac{f_S}{2} = \frac{fl}{2\,d_{CC}} \quad . \tag{7-26}$$

This is the highest MRT target that can be used with traditional laboratory procedures. The angle associated with the Nyquist frequency is

$$\theta_{NYQUIST} = 2\theta_{PAS} \quad . \tag{7-27}$$

7.3.7. OPTICAL ZOOM/ELECTRONIC MAGNIFICATION

We are all familiar with zoom lenses that are used with film-based cameras. As the focal length increases, the image size increases. The zoom lens provides more target detail. In addition, since the film has very high spatial resolution, it is possible to enlarge the image significantly and see further detail that is captured on the film negative.

This is partially true for thermal imaging cameras. The DAS decreases as the focal length increases and this allows you to see more detail on the target. Thus, a zoom lens on a thermal imaging system provides a similar capability as a zoom lens on a 35-mm camera (Figure 7-9).

With the advent of digital electronics and image processing techniques, we can enlarge the image (zoom) electronically. Here, the system's focal length is constant and the resolution of the camera does not change. Rather, the new image is created simply be replicating pixels. Electronic zoom is equivalent to moving closer to the monitor or using a larger monitor. No additional detail is available. If excessive electronic zoom is used, the image will appear blocky (Figure 7-10).

Some scanning systems have electro-optical zoom. Here, the scan mirror movement is reduced and the image is resized to accommodate the new scan geometry. While the displayed image appears larger (smaller field-of-view), the resolution has not changed since the focal length has not changed. Increasing the focal length increases the spatial resolution of a detector-based system.

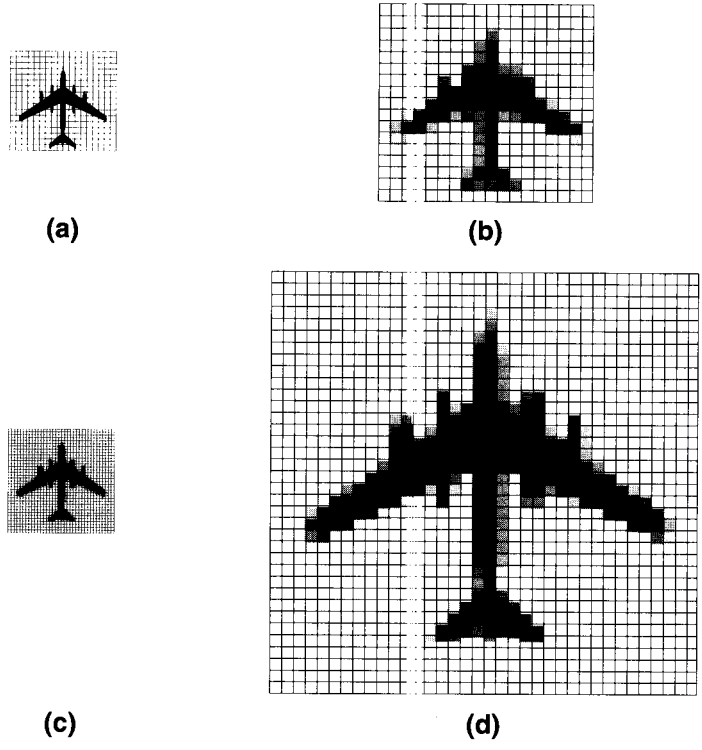
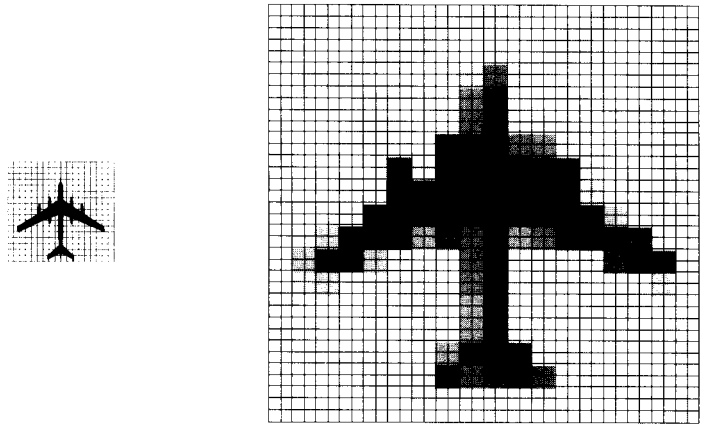


Figure 7-9. Changing the focal length. Each square on the left represents the projected area on a DAS onto the target. Each square on the right represents the image on a monitor. (a) Normal projection, (b) displayed image of normal projection, (c) projection of the DAS when the focal length is doubled, and (d) displayed image of zoomed projection. The image appears twice as large on the monitor. The detector output is an average on the scene detail impinging on it.



(a) (b)

Figure 7-10. Electronic zoom is simply pixel replication. Image (a) is identical with Figure 7-9a. The displayed image (b) is just an enlarged version of Figure 7-9b. Optical zoom (Figure 7-9d) provides more target detail than electronic zoom shown here.

7.4. OBSERVER RESPONSE

The eye provides significant temporal and spatial integration. The eye can easily perceive a well-defined target when the SNR is as low as 0.05. Here, well-defined means something that is easily recognized such as a square, triangle or alphanumeric characters. What this means is that the thermal imaging system may have difficulty in determining a temperature even though the target is easily perceived.

Figure 7-11 illustrates target visibility as a function of SNR when noise is present. With low SNRs, large targets are difficult to perceive. As the SNR increases, modest sized targets become visible. Finally, for high SNRs, fine detail (high spatial frequencies) can be discerned. This figure visually illustrates that MRT values can be less than the NEDT.

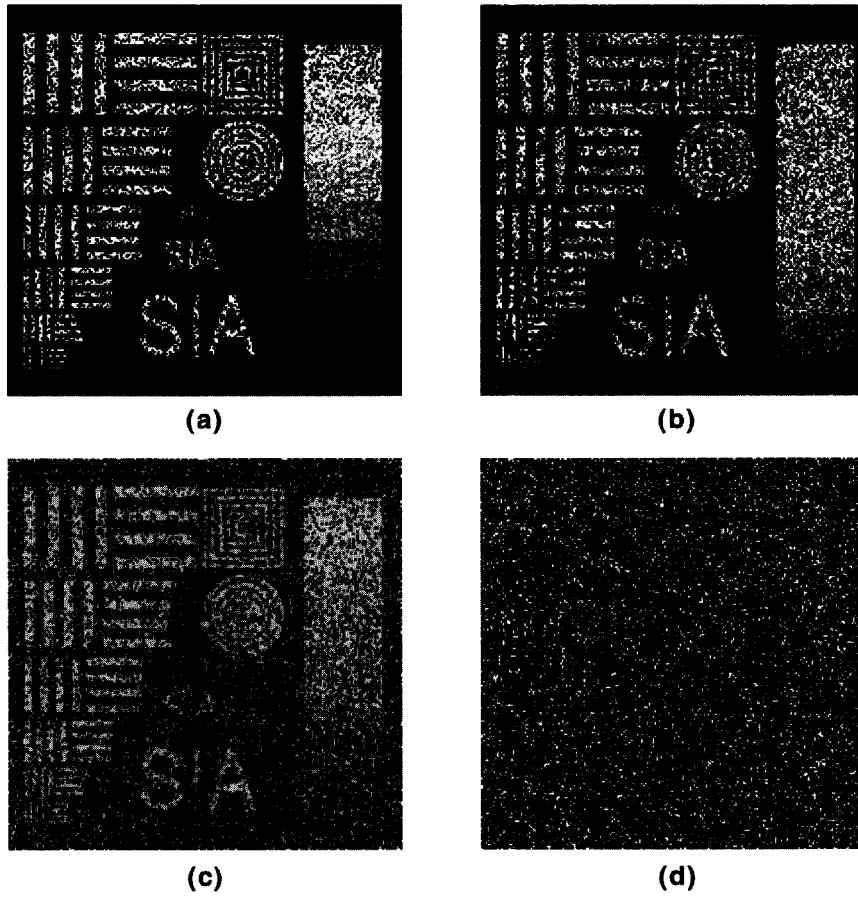


Figure 7-11. Target visibility as a function of the signal-to-noise ratio. (a) ***SNR*** = 0.5, (b) ***SNR*** = 0.3, (c) ***SNR*** = 0.2, and (d) ***SNR*** = 0.1. The imagery was computer generated with the SNRs indicated. It was sent to a laser printer and then reproduced. The SNR of this printed image has not been measured and therefore this figure should be considered as representative.

7.5. MRT AND MDT

Every time an imaging system is turned on, the observer subconsciously makes a judgment about image quality according to his internal rating scale. The military has selected the minimum resolvable temperature (MRT) and the minimum detectable temperature (MDT) as standard measures of image quality.

The military uses the MRT to predict the range at which a target can be detected, recognized, or identified. It is now used to predict the performance of all surveillance systems. This section highlights the MRT concept. Chapter 18, *Surveillance*, describes how the range is obtained from the MRT curve. MRT and MDT are rarely used for condition monitoring or predictive maintenance activities.

The MRT and MDT depend upon the thermal imaging system's resolution and sensitivity. MRT is a measure of the ability to resolve a 4-bar target, whereas the MDT is a measure to detect something. The MRT and MDT deal with an observer's ability to perceive low contrast targets embedded in noise.

MRT and MDT are not absolute values but are perceivable temperature differentials relative to a given background. Sometimes they are called the minimum resolvable temperature difference (MRTD) and minimum detectable temperature difference (MDTD). The term *difference* or *differential* is often omitted because it is understood that it is a differential measurement. The MRT has become a standard metric of image quality. On the other hand, the MDT is rarely used.

The theoretical MRT is

$$MRT = k_{SNR} \frac{NEDT}{MTF} K_{FACTOR} \quad , \tag{7-28}$$

where MTF is the system's modulation transfer function and k_{SNR} is an empirical constant that matches the theoretical prediction to measured values. The value K_{FACTOR} represents various eye "filters" that interpret the various noise component. Because the MTF decreases as the spatial frequency increases, the MRT increases with increasing spatial frequency.

The MRT curve is usually examined in three places (Figure 7-12a). First, the high spatial frequency asymptote is estimated. This is simply an indication of the maximum spatial frequency resolvable through the infrared imaging system. For staring arrays, the highest spatial frequency that can be faithfully reproduced is limited by the Nyquist frequency (Figure 7-12b). The mid-frequency value is a measure of average response and the low-frequency response is a measure of sensitivity.

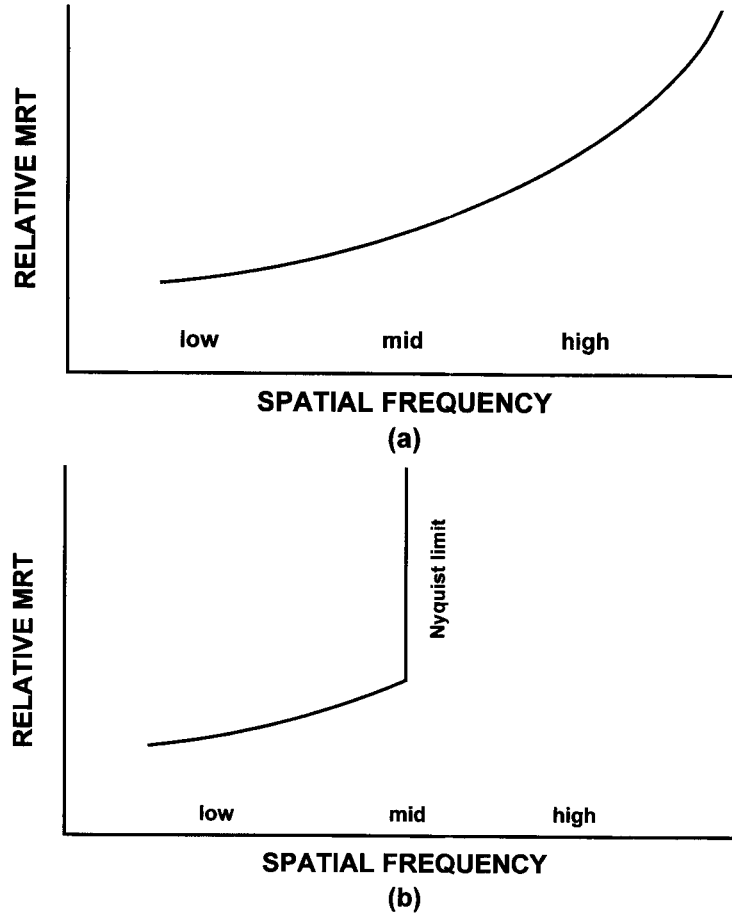


Figure 7-12. Typical MRT responses. (a) Analog scanning systems and (b) staring array. The staring array system response is limited by the system Nyquist frequency.

MRT has the same background temperature dependence as the NEDT. As the background temperature increases, MRT decreases (Figure 7-13). Reference 2 provides the complete MRT equation.

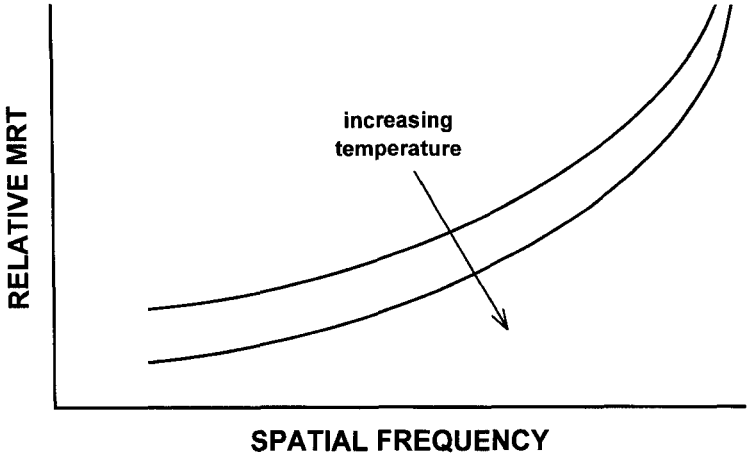


Figure 7-13. The MRT is a function of background temperature.

7.6. REFERENCES

1. G. C. Holst, *Electro-Optical Imaging System Performance*, page 111, JCD Publishing, Winter Park, FL (1995).

2. G. C. Holst, *Electro-Optical Imaging System Performance*, pp. 381-411, JCD Publishing, Winter Park, FL (1995).

8

CAMERA SELECTION

The previous chapters provided the physics of heat transfer, radiative properties of objects, and infrared camera design. Based upon that information (Table 8-1), you can select a system with the performance parameters that are appropriate for your application. Recall that target size is linked to the range and spatial resolution

$$Target\ size = \theta_{RESOLUTION} R \quad , \tag{8-1}$$

and the atmospheric transmittance also depends upon the range to the target:

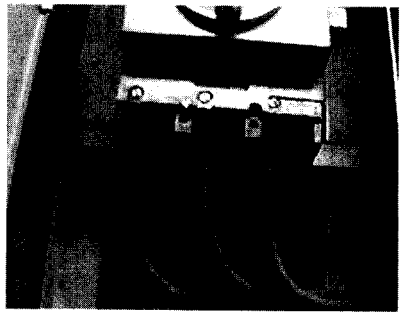
$$T_A = \tau_A^R \quad . \tag{8-2}$$

The required performance parameters are intertwined with the specific application (the environment) and data desired.

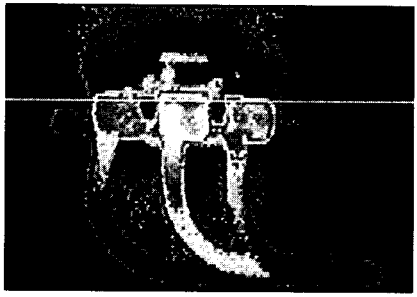
However, other factors must be considered before buying a system (Table 8-2 and Figure 8-1). While this chapter discusses the features listed in Table 8-2, it also poses a number of questions that must be answered before selecting a thermal imaging system. The answers can only be obtained from the manufacturer after you have carefully defined your operational requirements.

Table 8-1
SYSTEM SELECTION by PERFORMANCE PARAMETERS

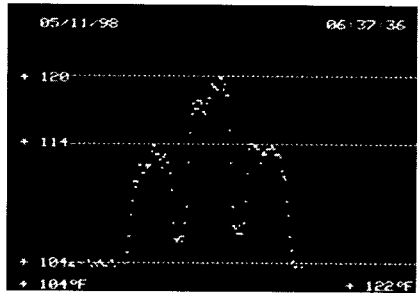
Environment	Camera
Target temperature Target emissivity Target size Atmospheric transmittance Ambient temperature Harsh environment Viewing geometry	NEDT Spatial resolution MRT Spectral response



(a)



(b)



(c)

Figure 8-1. Overheated 350-amp main circuit breaker. The high resistance in this poor connection has an elevated temperature of 19°F. (a) Visible image, (b) a low NEDT allows you to see small temperature changes and a high spatial resolution allows you to see detail (system parameters), and (c) a line trace provides the actual temperature profile (system features). (By courtesy of Gary J. Weil, president, EnTech Engineering).

Table 8-2
SYSTEM SELECTION by SPECIFIC FEATURES

Camera	**Storage and Output**	**Other Issues**
Power/size/weight Dynamic range Frame rate Image processing Calibration	Type of storage Storage capacity Computer interface Data rate Final report	Cost Training Service Repair

8.1. ENVIRONMENT

In a harsh environment that may contain salt spray, excessive moisture, manufacturing effluents, or pollutants, it may be necessary protect the optics with an additional window. As with the optics, the window transmittance is important. If a window is added, then the system must be calibrated with that window in place for accurate temperature measurements.

The ambient temperature affects the NEDT and may affect the calibration. The viewing geometry may increase the minimum target size that can be measured with accuracy.

8.1.1. HARSH ENVIRONMENT

Window materials are not completely transparent. They emit and reflect radiation. Windows can be heated by a variety of mechanisms. Any radiation absorbed will increase the temperature of the window. If mounted on a missile, the window can be aerodynamically heated. If near a hot source, such as a furnace, convection and radiation can heat the window. In all these cases, as the window heats up, the amount of radiation that it emits (self-emission) acts as noise in the same manner that atmospheric path radiance affects the signal-to-noise ratio. It may be possible to blow cool air across the window to reduce its temperature and thereby minimize emission.

Windows can reflect radiation. Since the window is mounted on the system, it will reflect any radiation that originated within the system. Discuss this concern with the manufacturer. Narcissus, a phenomenon that does not exist in the visible, occurs in the infrared. Since the detector is usually cool (particularly true for photon detectors that are cooled to 77K), the reflected radiation consists of the warm housing and the cool detector. Here, the detector can actually "see" itself. This is the narcissus signal. Narcissus becomes more pronounced and annoying as the reflected image becomes more in focus. This results in a dark spot (cold spike) in the displayed image. Tilting the window (Figure 8-2) minimizes the narcissus signal.

In a harsh environment, the window will become dirty. If a window is contaminated with a pollutant such as oil soot, how easy is it to clean?

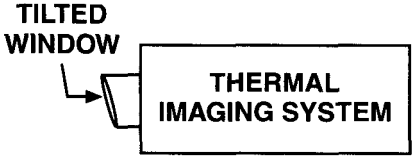


Figure 8-2. Narcissus is present in all thermal imaging systems. Appropriate optical design reduces the narcissus signal below perceptibility. Flat windows must be tilted to avoid narcissus.

8.1.2. AMBIENT TEMPERATURE

The working environment must be considered, If working in a manufacturing facility, the temperature may fluctuate by 10°C (18°F). In foundries and furnace locations, the temperature may be an extreme. Globally, the outdoor temperature may range from –40 to 50°C (-40 to 122°F). At low temperatures, dew or even frost can build up on the lens. While generally not harmful, water is opaque in the infrared. This may require warm air or a dry nitrogen purge across the window to prevent fogging.

Recall that the sensitivity (NEDT) is a function of the background temperature (Figure 7-5). It increases with decreasing temperatures. This means that the system will be noisier at low temperatures and the temperature resolution decreases. MWIR systems tend to have poorer (worst) sensitivity compared to LWIR when the ambient temperature drops. Systems are usually calibrated in an air-conditioned laboratory.

Will the calibration be valid at extreme temperatures and does it drift?

8.1.3. VIEWING GEOMETRY

The simple equation

$$\textit{Target size} = \theta_{RESOLUTION}\, R \quad , \tag{8-3}$$

assumes that the target is normal (perpendicular) to the line-of-sight. However, this is not always the case. When observing a roof from a distance, you are viewing it at an oblique angle. This is distorts the projected DAS (foot print).

Figure 8-3 illustrates the viewing geometry when looking downward. This typifies a roof surface where the observer is standing and is using a handheld camera. Figure 8-4 illustrates the footprint created during oblique viewing.

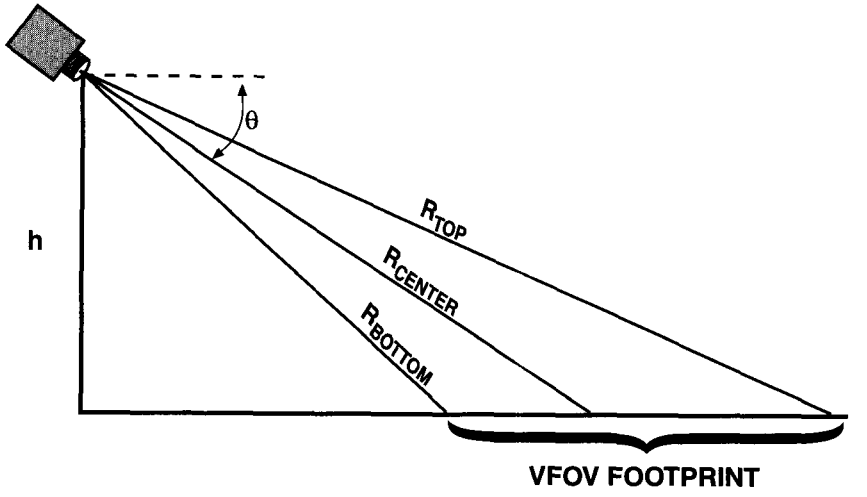


Figure 8-3. Viewing geometry. The depression angle is θ.

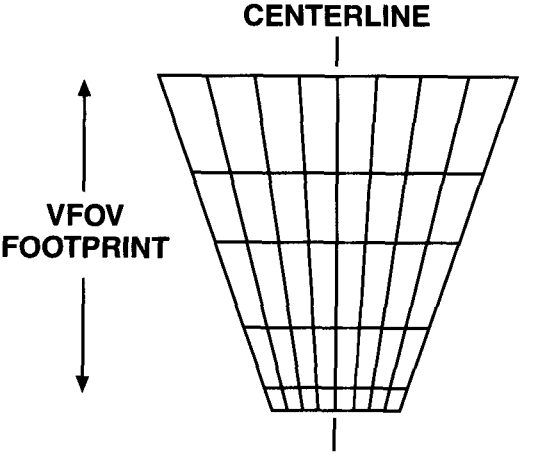


Figure 8-4. Keystone footprints of each pixel during oblique viewing.

In the center of the horizontal field-of-view, the distance to the target at the bottom of the field of view (when looking downwards) is

$$R_{BOTTOM} = \frac{h}{\sin\left(\theta + \frac{VFOV}{2}\right)}, \tag{8-4}$$

where $VFOV$ is the vertical field-of-view and θ is the depression angle. For the top of the FOV

$$R_{TOP} = \frac{h}{\sin\left(\theta - \frac{VFOV}{2}\right)}. \tag{8-5}$$

The vertical field-of-view footprint is

$$VFOV_{FOOTPRINT} = h\left[\frac{1}{\tan\left(\theta - \frac{VFOV}{2}\right)} - \frac{1}{\tan\left(\theta + \frac{VFOV}{2}\right)}\right]. \tag{8-6}$$

Figure 8-5 illustrates the range for a person using a handheld device. When standing, then the height, h, is approximately at 5.5 feet.

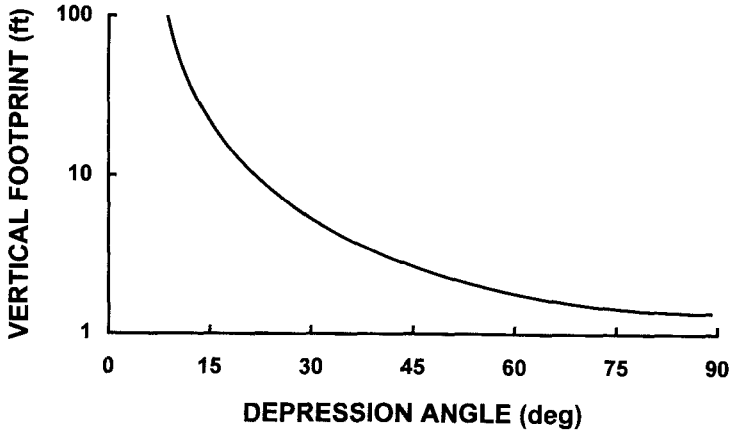


Figure 8-5. Vertical FOV footprint as a function of viewing angle with a 14°-VFOV system. The system is held at 5.5 feet.

Figure 8-6 illustrates the geometry when looking upward (e.g., viewing a tall building). The equations become

$$R_{BOTTOM} = \frac{h}{\cos\left(\theta - \frac{VFOV}{2}\right)} , \tag{8-7}$$

where θ is now the elevation angle. For the top of the FOV

$$R_{TOP} = \frac{h}{\cos\left(\theta + \frac{VFOV}{2}\right)} . \tag{8-8}$$

The vertical field-of-view footprint (Figure 8-7) is

$$VFOV_{FOOTPRINT} = h\left[\tan\left(\theta + \frac{VFOV}{2}\right) - \tan\left(\theta - \frac{VFOV}{2}\right)\right] . \tag{8-9}$$

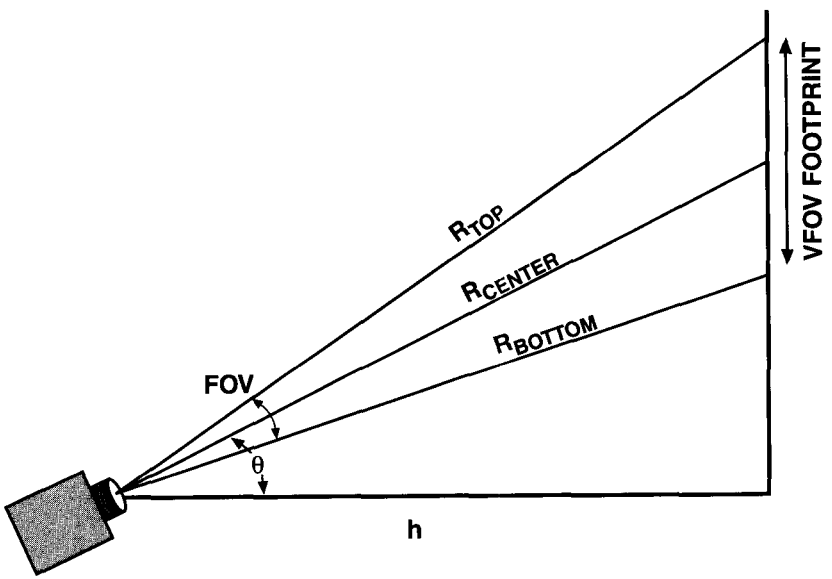


Figure 8-6. Viewing geometry when surveying tall buildings. The distance to the building is h and the elevation angle is θ.

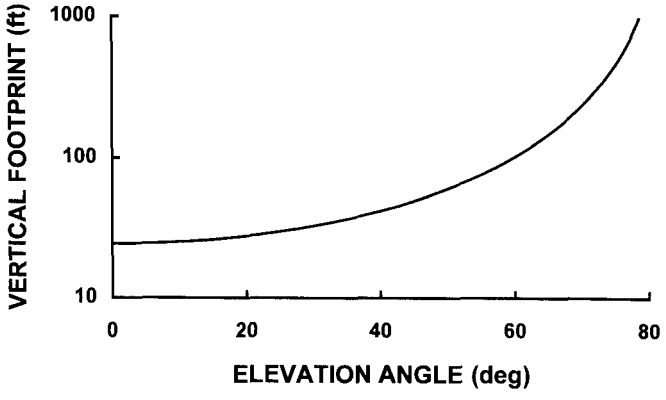


Figure 8-7. Vertical FOV footprint as a function of viewing angle. The observer is 100 feet from the structure and system ***VFOV*** is 14°.

For each pixel, ***VFOV*** is replaced by the ***DAS*** in the above equations. Now θ is the depression (elevation) angle of the specific pixel. Of more interest is the minimum size necessary to make accurate temperature measurements. Here ***VFOV*** is replaced by θ_{MIFOV} (Figures 8-8 and 8-9). As the viewing angle increases, the minimum measurable target size increases dramatically.

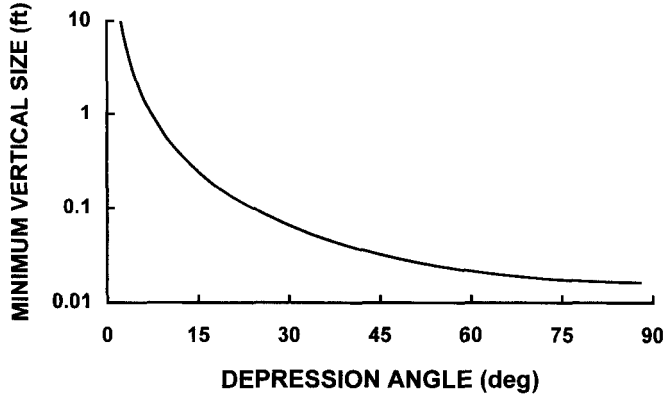


Figure 8-8. Minimum target size that can be accurately measured when θ_{MIFOV} is 3 mrad. The height is 5.5 feet (looking downward).

If the target is very large, then it is sometimes useful to combine many individual pictures to create a mosaic of the overall target. If each image was viewed normally, it is easy to create the mosaic. If viewed at an angle, then the footprint varies across the field-of-view (Figure 8-10). If the angle is large, extensive computer programming is required to rectify the image.



Figure 8-9. Minimum target size that can be accurately measured when θ_{MIFOV} is 3 mrad. The distance is 100 feet or 30.5 m (looking up).

If viewing the target (e.g., a roof) from an aircraft, aircraft motion must be considered to rectify the image. Pitch, roll, yaw, and altitude variations distort imagery. These quantities are difficult to control. Ideally, you should look straight down to avoid oblique imagery.

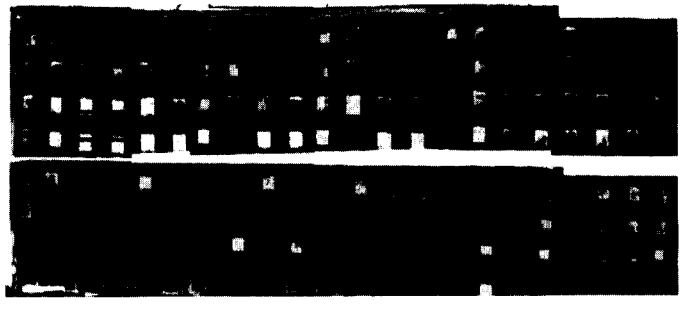


Figure 8-10. Mosaic of Harrah's Passport Casino Hotel in St. Louis. Each thermogram was taken at a slightly different distance and elevation. This produced different footprints. Although a computer algorithm could have rectified the image, this mosaic is adequate to identify problem areas. The heat loss through the windows is a function of the interior window dressing and room temperature. If the shades, curtains, or blinds are drawn, heat loss is minimal. (By courtesy of Gary J. Weil, president, EnTech Engineering)

8.2. CAMERA

The camera can be mounted on a host of platforms ranging from handheld to vehicle to aircraft. With aircraft mounting the system may have to be vibration isolated (line-of-sight stabilized). Note that vehicle or aircraft mounting probably will need special brackets and mounting plates. Safety considerations limit the location of brackets.

With mounted systems, are there any special restrictions?

8.2.1. PHYSICAL ATTRIBUTES

For handheld devices, weight and size are of concern. Here the weight of the entire system, including batteries and video recorder, must be included.

For battery operated devices, how long do the batteries last?

For all systems, ruggedized design is important. No matter how careful you are, the system will be subjected to shocks and bumps. It may even be accidentally dropped. For vehicle and aircraft mounting, the system must be able to withstand all stresses imposed by the engine, transmission, and flight envelope of the aircraft.

Ruggedization is expensive and a cost-benefit trade-off must be made. If protecting the system from damage due to an accidental drop is too expensive, treat the (un-ruggedized) system with extreme care: Do not drop it!

8.2.2. DYNAMIC RANGE

The temperature difference between the background and the target is crucial to thermal imaging system design. Both the background and target are radiating a large amount of energy whereas the difference can be very small. This leads to dynamic range problems and requires careful settings of both gain and level. Dynamic range can be extended at the expense of the minimum measurable signal at any particular gain setting.

Figure 8-11 illustrates two different gain and level settings. In Figure 8-11a, the input range, $T_2 - T_1$, is large and it produces a large output range, $V_2 - V_1$. This corresponds to a low gain system. Figure 8-11b illustrates a high gain system: $T_4 - T_3$ is small and output range, $V_2 - V_1$, is the same. In both cases, the lower voltage, V_1, appears as black and the higher voltage, V_2, appears as white on the monitor.

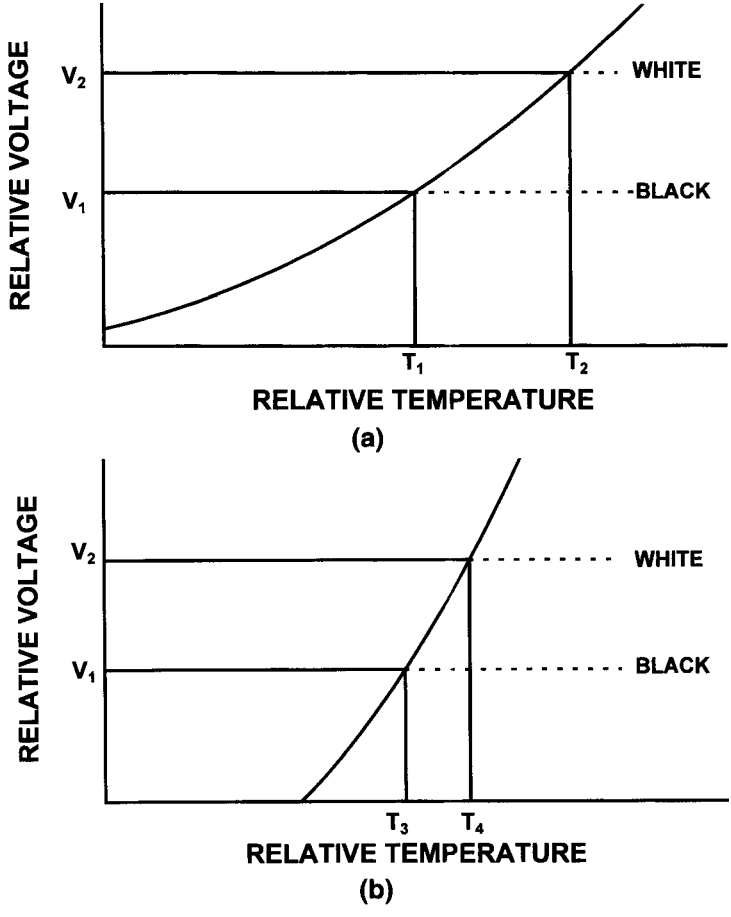


Figure 8-11. Gain and level variations. (a) Low gain and (b) high gain. The dynamic range is $T_2 - T_1$ or $T_4 - T_3$.

The voltage difference, $V_2 - V_1$, is usually digitized. Thus the difference is broken up into discrete levels. The smallest level, the least significant bit (LSB) represents the temperature resolution afforded on that particular gain setting. Although the relationship between input temperature and detector output is nonlinear, a look-up table in software provides a linear relationship between input temperature and camera output voltage.

The dynamic range is the temperature range measured from the minimum temperature. The level adjustment selects that minimum value. For example, a 100°C

(212°F) dynamic range could measure temperatures from 0°C to 100°C (32 to 212°F), 50°C to 150°C (122 to 302°F), or 70°C to 170°C (158 to 338°F). The minimum and maximum values depend upon the system design.

We are assuming that the zero level is mapped into black and the maximum level (255 on an 8-bit system) is mapped into white. Any temperature that is less than the minimum will appear as black. We would not see it. Any temperature above the maximum will appear as white. We will see that target but the signal is in saturation and we cannot measure its temperature accurately. In many of the images in this book, the heated component exceeds the dynamic range of the imaging system. The components appear white (saturate the system). No detail can be seen in a saturated image.

Suppose the input temperature range is 200°C (360°F) and an 8-bit digitizer is used. Then the thermal resolution on this gain setting is 200°C /256 = 0.77°C (1.39°F). If the gain is increased so that the input range is 100°C (180°F), then the thermal resolution becomes 100°C /256 = 0.39°C (0.7°F). Note that this limitation on thermal *resolution* may be much larger than the thermal *sensitivity* (NEDT).

To measure the NEDT accurately, several digital levels must be devoted to noise. Consider a system whose ***NEDT*** is 0.1°C. With an 8-bit system, there are 256 levels. For accurate noise measurement, assign 4 levels to noise. Then the dynamic range is

$$DR = 256\left(\frac{0.1}{4}\right) = 6.4\ ^{0}C \quad . \tag{8-10}$$

This represents a high gain system. With an 8-bit system, the operator must constantly change the gain and level settings to see all the detail present. Therefore, new systems digitize up to 16 bits. The number of bits selected depends upon the NEDT and the system's application (required dynamic range).

As the number of bits increases, the potential thermal resolution increases. Table 8-3 provides the thermal resolution for a 200°C dynamic range. If the NEDT is 0.1°C, there is no point in using more than 13 bits because any more will simply be devoted to noise. That is, the thermal *resolution* afforded by the digital step cannot decrease the thermal *sensitivity* as specified by the NEDT. On the other hand, if we devote 4 levels to noise, then the maximum dynamic range with a 16-bit digitizer *could* be

$$DR = 65536\left(\frac{0.1}{4}\right) = 1638\ ^{0}C \quad . \tag{8-11}$$

The required dynamic range depends upon the application (Table 8-4). Generally, manufacturers select the number of bits that permit both NEDT measurements and full dynamic range measurements without any gain or level adjustments. This makes the system easier to use. However, many computer systems only support 8-bit imagery. This creates a challenge in image transfer from the camera to the computer.

Table 8-3
THERMAL RESOLUTION for ΔT=200 °C

Number of bits	Number of Levels	Thermal Resolution
8	256	0.771
9	512	0.391
10	1024	0.195
11	2047	0.0976
12	4094	0.0477
13	7192	0.0244
14	16374	0.0122
15	32767	0.0061
16	65536	0.0030

Table 8-4
TYPICAL TEMPERATURE RANGES

Application	Temperature range
Thin film plastic, low temperature glass	50 to 500°C
Glass and ceramic processing	200 to 1500°C
See through clean combustion flames and hot gases	500 to 2000°C
Predictive maintenance	Ambient to 100°C
NDT	Ambient to 50°C
Life sciences, medicine	Ambient to 50°C

8.2.3. FRAME RATE

When taking images of static targets (e.g., roof, building, buried objects) or slow-moving targets (typical of surveillance activities), the standard frame rate of 30 Hz (US) or 25 Hz (European) is adequate. Using conventional frame rates ensures that imagery can be easily stored on videotape.

For fast moving objects such as rotating machinery or viewing transient events as with NDT inspections, higher frame rates are usually required. Here, a stop-action approach is necessary and the camera must be synchronized to the thermal event. With sufficiently high frame rates, image blurring will be minimal. This is in effect a strobe light condition. For rotating equipment, you do not have to capture every rotation. It is usually adequate to capture every 5th or 10th rotation. If the rotating object has a specific hot spot, then synchronization is necessary (see Figure 2-18).

If the object is uniformly heated, synchronization is not needed. However, the image will be blurred. But this is not important for certain applications such as locating overheating bearings. The mechanical applications illustrated in Chapter 16 do not require synchronization. Whether synchronization and high frame rates are required depend upon the application and desired results.

Note that as the frame rate increases, the integration time must decrease. For example, at a 30-Hz frame rate, each frame views (integration time) the target for a maximum of 1/30 s or 33 ms. If the frame rate increases to 100 Hz, then the viewing time (integration time) drops to 10 ms. For staring arrays, the signal produced by the camera is proportional to the integration time. Therefore, the voltage produced drops as the integration time decreases. This loss in signal can be overcome by increasing the camera's internal gain. However, for staring arrays, the NEDT is inversely proportional to the square root of the integration time. As the integration time decreases, the NEDT increases. Thus, high frame rates can reduce the signal-to-noise ratio in staring arrays significantly. This reduction in SNR can be overcome by frame integration. The SNR improves by the square root of the number of frames averaged. With repetitive events, such as rotating machinery, frame averaging is an important image processing technique. However, frame averaging will degrade the image of transient events. Note that scanning arrays are more difficult to synchronize to a thermal event.

This concept of noise versus integration time is similar to photographic film performance. For high quality, low noise imagery, slow film (e.g., ASA 100) is used. But the shutter speed must be long (e.g., 1/30 s). For fast moving objects, high-speed film (e.g., ASA 1000) is used with a commensurate reduction in shutter speed (e.g., 1/1000 s). However, the faster film provides a grainy (noisier) picture.

8.2.4. IMAGE PROCESSING

Many cameras have built-in image processing capability. Indeed, we can say the modern thermal imaging systems are mini-computers with a detector attached. Cameras come with a large variety of image-processing software. You select the camera that has the software of interest to your application. For surveillance systems, image processing includes automatic level and gain control. This insures that the image is optimized regardless of the time of day. Military systems may also have target cuers and automatic recognizers.

For temperature measuring devices, typical built-in functions include isotherms, color rendition, spot temperature measurements, temperature profile, and area-weighted temperature. Area weighted functions are also called region-of-interest (ROI) functions. Most systems offer emissivity correction that allows the user to enter both the target emissivity and the surrounding temperature.

Additional image processing software can be loaded into your computer. Large numbers of off-the-shelf imaging processing software programs are available. However, you must insure that the software is compatible with the image format created by the camera. Although third-party software providers claim 100% compatibility there are always glitches. These problems are usually unknown until they surface in your application. It is recommended to discuss your software needs with the your camera manufacturer and with other users.

Additional features, usually performed by the external computer, include pixel-by-pixel emissivity correction and time-temperature history. Pixel-by-pixel correction is useful when there are multiple targets and each has a different emissivity such as that encountered with printed circuit board analysis. The time-temperature feature allows you plot the temperature as a function of time. This is important for targets that undergo cycling effects: Motors, HVAC (heating, ventilation, and air conditioning) systems, conveyor belts, and manufacturing processes that turn on and off.

Of interest is the ability to subtract one image from another. The comparison of two images is called[1] differential infrared thermography (DIT). If the standard image is a baseline, then the difference will provide an image of components that are different from the baseline. If a preset tolerance table exists, then the components that are out of tolerance are highlighted. If the surrounding temperature is the same on the baseline and current image, the subtraction technique removes the surrounding temperature influence.

8.2.5. CALIBRATION

Standard performance parameters were discussed in Chapter 7. All thermal imaging systems must be characterized, and for those that provide temperature measurements, calibrated. Since lenses have different f-numbers and different transmittances, the system must be calibrated for each lens. Of prime concern is how long the calibration is valid.

How often does the system require recalibration?

What is the repeatability and drift?

What is the cost of recalibration?

Finally, who will calibrate the system and how long does it take? What is the down time for calibration?

To measure temperatures, commercial cameras usually have a target emissivity correction capability. While the manufacturers strive for excellent corrections, deviations may occur because you do not know the object's true emissivity. Error in emissivity is probably the biggest source of error in temperature measurements. The second source of error is not knowing the atmospheric transmittance. These errors are induced by the user and are not related to the system's calibration.

8.3. STORAGE AND OUTPUT

When operating in the field, it is necessary to store imagery for later interpretation. The imagery may be stored on a video tape player or PCMCIA card. In both cases, you must have the right computer interface to access the imagery. The "standard" video signal has a format that is consistent with black-and-white or color formats. Because of bandwidth limitations, analog signals are digitized into 8 bits. The camera may create more data: it may consist of 12 bits and have additional information such as dynamic range and level setting. If these additional data are present, then the computer must be able to read that data and also strip it off to display the image on the monitor.

Understand your video standards. For example, RS-170 timing supports a detector array that contains about 640×480 elements. As a result, commercial frame grabbers with convert an analog signal into about 640×480 pixels. This electronically created pixel resolution may not be related to the resolution of the camera. Today, many uncooled systems only have 320×240 detector elements. Thus the system resolution is determined by the array and not by the computer electronics. Note that

in common parlance, computer monitors support 24 bits. This is deceiving. There are three colors and each color has only 8-bits of information (3×8 = 24). The gray scale is only 8 bits.

If the camera produces more than 8 bits, how is the data transferred to the computer?

Most image processing software and computer interfaces are designed to operate at 30 Hz (standard U.S. frame rate) or 25 Hz (standard European frame rate). If a higher frame rate is required, such as that required to view transient events, you must ensure that your frame grabber can operate at the non-standard frame rate.

Always keep your final product in mind, which is typically the final report. Make sure that your computer program can easily generate that report. This includes text that describes the test, test conditions, and imagery. If you supply the imagery on a memory device (disk or PCMCIA card), then you must insure that your customer has the resources to view the imagery. Remember, "compatible" software may have glitches.

8.4. OTHER ISSUES

It is false economy to buy yesterday's components because they are cheaper. In general, a less expensive system provides less capability. It may have (1) lower spatial resolution, (2) more noise, (3) smaller dynamic range, (4) no data storage capability, (5) no on-board image processing, (6) or not be ruggedized. Consider the cost of the *entire* system: camera, data storage, interfaces, battery charger, computer, computer program, and printers. As always, the list is driven by the application and desired data. Although these systems may be less costly, it does not mean that they will not perform for your application. For example, lower spatial resolution can be overcome with higher magnification optics (longer focal length). However, this reduces the field-of-view.

Training issues are described in Chapter 9. It is part of the overall system cost and it takes time and time is money. The amount of training depends, in part, on the system's ease of use. Complex systems will take longer to master than simple systems.

8.5. REFERENCES

1. H. Kaplan, "An Application of Differential Infrared Thermography in Power Generation Facilities," in *Thermosense XVII*, S. A. Semanovich, ed., SPIE Proceedings Vol. 2473, pp. 67-74 (1995).

9

OBSERVER TRAINING

Interpretation of the results of an infrared inspection depends upon decisions made by an observer. The results vary with training, motivation, and visual capacity of the observer as well as the environmental setting. To obtain any degree of consistency, it is assumed that the observers are qualified.

The process of observing is somewhat a learned ability. It is a perceptual one, accomplished by the mind, affected by and incorporating other sensory systems such as emotions, learning, and memory. The relationships are many and not well understood. Seeing varies among individuals and temporally within an individual. Because each person is different, individual characteristics can affect detection threshold. Age, experience, personality, mood, and perception are just a few such characteristics. During the course of an evaluation, many changes take place that could influence the outcome. People learn new methods, have new experiences, change moods, and become fatigued.

Whether commercial or military, the user must fully understand the operation of the thermal imaging system. He must understand that real targets (discussed in Chapter 11, *Target Signatures*) have fluctuating temperature distributions. Outdoor targets are subjected to sun, wind, and rain, each of which can dramatically change the target's thermal signature. For both indoor and outdoor targets, the signature depends upon the operating conditions. For most commercial applications, you want the target to be operating under full load. This should create the maximum temperature difference or maximum temperature rise.

Given that a target signature exists, the observer must be trained in system usage. This includes selecting the appropriate field-of-view, gain, and level settings to optimize the displayed image and to reduce measurement error. When looking for relative changes over a long time period, it is necessary to set the camera to the same gain and level each time.

Both qualitative and quantitative infrared techniques require a high level of training and understanding. The observer must have a thorough understanding of target signatures to separate the true target (or defect) from false anomalies. Accurate temperature measurements can save millions of dollars in unnecessary downtime and maintenance.

Elements of a successful training program include infrared theory and principles, heat transfer theory, operation of infrared equipment, how to conduct inspections, and temperature measurement techniques. Training should include application specific information, how false anomalies might look, how to analyze data, and how to prepare a report. Signature analysis is based upon a combined knowledge base of schooling, personal experience, and methods learned from others.

Training is not a one-time event. One must strive for continual improvement. Operators need continual training to maintain current skills, learn new techniques and develop new applications. Training occurs in many venues, including formal short courses, attendance at conferences, and interaction with other industry professionals.

9.1. CERTIFICATION

The American Society for Nondestructive Testing (ASNT) provides guidelines for Level I, II, and III certification.[1] Briefly, they are:

Level I

An individual with Level I certification is qualified to perform specific calibrations, specific tests, and specific evaluations. He/she follows written instructions and is capable of recording the test results.

Level II

An individual with Level II certification is qualified to set up and calibrate equipment. He/she can interpret and evaluate results with respect to applicable codes and standards. He/she is thoroughly familiar with the scope and limitations of the method for which he/she is qualified. The Level II individual provides on-the-job training for Level I personnel.

Level III

An individual with Level III certification shall have the skills and knowledge to establish techniques and procedures and to verify the accuracy of procedures. He/she can interpret codes, standards, specifications and procedures. The Level III individual will also have general familiarity with the other NDT methods, as well as knowledge in material science, manufacturing methods, and product technology. He/she shall be capable of conducting or directing the training and examining of personnel in the methods for which he/she is qualified.

9.2. MILITARY USERS

The military is primarily interested in one application: To be able to detect and classify the enemy at a maximum range. This means that the system gain is maximized and this presents a somewhat noisy image to the observer. Although no certification exists for military users, they are trained to optimize system gain and level to maximize detection, recognition, and identification capabilities. In addition, the user must understand how environmental and battlefield conditions affect target signatures. Targets are more difficult to see during heavy cloud cover (no heating from the sun) and after rain. Water conducts heat away from hot spots and evaporating water cools objects. Mud and dirt act as insulators and thereby modify the target signature. The atmospheric transmittance can vary dramatically from location to location. For example, in a humid area, tanks may only be visible to 5 km (3.15 mi) whereas the same tank may be detected out to 10 km (6.3 mi) in the desert. The military user does not have the luxury of waiting for good weather.

9.3. MRT OBSERVERS

MRT is the laboratory assessment of image quality and is used to characterize and compare the imagery from different infrared systems. It is requires motivated, trained observer to get consistent results. Two different observers can obtain different detection thresholds (Figure 9-1) with either response being equally likely. The responses may be both above the average, below the average, or one above and one below. In addition, the same person may obtain different results depending upon the time of day.

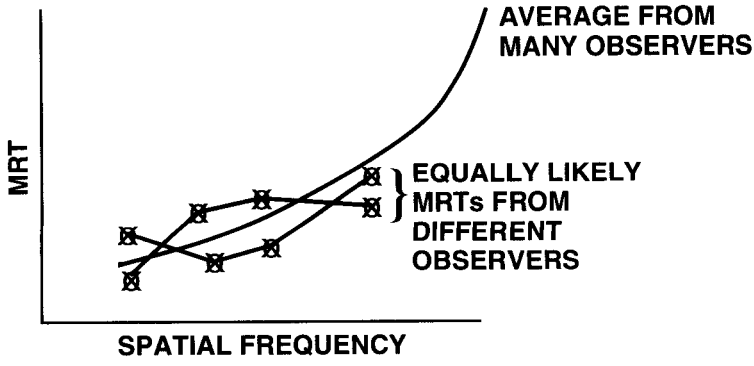


Figure 9-1. Equally likely observer MRT responses.

Visual performance can fluctuate considerably over a period ranging from a few minutes to several weeks.[2,3] The psychophysical frequency-of-seeing curve includes these fluctuations. At any particular moment in time, an individual's response may be significantly different from the population average.[4] MRT variability as high as 50% are often cited from laboratory-to-laboratory with 20% variability reported at one laboratory.[5] Differences in detection criteria, test procedure, test equipment, as well as fatigued observers may be contributors to the variability.

A qualified MRT observer is difficult to define. The qualified observer should be consistent, have a low detection threshold, and have good visual acuity. New observers should compare their detection thresholds to those obtained by existing qualified observers. As the individual's variability is reduced, he becomes a consistent observer. But this does not mean that he will have a lower detection threshold value. It simply means that he will perform consistently and that his particular frequency-of-seeing curve is sharp. This training may take up to six months. There is no industry wide standard by which to rate MRT observers nor any national school to train MRT observers.

There is a myriad of methods available to test visual capacity. The observer should have corrected 20/30 or better acuity with corrected astigmatism. Visual acuity tests only provide information about how well an observer can resolve high contrast targets. Good visual acuity does not ensure low threshold detection capability. But MRT and MDT are measures of threshold detection of low contrast targets embedded in noise (see Section 7.4, *Observer response* and Section 7.5, *MRT and MDT*).

Finally, sustained effort is required from well-trained staff to maintain consistency within a given laboratory. The observer must be healthy and alert. An operator who is neither tired or under stress should achieve the best consistency.

9.4. REFERENCES

1. The American Society of Nondestructive Testing (ASNT) provides general training requirements. Several independent organizations offer the training. ASNT is located at 1711 Arlingate Lane, PO Box 28518, Columbus, OH 43228-0518.

2. I. Overington, *Vision and Acquisition*, pp. 32-47, Pentech Press, London (1976).

3. I. Overington, "Image Quality and Observer Performance," in *Image Quality*, J. Cheatham, ed., SPIE Proceedings Vol. 310, pp. 2-9 (1981).

4. J. P. Mazz, "Analysis of Observer Variability in the Assessment of FLIR Performance," in *Infrared Imaging Systems: Design, Analysis, Modeling and Testing VII*, G. C. Holst, ed., SPIE Proceedings Vol. 2743, pp. 2-11 (1997).

5. C. W. Hoover, Jr., and C. M. Webb, "What is an MRT? And How Do I Get One," in *Infrared Imaging Systems: Design, Analysis, Modeling and Testing II*, G. C. Holst, ed., SPIE Proceedings Vol. 1488, pp. 280-288 (1991).

10
INTRODUCTION to APPLICATIONS

For many applications, a change in temperature may signify a change in an object's operating condition. By monitoring an object's temperature, we can assess its "health." Any thermal anomaly, whether the presence of heat or the absence of heat, may suggest that a problem exists.

Condition monitoring and predictive maintenance activities have many well-defined applications. Consequently, we hear the most about these activities. However, numerous other applications exist. The military, the early leader in thermal imaging system design, is primarily interested in target detection. As a surveillance tool, imaging systems are now used for border patrol, law enforcement, search and rescue, and drug interdiction.

Less advertised areas include medical, biological, geological, and remote sensing applications. Many research and development (R&D) endeavors have employed or at least entertained the possibility that a thermal imaging system can provide answers that cannot be elicited by other means.

Measurements can be either qualitative or quantitative. Qualitative measurements compare the thermal signature of one component to that of an identical (or at least similar) component under the same (or at least similar) operating condition. The object's "health" (or anomaly) is assessed by the intensity variations between the two similar objects without assigning temperature values. For many quality control and process monitoring activities, we have a baseline or "golden" thermogram. All future thermograms are compared to the "golden" thermogram. Any thermal difference may suggest a problem.

Qualitative measurements are appropriate for those applications where the precise temperature is not required. These include surveillance, location of buried objects, roof inspections, building inspections, and geological surveys. It is also used to find vacuum leaks, air leaks, pipe blockage, and the fluid level in a storage tank.

Quantitative measurements provide the true temperature of the object. Accurate values are required for most condition monitoring and predictive maintenance activities. When the temperature is outside a preset range (can be either higher or lower), a course of action is taken. This usually means the repair or replacement of the component.

A thermal anomaly (also called an exception, deficiency, or fault) refers to a component whose temperature is different than expected. The temperature may be either greater of less. Generally, the term *deficiency* or *exception* is restricted to those components that appear to be non-operational, not performing properly, or defective. This is most often applied to electrical and mechanical inspections.

Applications can be described by industry (e.g., automotive), component generic design (e.g., motors), scientific identification (e.g., geology), or quantitative versus qualitative. There is no best way to place similar activities into a single table or chapter. For example, the automotive industry uses motors to manufacture cars. Motors can be described by their electrical function or mechanical function: windings burn out and bearings wear out. But an overheating motor may also indicate an electrical distribution problem.

No book can provide details on all applications. This chapter is a potpourri of applications arranged in no particular order. Its purpose is to provide you with ideas that expand your horizon. This book covers only a very small portion (Table 10-1).

Table 10-1
CHAPTER TOPICS

Chapter	Topics	Typical test
Chapter 13 Building envelope inspection	Building science, windows, and insulation	Qualitative
Chapter 14 Roof inspection	Water ingress and solar loading	Qualitative
Chapter 15 Power distribution	Power lines and transformers	Quantitative
Chapter 16 Electrical/ Mechanical inspection	Electrical distribution within a building, circuit breakers, motors, pulleys, and gears	Quantitative
Chapter 17 Buried objects	Storage tanks and pipe lines	Qualitative
Chapter 18 Surveillance	Military requirements and search and rescue	Qualitative
Chapter 19 Nondestructive testing	Detection of voids, delaminations, and corrosion	Quantitative
Chapter 20 Process/quality control	Various applications	Qualitative and quantitative

As you read the remaining chapters, you will see many generic approaches that can be used for other applications. Chapter 11, *Target Signatures* and Chapter 12, *Temperature Measurements* are generic to all applications. Addition information on various applications can be found in Appendix C, *Thermal Sensing and Imaging 1980-1999.*

This book provides thermal signature theory and lists numerous applications supported by imagery. The proper blending of experience, knowledge of heat transfer, and accurate data collection is required for valid data interpretation.

10.1. CONDITION MONITORING

Tables 10-2 through 10-5 were supplied by the Academy of Infrared Thermography. The table entries represent their way to classify condition monitoring and predictive maintenance applications.

Table 10-2
ELECTRICAL INSPECTION
(By courtesy of the Academy of Infrared Thermography)

Component	Conditions detected
Bus duct	Unbalanced loads and high resistance in joints, bus plug-ins, and fuse connections.
Emergency power	Poor battery terminal connections, dead cells in batteries, defective or inoperative contacts, or stand-by switches.
Lighting	Poor connections and overheating ballasts.
Motors/generators	Unbalanced loads, shorted or open windings, blocked cooling passages, and overheating of brushes, slip rings and commutators.
Switches, load centers, motor control centers, power factor capacitors, bus bars, and fuses	Loose or corroded connections, poor contacts, unbalanced loads, overloading, harmonics, eddy currents, and hysteresis.
Transformers	Loose/deteriorated connections, overheated bushings, overloading, unbalanced 3-phase load, blocked/restricted cooling tubes, low fluid level, and bad pothead connections.
Transmission lines, lightning arrestors, circuit breakers, conductors, splices, disconnects, and compression clamps.	Loose/corroded/improper connections and splices, inoperative capacitors, failed lightning arrestors, poor breaker connections, overloading, and broken conductor strands.

Table 10-3
MECHANICAL INSPECTION
(By courtesy of the Academy of Infrared Thermography)

Component	Conditions detected
Drives, conveyors, and pillow blocks	Overloaded bearings or rollers and misalignment of shafts or pulleys.
Heavy-duty equipment: tires, bearings, brakes, pulleys, gears, and ball mills	Overheating brakes, tires, bearings, pulleys, gears, gear or pulley misalignment, and transmission/gearbox overheating.
Hydraulics	Defective seals, overheating lines, and unequal flow.
HVAC systems	Air leaks, energy loss, clogged condenser/ heat exchanger tubes, and refrigerator and air conditioner efficiency.
Internal combustion engines	Valve or injector malfunction, blocked radiator tubes and oil coolers.
Mechanical drive turbines and small turbine generator units	High lube oil temperature, high bearing temperatures, drain valve blockage, steam trap blockage, faulty stop/control valve operation, and leaking shaft seals.
Presses	Defective bearings and V-belts, gearing fit, adequacy of lubrication, and clutch and brake efficiency.
Pumps, compressors, fans and blowers	Overheated bearings, high compressor discharge temperature, high oil temperature, broken or defective valves, or rings, and misalignment of drive belts and gears.

Table 10-4
BUILDING/STRUCTURE INSPECTION
(By courtesy of the Academy of Infrared Thermography)

Component	Conditions detected
Concrete	Bridge deck delamination, rebar deterioration and problems with embedded heating systems and steam lines.
Envelope	Heat loss, missing/deteriorated/misapplied insulation, air leakage, moisture problems in wall structure, dew on inner walls, window seal failure, and room airflow
Heating system	Determine inefficiencies in radiant ceiling panel, slabs, radiators, panel heaters, carpet heaters, and electric blankets.
Roof	Leaks and moisture intrusion on flat roofs.

Table 10-5
GENERIC APPLICATIONS
(By courtesy of the Academy of Infrared Thermography)

Component	Conditions detected
Aircraft: fuselage, composites, engines, propellers, brakes, and tires	Delaminations, voids, and moisture intrusion in composites. Blocked surface cooling holes in hollow jet engine turbine blades and vanes. Leakage in fuselage pressurization systems, water egress and skin delamination. Windshield heating/defrost patterns.
Dryer rolls	Condensate build-up and high bearing temperatures.
Ovens, kilns, blast furnaces, and ladles	Refractory deterioration and inefficient or malfunctioning heaters.
Process fired furnace tubes, burners and refractory material	Flame impingement, coke build-up on internal tube surface, faulty burners, and flame analysis.
Storage tanks for fluid products and gases	Determination of fluid levels, inadequate insulation, leaks, and defective valves.

10.2. PROCESS CONTROL/QUALITY CONTROL

Table 10-6 lists numerous industries that employ thermal imaging systems for process control and quality control. While the table seems long, it is in fact, brief. A complete list would easily create a 20-page report.

Table 10-6
PROCESS CONTROL/QUALITY CONTROL BY INDUSTRY
(By courtesy of the Academy of Infrared Thermography)

Industry	Process control/quality control
Automotive	Metal casting, refractory material, molds, conveyors, bearings, plastics and composite testing, bumpers, tires, spot welding, defective weld tips, punch presses, forming equipment, lighting ballasts, paint process, paint curing, rear window defrosters, electronic parts, tires, brakes,
Cement/Lime	Product/burning zone, kiln shell, hot clinkers, and control of electrostatic filter for exhaust smoke purification.
Chemical/ Petrochemical	Pipe thinning, scaling, deposits, and corrosion, furnace tube coking, refractory, insulation, energy management, steam systems, material and chemical mixing, stacks, product levels, sludge levels, liquid level on storage tanks, exchanger fouling, and heat loss quantification.
Die castings and molding	Thermal distribution of mold surfaces, cooling channel blockages, prototype evaluation, and die hot spots.
Electronics	Malfunction of components on printed circuit boards, poor solder joints, shorts, and improper heat sinking.
Food	Energy loss, seals, and insulation of freezers, baking ovens, candy/chocolate mixing, deep fat fryers, and coffee roasters. Drying processors, conveyors, bearings, and packaging/ sealing. Temperature of continuous baking ovens and hot metal heads for packaging and sealing plastic wrap.
Glass	Refractory material, glass, molds, annealing, and tempering temperatures. Thermal monitoring of reinforced glass.
Metals	Temperature monitoring during melting, pouring and rolling of all metals.
Paper	Coating and printing of wallpaper and photographic paper. Moisture profile irregularities, drying, misaligned press rolls, irregular steam distribution, and bearing condition. Malfunctioning vacuum boxes, heat ducts, dryer hoods, defective press roll covers, irregular felt conditioning, and uneven felt construction.
Plastics	Thermoforming, bottle forming, vacuum forming, coating laminating, calendaring, fiber optic cable extrusion, and uniformity of product exiting extrusion process or mold.
Roofing	Roof leaks, welded seam uniformity, and asphalt and kettle mix temperature.
Rubber	Milling, mixing, molding, calendaring, extruding, quality evaluation, curing, vulcanizing, tire testing, and cooling and rolling of hot rubber sheets.
Thin films	Web monitoring, coating laminating, blown film, printing, packaging, and thermal consistencies.

11
TARGET SIGNATURES

A target is an object that is to be detected, located, recognized, or identified. Target signatures are the spatial (size), spectral (wave band), and intensity (temperature) features that distinguish the target from the background. Most imaging system applications exploit intensity differences. Signatures are the characteristic patterns that the thermographer must learn to identify.

Signatures are created by an apparent temperature differential between the target and its background. The radiation that appears to emanate from an object depends upon its emissivity. This chapter describes how signatures vary with environmental factors. Emissivity effects are described in Chapter 12, *Temperature Measurements*. Although the temperature of the target is independent of its signature, there must be a signature to find the target.

11.1. THERMAL ANOMALY IDENTIFICATION

The difference between normal and abnormal temperature distributions may be determined by comparison with known objects or symmetry. The temperature may have been caused by mass transport, thermal capacity differences, energy conversion, state changes, or direct heat transfer.

COMPARISON

Irregularities may be noted by comparing one object with another similar object that is known to be good. The similar object must be subjected to the identical conditions. For example, when comparing the individual phases of a three-phase circuit, it is important that the connections be manufactured by the same manufacturer, have the same electrical load, same surface quality (emissivity), and subjected to the same environmental load (e.g., sun versus no sun).

SYMMETRY

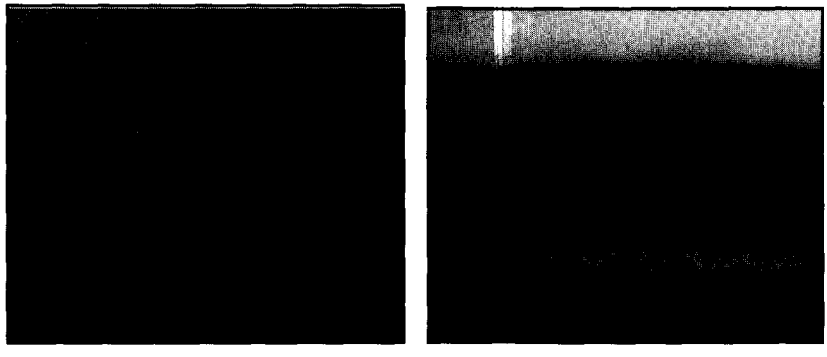
Many objects exhibit symmetrical or asymmetrical patterns. The human body should be symmetrical about a vertical axis in the center of the body. Any asymmetry (left different from the right) may indicate a medical anomaly.

MASS TRANSPORT

Mass transport occurs when a fluid diffuses through a surface. The temperature of the fluid will change the surface temperature. This is seen most often in energy conservation surveys. Heated air from a building seeps though cracks around windows and doors and the surface around the cracks becomes warm.

THERMAL CAPACITY

Objects with a high heat capacity will change their temperature more slowly than objects with a low heat capacity. Therefore, during a cooling or heating cycle, it is possible to locate a region of interest. This phenomenon is exploited to find moisture in roofs and fluid levels in storage tanks (Figure 11-1). It is the primary mechanism responsible for outdoor thermal signatures.



VISIBLE **THERMOGRAM**

Figure 11-1. A partially filled water storage tank. The bottom layer is sludge. The next is water and the dark band is a floating roof. The sludge, water, roof, and air above the roof have different heat capacities and therefore have different heating and cooling cycles. The sun provides the energy to heat the tank. (By courtesy of Advanced Integrated Technologies).

ENERGY CONVERSION

All electrical components (e.g., wires, connectors, electronics, transformers, and lights) dissipate energy through resistance. This energy is converted to heat and increases the temperature of the object. Similarly, all mechanical devices encounter friction. Friction creates heat.

STATE CHANGE

State changes delay temperature changes. For example, the sun will directly heat a dry roof. If there is standing water, a significant amount of the sun's energy is expended on water evaporation. Suppose moisture entered the roof and then froze because of very low temperatures. As the environment warms up, the roof temperature will remain near 32°F (0°C) until all the ice has melted.

DIRECT HEAT TRANSFER

Direct heat transfer is simply heat conduction. It is used to study a wide variety of applications, including the efficiency of brakes, the cooling efficiency of radiators, and the quality of composite materials. Poor heat conduction could mean blocked pipes, a clogged radiator, and hidden defects such as poor bonding, delaminations, or inclusions in multilayer composite structures.

11.2. THE ENVIRONMENT

The thermal signature is an integral part of its environment. Heat flows by conduction and convection and all objects radiate energy. Figure 11-2 illustrates the various sources of heat. Which component dominates depends upon the specific scenario. Note that heat may be lost or gained during a state change (e.g., melting of ice or freezing of water).

All objects eventually reach a steady state condition (thermal equilibrium). At steady state, heat gain is balanced by its heat loss. When at steady state, the temperature of the object can be measured without ambiguity since it does not change with time. Mathematically,

$$Q_{GAIN} = Q_{LOSS} \tag{11-1}$$

and the temperature remains constant.

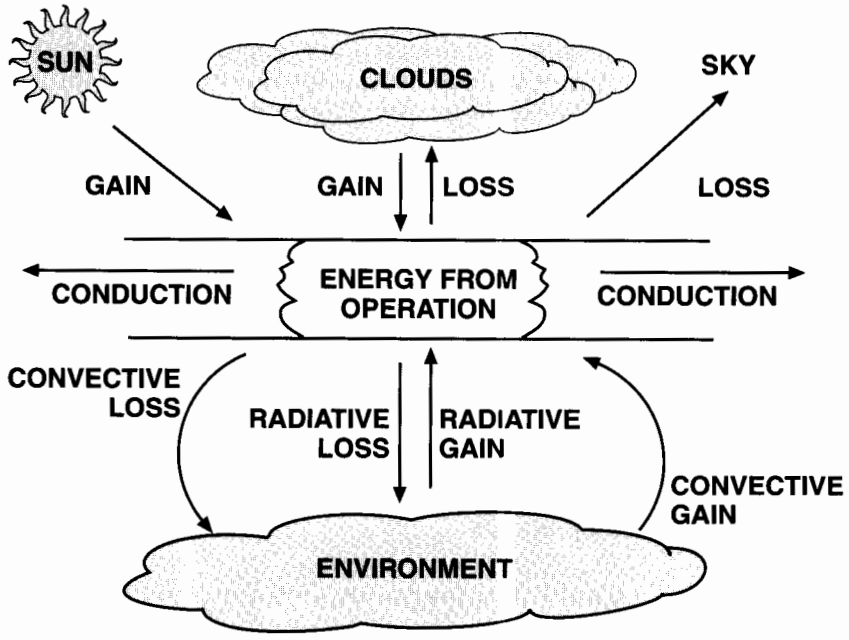


Figure 11-2. The environment affects the temperature of the object. Friction, fuel combustion, and energy conversion are sources of energy. The object's temperature depends upon the operational state and condition of the component.

The background can vary with application (Figures 11-3, 11-4, 11-5, and Table 11-1). The background may be natural (ocean, forest, desert, clouds, sky, or snow) or manmade (building, road, or walls). A vehicle viewed from the air could have diverse backgrounds such as sand, grass, water, concrete, asphalt, or dirt. Since vegetational growth varies with season, there is also a seasonal variation in the target signature. Similarly, a ship may have the sea or the sky as a background. A helicopter may have cold sky, clouds, mountains, or vegetation as a background depending upon the location of the observer with respect to the helicopter. In each case, the apparent target-background signature (apparent temperature) is different even though the target temperature is constant.

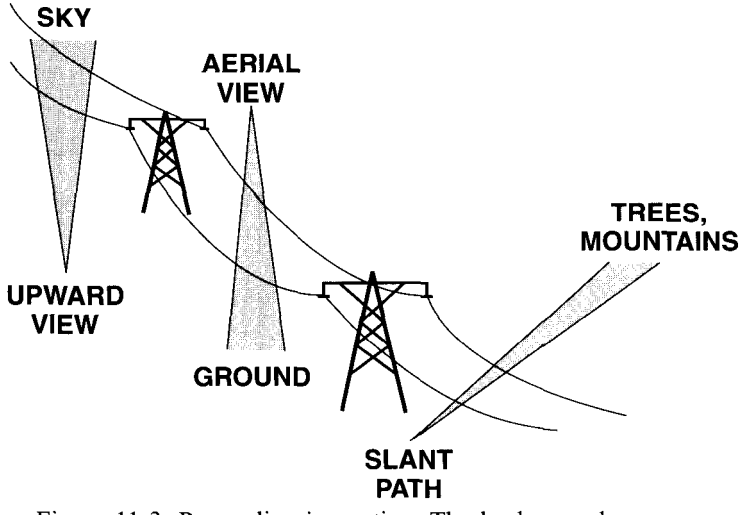


Figure 11-3. Power line inspection. The background can vary according to the viewing angle. Although the target temperature is constant, the ΔT varies. With slant path viewing, the apparent temperature of the background depends upon the atmospheric transmittance.



Figure 11-4. Solar heated utility pole. The sky is very cold. Solar heated connectors can be confused with defective connectors that are heated by undesirable electrical energy dissipation. (By courtesy of IRcameras.com).

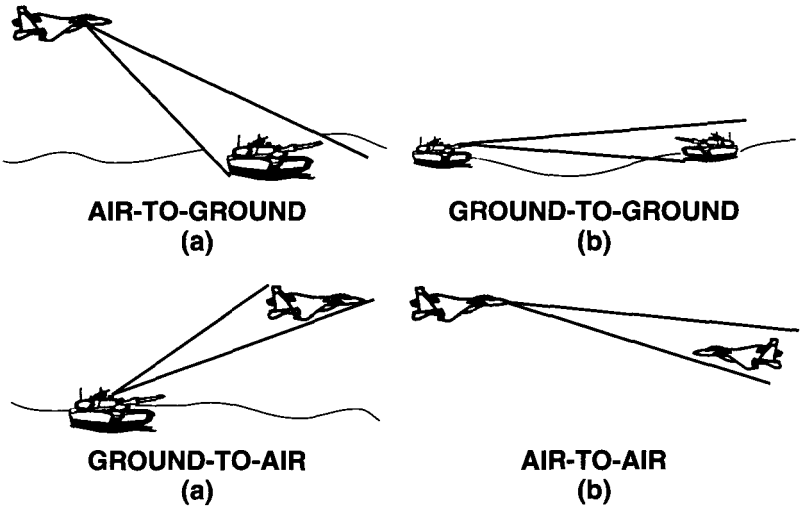


Figure 11-5. Military signatures vary with viewing angle. (a) Air-to-ground, (b) ground-to-ground, (c) ground-to-air, and (d) air-to-air.

Table 11-1
REPRESENTATIVE SIGNATURES

Application	Targets	Backgrounds
Surveillance	People, vehicles, boats, small planes	Vegetation, dirt roads, water, sky
Buried objects	Ground	Vegetation, dirt, sand, rocks
Electro-mechanical	Motors, conveyor belts	Cool (wall, floor, machinery, storage containers) or hot objects (boilers, ovens, steam lines)
Power generation	Power lines, transformers	Vegetation, dirt roads, water, sky, pavement

Deep space is very cold. If the atmospheric transmission is high, the sky will appear cold. As the atmospheric transmittance decreases, the path radiance increases and the sky *appears* warmer. Aircraft high in the sky may be against a 260K background. The same aircraft, when near the horizon, may be against an effective 293K background (See Figure 5-8). Extensive graphs on sky radiance can be found[1] in *The Infrared and Electro-Optical Systems Handbook.*

11.3. PASSIVE TARGETS

Passive targets rely on an external heat source to create a temperature differential. Outdoors, the sun is that source. Table 11-2 lists the heat transfer mechanisms that exist outdoors (see also Figure 11-2).

Table 11-2
OUTDOOR HEAT TRANSFER

Heat Gain	Heat Loss
Solar energy	
Radiation from clouds	Radiation
Radiation from surrounding objects	Conduction
Convection	Convection
State change	State change
Conduction	

Because the environment is constantly changing, the temperature of outdoor objects is constant changing. The intensity of the sun and direction constantly changes during the daytime. Buildings and trees may create shadows. To minimize environmental variations, measurements are often taken at nighttime (no solar loading) and with minimal wind speeds (reduces convective cooling).

11.3.1. SOLAR HEATING

Solar loading depends upon the season. In northern latitudes, maximum exposure occurs during June 21 and minimum exposure occurs during December 21. The sun angle also changes so that a slanted roof will receive different loading depending upon the sun angle.

All materials with high absorption in the solar spectral region will heat up. The temperature will depend upon the absorption coefficients at the solar wavelengths (α_{SUN}) and the emissivity in the infrared (ε_{IR}) where it re-radiates most of the energy. The current temperature of a target is a time history of radiation exchange between it and the environment.

If $\alpha_{SUN}/\varepsilon_{IR}$ is high, the target will heat up. If $\alpha_{SUN}/\varepsilon_{IR}$ low, it will not. Polished metals have a high ratio. If you leave metal tools out in the sun, they almost become too hot to handle. White paint has a low ratio whereas black paint has a high ratio. Consequently, white cars remain cool and black cars become quite hot. A roof with white asphalt shingle will not be as hot as a black roof. The ratio $\alpha_{SUN}/\varepsilon_{IR}$ is very important to spacecraft design to avoid overheating.

Naturally occurring objects such as trees, grass, rocks, and earth are heated passively through the absorption of solar energy. Daily heating begins at sunrise, and after midday, solar loading declines and natural objects begin to cool. After sunset, the background temperature approaches the air temperature. Low heat capacity objects such as grass, leaves, and the soil surface tend to track the solar radiation. When a cloud passes, these naturally occurring objects cool rapidly. Dense (high heat capacity) objects, such as rocks and tree timber, heat and cool slowly.

Since all objects have different absorption coefficients at the solar wavelengths, different emissivities, and different heat capacities, they heat up and cool at different rates (Figure 11-6). Therefore, target signatures are a function of all these parameters.

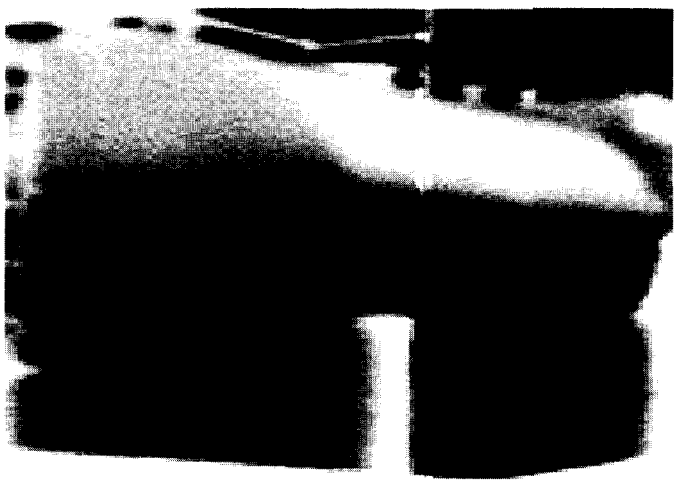


Figure 11-6. A passively heated storage tank. The tank is about 50% full. The morning sun has heated the ends of the cradle. The tank shields the lower portion of the cradle. This part will always be near ambient temperature. The top of the tank has also been solar heated. The solar heated area will cool in the afternoon. (By courtesy of the Academy of Infrared Thermography).

The amount of solar radiation absorbed depends upon the condition of the target's surface (e.g., covered with water from recent rain, dew, dirt, or mud). The temperature of large thermal mass objects such as armored vehicles tends to lag terrain temperatures. Thus the terrain will heat or cool faster than a parked armored vehicle and both positive and negative contrasts are possible.

As the sun rises, it heats that part of the target that faces east. During this time, the west side may still be cooling. Simultaneously, the grass on the eastern side will heat up. When viewing the western side in the morning, you see a cool side against a background that has heated. During the late afternoon, the situation is reversed. The east side is in a shadow and may start to cool while the west side starts to heat up. Figure 11-7 illustrates the diurnal cycle for different parts of a military tank. Depending upon the viewing angle and time of day, the target and its background may be at the same apparent temperature. This is known as thermal crossover.

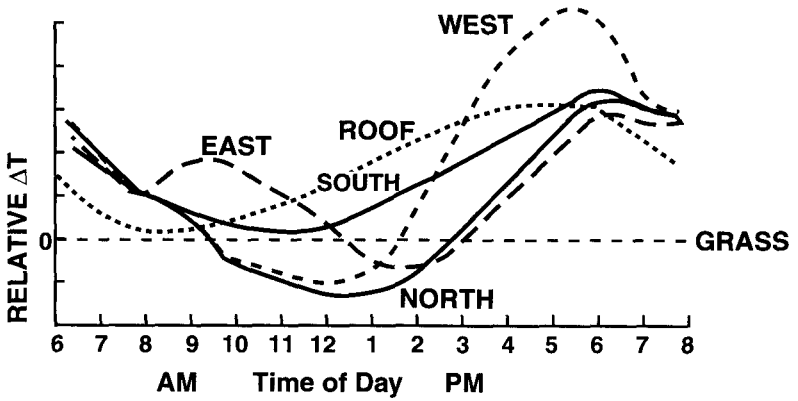


Figure 11-7. Representative ΔTs for a military tank on a grassy background for a northern latitude. As the sun's angle changes, different sides are heated. (From reference 2).

Figure 11-8 illustrates a typical diurnal cycle. At thermal crossover ($\Delta T=0$), the target cannot be detected. Note that while the ΔT has approached zero, both the target and background are still radiating energy. It is still possible to measure the target temperature (using the appropriate emissivity correction). However, with zero ΔT, you cannot find the target.

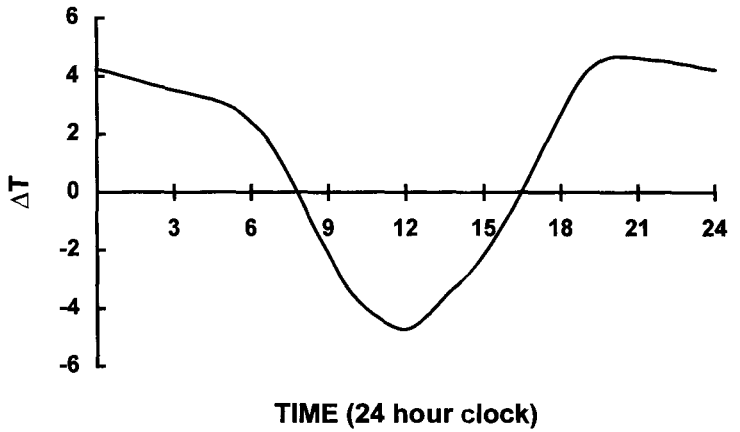


Figure 11-8. A typical ΔT diurnal cycle. The ΔT will vary according to season, location, and solar loading. This curve represents the area-weighted average ΔT for the front view of a military tank during a typical European summer day. (From Reference 3).

Figure 11-9 illustrates a typical diurnal cycle of houses in eastern Massachusetts. On January 15, the sunrise is about 7:15 AM and the sunset occurs about 4:30 PM. As a southerly view, the sun rises to the left and sets to the right of the houses. The metal slide always reflects the cold sky and appears dark in all images. The slide casts a shadow on the grass and that portion of the grass remains cool. The sun's location can be estimated from the location of this shadow.

At 10:00 AM, the sun heats the easterly side of the houses. By 1:00 PM, the scene becomes quite warm. The large temperature difference between the cold sky (black) and warm houses (white) exceeds the dynamic range of the imaging system. As a result, the thermogram appears partially saturated. The eastside of the houses is cooling and appears to be near the same temperature as the northerly sides. In the afternoon, the windows have experienced a contrast reversal. They are now warmer than the side. By 4:30 PM, the grass (low thermal capacity) has cooled significantly but the bushes retain some heat.

In the evening, the interior temperature heats up the windows and other uninsulated areas. By 10:30 PM, the temperature differential is small. The imaging system's gain has been increased to see this small ΔT, but it also increases the noise. Equivalently, the ΔT is near the system's NEDT so that the imagery appears "snowy."

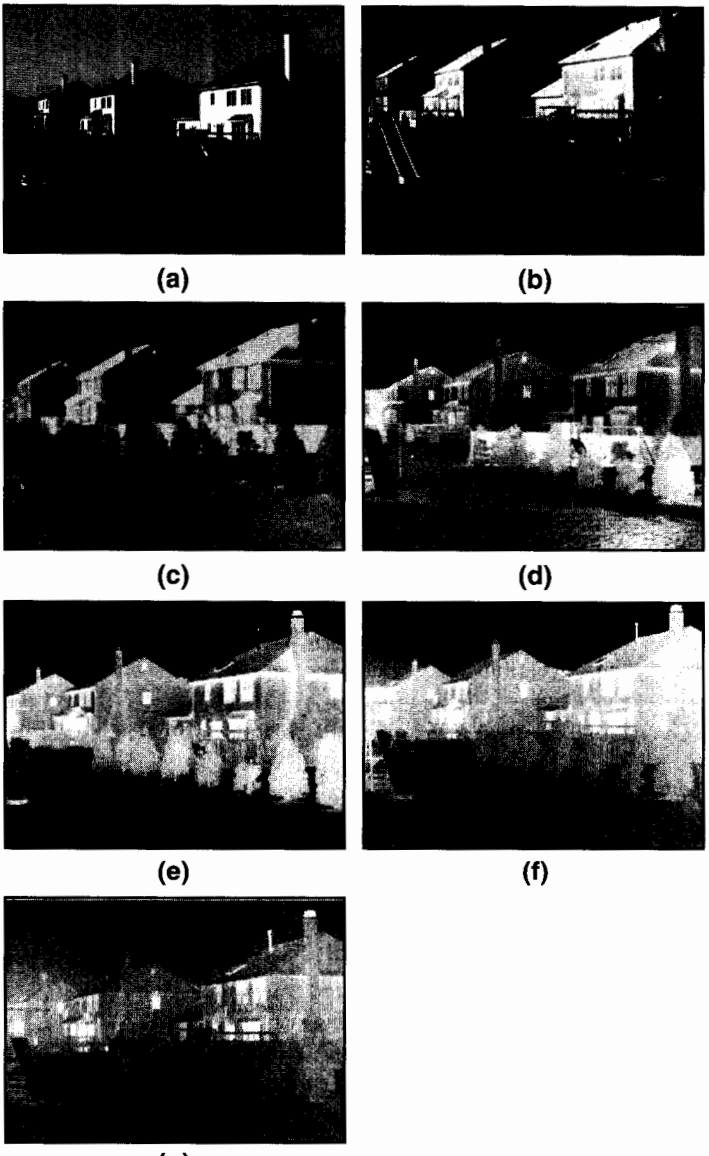


Figure 11-9. Wintertime (January 15) diurnal cycle taken with a LWIR uncooled microbolometer thermal imaging system. (a) Visible image taken at 10:00 AM. The thermograms are taken at (b) 10:00 AM, (c) 1:00 PM, (d) 3:15 PM, (e) 4:30 PM, (f) 6:30 PM, and (g) 10:30 PM. (By courtesy of IRcameras.com)

11.3.2. CLOUDS

Passing clouds modify the target signature. A heavy overcast lasting several days will nearly obliterate any signature as the earth and any target reach thermal equilibrium. Clouds block solar radiation and impede the heat transfer to the sky.

Depending upon the application, cloud cover can either be detrimental or helpful. No cloud cover is required when viewing objects that are passively heated. High cloud cover helps when the object is actively heated. For roof inspections, a clear evening following a sunny day is ideal. For building envelope inspections, cloud cover prevents solar gain thereby permitting daytime inspections. To find underground leaks, cloud cover eliminates the solar gain that could mask the leak. For outdoor electrical inspections, cloud cover prevents solar gain.

11.3.3. WIND

Wind is equivalent to forced convective cooling. Although there is no industry wide standard, it well recognized that wind reduces target signatures and target temperature (see Table 2-6 and Figure 2-10). Knowing the wind speed is vital to thermographers. The thermal images and temperatures observed during building (Chapter 13), roof (Chapter 14), and outdoor electrical (Chapter 15) inspections are dramatically affected by wind speed. For qualitative measurements such as building and roof measurements, a wind speed less than 15 mph (24 kph or 6.7 m/s) is probably adequate. Quantitative measurements require conditions that are more restrictive. Wind speeds must be less than 10 mph with less than 5 mph (8 kph or 2.2 m/s) desirable.

Table 11-3 is a guide for estimating the wind speed. Although the Beaufort scale has 13 categories ranging from calm (0) to hurricane (12), only the first six are of interest to the thermographer.[4] Higher wind speeds will significantly reduce temperatures and are well above recommended values for testing. High gusts of wind have a definite cooling effect on surface temperatures. Building projections may alter the wind speed and may locally increase the wind speed. This is evident in cities with tall buildings. The wind channeled through the streets can have a much higher speed than the overall average wind speed.

Table 11-3
BEAUFORT WIND SCALE

Beaufort Number	Name	Wind speed			Description
		mph	kph	m/s	
0	Calm	< 1	< 1.6	< 0.4	Smoke rises vertically
1	Light air	1-3	1.6-4.8	0.4-1.3	Direction of wind shown by smoke, but not wind vanes
2	Light breeze	4-7	6.4-11	1.8-3.1	Wind felt on face. Leaves rustle, wind vane moves.
3	Gentle breeze	8-12	13-19	3.6-5.4	Leaves and small twigs in constant motion and wind extends a small flag
4	Moderate breeze	13-18	21-29	5.8-8.0	Wind raises dust, loose paper and small branches move
5	Fresh breeze	19-24	31-39	8.5-10.7	Small-leafed trees begin to sway, crested wavelets form on inland waters

11.3.4. RAIN AND SNOW

While raining or snowing, solar loading is typically zero. Simultaneously, the high thermal conductivity of water aids in heat dissipation so that the scene is washed out. Evaporative cooling will remove additional heat. For several hours after a heavy rainfall, target signatures are faint. Target temperature measurements will not be accurate when there is standing water or snow.

11.3.5. THE SCANNING WINDOW

Climatic conditions and temperature extremes can have a significant effect on both the thermal signatures and the operation of the imaging equipment. The scanning window is the time available to make good measurements. The signal-to-noise ratio, ***SNR***, can be estimated from the back-of-the-envelope sensitivity approximation

$$SNR \approx \frac{\tau^R \, \Delta T}{NEDT} \quad . \tag{11-2}$$

The range is zero at thermal crossover. The amount of time the ***SNR*** is below a measurable value depends upon the ***NEDT***, the atmospheric transmittance, and the ΔT.

Figure 11-10 provides the ***SNR*** for the data given in Figure 11-8. The ***SNR*** must be above a threshold for good imagery. Although measurements could be performed anytime, they should be performed when the temperature is fairly constant. Testing should be performed during times of the day or night when the solar radiation or lack of solar radiation would produce the maximum temperature differential (Figure 11-11). As illustrated in Figure 11-12, the scanning window is reduced by cloud cover, rain, wind, and low atmospheric transmittance. Note that this approach assumes that the signature can be seen equally well during the day and the night. Sun glints often force nighttime viewing.

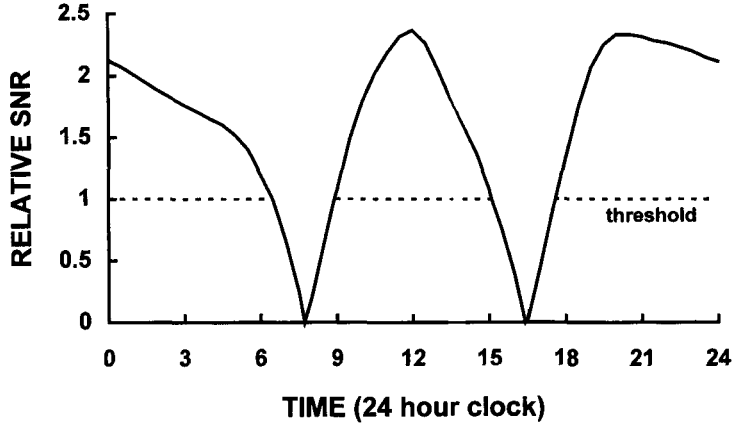


Figure 11-10. Representative SNR. The scanning window is the amount of time that the target signature is above threshold (Relative ***SNR*** = 1). This scanning window is about 19 hours. Both the negative and positive contrasts illustrated in Figure 11-8 are detectable.

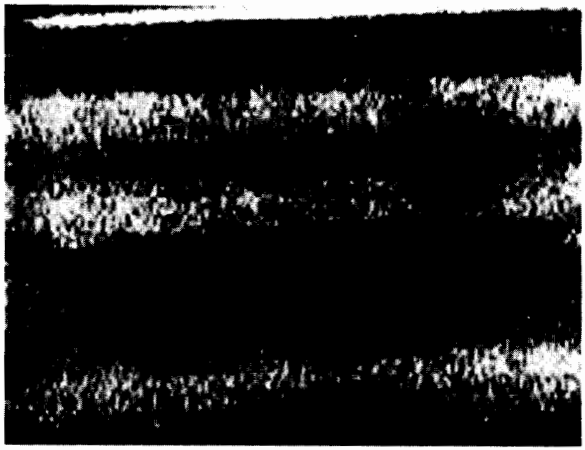


Figure 11-11. Aerial view of a bridge deck during the day. The road surface has delaminated from the supporting structure creating voids (dark areas). Tires polish the road surface and thereby change the emissivity. Thus, the traffic lanes become discernible. (By courtesy of the Academy of Infrared Thermography).

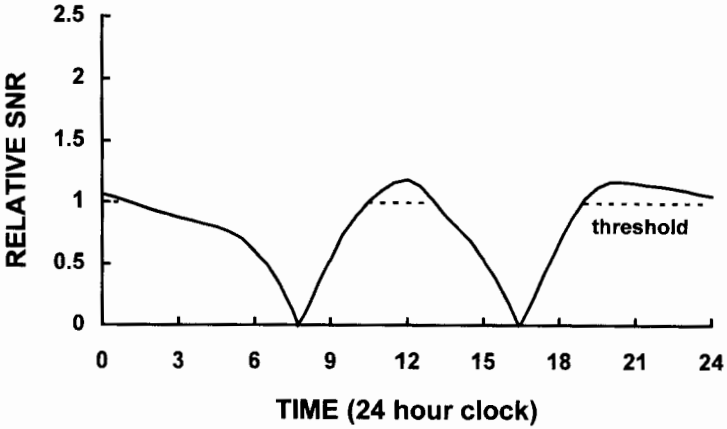


Figure 11-12. Adverse weather conditions reduce the scanning window. This window is about 9 hours. Although still a significant amount of time, ideal conditions provided a 19-hour window (Figure 11-10).

11.3.6. OUTDOOR CONSIDERATIONS

Figure 11-13 illustrates an aerial roof survey taken during the day. The sun, clouds, sky, and trees contribute to the radiation impinging onto the roof. The airplane also adds radiation. Figure 11-14 illustrates another roof survey. Here the roof is cooler due to the shading by a tall building and trees. The effect of adjacent buildings varies with the location (Figure 11-15).

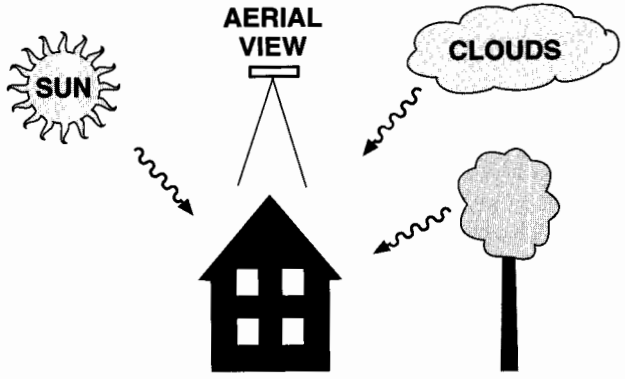


Figure 11-13. The entire environment affects the target temperature.

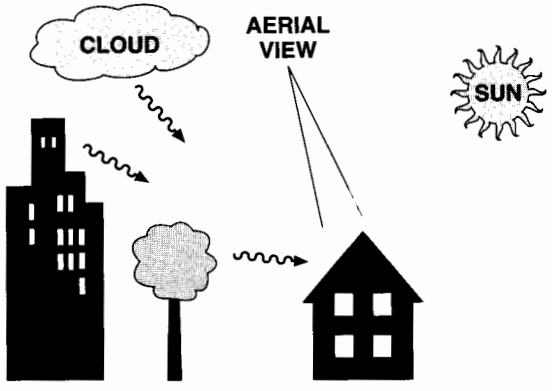


Figure 11-14. Tall buildings and trees minimize solar loading.

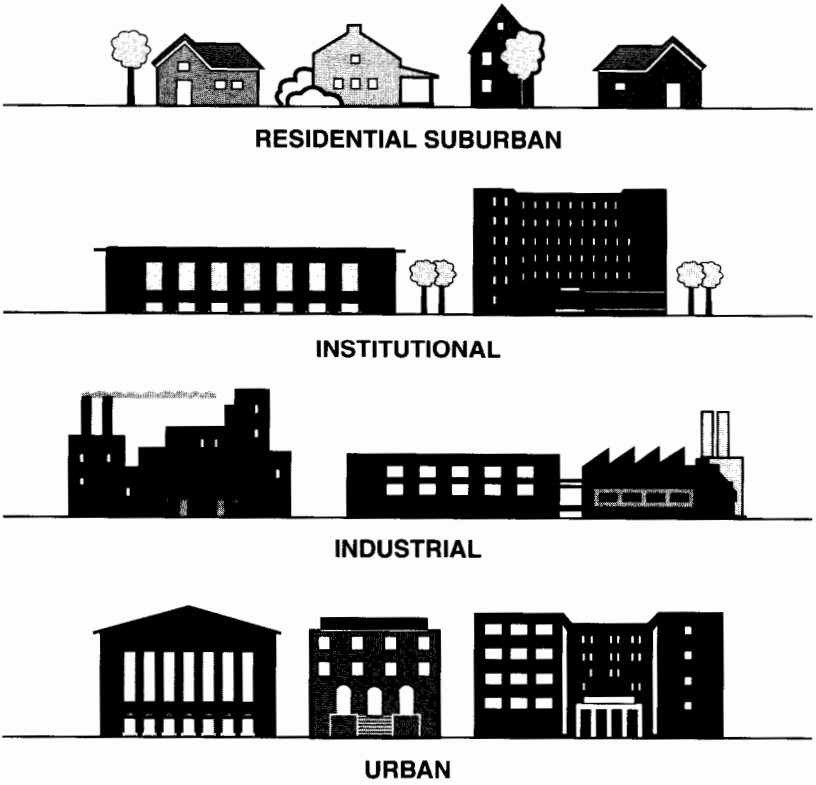


Figure 11-15. Building temperatures can differ in commercial and residential areas.

11.4. EMISSIVITY VARIATIONS

Although heat transfer mechanisms are well known, we do not measure the temperature directly. We measure the radiation that appears to emanate from the target. This measured radiation is due to target self-emission, path radiance, and reflections. The emissivity depends upon the surface quality and surface shape (geometric properties). The reflectivity, of course, depends upon the same factors. Surfaces may be smooth or rough. A polished surface provides a specular reflection (Figure 11-16). Polished surfaces can easily provide sun glints.

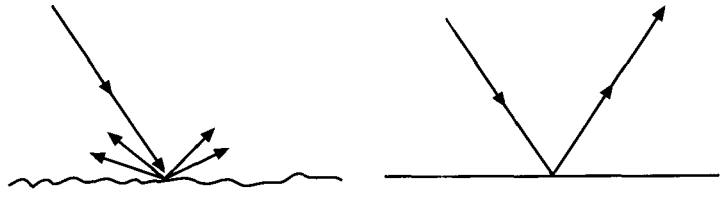


Figure 11-16. Surfaces can be either diffuse or specular. Polished metals provide a specular reflection (very low emissivity) whereas rough surfaces like asphalt shingles and brick create a diffuse surface (high emissivity).

The effects of a polished surface are illustrated in Figure 11-17. The aircraft's specific signature depends upon the exhaust plume, scattered and reflected radiation (earthshine, sunshine, skyshine), internal heat sources, and aerodynamic heating. Depending upon the viewing angle and background, the wings and fuselage may appear either warmer or colder than the background. The engines, of course, are always hotter than the background.

Glass is also a polished surface (Figure 11-18) and can be quite reflective. It is always reflective in the LWIR region (See Figure 4-12). As with all flat surfaces, the reflectivity increases as the angle if incidance increases (See Figure 4-4).

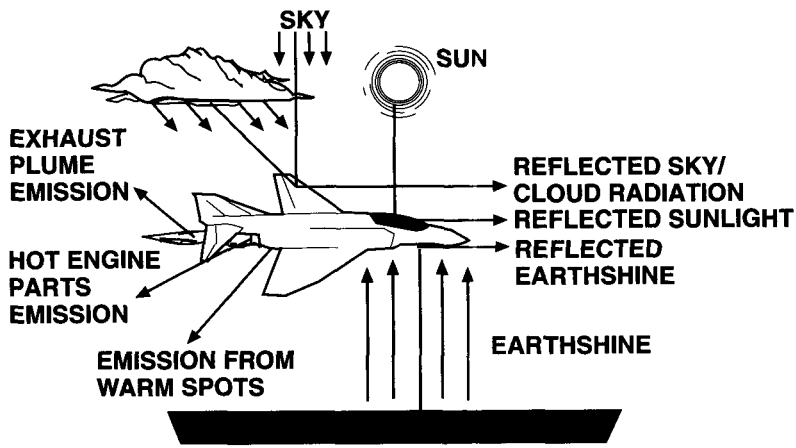


Figure 11-17. An aircraft signature cannot be separated from the environment. Earthshine, skyshine, sunshine, and cloudshine affect the apparent target temperature.

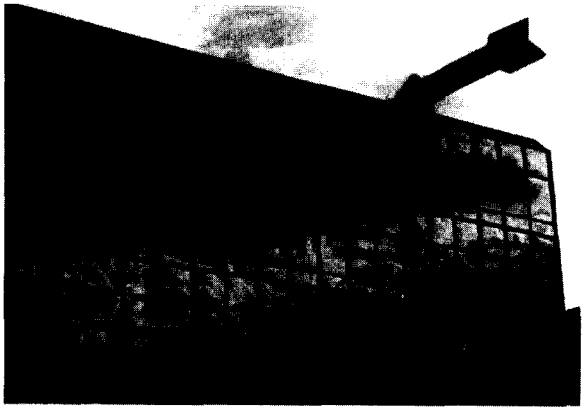


Figure 11-18. A visible image of a glass building that clearly illustrates reflectivity. The arrow points to an area where substantial heat loss is occurring. The heat loss can only be seen with a thermal imaging system. The thermogam is not shown. (By courtesy of Gary J. Weil, president, EnTech Engineering).

Most metals have a low emissivity (appear very reflective) when manufactured. Upon exposure to the weather and pollutants, they oxidize. Oxidized surfaces often have a relatively high emissivity. In machinery and motors, elevated temperatures can accelerate the oxidation process.

The magnitude of a solar glint depends upon the surface emissivity. If the emissivity is near unity, there are no reflections. As the emissivity drops, the reflectivity increases. While nighttime measurements avoid the solar glint problem, they are still plagued with reflectivity problems. If the reflectivity is high, then the thermographer's body may provide the heat source for a reflection. Outside, the sky is very cold and the object may appear cold (e.g., the slide in Figure 11-9). On the other hand, clouds have higher temperatures and the reflection may not be very noticeable (although it is still there).

Solar reflections appear as hot spots. They are unique to the angle at which the target is viewed. By changing the viewing angle, it is easy to determine if the hot spot is real or a reflection. Real hot spots will not move whereas the reflection will change or disappear (Figure 11-19). Emissivity differences create apparent temperature differences. If a spot on the target were truly hot, then there would be a temperature gradient due to heat conduction. An emissivity difference would not create a gradient. Consider paint chips on a piece of metal. The chips would be detected even though they are the same temperature as the metal and there would not be any temperature gradient.

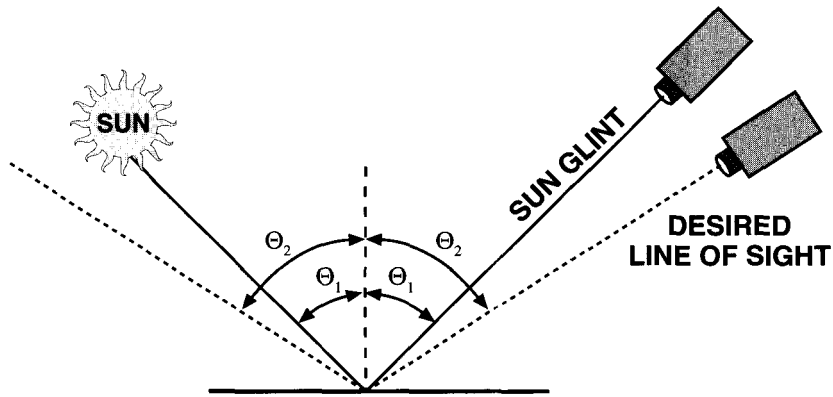


Figure 11-19. Solar glints occur when the angle of reflection equals the angle of incidence. By changing the viewing angle, sun glints should disappear. With multi-faceted or curved surfaces, solar reflections will appear at a variety of angles.

11.5. ACTIVE TARGETS

Active targets are those that generate heat. Fuel combustion, friction, chemical reaction, and electrical energy dissipation create heat. The amount of heat generated depends upon the operational state. Engines running at full throttle produce more heat than those at idle. The amount of heat generated by electrical energy dissipation depends upon the resistance and the current. While passively heated targets may experience thermal crossover, active targets generally do not.

Indoor targets are not affected by the sun, clouds, or sky (Table 11-4). However, forced convection may be significant if cooling fans are present of if the target is near an HVAC (heating, ventilation, and air-conditioning) duct.

Table 11-4
INDOOR HEAT TRANSFER

Heat Gain	Heat Loss
Radiation from surrounding objects	Radiation to surrounding objects
Convection	Conduction
Energy from operation	Convection
State change	State change

11.5.1. VEHICLES

Fuel related heat sources occur whenever the engine is operated and is nearly independent of vehicle motion. If the engine is water cooled, the engine compartment temperature is usually below 212°F (100°C). If the heat is piped into the passenger compartment for personnel heating, then that also will appear warm. Because of heat transfer, the engine compartment does not appear as a well-defined area but as a blob with a diffuse edge as the heat dissipates. Engine mufflers and exhaust pipe temperatures run quite high. These heated areas can be seen at very long distances. However, these areas are localized and therefore may not be oriented toward the imaging system. Consider, for example, the thermal image of a car. The engine compartment and grill will be clearly visible from the front whereas the rear view may provide only a small heated exhaust pipe.

Frictional heat is only generated when the vehicle is in motion. The heat is less intense than that created by the engine. Tracks, road wheels, drive sprockets, support rollers, and shock absorbers are the frictionally heated features on military tanks. Wheeled vehicles generate heat in the tires, shock absorbers, drive shafts, transmissions, axles, and differentials (Figure 11-20). Frictionally heated cues differentiate wheeled vehicles from tracked vehicles.

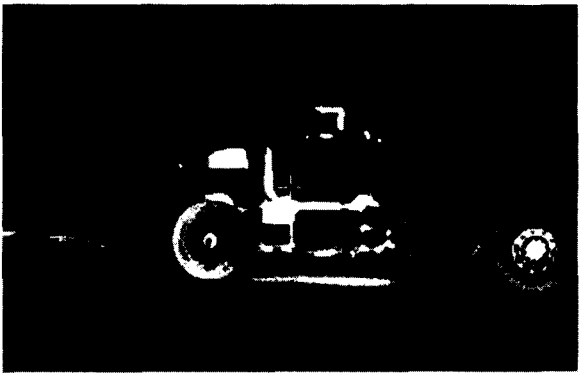


Figure 11-20. Moving truck. The engine compartment and exhaust are easily seen. Friction between the road and tires will always heat up the tires. At grazing angles, a paved road surface becomes reflective and reflects the heat from the underside of the truck. The front brakes on most vehicles provide about 70% of the stopping power. As a result the front wheels are typically warmer than the rear wheels. Since this is a wintertime image, the heater in the cab is on and is warming the window frame. (By courtesy of IRcameras.com).

If the vehicle is moving rapidly or if there is a large wind, both fuel related and friction related temperature gradients may be reduced. For military vehicles equipped with weapons, the gun tube can be significantly hot after firing. For high-speed aircraft, aerodynamic heating also provides a signature.

For several hours after a heavy rainfall, target signatures are faint. Water and mud reduce frictional cues through cooling and insulation. Wind aids in heat transfer so that under moderate wind conditions, target temperatures will be lower than under still air conditions.

11.5.2. SMALL TARGETS

There are many small active targets such as electrical components and bearings. If significant conduction occurs, then the temperature at the fault will be much lower than without conduction. This means faulty components may not exhibit a high temperature (Figure 11-21).

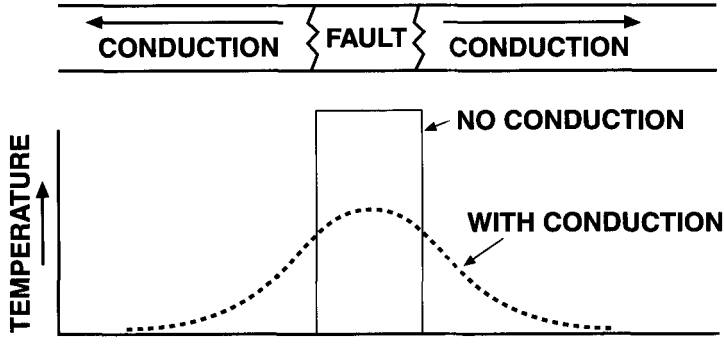


Figure 11-21. Heat conduction reduces the maximum temperature at the fault.

11.5.3. ESTIMATE OF THE SCANNING WINDOW

Under most situations, the scanning window is open as along as the target is active. However, there are special cases. Lyberg et. al.[5] were looking for heat losses from a buried heat distribution system in southern Sweden. Since this was performed from an airplane, low-lying clouds would obscure the ground. They estimated the number of hours available for aerial detection based upon the various criteria previously mentioned in this chapter. The following data should

be used as a guideline. Clearly, the number of hours available depends upon geographic location and the criteria depend upon the application.

Lyberg et. al. proposed the following meteorological criteria (in order of decreasing importance):

1. No precipitation (rain or snow)
2. Air temperature between 2°C (36°F) and 15°C (59°F)
3. Relative air humidity below 93 %
4. Cloudiness less than 2/8 or cloudiness less than 7/8 if the cloud base is above 2000 ft cloud
5. Wind speed below 5 m/s (11 mph).

Since the aircraft will fly at an altitude of less than 2000 feet, it is important that there be very few clouds below 2000 feet (cloud cover less than 2/8). The cloud cover above 2000 feet is of less importance for active targets. Table 11-5 provides the total number of hours per year available to the scanning window. Using these criteria, tests could be performed only 12% of the time. Table 11-6 provides the number of occasions of different duration that are available for aerial thermography in the Stockholm region. It is striking that the hours available for a single flight are relatively small. The average is only 3.5 hours.

However, there is a tendency for a concentration of the acceptable hours to be in certain months. This necessitates a concentration of aerial thermography to a number of occasions of very short duration. This requires a high degree of preparedness and access to detailed, short-term, weather forecasts.

Colantino[6] performed numerous building envelope inspections with emphasis on historic buildings in Northern Italy. To create an adequate thermal signature, he determined that the outdoor temperature must be greater than about 7°C and the relative humidity must be less than 70%. In Northern Italy, the number of days available for inspection is less than 180 days per year.

The scanning window depends upon the application (building inspection, roof inspection, surveillance, etc.), temperature, wind speed, path length (atmospheric conditions), and sun location. These vary with geographical location. Conditions (and hence the scanning window) can vary between locations that are only a few miles apart.

Table 11-5.
REPRESENTATIVE NUMBER of HOURS
AVAILABLE in SOUTHERN SWEDEN (From Reference 5)

Meteorological criterion	**Hours lost**	**Hours remaining**	**Remaining percentage**
Number of hours in a year		8760	100%
Precipitation	2000	6760	77
Air temperature below 2°C	1500	5260	60
Air temperature above 15°C	1300	3960	45
Relative air humidity above 93%	700	3260	37
Cloudiness between 3/8 and 6/8	900	2360	27
Cloudiness above 7/8 and cloud base below 2000 ft	600	1760	21
Cloudiness below 2/8 during daytime	500	1260	14
Wind speed above 5 m/s	200	1060	12

Table 11-6
NUMBER of OCCASIONS in a YEAR
AVAILABLE for AERIAL THERMOGRAPHY

Duration of occasion (hours)	**Total number of occasions**
2	2136
3	86
4	44
5	29
6	18
7	12
8	8
9	5
10	13
11	12
12	1

11.6. LIMITED ACCESS COMPONENTS

Nearly all electrical and moving mechanical components have safety enclosures. Circuit breakers, fuses, and switches are usually inside electrical boxes. Panels must be removed to view the defective components. Only trained personnel should remove these panels. Depending upon the size of the enclosure and the proximity of the electrical components to the panel, removal may upset thermal equilibrium. That is, panel removal upsets the local environment and the temperature measured may not be representative of the true temperature when the panel is in place, Further, for electrical inspections, the current must be measured. In some situations, the panel can only removed after the power has been turned off. The problem is that the power outage represents equipment shut down. Factory personnel would probably recommend shut down during an off-peak period. However, to measure the maximum temperature, we want to measure during maximum current time (peak period). This is further described in Chapter 16, *Electrical/mechanical inspection.*

Most machines have safety shrouds. The shroud limits your view of rotating parts. If the shroud is solid, it must be removed. Generally, the shroud can only be removed after the machinery has been turned off and this upsets thermal equilibrium. During removal, the components will cool down. Some shrouds consist of wire mesh. In this case, a thermogram can be taken. The ability to measure the correct temperature depends upon the size of the wire mesh opening and the system's MIFOV.

A front surface mirror allows you to view the backside of a component (Figure 2-18). The mirror surface can be polished gold, silver, or aluminum. These mirrors are available from most laboratory supply houses. These materials are soft and scratch easily. It is possible to buy mirrors with a durable overcoat. Verify with the supplier that the overcoat does not adversely affect the reflectivity. While the reflectivity of these materials is high, it is not 100%. For scientific studies, the reflectivity must be taken into account when estimating the temperature of the object.

Regular mirrors (those used in every day living) are back surface mirrors (Figure 11-22). The glass protects the silver or aluminum surface from scratching. Upon careful examination, you can visually see multiple images. This is due to reflections between the rear-silvered surface and the front surface. As illustrated in Figures 4-11 and 4-12, glass is opaque in the LWIR region and partially opaque in the MWIR region. Regular mirrors cannot be used for infrared inspection.

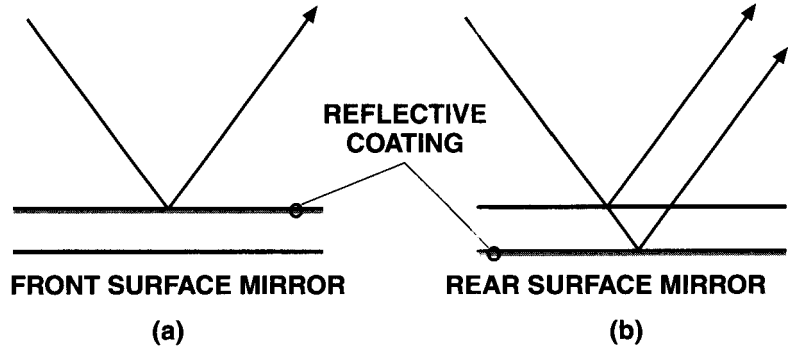


Figure 11-22. Front surface (a) and rear surface (b) mirrors. Only front surface mirror can be used for infrared testing.

11.7. REFERENCES

1. D. Kryskowski and G. H. Suits, "Natural Sources," in *Sources of Radiation*, G. J. Zissis, ed., pp. 139-316. This is Volume 1 of *The Infrared and Electro-Optical Systems Handbook*, J. S. Accetta and D. L. Shumaker, eds., copublished by Environmental Research Institute of Michigan, Ann Arbor, MI and SPIE Press, Bellingham, WA (1993).
2. F. A. Rosell, "Characterization of the Thermal Scene," in *The Fundamentals of Thermal Imaging Systems*, F. A. Rosell and G. Harvey, eds., page 16, NRL Report #8311, Naval Research Laboratory, Washington, D.C. (1979).
3. J. A. D'Agostino, "The SPACE Signature Model: Principles and Applications," in *Infrared Image Processing and Enhancement*, M. Weathersby, ed., SPIE Proceedings Vol. 781, pp. 2-9 (1987).
4. For the last 10 years, John Snell, Snell Infrared, has recommended that thermographers use the Beaufort wind scale.
5. M. D. Lyberg, R. Taesler, and M. Mattsson, "Conditions for Detecting Malfunctions of Buried Heat Distribution Systems by Thermographic Methods," in *Thermosense X*, R. D. Lucier, ed., SPIE Proceedings Vol. 934, pp. 78-82 (1988).
6. A. Colantino, "Thermal Performance Patterns on Solid Masonry Exterior Walls of Historic Buildings," in *Thermosense XX*, R. N. Wurzbach and D. D. Burleigh, eds., SPIE Proceedings Vol. 3056, pp. 87-95 (1997).

12
TEMPERATURE MEASUREMENTS

With non-contact measurements, there is no way of knowing what the actual temperature is! We only measure the radiation that appears to emanate from the target. The total radiation includes the self-emission of the target (a function of the emissivity and temperature), reflected ambient radiation, and path radiance. It is possible to calibrate a thermal imaging system such that its output is proportional to the object's temperature. Key to this calibration is knowing the object's emissivity and ambient temperature. Path radiance can be considered small if the spectral response of the system coincides with those regions where the atmosphere is fairly transparent. This, of course, implies a relatively short path length. This is typical for most condition monitoring activities.

For most surveillance applications, the emissivity of the target is unknown. While the emissivity of new paint may be known, the surface of the target may be oxidized, covered with dirt, or wet. Likewise, the temperature of the immediate environment surrounding the target is often unknown. As such, it is extremely difficult to make accurate temperature measurements. Further, with long path lengths, path radiance could be significant. Therefore, surveillance activities only provide qualitative results: can we detect, recognize, and identify the target? For convenience, the military attaches an apparent temperature to each target. This serves as a standard against which systems are designed. For example, a military system may be designed to detect a tank at 10 km (6.3 mi) whose apparent differential temperature, $\Delta T_{APPARENT}$, is 0.1°C. This is further discussed in Chapter 18, *Surveillance*.

12.1. APPARENT TEMPERATURE

An apparent temperature exists when the emissivity is less than one. The Stefan-Boltzmann law is used for illustrative purposes. The actual radiation detected depends upon the spectral response of the system. Neglecting atmospheric effects, the amount of radiation reaching the detector that is emanating from an opaque target is

$$M_{MEASURED} = \sigma(\varepsilon T_T^4 + \rho T_S^4) \quad . \qquad (12\text{-}1)$$

We assume this radiation is from an ideal blackbody whose apparent temperature is

$$M_{MEASURED} = \sigma T^4_{APPARENT} \quad . \tag{12-2}$$

Solving these two equations provides

$$T_{APPARENT} = (\varepsilon T_T^4 + \rho T_S^4)^{1/4} \quad , \tag{12-3}$$

where $\rho = 1\text{-}\varepsilon$. If the emissivity is one, then the apparent temperature is equal to the true temperature. When the emissivity is zero, the target appears as the same temperature as the surroundings. Intermediate values of the emissivity provide various apparent temperatures (Figure 12-1)

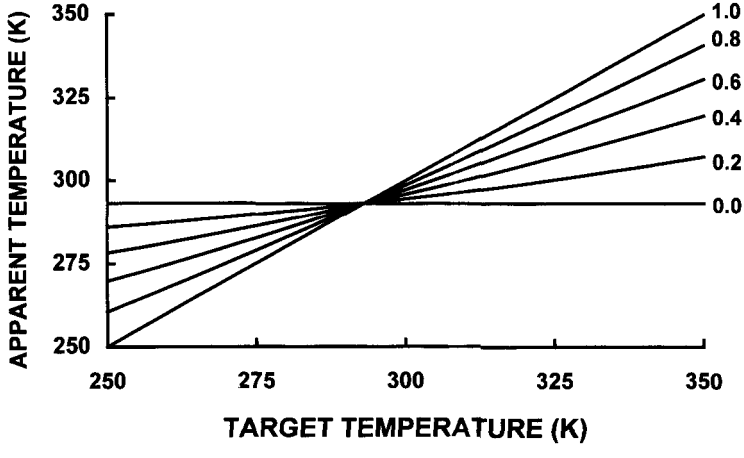


Figure 12-1. Apparent temperature as a function of emissivity. $T_S = 293$K.

The apparent temperature differential is

$$\Delta T_{APPARENT} = \left[(\varepsilon_T T_T^{\ 4} - \rho_T T_S^4) - (\varepsilon_B T_B^{\ 4} - \rho_B T_S^{\ 4}) \right]^{1/4} \quad . \tag{12-4}$$

Note that even if the target temperature and background temperatures are the same, $\Delta T_{APPARENT}$ can exist if the emissivities are different. For many condition-

monitoring activities, the temperature of a tested component is compared to the temperature of a good component. That is, we measure the $\Delta T_{APPARENT}$ between the tested component and the good one. Here, it is assumed that the emissivities (and reflectivities) are the same:

$$\Delta T_{APPARENT} = \left[\varepsilon_T \left(T_{TESTED}^4 - T_{GOOD}^4 \right) \right]^{1/4} . \qquad (12\text{-}5)$$

In this case, the contribution from the reflected radiation cancels. The good component imagery was previously called the baseline or "golden" thermogram. When $\Delta T_{APPARENT}$ deviates by a preset amount, the tested component must be repaired or replaced.

12.2. TEMPERATURE CALIBRATION

When calibrating a thermal imaging system, we view a standard laboratory blackbody whose temperature is known. In the laboratory, the path length is small so that we can assume that the atmospheric transmittance is unity. This also means that the path radiance is zero. Since calibrated black bodies have unity emissivity, the output voltage is

$$V_{CALIBRATION} = kR_D M_{BB} . \qquad (12\text{-}6)$$

Calibration is straightforward. The camera views a blackbody source and the voltage output is recorded for each temperature. Then a table with the inverse relation is created (Figure 12-2). This becomes the software look-up table. Now the thermal imaging system output can be in units of temperature (Figure 12-3).

This calibration is only valid when the target is an ideal blackbody and the atmospheric transmittance is unity. Changing the lens may change the f-number and the optical transmittance. Ideally, the calibration should be performed for each lens available. Chapter 4, *Emissivity*, provided guidelines on selecting narrow filters for accurate temperature measurements of furnaces (flame filter), and a variety of filters for plastic. The system must be calibrated with these filters in place. If the filters are changed, then the system must be recalibrated.

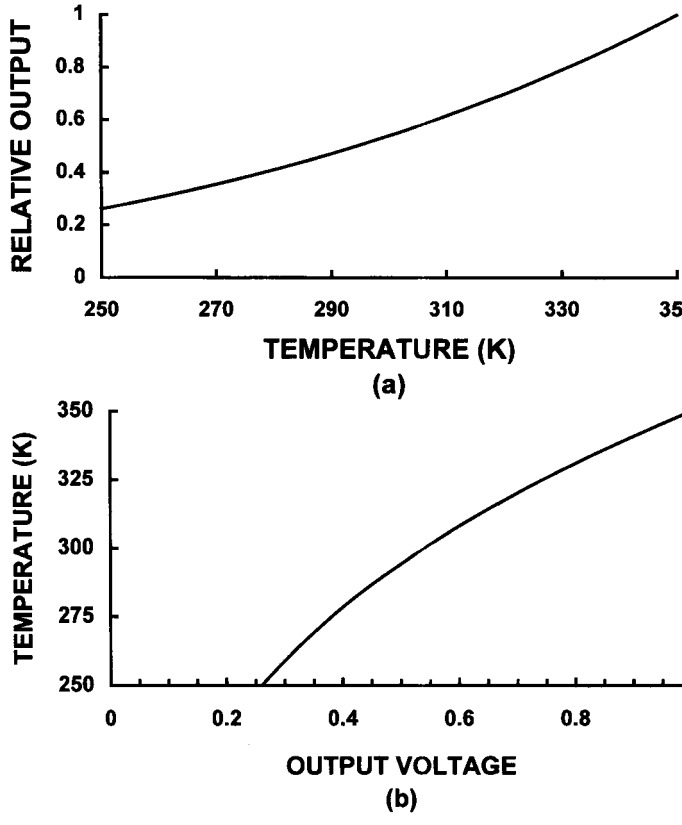


Figure 12-2. Temperature calibration. (a) Voltage output as a function of temperature obtained in a laboratory. (b) The temperature as a function of voltage. This calibration appears in a look-up table. Although the output is shown as an analog voltage, most systems operate in the digital domain.

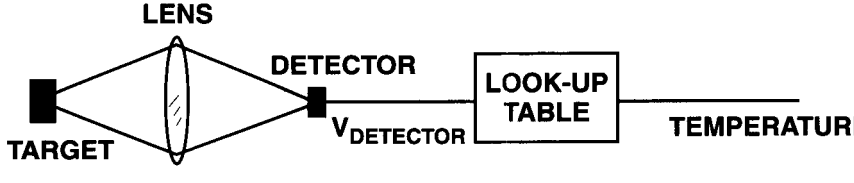


Figure 12-3. A thermal imaging system whose output is provided in temperature units (Fahrenheit, Celsius, Kelvin, or Rankine).

12.3. EMISSIVITY

There are three different generic measuring conditions.

CASE 1. THE TEMPERATURE DIFFERENTIAL IS SMALL ($T_T \approx T_S$).

This case is encountered during electrical and mechanical inspections. Both the emissivity and surrounding temperature must be known for accurate temperature measurements. As the emissivity increases, the influence of the surrounding temperature decreases. Black paint or tape may be used to increase the emissivity.

CASE 2. THE TARGET TEMPERATURE IS VERY HIGH COMPARED TO THE SURROUNDING ($T_T >> T_S$).

This case is encountered in many industries such as paper manufacturing and refineries. Here, the influence of the surrounding is minimal. As an approximation

$$M_{MEASURED} \approx \sigma \varepsilon T_T^4 \quad . \tag{12-7}$$

This suggests that the surrounding temperature has no effect. This is not entirely true. It simply means that it is sufficient to *estimate* the surrounding temperature.

CASE 3. THE TARGET IS COOLER THAN THE SURROUNDING ($T_T < T_S$).

As the emissivity decreases, the reflected radiation can be much greater than the target self-emission. This case is encountered in steel and aluminum manufacturing. Polished metal has a low emissivity. During processing, the material is heated in a furnace. The furnace provides the surrounding temperature and is hotter than the metal. A similar situation can occur in boiler stream pipes and refinery heater tubes. Here, a small error in emissivity can lead to a large error in the calculated temperature.

12.3.1. EMISSIVITY CORRECTION

We need a look-up table that also includes emissivity. In principle, it is straightforward. Using the Stefan-Boltzmann relationship as an approximation, the detector output is

$$V_{DETECTOR} = kR_D \left[\varepsilon \sigma T_T^4 + (1 - \varepsilon) \sigma T_S^4 \right] \quad . \tag{12-8}$$

The detector output is plotted in Figure 12-4 for three different emissivities when T_S = 293K. A family of curves exist for each surrounding temperature.

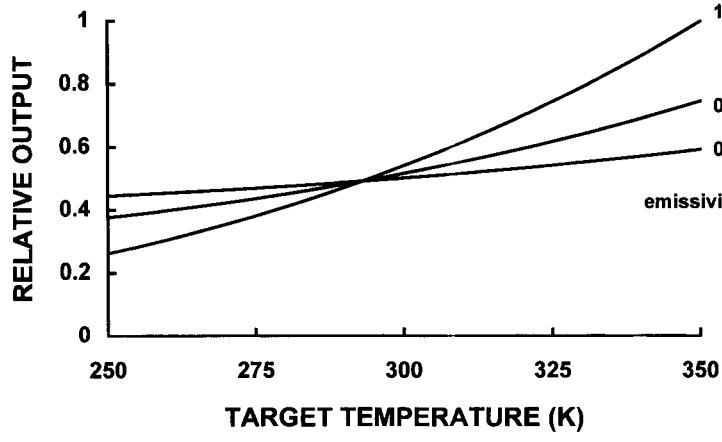


Figure 12-4. Relative output as a function of target temperature when T_S = 293K. When the emissivity is unity, the apparent temperature is equal to the actual temperature (same values as Figure 12-2a). When the emissivity is zero (a perfectly reflecting target), the target appears to have the same temperature as the surrounding. These curves are approximations. The precise response depends upon the system's spectral response.

12.3.2. ANGLE OF INCIDENCE

As indicated in Figure 4-4, the emissivity decreases as the angle of incidence increases. While the emissivity may be known for normal incidence, its angular dependence is not usually known. When the angle exceeds 45°, the emissivity decreases (reflectivity increases). At grazing angles, the emissivity can approach zero (reflectivity approaches unity). As indicated in Figure 12-5, the emissivity can have a strong angular dependence. Even if the angular dependence is known, a small error in test setup in terms of angle can lead to a large error in emissivity. This suggests that accurate temperature measurements can only be made when the angle of incidence is less than 30°. As the angle increases to 60°, a small error is introduced. When the angle is greater than 60°, large errors can occur.

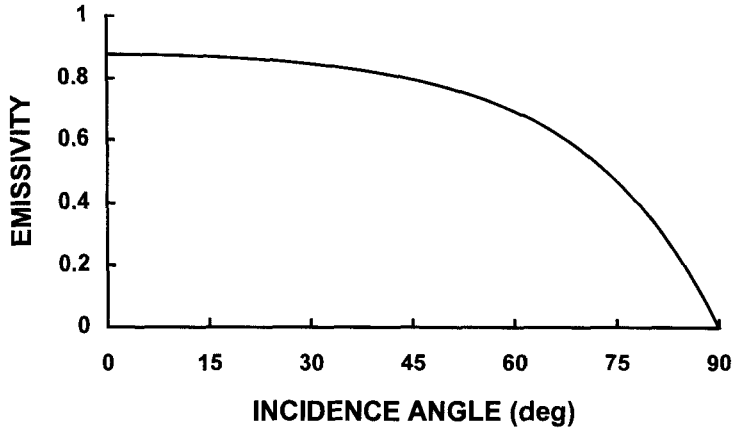


Figure 12-5. At normal incidence, the emissivity may be high. For most materials, it approaches zero at grazing angles.

Comparing Figures 12-1 and 12-5, if the target temperature is greater than the surrounding, then as the angle of incidence increases the apparent temperature decreases. This occurs for all targets that are not normal to the line-of-sight (Figure 12-6).

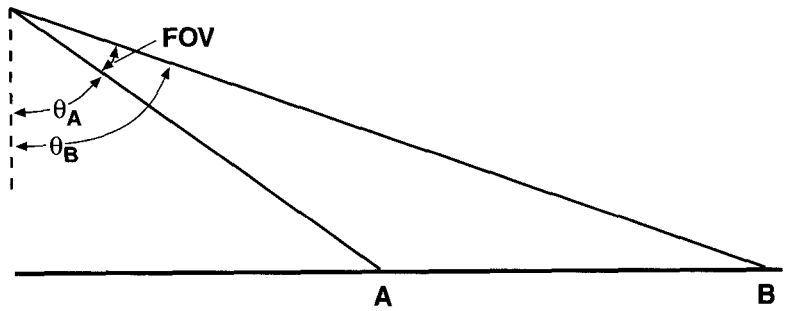


Figure 12-6. Viewing a target at an angle. Because the emissivity decreases with increasing angle, Point A will appear to have a higher apparent temperature than point B when $T_T > T_S$. That is, the apparent temperature changes across the system's field-of-view. The viewing angles are θ_A and θ_B.

12.3.3. EMISSIVITY UNCERTAINTY

Many texts refer to uncertainty analysis as error analysis. While technically correct, some claim that errors are mistakes that should be avoided. In principle, errors can be eliminated or at least reduced significantly so that they do not affect the measured value. Careful planning and following the test plan to the letter eliminate accidental errors (blunders). Accidental errors include (a) failure to account for external heat sources, (b) recording wrong voltages, and (d) failure to turn on all test equipment. Measurement uncertainty cannot be avoided.

Our largest uncertainty is the emissivity. We do not know the emissivity precisely and must estimate it. It depends upon the surface characteristics (age of paint, dust, dirt, dew, frost, chips, scratches, and weathering effects) and viewing angle. It also a function of temperature and this makes high temperature measurements (e.g., a furnace) difficult. Madding[1] provides a formal approach to emissivity uncertainty analysis.

Emissivity can vary depending upon surface conditions and environmental conditions. At any particular location, the variation can be small. That is, the emissivity in a "clean" environment may be different from the emissivity in a "dirty" environment. It is reasonable to assume that the emissivities (although different) will remain constant at their respective locations. The emissivities may vary because of different material used, different manufacturers of the same equipment, or that the plant may be subjected to environmental parameters such as excess moisture, sun exposure, weathering, dirt, and dust.

Emissivity uncertainty creates an uncertainty in the measured temperature. Figure 12-7 illustrates the calculated temperature differential when the true differential is 10K and $T_S = 293$K. For illustrative purposes, the Stefan-Boltzmann law was used. The emissivity selected can either be higher or lower than the true emissivity. When the selected emissivity is lower, the calculated temperature will always be higher than the true temperature (assuming that the target is warmer than the background).

Generally, the error in emissivity will be relatively small. Figure 12-8 illustrates the apparent temperature differential as a function of two different uncertainty levels. Note that the emissivity uncertainty is given as an absolute value and not a percentage. For example if $\varepsilon = 0.5$ and the uncertaintly is ± 0.1, then the emissivity can vary from 0.4 to 0.6.

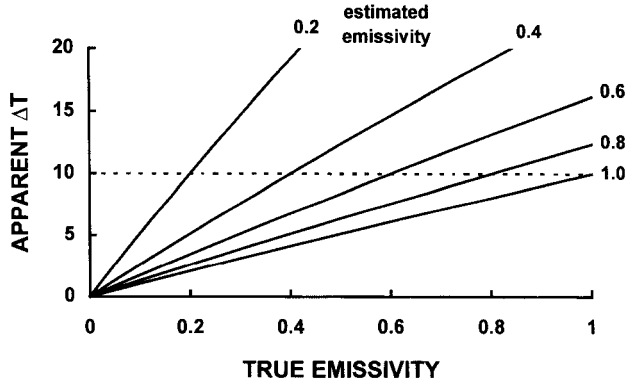


Figure 12-7: Representative apparent temperature differential as a function of emissivity. The true differential is 10K and $T_S = 293$.

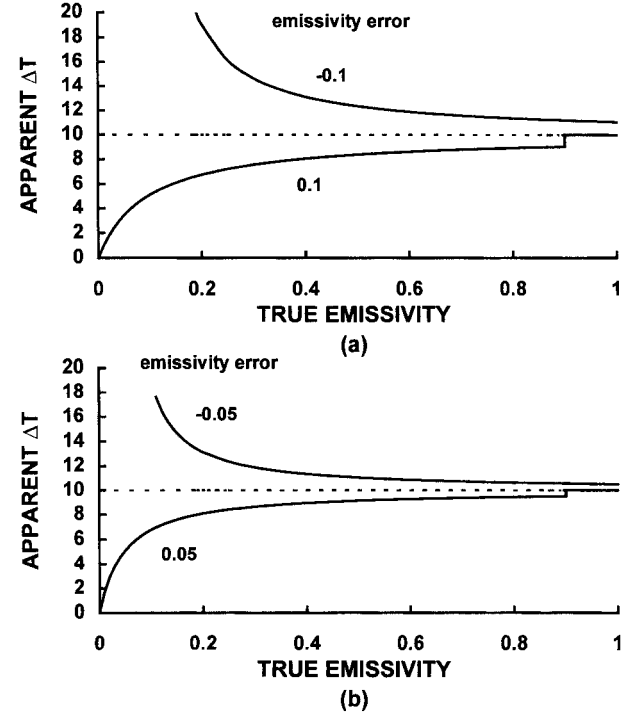


Figure 12-8. Representative range of calculated ΔTs for emissivity uncertainty of (a) ±0.05 and (b) ±0.10. The true temperature differential is 10K and $T_S = 293$K. The emissivity cannot be greater than unity. This places an upper bound on the value and creates a "dog-leg" in the curve.

If the wrong emissivity is assumed, then an error is made in calculating the temperature. However, temperature measurements should be completely repeatable as long as the emissivity control is set to the same value. This leads to the concept of standardized emissivities (discussed in Section 16.4, *Emissivity*).

Table 12-1 provides selected values. The shapes of the curves do not change dramatically for different ΔTs or different surround temperatures. The temperature error becomes unacceptable when the emissivity is less than about 0.5 (e.g., polished metals). How much error can be tolerated depends upon the task. For scientific studies, an emissivity error of 0.1 is probably unacceptable.

Table 12-1
RANGE OF CALCULATED ΔTs
TRUE ΔT = 10K and T_S = 293K

True emissivity	Estimated emissivity	Calculated ΔT
0.5	0.4 to 0.6	8.39 to 12.4
0.6	0.5 to 0.7	8.62 to 11.9
0.7	0.6 to 0.8	8.80 to 11.6
0.8	0.7 to 0.9	8.93 to 11.4
0.9	0.8 to 1.0	9.04 to 11.2
1.0	0.9 to 1.0	10.0 to 11.1

While the thermographer can correct for the object's emissivity, a basic underlying assumption is made: The surrounding has a uniform temperature. This is rarely true. The thermographer himself provides radiation that can be reflected. This means that the ambient temperature can only be estimated. For low emissivity material (polished metals), it is prudent to modify the surrounding so that the target is uniformly illuminated. Employing an appropriate barrier (Figure 12-9) can minimize the effects of a hot source in the surrounding.

The above equations provided the phenomenology associated with an emissivity error. Neglecting reflections, we can mathematically approximate the error in temperature measurement with the error in the emissivity. It was shown in Section 3.2.2, *The background*, that the thermal derivative is

$$\frac{\partial M(\lambda, T_B)}{\partial T} = M(\lambda, T_B) \frac{c_2 e^{c_2/\lambda T_B}}{\lambda T_B^2 \left(e^{c_2/\lambda T_B} - 1\right)} . \qquad (12\text{-}9)$$

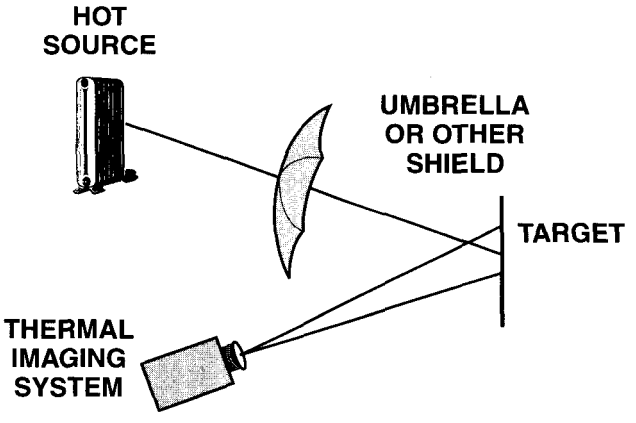


Figure 12-9. Shielding hot sources.

For most applications, $c_2/\lambda T_B >> 1$. For LWIR systems, this is true when $T_B << 1438$K and for MWIR when $T_B << 3597$. Then

$$\frac{\partial M(\lambda, T_B)}{\partial T} \approx M(\lambda, T_B) \frac{c_2}{\lambda T_B^2} . \tag{12-10}$$

Replacing the thermal derivative with $\Delta M/\Delta T$ and rewriting provides

$$\frac{\Delta T}{T_B} = \frac{\lambda T_B}{c_2} \frac{\Delta M}{M} = \frac{\lambda T_B}{c_2} \frac{\Delta \varepsilon}{\varepsilon} , \tag{12-11}$$

where $\Delta\varepsilon$ is the uncertainty in the emissivity and ΔT is the uncertainty in the calculated temperature. For refineries, where the reflectivity can be neglected (Case 2 described at the introduction to this section), let $T_B = 500$K and $\lambda = 10$ μm (LWIR system), then

$$\Delta T = \frac{10(500)(500)}{14388} \frac{\Delta \varepsilon}{\varepsilon} = 174 \frac{\Delta \varepsilon}{\varepsilon} . \tag{12-12}$$

If $\varepsilon = 0.2$ and $\Delta\varepsilon = 0.05$, then the error in temperature is $\Delta T = 43.5$K. As the uncertainty in the emissivity decreases, the uncertainty in the calculated temperature decreases.

12.3.4. INCREASING THE EMISSIVITY

Adding an emissivity "improver" to the surface can increase the emissivity. This could either be paint or tape. The apparent emissivity can be increased by locating a part of the target that approximates a cavity (wedge method) or by adding a "gold cup." Another method employs the image transfer concept. If a highly emissive component comes into thermal contact with the target, then that component's temperature can be measured and thus avoid emissivity uncertainty issues. Develop a safe procedure for applying the "emissivity improver." This is particularly true with energized electrical components and operating machinery.

PAINT/ BLACK TAPE

Black paint and black tape enhance radiation dissipation and hence small objects may be cooler than normally. This is particularly true for printed circuit boards. The application of paint or tape and its removal (if required) may be difficult. Experiment with the paint and tape. Verify that it is truly opaque. Many tapes are made of plastic and many plastics are semi-transparent at the infrared wavelengths (see Figure 4-6). Painting is an art (like painting a car) and may be difficult to apply uniformly.

GEOMETRIC CONSIDERATIONS (WEDGE METHOD)

The wedge method[2] relies upon multiple reflections. In those manufacturing areas where continuous sheets are created, the material usually comes in thermal contact with rollers. The roller forms a wedge with the material (Figure 12-10). This wedge-material combination provides multiple reflections and thus acts as a cavity. This improves the apparent emissivity. The wedge or "multiflex" method has been successfully used at continuous strip annealing furnaces.

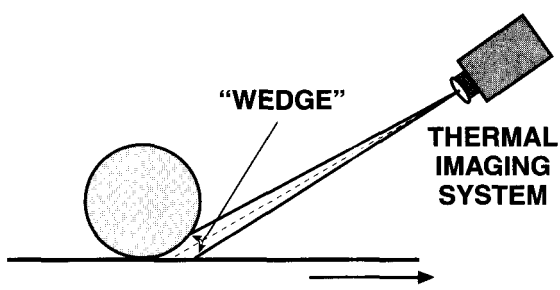


Figure 12-10. The wedge method. By looking at a region where multiple reflections can occur, the emissivity approaches unity. Both the roller and sheet material must be at the same temperature. (From reference 2).

GOLD CUP

The "gold cup" method also relies on multiple reflections.[2] When it is placed near a surface it blocks out any reflecting sources (Figure 12-11). It acts as a blackbody cavity and provides an apparent emissivity of unity.

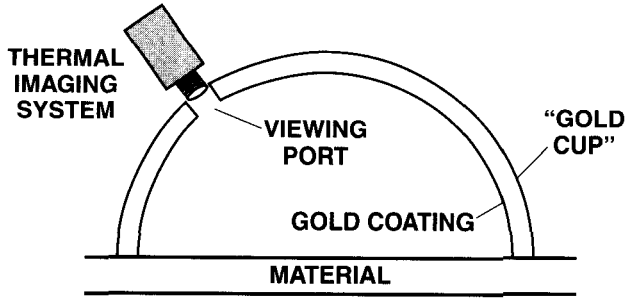


Figure 12-11. The gold cup method. The highly reflective cup increases the reflections and thereby increases the emissivity. (From reference 2).

IMAGE TRANSFER

Image transfer relies upon a highly emissive surface that comes into thermal contact with the target. This technique is appropriate for industries that manufacture continuous sheets. As the roller contacts the sheet, the temperature distribution of the sheet is transferred to the roller.[3] The roller is viewed with a thermal imaging system (Figure 12-12). The technique requires a method that continuously removes the heat distribution from the roller before it contacts the sheet. The roller could be replaced by a membrane.

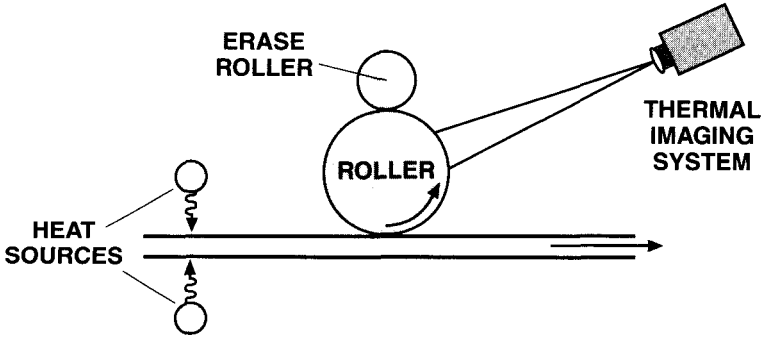


Figure 12-12. Image transfer with a roller. The material can be heated either by the manufacturing process or by an external heater (illustrated here). (From reference 3).

12.4. MEASUREMENT OF T_S

The surround temperature is an input to the equations for emissivity correction and it should be constantly monitored. If the measurements only take a few minutes, then this is not a problem. But if the measurements span tens of minutes, the ambient temperature may change – necessitating changing its value in the thermal imaging system.

Outdoors, the reflected radiation depends upon all objects in the immediate area of the target (for example, see Figure 11-13). These temperatures vary hourly. This creates some uncertainty in the precise ambient temperature to use. Indoors, the environment is usually fairly constant.

If the target is reflective, then point the camera in the direction of the reflected energy source (Figure 12-13) and measure its apparent temperature. The emissivity and surrounding temperature are entered into the camera's look-up table. The camera uses these values to calculate the true temperature of the target.

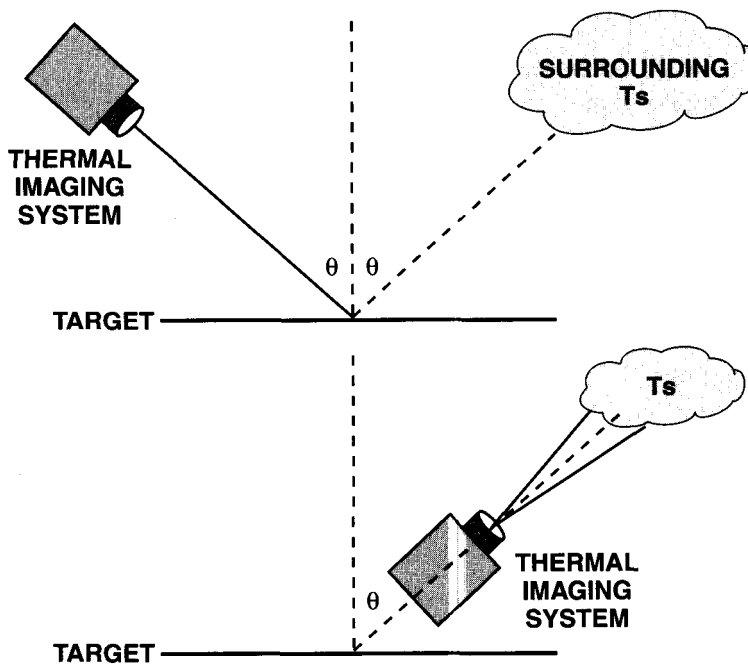


Figure 12-13. Temperature measurements of a (a) reflective target and (b) its environment. It is important to measure T_S at the angle of incidence.

If the target is diffuse, then point the imaging system at the surrounding background (i.e., the sky if outside) and measure the average temperature. This is accomplished by selecting a large region of interest (ROI) and letting the camera calculate the average temperature within the ROI. The emissivity of the surroundings is assumed to be unity. If the camera does not have an averaging function, then defocus the camera. Defocusing tends to average out any nonuniformity that may exist.

12.5. ATMOSPHERIC CORRECTION

If viewing a target at a long path length, the atmospheric transmittance and path radiance must be included in the target temperature calculation. A simple correction for the atmospheric transmittance is difficult. The average values provided in Table 5-3 should only be used for back-of-the-envelope calculations. Removing the atmospheric transmittance and path radiance requires a computer program such as MODTRAN. In addition, you must make many educated guesses about the weather conditions. This is NOT trivial! It is difficult to measure accurately temperatures over long path lengths.

So far, this chapter illustrated the potential error encountered if the emissivity and surrounding temperature were unknown. The precise response of a system depends upon its spectral response. When viewing a real target, the radiation that appears to emanate from the target includes reflected radiation (M_S) and path radiance (M_A). The target signal is attenuated by the atmospheric transmittance (T_A):

$$V_{DETECTOR} = kR_D \left[T_A \left\{ \varepsilon M_T + \rho M_S \right\} + M_A \right] \qquad (12\text{-}13)$$

We must know the emissivity, atmospheric temperature, and the average temperature of the reflected radiation. The detector output is measured and the temperature is inferred from Planck's blackbody radiation law. Since all quantities are a function of wavelength, it is easier to obtain empirical curves rather than theoretical values.

12.6. DUAL BAND MEASUREMENTS

Because of the difficulty of estimating the emissivity, a dual band technique has been recommended.[4-8] The object is viewed by two different thermal imaging systems. Generally, MWIR and LWIR are recommended. Key to the success of dual band imaging is that the emissivity is constant and the same in the two bands. The capability has been demonstrated but is not used extensively since it requires two expensive thermal imaging systems.

Since wavelength dependence is important in dual band measurements, we must use $M(\lambda,T)$:

$$V_{MWIR} = kR_D\left[\varepsilon_{MWIR}M_{MWIR}(\lambda,T_T)+(1-\varepsilon_{MWIR})M_{MWIR}(\lambda,T_S)\right] \quad (12\text{-}14)$$

and

$$V_{LWIR} = kR_D\left[\varepsilon_{LWIR}M_{LWIR}(\lambda,T)+(1-\varepsilon_{LWIR})M_{LWIR}(\lambda,T_S)\right]. \quad (12\text{-}15)$$

If the emissivities are the same in both bands, then

$$\frac{V_{LWIR}-kRM_{LWIR}(\lambda,T_S)}{V_{MWIR}-kRM_{MWIR}(\lambda,T_S)} = \frac{M_{LWIR}(\lambda,T_T)-M_{LWIR}(\lambda,T_S)}{M_{MWIR}(\lambda,T_T)-M_{MWIR}(\lambda,T_S)} \quad (12\text{-}16)$$

If $\varepsilon M(\lambda,T_T) >> (1\text{-}\varepsilon)\, M(\lambda,T_S)$, then

$$\frac{V_{LWIR}}{V_{MWIR}} = \frac{M_{LWIR}(\lambda,T_T)}{M_{MWIR}(\lambda,T_T)} \quad (12\text{-}17)$$

Equations 12-16 or 12-17 can be easily be solved by a computer algorithm.

12.7. SIGNAL AVERAGING

The ***NEDT*** represents an uncertainty in measuring a temperature. Suppose that the uncertainty is given by

$$T_{MEASURED} = T_{TRUE} \pm 3NEDT \quad . \quad (12\text{-}18)$$

That is, we can only say that the true temperature lies between $T_{MEASURED}$ + $3NEDT$ and $T_{MEASURED}$ - $3NEDT$. Suppose N frames are averaged together or N pixels are averaged. Then the uncertainty is reduced to

$$T_{TRUE} = T_{MEASURED} \pm \frac{3NEDT}{\sqrt{N}} \quad . \quad (12\text{-}19)$$

Averaging decreases the uncertainty in temperature measurements. The uncertainty, $3NEDT/\sqrt{N}$, is a measure of repeatability and temperature accuracy.

12.8. REFERENCES

1. R. P. Madding, "Emissivity Measurement and Temperature Correction Accuracy Considerations," in *Thermosense XXI*, D. H. LeMieux and J. R. Snell, Jr., eds., SPIE Proceedings Vol. 3700, pp. 393- 401 (1999).
2. G. R. Peacock, "A Review of Non-contact Process Temperature Measurements in Steel Manufacturing," in *Thermosense XXI*, D. H. LeMieux and J. R. Snell, Jr., eds., SPIE Proceedings Vol. 3700, pp. 171- 174 (1999).
3. X. P. V. Maldague, *Nondestructive Evaluation of Materials by Infrared Thermography*, pp. 141-144, Springer-Verlag, London (1992).
4. J. D. Fehribach and R. B. Johnson, "Temperature Measurement Validity for Dual Spectral-band Radiometric Techniques," Optical Engineering Vol. 28(12), pp. 1255-1260 (1989).
5. N. K. Del Grande, P. F. Durbin, M. R. Gorvad, D. E. Perkins, G. A. Clark, J. E. Hermandez, and R. J. Sherwood, "Dual-band Infrared Capabilities for Imaging Buried Object Sites," in *Underground and Obscured-Object Imaging and Detection*, N. K. Del Grande, I. Cindrich, and P. B. Johnson, eds., SPIE Proceedings Vol. 1942, pp. 166-177 (1993).
6. N. K. Del Grande and P. F. Durbin, "Dual-band Infrared Imaging to Detect Corrosion Damage within Air-frames and Concrete Structures," in *Thermosense XVI*, J. R. Snell, ed., SPIE Proceeding Vol. 2245, pp. 202-207 (1994).
7. H. Kourous, B. N. Shabestari, S. Luster, and J. Sacha, "On-line Industrial Thermography of Die Casting Tooling using Dual-Wavelength IR Imaging," in *Thermosense XX*, J. R. Snell and R. N. Wurzbach, eds., SPIE Proceeding Vol. 3361, pp. 218-227 (1998).
8. G. Barani and A. Tofani, "Comparison of Some Algorithms Commonly used in Infrared Pyrometry: A Computer Simulation," in *Thermosense XIII*, G. S. Baird, ed., SPIE Proceeding Vol. 1467, pp. 458-468 (1991).

13
BUILDING ENVELOPE INSPECTION

The building envelope consists of those walls that separate the environmentally controlled interior from the outdoors. The interior may be either heated or air-conditioned. To minimize energy costs, the exterior walls are insulated to reduce heat conduction and all joints are sealed to prevent air leakage.

Defects and faults such as moisture accumulation, missing insulation, thermal bridges, and air leakage will change the temperature of the surface around the defect. Surface temperature patterns are indirect indicators of subsurface anomalies. Considering that every window, door, pipe, electrical connection, and HVAC duct is a potential location of heat loss, it is amazing that most building are reasonably energy efficient.

Building envelope inspections are carried out for two specific purposes: (1) quality control of new or retrofitted wall assemblies and (2) existing building condition assessment. The purpose of quality control of new construction is to verify that there are no hidden defects that could result in premature material deterioration. Quality control of new construction is the more difficult task: the thermographer does not have the luxury of visual symptoms of material deterioration or failure. The thermographer has to make assessments and recommendations based on available construction drawings and thermal imagery of assemblies that do not show any visible evidence of problems.

This chapter describes heat loss through exterior walls and the next chapter is devoted to roofs. The primary difference is that a roof survey usually relies on the sun to heat entrapped moisture. Since the walls are often shielded from the sun, a temperature difference between the interior and exterior is necessary. This is generally requires heating or cooling the interior. Evaporative cooling can also identify entrapped moisture. Building inspections are usually qualitative.

This chapter draws heavily upon the information provided in references 1-6. Appendix C, *Thermal Sensing and Imaging 1980-1999*, contains numerous papers on building envelope inspections.

13.1. BUILDING SCIENCE

Since building construction changed over the years, it is instructive to briefly study architecture and building materials. The building periods chosen are not static. Different building constructions are normally used over a long period, and new constructions and building materials are gradually introduced into the market. The skill of the builders changes over time. Some knowledge of old building construction and building materials has vanished with past generations.

Water ingress into masonry and mortar can be a problem in climates where there are many freeze-thaw cycles. The continual expansion of ice as it forms acts as tiny crowbars that eventually break down the walls and joints.[1] This problem is acute in cold wet environments. Melt water damage occurs on interior sections of wall assemblies when drainage is towards the interior at floor slabs. Interior wall deterioration is one symptom of this problem.

Building envelopes often contain numerous highly conductive heat flow paths called thermal bridges. Thermal bridges are normally due to the insertion of architectural structures made of more conductive materials than ordinary wall. An uninsulated metal window frame is a prime example of a thermal bridge.

Air leakage leads to increased heating and cooling costs. Warm interior moist air will condense if the exterior temperature is below the dew point. Vapor barriers, placed on the inside, prevent this moisture from condensing. Older buildings without vapor barriers or those with defective barriers permit condensation within the wall when the outside temperature is low. Condensation decreases the thermal efficiency of the insulation and thereby increases heating or cooling costs. Condensation within a defective wall or roof will, over time, lead to deterioration that is costly to repair. If the damage is serious enough, it may not be possible to repair.

13.1.1. HISTORIC BUILDINGS

The thick walls of historic buildings may consist of solid stone (granite, sandstone, or other rock) or thick bricks and may have a cement plaster. The interior walls may be covered with plaster and frescos.

Dampness[2-4] is a major problem affecting the preservation of ancient buildings. Dampness damages decorations, reduces paint adhesivity, causes mildew (black stains), and may allow the growth of micro and macro flora. The extent of decay is mainly related to the permeability of the wall and to water content present. Buildings are often built on fertile ground that have a high water content and near

rivers or canals. This exacerbates the water problem. Water can travel up the wall by capillary action. Water enters during periods of high humidity or excessive condensation (Figure 13-1). The thermal and hydrologic status of the wall is created by weather cycles and man's activities (e.g., area heating, plants and shrubs, and occupancy level).

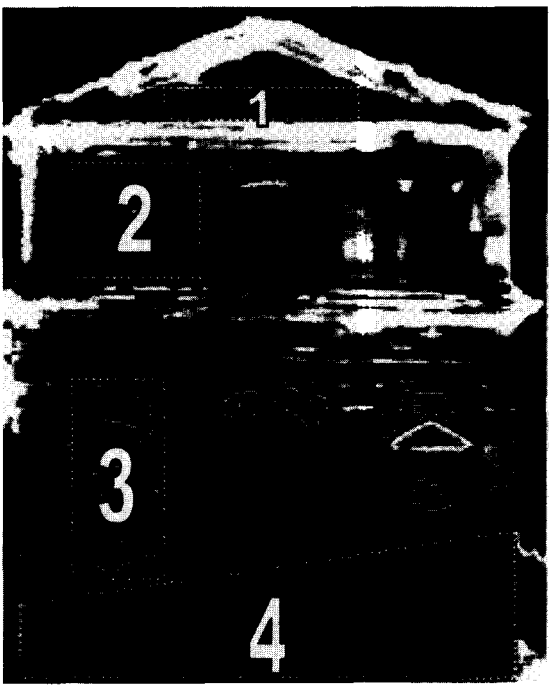


Figure 13-1. Evaporation cools the façade of this 17th century church. Cooling at location 1 is due to rainfall and vegetation. At location 2, plants provide a constant source of moisture. Location 3 variations are due to emissivity differences caused by different types of damage. Capillary action from ground water appears in location 4. The regions labeled A and B are discussed in Reference 2. (By courtesy of E. Rosina et. al.).

Uninsulated solid masonry walls experience low interior temperatures because of the relatively high thermal conductivity. Radiant heating or HVAC is added to make the interior more comfortable for the occupants (the original structure had no heat). Further, the HVAC system may introduce humidification

to reduce static electricity and to protect valuable furniture. The potential for interior water vapor migration into the exterior wall increases dramatically under these conditions.

A phase change is dangerous for wall surfaces. When the water evaporates, the salts in the water crystallize into the pores of the wall. This causes superficial layers to break into chips that lead to the complete disintegration of the wall surface.

For old buildings, neither the underlying materials nor the finishing techniques may be known. The finish affects surface porosity. Decay changes the surface and bulk conduction characteristics. Further, the building may have been repaired with unknown material.

13.1.2. 1880 to 1940 CONSTRUCTION

Most buildings[5] built from 1880 to 1940 have a solid construction with a high quality of craftsmanship. These buildings usually have a heavy wooden and timber construction or heavy bricks and stone constructions. Wood has a low thermal conductivity and therefore these structures offered relatively good thermal insulation.

The weakest part of those buildings seems to be the construction of the wall/roof and wall/wall joints. This leads to severe moisture damages in eaves and in roof connections. The doors and windows were not well sealed and hence allow air infiltration. However, these buildings often had a minimal number of windows and therefore, while air leaks were present, they did not permit significant ventilation. These buildings tend to have a musty smell.

13.1.3. 1940 to 1960 CONSTRUCTION

Buildings from 1940 to 1960 could be of either a heavy or light stone construction or a light wooden frame construction. The quality of construction, thermal performance, and craftsmanship seem to vary a lot during this period. The most obvious defects are air infiltration, high-energy loss, and moisture damage. During this period, vapor barriers and insulation were introduced as standard building materials.

Hollow concrete block was introduced in the early 1900s and became a popular building material around 1950 as a low cost building material. Note that building costs include both the material and labor. Since labor costs are significant, emphasis was placed on selecting materials that were very easy to install (requiring

less skilled and, hence, lower-paid workers). Time is money; a slogan for the building industry was created during this period and is still true today.

13.1.4. 1960 to 1990 CONSTRUCTION

For this period, one finds here the greatest variety of problems, such as high-energy loss, air infiltration, moisture damage in roofs and walls, and thermal bridges. These are due to a combination of constructional mistakes, and poor craftsmanship. Some buildings also have the "sick-house syndrome." Bad indoor air quality was caused by wrong dimensioning, poor adjustment of the ventilation systems, and modern allergenic building materials.

13.1.5. MODERN CONSTRUCTION

Modern construction includes a variety of materials such as aluminum, weathering steel, plastics, and manmade stone.[6] New building construction and materials are often not sufficiently tested to determine damage potential over time.

Exterior wall assemblies[7] on medium and large buildings can be classified into four generic wall types: (1) masonry, (2) architectural precast, (3) metal and glass curtain wall, and (4) insulated steel assemblies. Within these generic types of assemblies, there are variations within the cladding type as well as the assembly configuration. Each generic type performs in a different way. Therefore, the inspection methodology may vary by design to isolate specific problems. Sealants are used around the interior joints of all the panels to achieve air tightness and air barrier integrity. Once constructed, sealed joints are hidden from sight and deficiencies can only be determined thermographically.

The most common masonry wall used in single-story commercial construction is load bearing concrete block that is partially reinforced. These reinforcements can be seen in the IR. The walls are, otherwise, hollow.

13.1.6. WINDOWS

Windows, while simple in construction, provide unique thermograms. Heat is lost through the glass and frame by conduction and by air leakage through poorly sealed frames, ill fitting operable windows, and hinges. The glass may be of varying thickness and the window may be multi-paned (Figures 13-2 and 13-3). The frames

may be wood or metal. The heat conducted depends upon the interior temperature and window treatment (see Figure 8-10). There appears to be an infinite variety of window treatment materials and therefore, an incredible variation in heat loss. Further, the window is semi-transparent in the MWIR spectral region. Typical residential glass (single-thickness) is about 1/4 inch thick and is opaque for wavelengths greater than 4.5 μm (see Figure 4-11).

In some locations, it is common practice to place the central heating radiators under windows to help reduce cold convection currents on the occupants. This can have a dramatic effect on the thermal environment around the window.

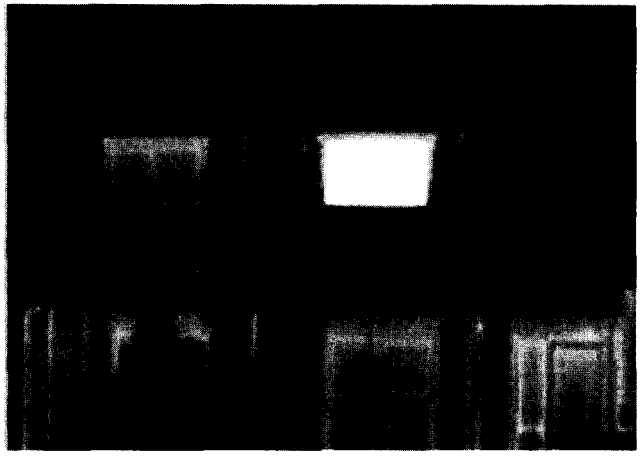
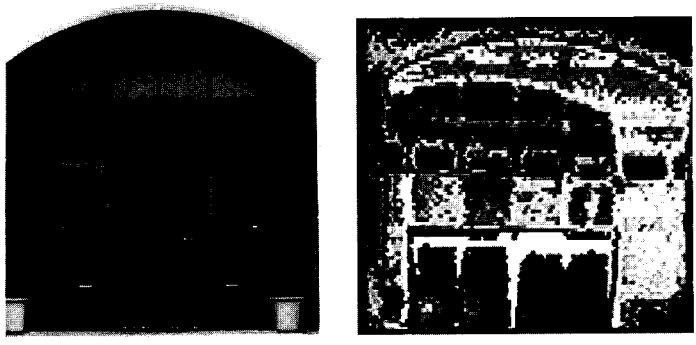


Figure 13-2. The metal studs used in this home have higher heat conductivity than wood and therefore are clearly visible during cold weather. They create thermal bridges. The double-paned windows have a partial vacuum to reduce heat conductivity (see Figure 2-6). The seal on the second-story window broke and the conductivity increased significantly. This interpretation is based upon information provided by the owner. An alternate interpretation is given in Figure 18-6. (By courtesy of the Academy of Infrared Thermography).



VISIBLE **THERMOGRAM**

Figure 13-3. Lobby entrance. The triple-paned windows on the top have excellent insulating properties. The double-paned windows in the center are good. Significant heat is lost around the doors. (By courtesy of Gary J. Weil, president, EnTech Engineering).

13.2. HEAT TRANSFER

There are basically three different measurements: (1) Determination of missing insulation, thermal bridges, or presence of water by differences in thermal conductivity, (2) determination of the presence of water by relying upon evaporative cooling, and (3) air leakage by pressuring the building to create the mass transport phenomenon. Each has its own environmental consideration to insure that there is a significant thermal signature (Figures 13-4 and 13-5).

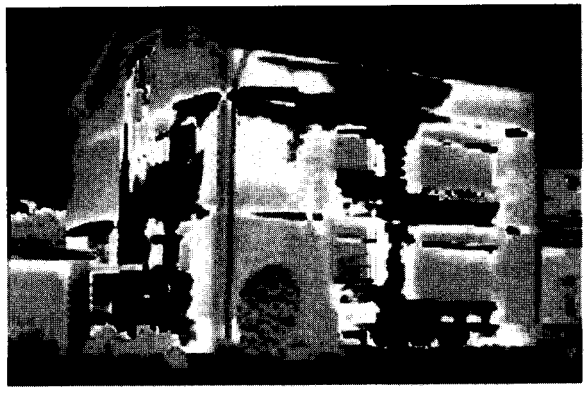


Figure 13-4. This image illustrates heat loss by conduction and air infiltration as well as moisture buildup problems. Proper environmental conditions and careful image interpretation will locate the source of the problem and identify the root cause. (By courtesy of the Academy of Infrared Thermography).

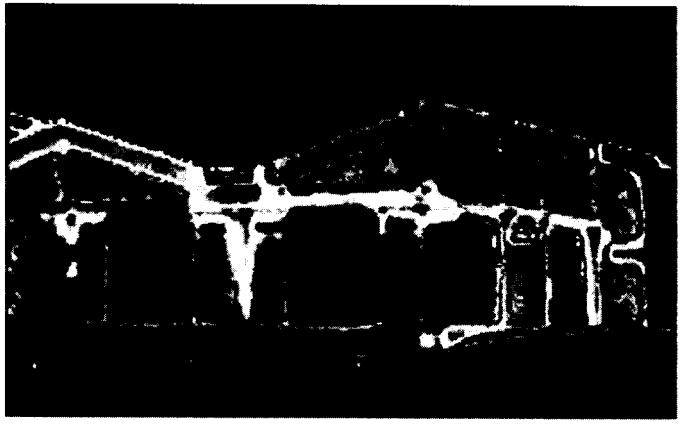


Figure 13-5. Heat leakage at wall/wall, wall/roof, and wall/window joints. (By courtesy of Gary J. Weil, president, EnTech Engineering).

13.2.1. CONDUCTIVITY

Temperature differentials of about 15°C between the inside and outside are sufficient to see water penetration (Figure 13-6). For condensation (Figure 13-7), the internal wall temperature must be below the dew point. Due to the insulating properties of the exterior surface, this suggests that the outside should be near freezing.

When exterior temperatures drop below 0°C, thermal patterns caused by a phase change of water on or underneath the surface of the cladding can be detected. These dark patchy areas on masonry surfaces only exist at or slightly below the freezing mark. These patterns are associated with exterior temperatures falling from above freezing to below freezing during the inspection.

If the outside is cooler than the interior, then a moisture-laden area will appear warm when viewed for outdoors. Simultaneously, it will appear cool when viewed from indoors (Figure 13-8). Missing insulation (Figure 13-9) provides a thermogram similar to moisture intrusion. Additional information is needed to discern the cause of heat loss.

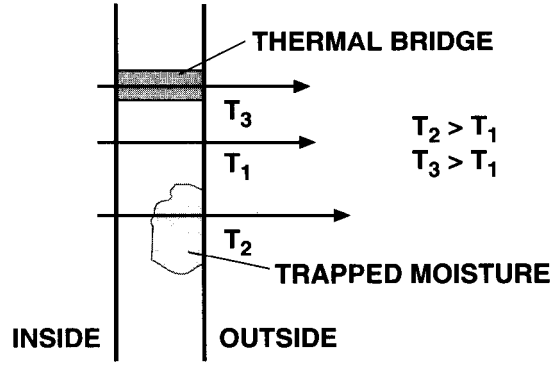


Figure 13-6. Trapped moisture and thermal bridges have a higher thermal conductivity than the insulated wall. The arrow indicates the heat flow from the warm interior to the cool outdoors. The outside temperature must be 15°C less than the inside to see the temperature pattern. When viewed from the outside, the surface temperature at these defects will be higher than at the insulated section.

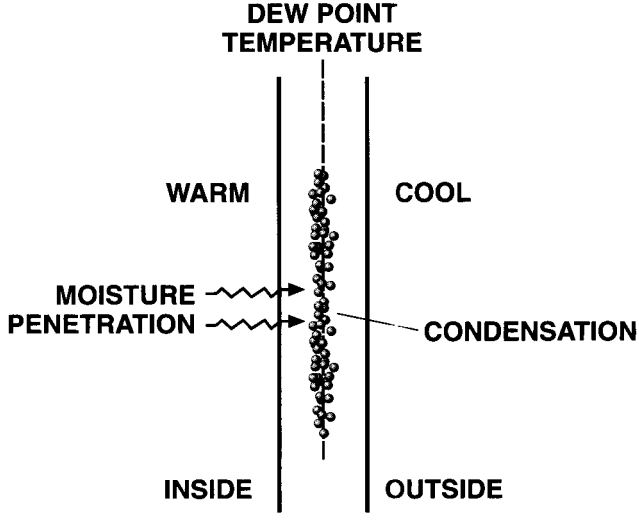


Figure 13-7. Condensation can occur when the interior moisture diffuses through the wall. The internal temperature of the wall must be below the dew point.



Figure 13-8. Moisture increases heat transfer. From the inside, it appears as a cool area. (By courtesy of Academy of the Infrared Thermography).

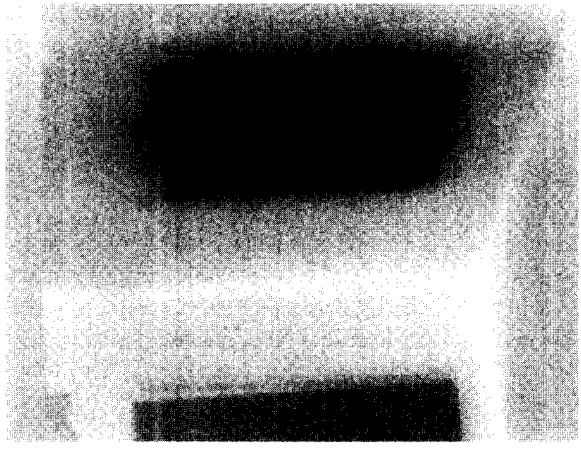


Figure 13-9. A newly constructed house with missing ceiling insulation. (By courtesy of the Academy of Infrared Thermography).

13.2.2. EVAPORATION

Each evaporating gram of water absorbs 539 kcal and this cools the surface very effectively. Therefore, moist areas are colder than the dry ones if submitted to the same boundary conditions (Figure 13-10). The appearance depends on air temperature and relative humidity. Air movement, enhanced by fans will increase evaporative cooling.

Since warm air has lower relative humidity, heating accelerates evaporation. However, it upsets the ambient thermal conditions and heating should be avoided because wet and dry zones have different thermal capacity. If heating is used, the air must be sufficiently cool (not more than 5°C above ambient) to avoid heat transfer from air to the wall. Wall heating will complete with evaporative cooling.

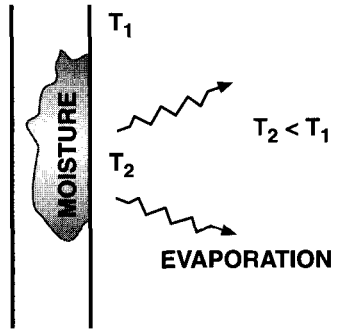


Figure 13-10. Evaporative cooling. The temperature of the wet area will be lower than the dry area. Figure 13-1 illustrated a thermal signature created by evaporative cooling.

13.2.3. MASS TRANSPORT

Air can either enter (infiltrate) or exit (exfiltrate) through cracks in the building envelope (Figure 13-11). This air leakage is accompanied by water vapor from the building interior. When the water vapor reaches the dew point, it condenses within the cavity space. This results in the deterioration of structural members.

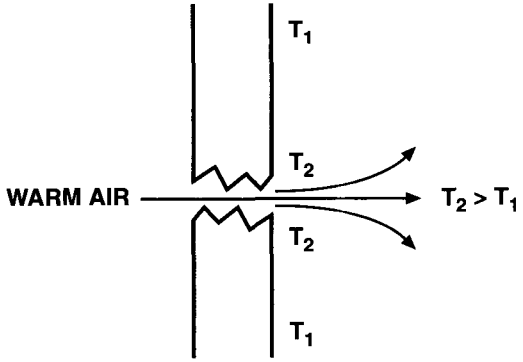


Figure 13-11. Mass transport. As the warm interior air seeps through cracks, the exterior surface is heated.

If there is minimal wind, the area around the crack will heat up (assuming the inside is warmer). This heating is the mass transport phenomenon. The magnitude of the temperature seen depends upon the nature and size of the leak, pressure differential, and temperature differential.

Pressurizing the building can force the warm interior air through the cracks. The resultant temperature distribution is nearly impossible to distinguish from heat conductivity temperature distributions (Figure 13-12). Negative pressure reverses the airflow: the cooler outside air will cool the cracks and the cracks will be at a cooler temperature compared to high heat conductivity areas. Conductive losses are independent of building pressure. This allows differentiation between thermal patterns produced by air leakage and conduction. Depressurization also allows the cool outdoor air to cool the interior surface. Thus, mass transport can be viewed from either the interior or exterior.

In cold climates, buildings generally experience outward air leakage on the upper sections due the stack effect. The stack is generated by the temperature differential between the interior and exterior environments. Wind pressures also increase outward air leakage on the leeward sides. Air leakage can be confirmed by tracer gas and smoke pencil techniques. This will help in quantifying the air infiltration rate.

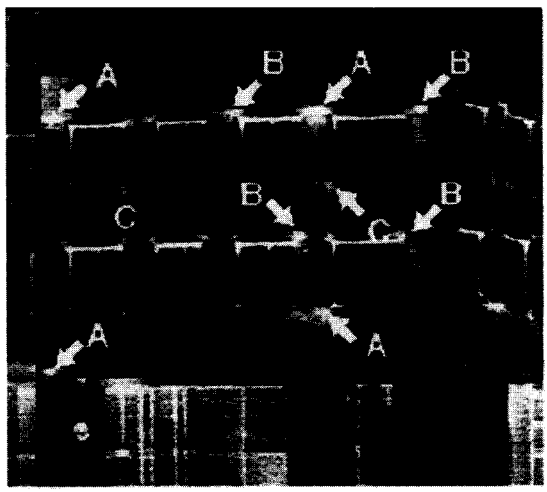


Figure 13-12. Mass transport seen when the insulated masonry-cladded building is under positive pressure. Smoke bomb testing verified mass transport at the locations marked A. Heat loss at locations marked B is a result of openings in the interior air barrier assembly. Locations marked C were not independently verified but are believed to be where leaking interior air first encountered the cladding. (From reference 8, by courtesy of A. Colantonio).

13.3. BUILDING INSPECTION

Because the sun does not directly heat walls, it is necessary to perform measurements when a significant temperature exists between the inside and outside. This suggests that the winter months are desirable. Wind can significantly affect the thermal pattern. Wind speeds should be less than 15 mph (6.7 m/s or 24 kph) for qualitative measurements (see Section 11.3.3. *Wind*).

Inspections of exterior wall assemblies are easier and more cost effective. Apart from the vast amount of walking and time it would take to carry out an interior inspection, in most commercial office buildings access to the individual tenant spaces can be difficult. Interior inspections are generally used to verify thermal anomalies originally found during exterior testing.

Often, high-rise buildings are adjacent to other large buildings. The roofs of adjacent building offer the best vantage points to viewing buildings in high-density urban settings. They should be used as much as possible when available. However, the reflective patterns from adjacent buildings (See Figure 11-14) represent a potential data analysis problem.

13.4. REFERENCES

1. A. Colantino, "Thermal Performance Patterns on Solid Masonry Exterior Walls of Historic Buildings," in *Thermosense XX*, R. N. Wurzbach and D. D. Burleigh, eds., SPIE Proceedings Vol. 3056, pp. 87-95 (1997).
2. E. Rosina, N. Ludwig, and L. Rosi, "Optimal Environmental Conditions to Detect Moisture in Ancient Buildings. Case Studies in Northern Italy," in Thermosense *XX*, J. R. Snell and R. N. Wurzbach, eds., SPIE Proceedings Vol. 3361, pp. 188-199 (1998).
3. E. Grinzato, F. Peron, and M. Strada, "Moisture Monitoring of Historical Buildings by Long Period Temperature Measurements," in *Thermosense XXI*, D. H. LeMieux and J. R. Snell, Jr., eds., SPIE Proceedings SPIE Vol. 3700, pp. 471-486 (1999).
4. P. G. Bison, M. D. Bardeschi, E. Grinzato, T. Kauppinen, E. Rosina, and G. Tucci, "Survey of Facades Based on Thermal Scanning: Palazzo della Ragione, Milan, Italy," in *Thermosense XVIII*, D. D. Burleigh and J. W. M. Spicer, eds., SPIE Proceedings SPIE Vol. 2766, pp. 55-64 (1996).
5. S-A. Ljungberg "Infrared Survey of Fifty Buildings Constructed During 100 Years – Thermal Performances and Damage Conditions," in *Thermosense XVII*, S. A. Semanovich, ed., SPIE Proceedings Vol. 2473, pp. 36-54 (1995).
6. T. C. Jester, ed., *Twentieth Century Building Materials*, McGraw Hill, New York (1995).
7. A. Colantonio "Infrared Thermographic Investigation Procedures for Four Types of Generic Exterior Wall Assemblies," in *Thermosense XXI*, D. H. LeMieux, and J. R. Snell, Jr., eds., SPIE Proceedings Vol. 3700, pp. 458-462 (1999).
8. A. Colantonio, "Identification of Convective Heat Loss on Exterior Cavity Wall Assemblies," in *Thermosense XXI*, D. H. LeMieux and J. R. Snell, Jr., eds., SPIE Proceedings Vol. 3700, pp. 514-20 (1999).

14
ROOF INSPECTION

Infrared inspections are routinely used to locate wet insulation in flat roofs. Here the insulation is between the deck and membrane and is in direct contact with the underside of the membrane (Figure 14-1). This construction is found in commercial, industrial, and institutional buildings. It is less common in residential construction.

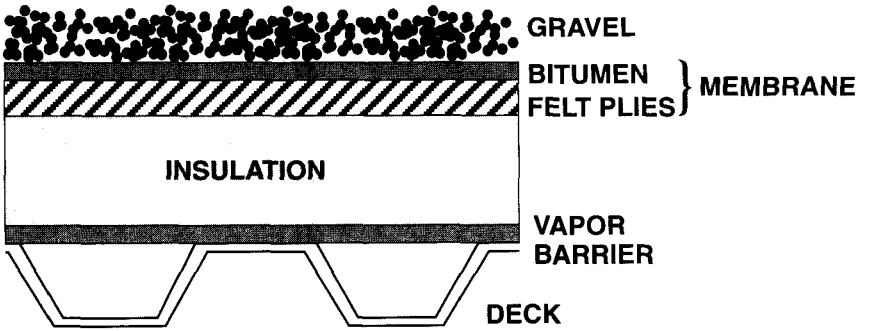


Figure 14-1. Cross-section of a flat roof. The gravel shields the bitumen from the sun's damaging ultraviolet radiation.

Entrapped moisture will ultimately destroy a roof system (Figure 14-2). The roof membrane and insulation will rot. Water may cause decay or rusting of the structural deck. Rotting, blistering, and other degradation of the roof membrane will eventually lead to the demise of at least a portion of the roof system. Water can dangerously increase the weight load of the roof. It decreases the thermal efficiency of the insulation and thereby increases heating or cooling costs. In northern climates, freeze-thaw cycles can cause major damage. Moisture intrusion into a roof system can be caused by several factors (Table 14-1).



Figure 14-2. Because of extensive water intrusion, this roof must be replaced. At nighttime, the waterlogged areas are warmer and appear white in this thermogram. (By courtesy of the Academy of Infrared Thermography).

Table 14-1.
POSSIBLE CAUSES for WATER INTRUSION

Original design inadequacies
Incompatibilities of materials
Poor workmanship
Improper installation of equipment on the roof
Lack of proper maintenance (neglect)
Normal weathering, pollution, and age
Improper drainage
Damage caused by people or animals

Variations in temperature can indicate the location of entrapped water or unusual construction. This requires a thorough understanding of the construction (including repairs) and functioning of the roof. While thermography can be used to locate entrapped water, the source of the leaks usually is determined by some other means.

Roof problems are not normally emergencies (as with electrical equipment). With small leaks, buckets are used to protect the floor. Since it does not rain every day, the leak is forgotten until the next heavy rain. Therefore, people do not deem roof surveys important unless a severe leak is present. Remember the problem will not get better by itself, and the longer it goes uncorrected, the more costly the repair. At current roof replacement costs, any loss would be extremely expensive. Therefore, the early detection of entrapped moisture is of paramount importance in maintaining the integrity of a roof.

Generally, a good roof will last 15 to 25 years. Severe weather or excessive pollution can shorten the lifetime. The roof should be surveyed about five years before the end of its expected lifetime, or sooner if adverse conditions are present and definitely if leaks occur.

Uninsulated roofs (with the exception of lightweight concrete decks) usually do not retain sufficient quantities of water to provide a good thermal signature. Visual inspection of an uninsulated roof is usually adequate to locate damage.

14.1. ROOF CONSTRUCTION

In cold climates, the roof is subjected to snow, ice, and rain. Large quantities of moisture can diffuse into the insulation and condense beneath the roof membrane. The insulation is often protected by a vapor barrier located, as near as possible, to the warm side. As long as the vapor barrier is maintained at a temperature above the dew point, condensation is avoided. If the vapor barrier is in poor condition, the moisture will diffuse to the cold insulation and condense.

If there are hot summers, the moisture generally will evaporate. However, if small amounts of water enter and subsequently evaporate, some permanent damage will result. Significant damage occurs when roof components are exposed to water over long periods.

The insulation may act as a sponge, soaking up the water from leaks and permitting no visual indication of a problem at its inception. The water in the insulation may tend to permeate laterally (particularly with the presence of a vapor barrier) damaging more insulation with a self-propagating cancer-like effect.

The insulation isolates the roof membrane from the thermally stabilizing effects of the building, causing the roof to reach higher temperatures during the hot sunny day and lower temperatures during a cold night. These extreme temperatures significantly increase the thermal stresses placed on the roof membrane. On a clear day, the roof acts a large thermal collector and can reach 70°C (160°F).

Certain constructions can make the detection of moisture more difficult. These include roofs with surfaces that are reflective (typically aluminum), roofs with thick insulating gravel, and roofs with a very heavy top pour of bitumen. A roof surface with extremely heavy gravel, such as a ballasted single ply roof, places an unusually large mass of material above the insulation. This material

will retain sufficient heat to prevent temperature differentials due to the moisture content of the insulation from occurring. These roofs are difficult to survey.

14.2. TEMPERATURE DIFFERENTIAL

Environmental factors play an important role in infrared roof moisture inspections. The sun is the usual source of energy, so a sunny day before the survey is generally required. A roof shadowed by clouds, trees, or building appurtenances may not receive sufficient solar energy to permit a good survey (See Figure 11-14).

However, if there is a minimum of 10°C difference between the interior and exterior for at least 24 hours, a reasonable inspection can be performed. This suggested requirement is based upon heat loss rather than solar gain. The saturated roof sections are good heat conductors. More heat will move through the wet sections. If the outdoors is cooler, then the wet areas will appear warmer.

The 10°C differential requirement suggests that the winter is a better time than the summer. If the roof is surveyed in the winter and then replaced in the summer, the summer heat may have totally dried out the roof – thus leading to skepticism as to the validity of the results. Note that even if the insulation dries out, it rarely returns to its original R-value.

14.2.1. SOLAR LOADING

During the day, the sun heats the roof surface. Water in the wet insulation will tend to remain cool, because of its ability to store vast quantities of energy with little temperature change (high heat capacity). The insulation has a low thermal capacity and allows the roof membrane to heat. When viewed from outside, the roof over the wet insulation will be cooler than that over the dry area.

Since water has a high thermal conductivity, heat will flow into the building. The insulation, with its low thermal conductivity, will have reduced heat transfer. When viewed from the inside, the wet area will appear warmer than the dry area. With good insulation, the dry-area's temperature will be near that of the interior temperature.

At night, an upward-looking surface quickly cools by radiation losses. Well-insulated roofs may cool to 5°C below air temperature. Those areas of roof with wet insulation will tend to remain warm for a longer period compared to the dry insulation due to the stored energy in the water. Additionally, during winter

months, the inside temperature is generally greater than the outside. This causes a heat flow from inside to outside. The high thermal conductivity of the wet insulation will keep the roof surface warmer. These two effects make the roof over the wet-insulation area warmer at night than the dry-insulation area (Figure 14-3).

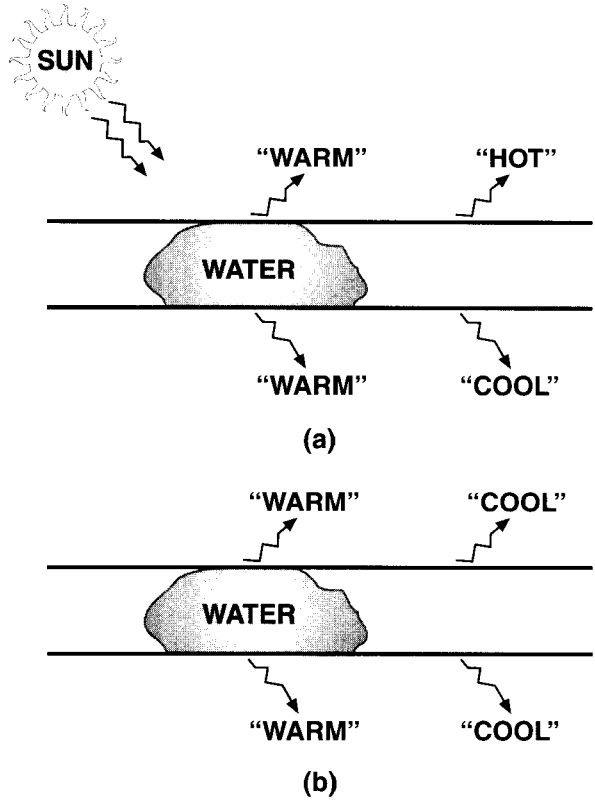


Figure 14-3. Heat transfer during the (a) day and (b) night.

As seen in Figure 14-4, significant temperature differentials between wet and dry insulation exist both during the day and at night. At thermal cross-over, the wet and dry areas have the same temperature. This limits inspections to a few hours during the day and a few hours during the night. The actual ΔT depends upon cloud cover, wind, location (latitude), and season. Figure 11-8 illustrated the ΔT of a tank. The roof, also heated by the sun, follows the same diurnal cycle.

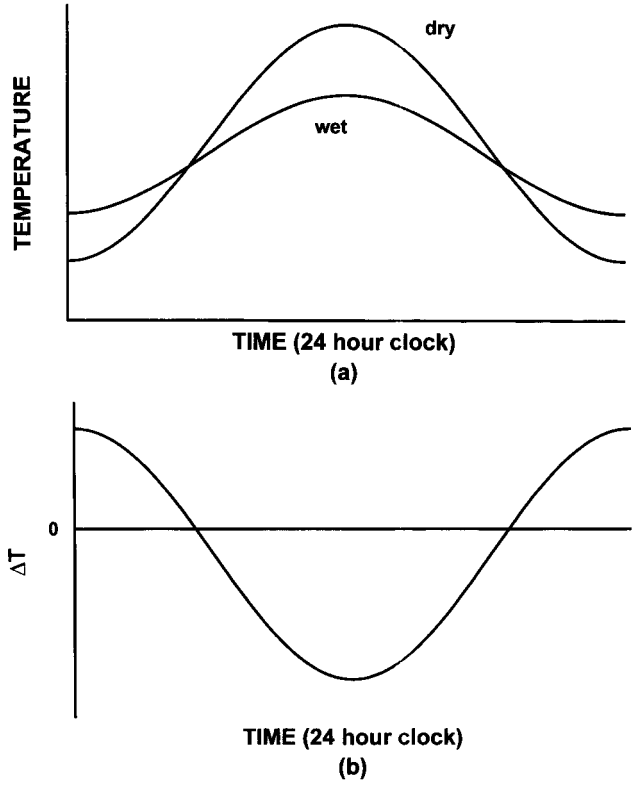


Figure 14-4. Diurnal temperature variation. (a) Actual temperatures and (b) the temperature differential of "wet" minus "dry" temperatures. Thermal crossover occurs just after sunrise and sunset.

In the Northern Hemisphere, the angle of incidence of the sun's radiation is a maximum on June 21 and a minimum on December 21. Thus, solar loading is at a maximum in the summer. However, to achieve a large ΔT, the nighttime outside temperature should be cooler than the inside. This suggests that the inspection should be performed in the winter. With competing phenomena, there is no ideal time of year. Because the inspections are qualitative in nature, roof moisture inspections may be successfully carried out over a wide range of less than optimal conditions.

During a sunny day, the ΔT may be greater than the ΔT at night. However, because of the solar glints and the rapid differential cooling rates observed as clouds shadow the roof, nighttime viewing is preferred.

14.2.2. CLOUDS

The amount of solar loading depends upon the cloud cover. Low solar heating creates a low temperature differential. On hot sunny days the variations are greater and will last longer than on overcast days. A cloudy night will reduce radiative losses from this roof surface. This reduces cooling and affects the ΔT. Figure 14-5 illustrates the temperature differential for two different solar loading. As the solar loading decreases, the ΔT decreases. When the ΔT drops below a predetermined ***SNR***, it is impossible to measure the ΔT. This reduces the amount of time available for an inspection. Figures 14-5a and 14-5b are equivalent to Figures 11-10 and 11-12, respectively.

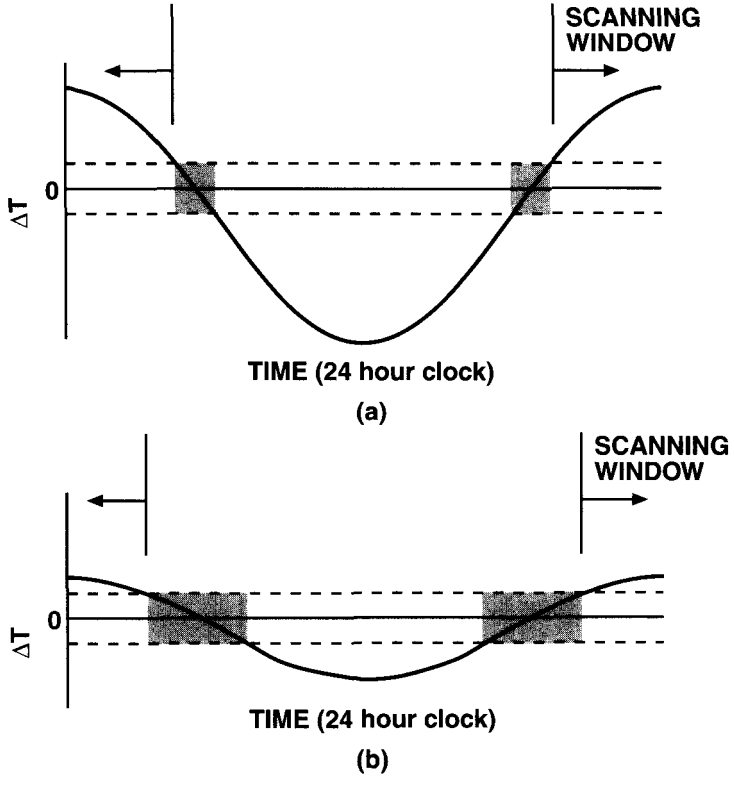


Figure 14-5. Available inspection times. (a) High solar loading and (b) low solar loading. The shaded area represents the time that the ΔT is less than a predetermined value. No inspection can take place during this time. The nighttime scanning window is shown. Conservatively, the magnitude of the temperature differential should be greater than 3 times the NEDT.

14.2.3. WIND

A strong wind can cause the thermal signatures on the roof to virtually disappear due to its cooling effect (See Section 11.3.3. *Wind*). The effect is noticeable when the wind velocity approaches 15 mph (6.7 m/s or 24 kph). Even when the wind in the open may be less than this 15-mph threshold, eddy and vortex wind currents may exceed this threshold. Building projections can channel wind and increase the local velocity. Short-term wind gusts can also alter or mask the thermal signature significantly. Similarly, air movement due to exhaust fans, air handling units, open windows, and open doors can mask variances on the roof.

The effect of the wind can often be gauged by observing the thermal patterns around vent stacks on the roof. When the wind flow is significant, the vent stack disrupting the wind flow produces what appears to be a shadow on the leeward side, as if a light were on one side of the object casting a shadow. This occurrence can sometimes be a sign to the thermographer that the scanning window has closed.

14.2.4. SURFACE MOISTURE

Inspections cannot be carried out when there is standing water on the roof. It is not advisable to do an inspection after a rainfall. Sufficient time must be allowed for the roof surface to dry out. The surface water will eventually evaporate. However, evaporation requires heat and cools the surrounding area. This, too, affects the thermal signature of the roof and leads to false conclusions about the roof integrity. Simply, the presence of surface moisture reduces the scanning window time. This leads to the generally accepted rule: No appreciable precipitation shall have fallen in the 24 hours before the inspection. There shall be no standing water.

14.2.5. HIGH RELATIVE HUMIDITY

As the relative humidity increases, the atmospheric transmittance decreases. For inspections carried out on the roof, this effect is minimal. For airborne inspections, the path length may be greater then 500 meters. Although roof inspections are qualitative, the reduced atmospheric transmission reduces the apparent ΔT, which in turn reduces the scanning window time.

When the roof temperature drops below the dew point (temperature), water will condense on the roof. Water has a different emissivity than the roof and thereby

alters the thermal signature. While the presence of water is easily discerned with an on-the-roof inspection, it is nearly impossible to see with an aerial inspection. However, dew generally will not occur on a cloudy night or a night with a strong wind. It is also interesting to note that dew will not usually occur on areas of wet insulation since these areas are warmer than the air.

14.2.6. PHASE CHANGE

When the outside ambient temperature is near the freezing point, entrapped water can change from a liquid to ice. The temperature of the wet area will remain constant until all the water is converted into ice. This results in a uniform temperature across the roof. Both good and bad roofs will look the same. This can significantly reduce the scanning window time.

On cold clear nights, entrapped water can freeze when the air temperature is as much as five degrees Celsius above zero. Heat transfer to the cold sky causes the surface temperature to drop below freezing. It will take significant solar loading to convert the ice into liquid. In the winter, this is a problem since the solar loading is at a minimum.

14.2.7. REFLECTIONS

Low emissivity (high reflectance) roofs will not heat or cool as quickly as high emissivity roofs. Because of this, it may be difficult to locate moisture in newly aluminized roof surfaces. The emitted energy increases when the surface has oxidized with age or has become dirty. At this point accurate surveys are possible.

High temperature exhaust stacks can also cause thermal shadowing effects on the roof surface. When scanning a roof, it is best to point the infrared system away from these objects to avoid any thermal reflections.

14.2.8. INTERIOR EFFECTS

It is important to know the internal environment of the building. The thermal signature of the roof will be different for cold storage buildings, air-conditioned buildings, and heated buildings. Cool interiors will draw heat from the insulation and thereby reduce the sun's heating effect.

In some buildings, the air handling system uses the drop ceiling as the return air plenum. This return air can cool the entire underside of the roof deck and reduce the heating effect of the sun. This reduces the scanning window time.

14.3. INSPECTION

Many objects in the interior and on the exterior can affect the roof surface temperature. Extremely hot processing areas, refrigerated areas, and the use of the ceiling-to-deck air space as a plenum will affect the inspection interpretation. Of particular concern are air-conditioners, fan housings, ductwork, transformers, drains, and vents installed in the roof (Figures 14-6 and 14-7). Normally, problems associated with surface mounted units and small internal heat sources may be circumvented by appropriate verification techniques. The thermographer will need detailed information to separate expected warm areas from moisture intrusion (Table 14-2).



Figure 14-6. The heating vent is directly underneath this portion of the roof. Spray paint identifies it as area #4. (By courtesy of the Academy of Infrared Thermography).

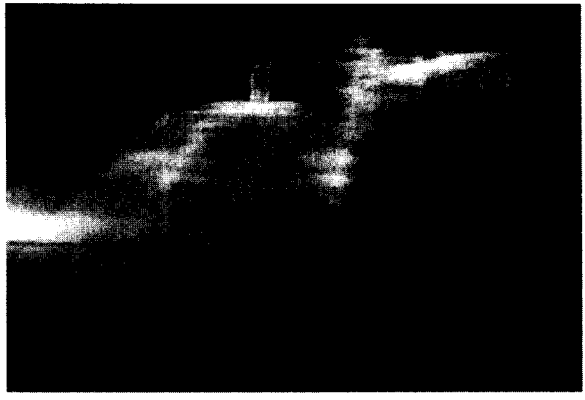


Figure 14-7. A large portion of this roof has a problem. Note the heat loss around the vent. It is difficult to fully insulate protrusions. (By courtesy of the Academy of Infrared Thermography).

Table 14-2
NECESSARY INFORMATION

Repaired areas
Wall location
Insulation voids
Location of HVAC units and duct work
Detailed drawing of the roof edge and supporting structure
Detailed drawing of the roof-wall joint
Details about how projections were installed on the roof

Visual inspection will locate obvious defects such as open joints in the flashing, missing flashing, punctures, blisters, bare spots on aggregate-covered roofs, missing ventilator hoods, cracks in adjacent masonry walls, open joints in coping, and standing water. Once discovered, these problems should be dealt with immediately.

Lightweight concrete materials often retain significant quantities of construction water and this can make it difficult to determine those wet areas caused by unwanted post construction moisture infiltration. Closed-cell insulation has a different wetting pattern than other roof insulation. Because of their closed-cell nature, it takes an increased exposure to moisture for the water to significantly infiltrate. For this reason, surveys on roofs with slow wetting, closed-cell insulation should be delayed until they are at least 8 months old.

WHEN TO INSPECT

When a new roof has been installed or a patch made, thermography should be used to verify job success. An additional inspection should then be carried out just before the end of the warranty period. If anomalies are found the contractor can return and correct the problem at his cost. After the warranty period, the owner must pay for all repairs.

The American Society for Testing and Materials (ASTM) has provided uniform, generally accepted standards for testing for over 90 years. ASTM C1153-90 applies to Roofing Systems.[1] It recommends nighttime surveys to delineate areas of wet insulation located above the deck and below the waterproofing system (membrane). ASTM C1153-90 outlines the minimum criteria for infrared imaging systems, the effect of meteorological conditions, roof construction, and verification criteria.

14.4. REFERENCES

1. ASTM C1153-90, "Standard Practice for the Location of Wet Insulation in Roofing Systems Using Infrared Imaging," Annual Book of ASTM Standards, Vol. 4.06, American Society for Testing and Materials (ASTM), Philadelphia, 1990.

15
POWER DISTRIBUTION

Nearly everything is powered by electricity. Living nearly stops without electricity. We would lose office lighting, street lighting, and traffic lights. Elevators would stop. All communications would stop (radio, television, and telephones). No heat in the winter can place an extreme hardship on people. Food in refrigerators spoils and ice cream melts in the summer. Factories would shut down losing millions of dollars. Granted, critical areas have emergency back-up power, but power loss is a serious problem.

It has become imperative that electricity be available at all times. To insure constant flow, the generation and distribution systems must be inspected on a regular basis for potential degradation. Fortunately, degradation is usually accompanied by an increase in resistance. As the resistance increases, the power dissipated by the degradation increases and appears as heat.

The temperature rise is a measure of resistance. Loose connectors, corroded connectors, and partially broken wires have increased resistance (Figure 15-1). Increased temperature often accelerates corrosion and may lead to total failure. Faults, if not repaired, may lead to catastrophic failure (explosion or fire), unplanned plant shutdowns, and production losses.

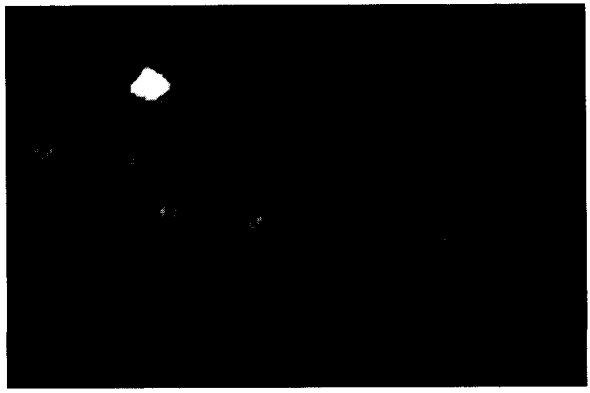


Figure 15-1. A poor electrical connection has a relatively high resistance. Its temperature depends upon the electrical current and wind speed. (By courtesy of the Academy of Infrared Thermography).

Electrical inspections are usually quantitative in nature. The applications fall into five generic categories (Table 15-1). Although transmission and distribution are considered different by some, they are both considered in this chapter as part of the overall distribution system. Transmission equipment includes suspension structures, insulators, and lines. These lines are the main arteries of the utility system and are quite important. Distribution systems consist of lines, poles, associated lightning protection, and power takeoff equipment.

The material in this chapter draws heavily from references 1-4. Addition information on electrical inspections is in Appendix C, *Thermal Sensing and Imaging 1980-1999.*

Table 15-1
POWER GENERATION, DISTRIBUTION, and USE

Category	Example
Power generation	Hydroelectric, fossil fuel, nuclear
Power distribution	Power lines, transformers, substations
Industrial users	Process and manufacturing industries
Commercial users	Warehouses, office buildings, schools
Residential users	Lighting, heating, air conditioning

15.1. RESISTANCE

The resistance of a homogeneous conductor is

$$R = \frac{\rho L}{A} \quad , \tag{15-1}$$

where ρ is the material's resistivity, L is the length, and A is the cross-section. Since the resistance is measured in ohms, the units of each variable must be consistent (Table 15-2). Then

$$\rho = 1\ \Omega - m = 10^{-2}\Omega - cm = 0.305\ \ \Omega - ft\,. \tag{15-2}$$

Table 15-2
UNITS

Resistivity, ρ	**Length, L**	**Area, A**
ohm-cm	cm	cm^2
ohm-m	m	m^2
ohm-ft	ft	ft^2

Copper wire is usually found within factories, commercial buildings, and residences. Because copper is relatively expensive, power distribution systems generally employ aluminum wire. The resistivity depends upon manufacturing techniques. For copper, the resistivty is approximately 1.77×10^{-8} ohm-meters or 5.81×10^{-8} ohm-ft. For aluminum, it is approximately 2.82×10^{-8} ohm-meters or 9.26×10^{-8} ohm-ft.

In the scientific community, resistivity has units of ohm-meters. The U.S. power industry uses ohms-circular mils per foot (usually abbreviated to mil-foot). A mil is 1/1000 of an inch. Since most wires are circular in cross section, the circular mil (CM) is equal to the diameter squared when the diameter is measured in mils. This approach eliminates the factor π that appears in area calculations:

$$A = \pi\frac{D^2}{4} \quad , \tag{15-3}$$

and

$$CM = D^2 \quad . \tag{15-4}$$

The current carrying capacity of wire depends upon an allowable temperature rise. As the resistance decreases, capacity increases. Since resistance decreases with diameter, larger wires can carry more current. While indoor wiring and feed-in lines are insulated for safety, power distribution systems generally are not. Electrical insulation also acts a heat insulator: an uninsulated wire has a higher current capacity. The values in Table 5-3 are from the U.S. National Electrical Code. Depending upon the insulation, these values may be reduced. Since aluminum has a higher resistivity, the allowable current capacities are 84% of the values in Table 15-3.

Ohm's law provides the relationship among resistance, current (I), and voltage (V):

$$V = IR \quad . \tag{15-5}$$

Table 15-3
ALLOWABLE CURRENT of UNISULATED COPPER WIRE
(American Wire Gauge or AWG)

AWG Wire Size	Diameter (inches)	Area (CM)	Allowable current (amps)
0000	0.460	211,600	325
000	0.4096	167,800	275
00	0.3648	135,100	225
0	0.3249	105,560	200
2	0.2576	66,358	125
4	0.2043	41,738	100
6	0.1620	26,244	70
8	0.1285	16,512	50
10	0.1019	10,384	35
12	0.08081	6,530	30
14	0.06408	4,106	20

Figure 15-2 illustrates a power generation facility with a load connected by a power line. Both the load and line can be treated as resistors (Figure 15-3). Since the current is constant in a series circuit, the voltage drop across the load is

$$V_{LOAD} = \frac{R_{LOAD}}{R_{LOAD} + R_{LINE}} V_G \qquad (15\text{-}6)$$

and the load across the line is

$$V_{LINE} = \frac{R_{LINE}}{R_{LOAD} + R_{LINE}} V_G \quad . \qquad (15\text{-}7)$$

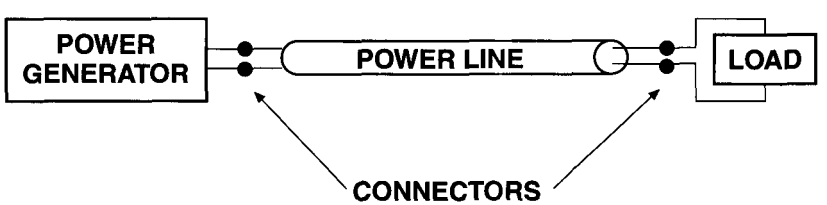


Figure 15-2. Power supplied to a load.

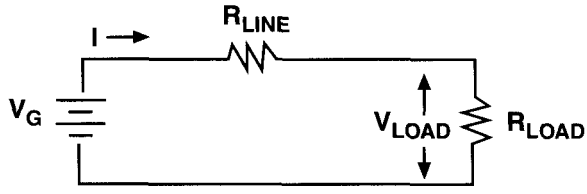


Figure 15-3. Electrical representation of Figure 15-2.

As line resistance increases, the voltage across the load decreases. While the wire resistivity seems low, very long power lines can have a significant resistance. For comparison, Table 15-4 lists the resistance of some common residential appliances. If the voltage drop across the line is large, then there is insufficient voltage to power the appliances.

Table 15-4
RESISTANCE of TYPICAL RESIDENTIAL APPLIANCES

Appliance	Voltage (V)	Current (A)	Resistance (Ω)
150W light bulb	120	1.25	96
Hot water heater	240	20	12
Air conditioner	240	45	5.3

The power loss in the line is sometimes called copper loss. A power generating facility provides the power ($P = VI = I^2R$) that is consumed by the load. Since power is constant, a step-up transformer may increase the voltage to 500,000V with an equivalent drop in current. Then a step-down transformer provides the voltage required at the load. With a low current flowing through the power line, copper loss is minimal. For illustrative purposes, Figure 15-4 illustrates a 1000:1 variation in voltage and current. Since the current decreases by 1000, the copper loss (power loss) decreases by 10^6.

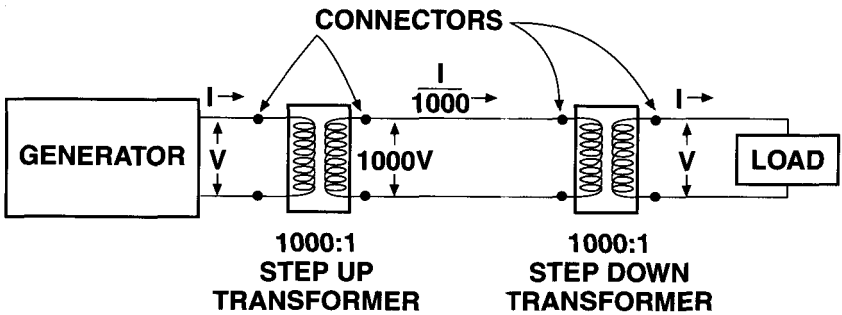


Figure 15-4. Step-up and step-down transformers in a power transmission system. If corroded or loose, the connectors can create additional resistance.

15.2. TEMPERATURE

When a resistor dissipates electrical energy, its temperature will increase by

$$\Delta T = \frac{Q_{ELECTRICAL}}{m\,c} \quad , \tag{15-8}$$

where c is the heat capacity (See Equation 2-2). Since energy is the power delivered over time t,

$$Q_{ELECTRICAL} = I^2 R t \quad . \tag{15-9}$$

This suggests that the temperature would increase without bound. However, as the resistor starts to heat up, it loses energy through radiation, convection, and conduction. Since electrical circuits use metallic components, significant heat can be conducted away from the resistor (see Figure 15-5 and Section 11.5.2. *Small targets*). This, combined with convective cooling, lowers the steady state temperature. Even if the resistance at the site of the fault is constant, one cannot assume that the temperature rises proportionally with the power dissipated. It is a nonlinear function of heat capacity, conduction, convection, and radiation. At steady state (resistance reaches a constant temperature), the heat transfer is

$$Q_{RADIATION} + Q_{CONDUCTION} + Q_{CONVECTION} = Q_{ELECTRICAL} \quad . \tag{15-10}$$

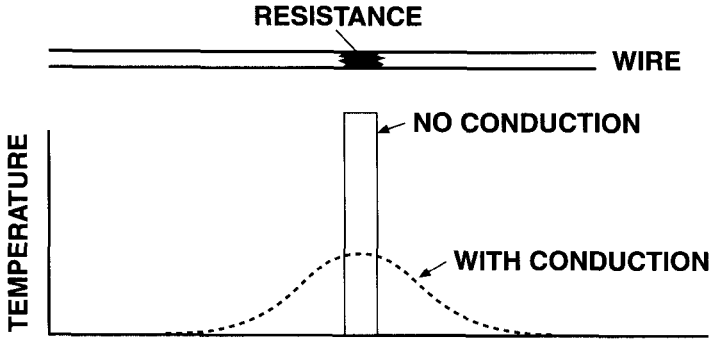


Figure 15-5. Effects of thermal conductivity. Without conductivity, the local temperature is high. With conduction, heat flows away from the source and provides an overall lower temperature.

15.2.1. RADIATION

When conduction and convection are negligible, the electrical power dissipated (I^2R) is balanced by the radiation at an elevated temperature. It is convenient to express the temperature increase as

$$\Delta T = k I^2 R \quad , \tag{15-11}$$

where k is a constant and ΔT is the temperature above ambient. When ΔT exceeds a preset value, the component must be repaired or replaced. The maximum temperature difference, $\Delta T_{FULL\text{-}LOAD}$, occurs when the maximum current, $I_{FULL\text{-}LOAD}$, is flowing (Figure 15-6). The value $I_{FULL\text{-}LOAD}$ is the maximum current for which the circuit is designed. Generally, measurements are not made under full load. Rather, the circuit is partially energized and the thermographer has to estimate the temperature at full load:

$$\Delta T_{FULL-LOAD} = \Delta T_{MEASURED}\left(\frac{I_{FULL-LOAD}}{I_{MEASURED}}\right)^2 \quad , \tag{15-12}$$

where $\Delta T_{MEASURED}$ is the temperature of the resistance when $I_{MEASURED}$ amps flows. Equivalently,

$$T_{FULL-LOAD} = T_{AMBIENT} + \left(T_{MEASURED} - T_{AMBIENT}\right)\left(\frac{I_{FULL-LOAD}}{I_{MEASURED}}\right)^2 . \tag{15-13}$$

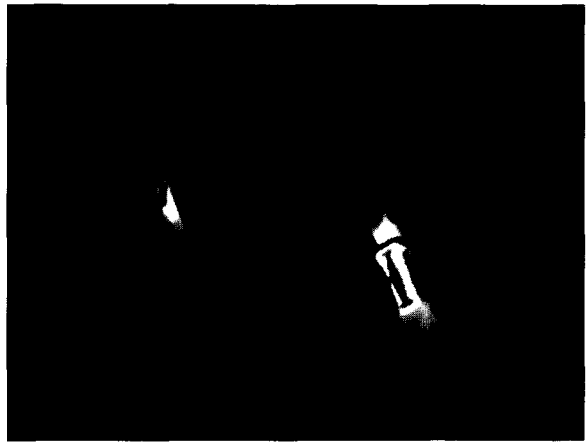


Figure 15-6. Fully loaded main bus bars at an aluminum processing plant. The difference in temperature between the two suggests a poor connection. (By courtesy of IRcameras.com).

15.2.2. CONDUCTION

When conduction is included, it is convenient to modify the equations[5] to:

$$\Delta T_{FULL-LOAD} = \Delta T_{MEASURED}\left(\frac{I_{FULL-LOAD}}{I_{MEASURED}}\right)^{N}, \qquad (15\text{-}14)$$

and

$$T_{FULL-LOAD} = T_{AMBIENT} + \left(T_{MEASURED} - T_{AMBIENT}\right)\left(\frac{I_{FULL-LOAD}}{I_{MEASURED}}\right)^{N}. \qquad (15\text{-}15)$$

As heat conduction increases, the exponent decreases (Table 15-5). Note that with low conduction, the equations are identical to those presented in the previous section: $N = 2$.

Table 15-5
EMPIRICAL EXPONENT for TEMPERATURE
(From Reference 5)

Thermal conductivity	Exponent
High	1.6
Fair	1.8
Low	2.0

High thermal conductivity occurs in large connectors and large diameter cables. Recall the conductivity equation:

$$\frac{Q}{t} = \frac{kA(T_2 - T_1)}{L} \quad . \tag{15-16}$$

As the cross-sectional area increases, the heat flow increases.

15.2.3. CONVECTION

Wind speed (forced convection) has a major effect on the temperature of power lines. Power lines do not have much mass and a relatively large surface area. Therefore, they are easily cooled by wind. Figure 15-7 illustrates the drop in temperature as a function of wind speed and direction. Wind traveling perpendicular (cross wind) to the wires provide the greatest cooling. The temperature equations should be further modified to include the effects of convection. Although no definitive data exists, limited experiments[6] provided exponents with values of between 0.6 and 1.1 for Equations 15-14 and 15-15. Recent laboratory data[7] confirm the cooling effect of wind: the temperature decreases significantly as the wind speed increases. Noteworthy is the dramatic drop in apparent temperature as the speed increases from 1 m/s to 4 m/s.

Wind effects were discussed in Section 11.3.3. *Wind*. For qualitative measurements such as building and roofs, the wind speed should be less than 15 mph (24 kph or 6.7 m/s). Qualitative measurements require much lower wind speeds with speeds less than 5 mph (8 kph or 2.2 m/s) recommended (Figures 15-8 and 15-9). The only thing that appears to be true about environmental influences is that fewer components fail outside during cold windy days.

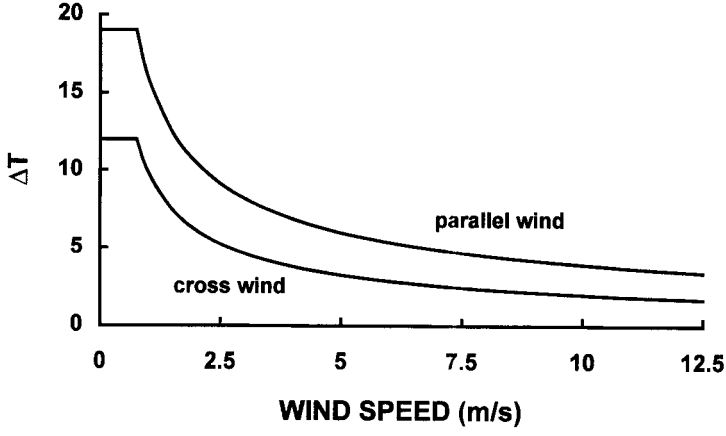


Figure 15-7. Variations of power line temperature with wind speed and direction. The temperature is constant for speeds less than 1 m/s (2.2 mph or 3.6 kph) (From reference 6)

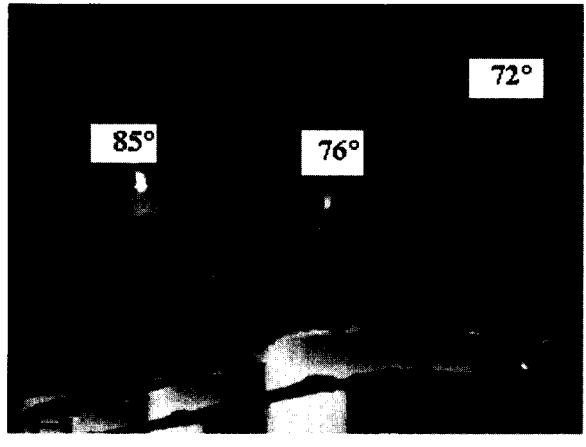


Figure 15-8. Wind effects on the temperature of an oil-filled circuit breaker. A moderate wind cooled the connectors to the temperatures shown. (By courtesy of J. Fritz, Snell Infrared)

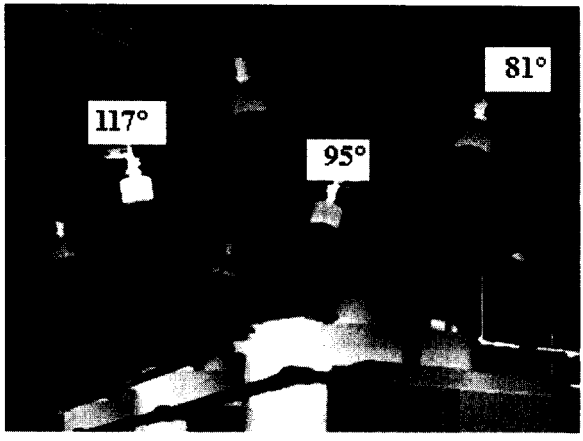


Figure 15-9. With a light wind, the connector temperatures approached the calm-air, steady state values. The true temperature differences (masked by the wind in Figure 15-8), suggest that a problem exists. (By courtesy of J. Fritz, Snell Infrared)

15.3. POWER DISTRIBUTION INSPECTION

Transmission lines are largely cross-country and therefore aerial inspection is preferred. The three items of prime interest are line clamps, connections, and insulators (Figure 15-10). While the inspection, ideally, should be carried out at nighttime to avoid solar loading and possible sun glints, it is difficult to locate power lines in the darkness. In the early morning, there is sufficient light without significant solar loading.

When possible, position the airplane such that the wire is against a neutral background to avoid confusion between hot spots and ground clutter. The inspection may appear somewhat boring since faults are typically far apart. It may difficult to measure the temperature from an aircraft due to vibration of the aircraft, wind swaying the wires, and the fault being smaller than the MIFOV. It may be appropriate to locate problem areas from the air and then to perform a ground inspection to verify the temperature.

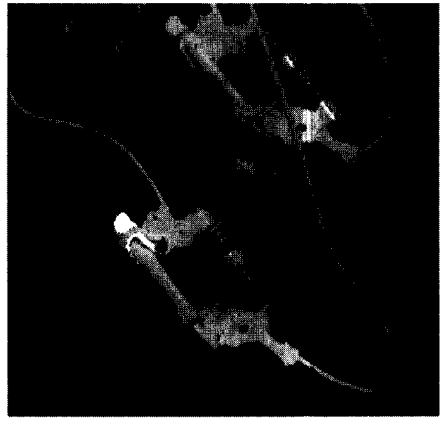


Figure 15-10. Overheated electrical connection. (By courtesy of the Academy of Infrared Thermography).

Transformer bushings insulate the electricity from the ground plane. They are also waterproof to prevent water from entering the transformer. The question is whether the heat is being generated in the external bushing connection or whether the bushing is acting as a heat sink for an internal problem. We cannot see inside the transformer and therefore cannot see the precise location of the defect (Figures 15-11 and 15-12). To allow for seasonal load changes, electrical inspections should be performed at least twice a year. Many transformers are oil-filled and have cooling fins. When operating properly, the cooling fins will have a uniform temperature distribution. Blocked fins (Figure 15-13) will be cooler.

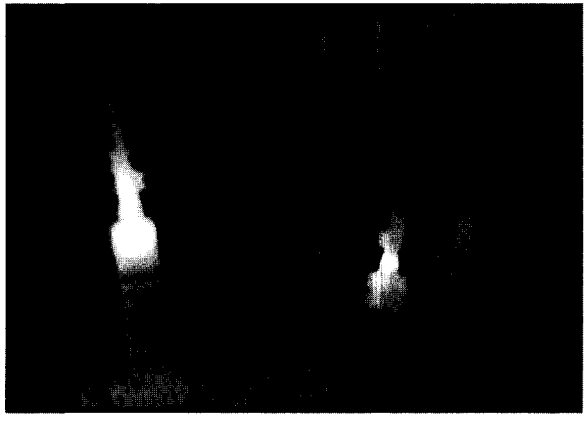


Figure 15-11. Overheated transformer bushing. (By courtesy of the Academy of Infrared Thermography).



Figure 15-12. Overheated bushing. (By courtesy of IRcameras.com).

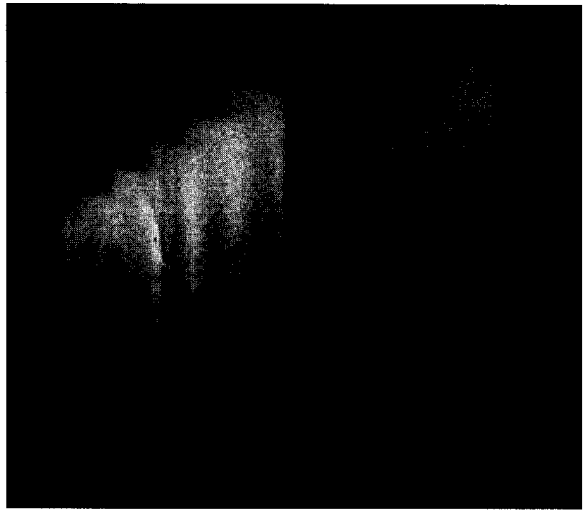


Figure 15-13. Blocked cooling fins on an oil-filled transformer (By courtesy of Gary J. Weil, president, EnTech Engineering).

15.4. REFERENCES

1. G. S. Baird, "Quality Aspects of Electric Utility Inspections," in *Thermosense VIII*, H. Kaplan, ed., SPIE Proceedings Vol. 581, pp. 98-102 (1985).
2. J. L. Giesecke, "Substation Component Identification for Infrared Thermographers." in *Thermosense XIX*, R. N. Wurzbach and D. D. Burleigh, eds., SPIE Proceeding Vol. 3056, pp. 153-163 (1997).
3. T. L. Hurley, "Infrared Qualitative and Quantitative Inspections for Electric Utilities," in *Thermosense XII*, S. A. Semanovich, ed., SPIE Proceedings Vol. 1313, pp. 6-24 (1990).
4. J. R. Snell, Jr., "Problems Inherent to Quantitative Thermographic Electrical Inspections," in *Thermosense XVII*, S. A. Semanovich, ed., SPIE Proceedings Vol. 2473, pp. 75-81 (1995).
5. T. Perch-Nielsen and J. C. Sorrensen, "Guidelines to Thermographic Inspection of Electrical Installations," in *Thermosense XVI*, J. R. Snell, ed., SPIE Proceedings Vol. 2245, pp. 2-13 (1994).
6. S. G. Burney, T. L. Williams, and C. H. N. Jones, *Applications of Thermal Imaging*, page 86, Adam Hilger, Philadelphia, PA (1988).
7. R. Madding and B. R. Lyon, Jr., "Environment Influences on IR Thermography Surveys," *Maintenance Technology*, pp. 36-41 (December 1999).

16
ELECTRICAL/MECHANICAL INSPECTION

The motor provides the link between electrical power and mechanical power. During normal operation, motors will heat up due to electrical and mechanical energy dissipation. The windings have resistance and heat is a by-product of friction. As with electrical components, it is important to be able to identify faulty components. This chapter discusses the electrical connections to the motor (via a distribution panel, fuses, and bus bars) and the mechanical output (bearings, pulleys, and belts).

In order to determine if a motor is operating outside of its normal temperature, the following questions must be answered: What is the capacity of the motor? What are its ratings? What temperature rise (absolute or differential above ambient) is significant? Is it operating under different conditions than normal? To evaluate a motor properly requires a tremendous amount of information. It is extremely valuable to have a baseline thermograph that indicates the temperature distribution when operating under normal load. Thermal anomalies are any deviations from this baseline or "golden" thermogram. While always looking for hot spots, a cool spot may indicate an open circuit or inoperative element. Interestingly, an open in one part of a circuit may cause an overload (and hence heat) in another part of the circuit. The current must always be checked.

A thermal anomaly (also called an exception, deficiency, or fault) refers to a component whose temperature is different than expected. The temperature may be either greater of less. Generally, the term *deficiency* or *exception* is restricted to those components that appear to be non-operational, not performing properly, or defective.

The material in this chapter draws heavily from references 1-4. Additional information on electrical inspections is in Appendix C, *Thermal Sensing and Imaging 1980-1999.*

16.1. BASELINE THERMOGRAM

To determine an adverse operating temperature of a component it is necessary to have a baseline thermogram (or "golden" thermogram). With a clear understanding of normal operation it is easy to quickly identify a thermal anomaly.

Baselines vary with manufacturer, materials used, surface finish, paint or other coating, environment, location, and proximity to other heat producing equipment. Consequently, the baseline may be unique to the particular unit being tested. Under ordinary operating conditions, a machine may develop hot spots that are perfectly normal, expected, and even by design.

For rotating machinery, two choices are possible. (1) Stop the machinery and take a thermogram. The image must be captured quickly to avoid cool down. (2) Synchronize the camera with the rotation. The frame time must be fast to prevent blurring. This is similar to using a strobe light to stop action (See Figure 2-18). However, most rotating machinery have safety shrouds. The shroud, of course, limits your view of the rotating parts.

16.2. ELECTRICAL CONNECTIONS

Figure 16-1 illustrates a distribution panel. Each connection and fuse has a very small resistance. When current passes though the circuit, all components will heat up (Figures 16-2 through 16-4). As a connection corrodes, the resistance increases with a commensurate increase in temperature. The fundamental question is "Is the temperature rise excessive?" When the temperature is above a predetermined value, then the component is deemed defective and must be replaced.

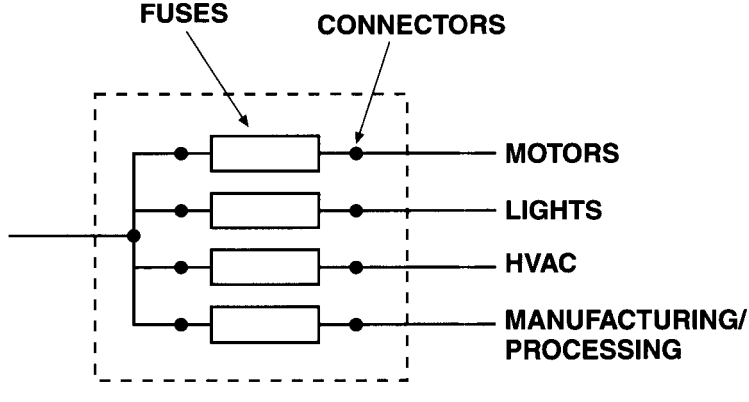


Figure 16-1. Distribution panel.

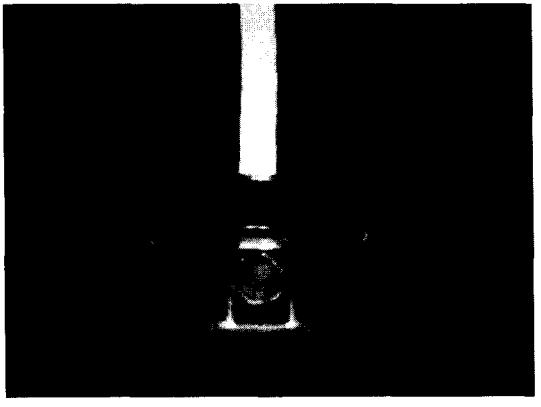


Figure 16-2. A poor connection that is underneath the bolt and hidden from view. The wire conducts the heat away from the fault. If the wire were overloaded, the entire length would be at a uniform elevated temperature. (By courtesy of the Academy of Infrared Thermography).



Figure 16-3. Overloaded wires. (By courtesy of IRcameras.com).

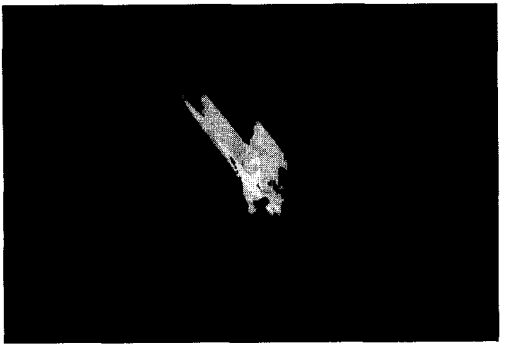


Figure 16-4. Poor connection on a knife switch. (By courtesy of IRcameras.com).

There are two considerations for identifying anomalies. Temperature guidelines specify the maximum temperature by an absolute temperature and differential temperature above ambient. The second is by comparison to companion components in similar circuitry. The latter refers to three-phase systems where all phases usually carry the same current. If a component in one phase has a different temperature than the other two components, then that component is suspect. Causes of excessive heat include overloaded circuits, corroded connectors, broken wires, loose connectors, phase imbalance, and defective components. While Figures 16-2 through 16-4 illustrated overheating, it is important to measure the actual temperature and differential temperature (Figures 16-5 and 16-6).

To have a good connection, two elements must be taken into account: clean contact surfaces and proper pressure. It is important to understand that just because a connection is identified as a thermal anomaly does not mean it is loose.[1] It could be oxidized, corroded, or have dirty contact surfaces. There may be a problem with cross threading, the wrong bolt or screw may be in place, the connection may be wrongly sized, or conductor strands may be broken away from the fitting. In these situations, applying a specified torque will not result in a good electrical connection.

We know when our car does not start (insufficient power to turn over the engine), that the battery is probably at fault. If the battery connections are corroded, they are immediately suspected. Corrosion is probable since car batteries are based upon a lead-acid combination. We also learned that trying to tighten the connection may provide temporary relief – the car starts a few more times. But we know that the connections must be completely cleaned to restore full electrical contact.

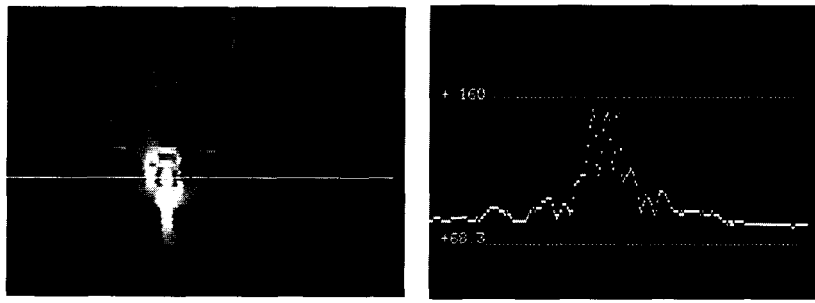
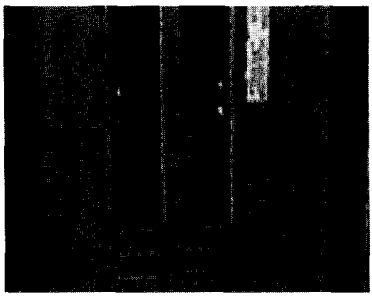


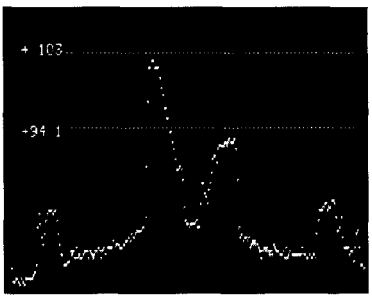
Figure 16-5. Overheated connection. The temperature profile across one line of the thermogram (indicated by the horizontal white line) shows a temperature rise of nearly 90°F (50°C). (By courtesy of Gary J. Weil, president, EnTech Engineering).



VISIBLE



THERMOGRAM



LINE PROFILE

Figure 16-6. Overheated circuit breakers. The temperature profile shows a temperature rise of nearly 30°F (16.7°C). (By courtesy of Gary J. Weil, president, EnTech Engineering).

Interestingly, although we know that corroded car battery connections must be thoroughly cleaned, we do not think so with other electrical connections. Probably because the corrosion is not as evident as that seen on a car battery. Even if the connection is loose (which will have an elevated temperature), it prudent to clean it before retightening it.

16.3. MOTORS: ELECTRICAL COMPONENTS

In general, the motor life is halved for each 10°C (18°F) temperature increase. Moisture, bearing lubrication, and chemicals react with the insulation and short out the windings. When a turn of the winding shorts to another, it forms an inductive loop. This inductive loop, subjected to 60-cycle alternating current, generates heat. The heat breaks down more insulation. This causes more shorts and ultimate failure of the entire winding.

A three-phase motor with a five-amp difference between leads is considered to have a phase imbalance. A short in the motor or undersized terminals, resulting in current flow restriction can cause phase imbalance. The heat buildup causes the wire insulation to break down, exposing bare wires. If bare wires are in the housing, the wires will contact the housing and create a short.

Motors create inductive fields that can cause excessive heating within ferrous components. If not properly shielded, these fields can heat up ferrous components external to the motor. Ferrous bolts may have been used to replace non-ferrous fasteners. Hot spots due to inductive heating may not be considered dangerous.

While simple in theory, motors are quite complex. Brown[2,3] has identified the following motor components that can create heat as they degrade:

Direct Current (DC) motors

Bad solder connections on a commutator riser, unequal brush tensions, shorted armature coils, pin-pointed electrical ground locations in armatures, grounded interpoles, shorted field coils, external cooling fans running backwards, loose field coils, bad couplings, and loose brush pigtails.

Alternating Current (AC) motors

Shorted stator coils, loose ring connections on wound rotor motors, loose armortisseur winding connections on synchronous motors, shorted stator iron, open winding connections, and grounds in stators and rotors.

16.4. MOTORS: MECHANICAL COMPONENTS

Bearings reduce friction between a rotating shaft and the fixture that holds the shaft in place. Figure 16-7 illustrates that all motors have two bearings. A variety of bearing configurations exists from lubricated roller bearings to simple unlubricated Teflon sleeves. With no load, the bearings in Figure 16-7 only have to support the weight of the rotor. When attached to machinery, an additional load is added. The motor power and the bearing strength limit the maximum mechanical load.

Immediate evaluation of the bearing condition is determined by comparing duplicate motors in the area running under the same load and by comparing the bearing temperature with its own housing. A bearing should not be warmer than its housing.

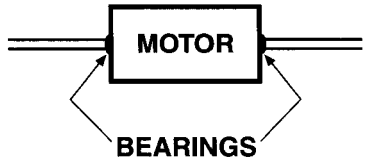


Figure 16-7. Motor bearings.

Bearings do not fail instantaneously. It is a progressive failure where continual rotation increases the temperature and further damages the bearing. Bearing fail due to excessive loading, lack of lubrication, and dirt in lubrication (Figures 16-8 and Figure 16-9). The problem of determining heat flow from a bearing in a specific application is rather complex. Factors affecting the rate of heat dissipation include:

1. Temperature gradient from bearing to housing. Size and configuration of the housing, and external cooling created by fans or HVAC ducts affect the temperature gradient.

2. Temperature gradient from bearing to shaft. Other heat sources such as gears and additional bearings affect the temperature of the shaft.

3. The heat carried away by a circulating oil system, such as that found in the gearbox of a pumping unit.

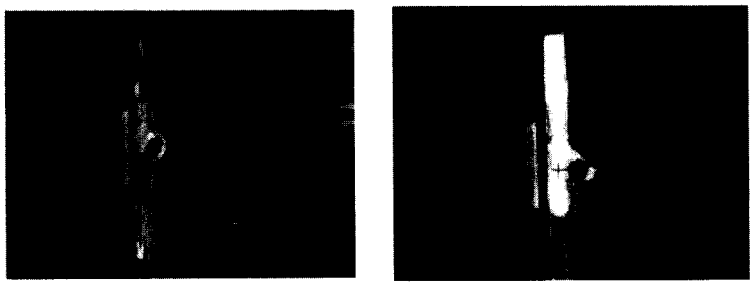


Figure 16-8. A close-up of an enclosed motor bearing. Only a small portion of the motor is shown. The bearing cannot be seen. Its temperature is estimated from the temperature of the motor housing. (By courtesy of the Academy of Infrared Thermography).



Figure 16-9. Overheated pinion gear shaft on a ball mill. (By courtesy of the Academy of Infrared Thermography).

16.5. MACHINERY

Figure 16-10 illustrates a motor connected to another mechanical component via a flexible coupling. The coupling may be a universal joint that has bearings or a material that flexes. The flexible joint is used to overcome any misalignment that might exist between the motor shaft and the mechanical shaft. As the misalignment increases, the flexible coupling flexes more and, since friction is associated with all mechanical components, will heat up (Figures 16-11 and 16-12).

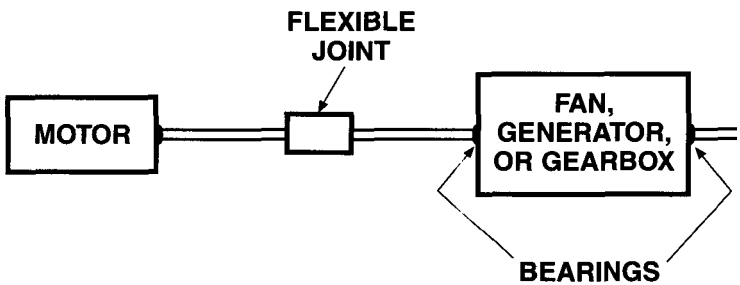


Figure 16-10. Mechanical coupling via a flexible shaft.

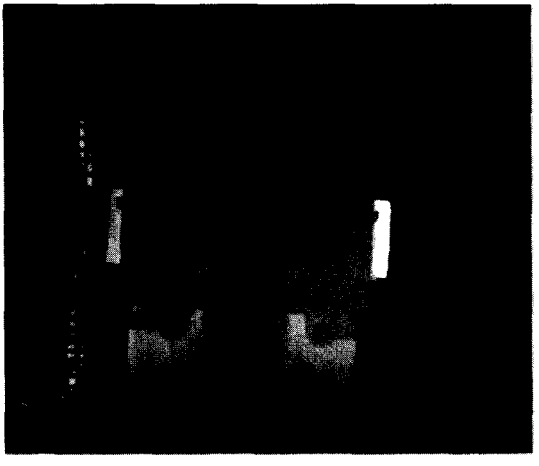


Figure 16-11. Flexible coupling with one side warmer than the other. The coupling is underneath the safety shroud and cannot be seen. (By courtesy of the Academy of Infrared Thermography).

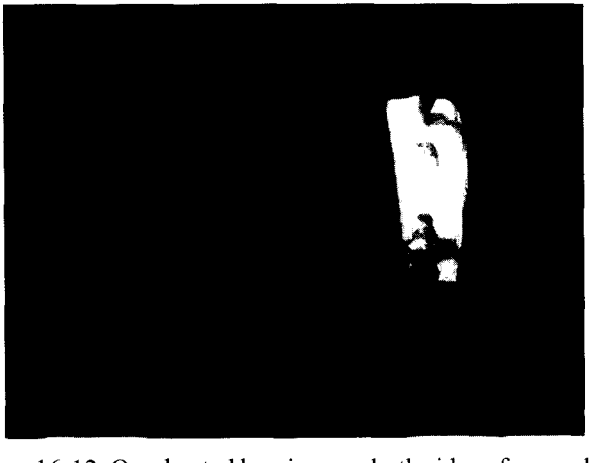


Figure 16-12. Overheated bearings on both sides of a coupling. As with nearly all machinery, safety shrouds prevent viewing rotating components. (By courtesy of the Academy of Infrared Thermography).

No temperature guidelines exist for flexible couplings. Kelch and Grover[4] performed a series of experiments to determine the temperature rise as a function of

misalignment. They attached a 10-hp motor to an 8000W generator with a flexible rubber coupling. The generator was operating at 50% load and they obtained the results given in Table 16-1. These data should not be construed as guidelines for flexible couplings. Rather, they indicate that misalignment adversely affects the temperature of the coupling. It is clear that as the misalignment increases, the temperature increases. At some (undefined) misalignment value, the temperature of the coupling will reach a value that is deleterious to the coupling material.

Table 16-1
COUPLING TEMPERATURE DUE to MISALIGNMENT
(From reference 4).

Misalignment (inches)	**Rubber Insert Temperature**	
0.000	80.8°F*	27.1°C*
0.010	87.5°F	30.8°C
0.020	98.9°F	37.2°C
0.030	103°F	39.4°C
0.040	109°F	42.8°C

* Near ambient temperature

Figure 16-13 illustrates mechanical connection by pulleys and a belt. Mechanical friction and stress points will heat up the pulleys, belt, and bearings. The mechanical coupling could also be a gear train. Each gear within the gear shaft will have two bearings (Figure 16-14).

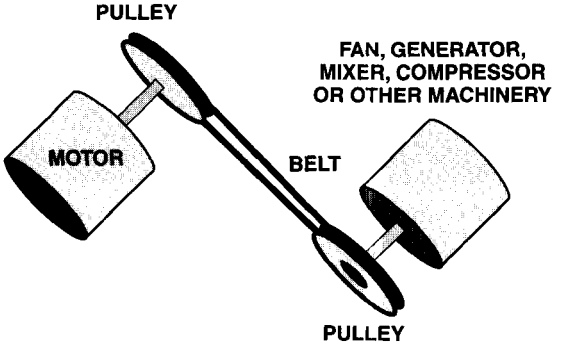


Figure 16-13. Mechanical coupling by a belt. Gear trains also connect mechanical components. Depending upon the shaft length and load, the shaft may be supported by additional bearings.



Figure 16-14. Overheated gearbox. Disassembly is required to locate the defective component. It could be a bearing, bent shaft, or misaligned gears. (By courtesy of the Academy of Infrared Thermography).

Fans can be direct-drive or belt driven. Single or multiple belts may be used.[5] The interaction of the sheaf and the belt generates friction. Additionally, cyclic tension and compression in the elastic belt creates internal friction. By establishing the normal amount of heat generated in a properly operated system, criteria can be established for identifying improper operation. Excessive belt pressure can increase the load on the fan motor and bearings. Too little pressure will result in belt slippage. For multi-belt systems, it is important that the belts be from a matched set. Matched sets will have the same size so that when tightened, they all have the same pressure. Otherwise, the looser belts will slip and require the tighter belts to work harder Figure 16-15).

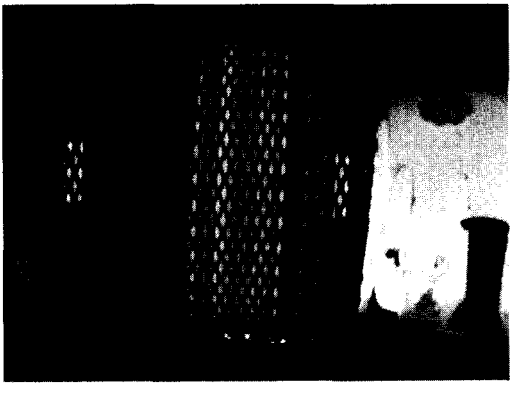


Figure 16-15. Multi-belt pulley. The pulley shaft is horizontal and the drive motor (not seen) is below the pulley. A wire mesh safety shroud covers the pulley and belts. The pulley shaft is misaligned from the motor shaft. Consequently, the belts on the right-hand side are under greater tension and become hot. The looser belts on the left-hand side are cool and cannot be seen in this thermogram. (By courtesy of the Academy of Infrared Thermography).

16.6. EMISSIVITY

All electrical components and most mechanical components are made of metal. Unfortunately, the emissivity of polished metal is low. Small errors in estimating the emissivity or surrounding temperature leads to large errors in the calculated temperature (see Section 12.3.3. *Emissivity uncertainty*). With highly reflective components, the surrounding temperature is a major contributor to the measured radiation. If the distance between the thermographer and the reflective component is only a few feet, then the thermographer's body temperature contributes to the surrounding temperature. This further complicates quantifying the surrounding temperature and leads to a larger component temperature uncertainty.

While the emissivity may not be know precisely, it may be permissible to assign a "default" value to commonly measured components. This creates an arbitrary baseline. At the Peach Bottom Atomic Electric Power Station, Wurzbach and Hammaker used the values[6] listed in Table 16-2 for electrical surveys. The materials are those commonly used in electrical equipment and connections. "Default" values vary with surface conditions and environmental conditions. Components built by different manufacturers may also have different surface conditions. However, at any particular location the variation can be small. That is, it is reasonable to assume that the emissivities (although different) will remain constant at their respective locations.

Table 16-2
REPRESENTATIVE DEFAULT EMISSIVITY VALUES
(From reference 6)

Material	Emissivity
Aluminum motor boxes, aluminum panels	0.2
Copper (bus bar)	0.4
Stainless steel (bolted connections in electrical equipment)	0.6
Painted surfaces	0.9

Rotating shafts and couplings frequently show surface anomalies (such as paint drops, grease, or scuffed or polished spots) and thus make a quantitative determination difficult, as these differences can appear as relative hotspots. It is

possible to distinguish a rotating hotspot from a rotating emissivity difference. Any spot of uniform temperature is probably due to an emissivity difference since thermal conductivity would dissipate heat into the surrounding material. That is, a true hot spot would not have sharp edges but a temperature gradient that starts at the background temperature and increases to a maximum value.

16.7. TEMPERATURE GUIDELINES

Manufacturers have established threshold temperatures for many component materials. However, these are very conservative and cannot readily be translated to the needs of thermographers. No universal standard exists for determining when equipment should be repaired or replaced. Each industry has created a list of guidelines based upon practical knowledge.

16.7.1. ELECTRICAL CIRCUITS

Temperature guidelines should include both the component's absolute temperature, $T_{COMPONENT}$ and the temperature differential, $\Delta T = T_{COMPONENT} - T_{AMBIENT}$. For 3-phase installation, the difference between phases, ΔT_{PHASE}, is also important. To ensure that the temperature has reached equilibrium, the load must have been constant for at least 45 minutes before the examination takes place.

Note that if any resistance exists, there will be a temperature increase. The ideal connection is perfect: It does not have any resistance, and an ideal circuit will not experience any temperature increase. By definition, a temperature increase represents a defective connection. The only question is when to repair or replace the connection. Table 16-3 lists representative temperatures for electrical circuits. The precise values depend upon the specific equipment involved. Repair priority also depends upon the need for continuity of operation and the seriousness if the component fails (fire or explosion). The ultimate decision to repair must be made by plant personnel familiar with the impact of component failure.

Table 16-3
REPRESENTATIVE ELECTRICAL REPAIR PRIORITY
Precise values depend upon specific equipment

Temperature rise	Situation	Repair priority
Greater than 50°C (Greater than 90°C)	Acute overheating	Immediate repairs required
30°C to 50°C (54°F to 90°F)	Excessive overheating	Repair as soon as possible
10°C to 30°C (18°F to 54°F)	Second stage of overheating	Should be attended to at the first opportunity
Less than 10°C (Less than 18°F)	First stage of overheating	Should be monitored and repaired during next scheduled maintenance

As discussed in Chapter 15, *Power distribution*, the temperature rise is related to the current at the time of measurement. Ideally, the system is working at full capacity so that you measure the highest temperature that the component will reach. Unfortunately, this is not always the case. The temperature at full load must be calculated from the measured values:

$$T_{FULL-LOAD} = T_{AMBIENT} + \left(T_{MEASURED} - T_{AMBIENT}\right)\left(\frac{I_{FULL-LOAD}}{I_{MEASURED}}\right)^{N} \quad (16\text{-}1)$$

and

$$\Delta T_{FULL-LOAD} = \Delta T_{MEASURED}\left(\frac{I_{FULL-LOAD}}{I_{MEASURED}}\right)^{N} . \quad (16\text{-}2)$$

$$\Delta T_{PHASE-RATED} = \Delta T_{PHASE}\left(\frac{I_{FULL-LOAD}}{I_{MEASURED}}\right)^{N} . \quad (16\text{-}3)$$

where the exponent N depends upon the estimated thermal conductivity (Table 16-4).

Table 16-4
EXPONENT for TEMPERATURE
(From Reference 7)

Heat conductivity	Exponent
High	1.6
Fair	1.8
Low	2.0

LOW VOLTAGE CIRCUITRY

For low voltage circuitry, an anomaly is identified when the measured temperature exceeds the values given in Table 16-5. Once an anomaly has been identified, some corrective action is required.

Table 16-5
REPRESENTATIVE LOW VOLTAGE MAXIMUM ΔT
Precise values depend upon specific equipment
(From reference 7)

Measured temperature	Temperature difference, ΔT
ΔT_{PHASE} (3-phase system)	3°C (5.4°F)
$T_{COMPONENT} - T_{AMBIENT}$	35°C (63°F)
$T_{COMPONENT}$	70°C (126°F)

3-PHASE SYSTEMS

Table 16-6 lists those corrective actions (repair priority) recommended when ΔT_{PHASE} is high.

Table 16-6
REPRESENTATIVE PHASE REPAIR PRIORITY for 3-PHASE SYSTEM
(From reference 7)

Temperature difference, ΔT	Situation	Repair priority
Greater than 30°C (Greater than 54°F)	Acute overheating	Immediate repairs required
5 °C to 30°C (9°F to 54°F)	Developed overheating	Repair as soon as possible
3 °C to 5°C (5.4°F to 9°F)	First stage of overheating	Should be monitored and repaired during next scheduled maintenance

HIDDEN CONTACTS

Although the above tables provide temperature limits, heat conduction must also be considered. The temperature of hidden connections or contacts can only be estimated from surface temperature measurements. Since conduction will disperse the heat, the temperature of components overlaying hidden components will be lower than the values given in the above tables. Table 16-7 provides representative values and repair priority for hidden connections.

Table 16-7
HIDDEN CONNECTIONS/CONTACTS
(From reference 7)

Temperature difference, ΔT	**Repair priority**
Greater than 3°C (Greater than 5.4°F)	Must be repaired immediately
1°C to 3°C (1.8°F to 5.4°F)	Must be repaired during the next scheduled maintenance

16.7.2. MECHANICAL SYSTEMS

During normal operation, motors will heat up due to electrical and mechanical energy dissipation. Friction creates heat in all mechanical devices. Simply stated, all mechanical components will experience a temperature increase during normal operation. This increase depends upon the design and load. Table 16-8 provides a representative mechanical repair priority. It is similar to the electrical repair priority (Table 16-3) but has one major difference. Under normal operation, mechanical components will heat up due to friction. The ideal circuit does not have any resistance and therefore will not heat up when current flows. Any heat in an electrical circuit represents a potential problem.

Table 16-8
REPRESENTATIVE MECHANICAL REPAIR PRIORITY
Precise values depend upon specific equipment

Temperature rise above ambient	Situation	Repair priority
Greater than 50°C (Greater than 90°F)	Acute overheating	Immediate repairs required
30°C to 50°C (54°F to 90°F)	Excessive overheating	Repair as soon as possible
10°C to 30°C (18°F to 54°F)	Second stage of Overheating	Should be attended to at the first opportunity
5°C to 10°C (9°F to 18°F)	First stage of Overheating	Should be monitored and repaired during next scheduled maintenance
Less than 5°C (Less than 9°F)	Normal operation	None

16.8. REFERENCES

1. R. Newport, "Infrared Electrical Inspection Myths," in *Thermosense XIX*, R. N. Wurzbach and D. D. Burleigh, eds., SPIE Proceedings Vol. 3056, pp. 124-132 (1997).
2. R. Brown, "Infrared Evaluation of Electrical Machinery," in *Thermosense VI*, G. .J. Burrer, ed., SPIE Proceedings Vol. 446, pp. 197-199 (1983).
3. R. Brown, "Electric Motor Care using Infra-Red Diagnostics" in *Thermosense VIII*, H. Kaplan, ed., SPIE Proceedings Vol. 581, pp. 108-109 (1985).
4. C. K. Kelch and P. Grover, "Using Thermography To Detect Misalignment In Coupled Equipment," in *Thermosense XVIII*, D. D. Burleigh and J. W. Spicer, eds., SPIE Proceedings Vol. 2766, pp. 91-100 (1996).
5. R. N. Wurzbach, "Infrared Thermography of Fan and Compressor Systems in a Predictive Maintenance Program," in *Thermosense XX*, J. R. Snell and R. N. Wurzbach, eds., SPIE Proceedings Vol. 3361, pp. 118-123 (1998).
6. N. Wurzbach and R. G. Hammaker, "The Role of Comparative and Qualitative Thermography in Predictive Maintenance," in *Thermosense XIV*, J. K. Eklund, ed., SPIE Proceedings Vol. 1682, pp. 3-11 (1992).
7. T. Perch-Nielsen and J. C. Sørensen, "Guidelines to Thermographic Inspection of Electrical Installations," in *Thermosense XVI*, J. R. Snell, ed., SPIE Proceedings Vol. 2245, pp. 2-13 (1994).

17
BURIED OBJECTS

Thermal imaging is useful for finding a variety of buried objects such as grave sites[1] (Figure 17-1), buried land mines,[2] storage tanks, pipelines, and defects in bridges (Figure 17-2). Most pipelines,[3] whether they contain oil, chemicals, water, steam, gas, or sewage, fail slowly through corrosion and small cracks and then gradually progress to a catastrophic ending. This disastrous failure can be expensive in terms of both dollars and lives. When a sewer caves in, it often takes the street, sidewalks, and surrounding buildings along with it, endangering public health and safety.



Figure 17-1. Graves at a cemetery. (By courtesy of Gary J. Weil, president, EnTech Engineering).

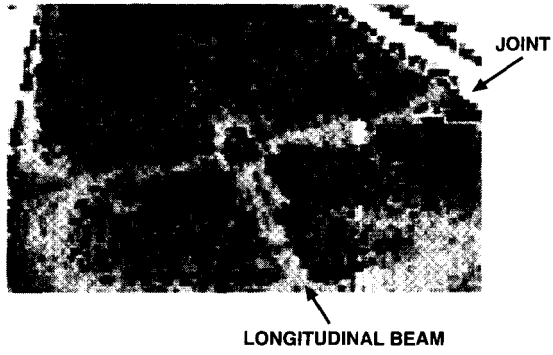


Figure 17-2. Corrosion at a joint and longitudinal beam on a bridge deck. (By courtesy of Gary J. Weil, president, EnTech Engineering).

Finding buried objects is a qualitative task. The thermal signature depends upon the thermal properties of the overlaying material (soil, dirt, rocks, or concrete). With lateral heat conduction, the signature of the buried object is typically larger than the object. Signatures are not well defined and object detection often depends upon other clues. For example, pipes are typically laid in straight lines or it is known that there are buried items – but the precise location is not known. Target recognition and identification is usually not possible. It can only be confirmed by digging up the buried object.

Numerous papers have been presented at several annual SPIE conferences. These conferences have printed proceedings available from SPIE. They are *Detection and Remediation Technologies for Mines and Minelike Targets, Nondestructive Evaluation of Utilities and Pipelines*, and *Infrared Technology and Applications*. This chapter draws heavily from References 1-8. Addition information can also is in Appendix C, *Thermal Sensing and Imaging 1980-1999.*

17.1. HEAT TRANSFER

The surface temperatures that are measured above a buried pipeline are dependent upon the soil properties, surface condition, environment, and heat source. For a single object (e.g., empty or filled storage tanks) solar loading provides the heat. Many pipes carry heated fluids such as steam and chemicals. These fluids provide the heat that creates the temperature differential on the surface.

Figure 17-3 illustrates a buried object. It may be either an empty container (storage tank) or a solid object (land mine or filled container). Solar loading heats up the ground and the object. If the object is empty, the air acts as a thermal insulator and prevents heat from penetrating to the ground beneath the object (Figure 17-4). Thus, the ground above the empty object becomes warmer than the surrounding. During nighttime, the heat escapes to the sky and the area over the empty object appears cooler. Undocumented underground storage tanks are usually removed because they may contain environmentally sensitive material.

If the object is filled with hazardous waste, gasoline, or oil, then the material has a different heat capacity than the surrounding soil. Since heat is stored in the higher heat capacity material, the surface over the object will appear warmer than the surrounding soil during nighttime.

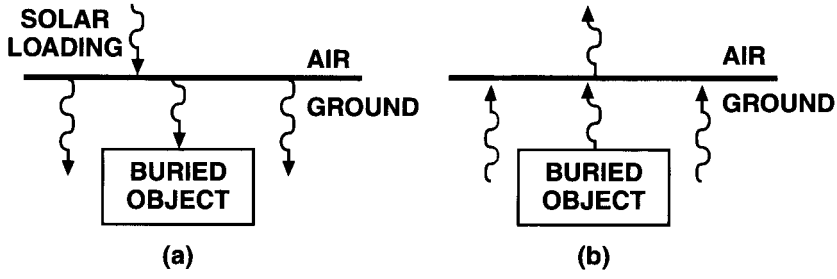


Figure 17-3. Heat flow at (a) daytime and (b) nighttime.

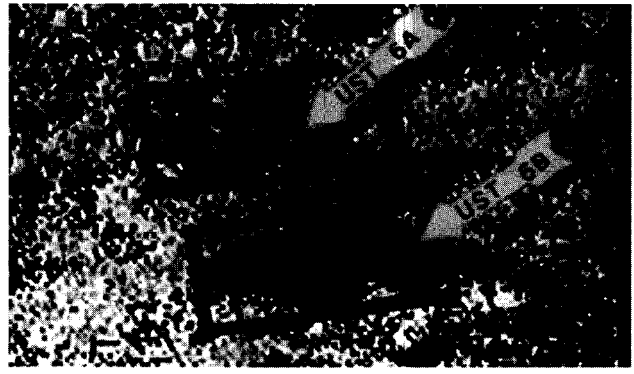


Figure 17-4. Underground storage tank (UST). Both filled and empty tanks produce thermal signatures. (By courtesy of Gary J. Weil, president, EnTech Engineering).

Figure 17-5 illustrates a pipe whose temperature is different from the ground. It may be a steam line or a refrigeration line in an ice skating rink. Since the material passing through the pipe is at a different temperature than the soil, the thermal signature should be visible during the day and night. The heat travels radially from the pipe. This provides a flared temperature distribution on the surface. That is, the image is much wider than the heated pipe.

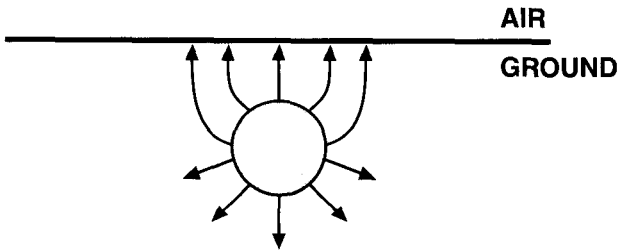


Figure 17-5. A heated (illustrated) or cooled pipe will provide a thermal signature all the time. The heat conduction will provide a flared temperature distribution on the surface.

A buried land mine may be more difficult to detect because its signature may be similar to that of buried rocks or other natural ground variations. Land mines are usually randomly located whereas pipes run in consistent directions (Figure 17-6). Further, animals may burrow (e.g., prairie dogs, mice, and moles) or dig holes (e.g., rabbits) that create local temperature variations. These may be similar to the mine signatures and thus act as thermal clutter.

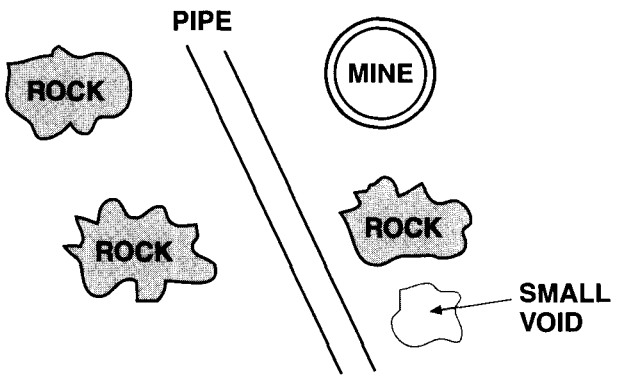


Figure 17-6. Buried pipes have a distinctive thermal signature. The signature of small buried objects such as land mines can be similar to rock signatures. Voids and small holes may produce a signature similar to the mine signature.

17.2. ENVIRONMENT

Buildings and vegetation produce shadows that reduce solar loading (Figure 17-7). Since shadows constantly move, solar loading variations tend to average out to a uniform level. Nevertheless, to improve solar loading, grass should be mowed and shrubs should be removed. Vegetation prevents the sun's energy from entering the ground and also prevents you from measuring the true ground temperature.

Good, compacted backfill should provide good thermal conductivity. However, soil erosion and poor backfill increase the insulating ability of the soil by reducing the heat conduction properties. This makes it more difficult to locate buried objects.

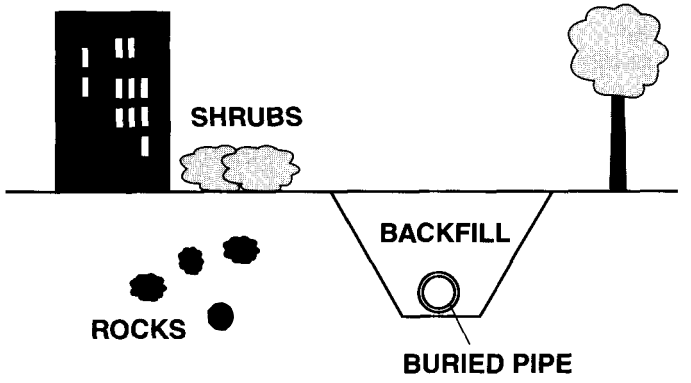


Figure 17-7. Trees, shrubs, other vegetation, and buildings can block solar loading. Usually, clean backfill is used to fill up the trench after the pipe or tank is buried.

17.3. UNDERGROUND OBJECTS

Small objects may be found by an inspection on foot. Buried pipelines are probably best viewed from an airplane.

17.3.1. HOT FLUIDS

The heat from a steam line is transferred through the ground by conduction, and once it reaches the surface of the ground the energy is transferred by radiation, convection, and conduction to surrounding surfaces. Because the sys-

tem is in a steady state condition, the heat transfer from the surface of the ground to the environment is equal to the heat transfer from the steam line to the surface. By calculating the heat released at the surface, it is possible to estimate[4] the heat loss from a steam pipe and calculate the temperature of the steam pipe.

As expected, the temperature over the centerline of the pipe is highest for the shallowest depth of pipe.[5] The surface temperature decreases as the pipe depth increases. Figure 17-8 illustrates the surface temperature of a concrete-buried pipe starting at the centerline and moving 25.4 cm laterally. Figure 17-9 illustrates the temperature as a function of wind speed. The temperature decreases dramatically as the depth increases and the wind speed increases. Further, it indicates that the apparent width of the pipe increases with depth. However, this is not a problem if the only requirement is to locate the pipe. If the soil or concrete is homogenous, the pipe will always be in the center of the flared image. As with most outdoor thermal imaging system applications, the wind speed should be less than 15 mph (24 kph or 6.7 m/s) (See Section 11.3.3. *Wind*).

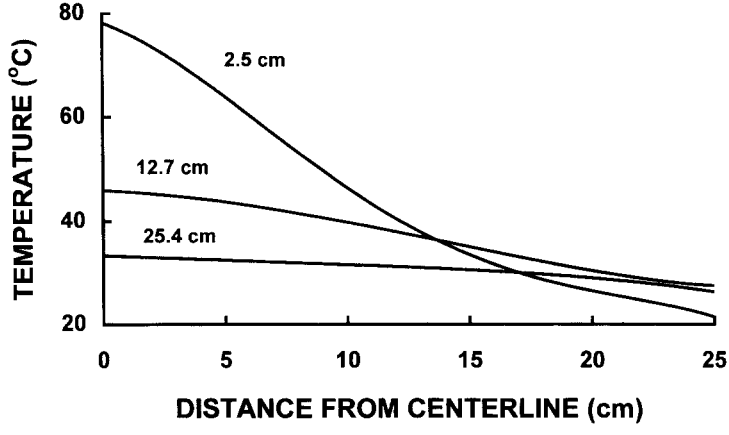


Figure 17-8. Calculated temperature distribution for a 2-inch diameter pipe buried in concrete for three different depths. The pipe is carrying a fluid whose temperature is 93°C (200°F) and the ambient temperature is 15°C (60°F). (From Reference 5).

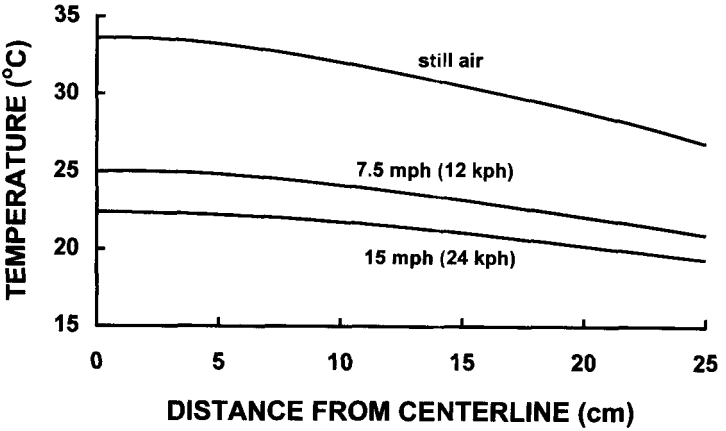


Figure 17-9. Calculated temperature distribution for a 2-inch diameter pipe buried at 25.4 cm in concrete as a function of wind speed. (From reference 5).

While it may be necessary to simply locate a buried pipe, it is more important to determine if it is leaking. A leaking pipe will create an underground pool of liquid (Figure 17-10). The utility companies in many older cities supply steam heat to a large number of customers. Steam leaks are easily found[6,7] since a great deal of heating on the ground occurs.

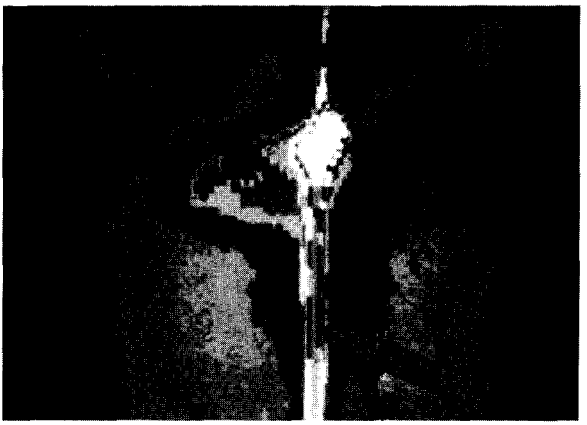


Figure 17-10. Thermogram of a buried oil pipeline, leak, and leak plume. Since the liquid has a different heat capacity than the ground, it will have its own unique thermal signature. (By courtesy of Gary J. Weil, president, EnTech Engineering).

The size, shape, and location of the pool depend upon the soil properties. The fluid will enter existing cracks and crevices and the pool can be any shape. For example, Salt Lake City, Utah heats the pavement during the winter months in order to melt ice and snow before it could become dangerous to pedestrians and traffic. Leakage is easily determined thermographically (Figure 17-11). As G. J. Weil[3] stated:

> *Most leaks though, were more difficult to locate because they did not start with a "hot" spot and radiate in a circular pattern from the leaks. Instead, these leaks started with a smaller "hot" spot and spread out along the pipeline for just a short distance. It was determined this signature signified smaller leaks that had not cracked the pipeline concrete encasement, but rather, exited the water pipe and traveled along the outside of the pipeline until it found an exfiltration point somewhere downstream in the pipe casement. The reason the heat dissipated so quickly was that the line acted as a heat sink and quickly brought the outside water temperature to the temperature of the line.*



Figure 17-11. Thermogram of buried hot water pipeline grid used to melt snow and ice on roadway pavement at Salt Lake City, Utah. The arrow points to a leak. (By courtesy of Gary J. Weil, president, EnTech Engineering).

17.3.2. VOIDS

Water leaking from a pressurized water main can cause the formation of voids in soil surrounding pipes by washing away soils (Figure 17-12) or compacting adjacent soil. For leaking sewer lines, the water can compact the soil but also can wash the soil down through the sewer line. Voids around sewers can be detected on exposed asphalt parking lots from the air.[8] Voids will provide the essentially the same thermal signature as an empty container. Large voids are dangerous since they can cave in.

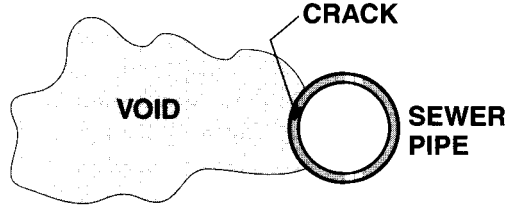


Figure 17-12. Leaking water pipes or leaking sewer lines can form a void in the ground.

17.4. REFERENCES

1. G. J. Weil and R. J. Graf, "Infrared Thermographic Detection of Buried Grave Sites," in *Thermosense XIV*, J. K. Eklund, ed., SPIE Proceedings Vol. 1682, pp. 347-353 (1992).

2. N. K. Del Grande, P. F. Durbin, M. R. Gorvad, D. E. Perkins, G. A. Clark, J. E. Hernandez, and R. J. Sherwood, "Dual-band Infrared Capabilities for Imaging Buried Object Sites," in *Underground and Obscured-Object Imaging and Detection*, N. K. Del Grande, I. Cindrich, and P. B. Johnson, eds., SPIE Proceedings 1942, pp. 166-177 (1993).

3. G. J. Weil and R. J. Graf, "Infrared Thermography Based Pipeline Leak Detection Systems," in *Thermosense XIII*, G. S. Baird, ed., SPIE Proceedings SPIE Vol. 1467, pp. 18-33 (1991).

4. J. H. MacDavid, "Buried Steam Line Temperature and Heat Loss Calculation," in *Thermosense XIII*, G. S. Baird, ed., SPIE Proceedings Vol. 1467, pp. 11-17 (1991).

5. J. M. Kleinfeld, "Finite Element Analysis as a Tool for Thermography," in *Thermosense XXI*, D. H. LeMieux and J. R. Snell, Jr., eds., SPIE Proceedings Vol. 3700, pp. 6-12 (1999).

6. D. J. Templeton and M. B. Palmer, "Infrared Evaluation of an Underground Steam Distribution System," in *Thermosense IX*, R. P. Madding, ed., SPIE Proceedings Vol. 780, pp. 42-46 (1987).

7. H. W. MacKay and G. R. Lawrence, "Application of Airborne Thermal Infrared for Steamline Maintenance," in *Thermosense VI*, G. J. Burrer, ed., SPIE Proceedings Vol. 446, pp. 106-111 (1983).

8. G. J. Weil, "Infrared Thermal Sensing of Sewer Voids," in *Thermosense VI*, G. J. Burrer, ed., SPIE Proceedings Vol. 446, pp. 116-121 (1983).

18
SURVEILLANCE

Although surveillance refers to the observation of a person, this definition is extended to include the detection, recognition, and identification of both people and objects. It includes search and rescue, endangered species monitoring, border patrol, law enforcement, and military applications. Systems designed for surveillance tend to be different than those designed for condition monitoring and predictive maintenance (Table 18-1). Surveillance activities are usually qualitative. In a very broad sense, all qualitative applications (building envelope, roof, and electro-mechanical inspections) may be considered a form of surveillance.

Table 18-1
TYPICAL DIFFERENCES BETWEEN SURVEILLANCE and INSPECTION

Category	Surveillance	Inspection
Minimum target size	Limited by the detector size or detector pitch	3 pixels (recommended)
Target contrast	May be low contrast	High contrast
Image quality	May be noisy	Low noise, high quality imagery
Range	Long range, atmospheric transmittance affects detection	Usually short range, atmospheric transmittance near unity

The minimum resolvable temperature (MRT) is a measure of an observer's ability to detect a four-bar target embedded in noise. The Johnson criterion relates real targets to equivalent bar-chart targets. Thus, the link between real targets and the MRT is the spatial frequency associated with the real target and the four-bar targets. Range to the target is increased at the expense of image quality. This is achieved by increasing the system gain until noise is apparent and the imagery is "snowy."

The U.S. Army developed the first thermal imaging performance model in 1975. While officially titled "Night Vision Laboratory Static Performance Model," it is commonly called the Ratches model in honor of the principal author. We will call it the 1975 NVL model. In 1992, the U.S. Army upgraded the model to include performance parameters of staring arrays. This new model was simply called FLIR92. These models are the main analytic tools for deriving system

requirements and predicting performance. While these models are used routinely for military applications, they generally are used only during system development for other surveillance activities.

18.1. SURVEILLANCE APPLICATIONS

Since all objects emit radiation, they cannot hide from detection by thermal imaging systems. Even in total darkness, people and objects can be detected. Consequently, surveillance can be effective 24 hours a day. The primary advantage of a camera is that it never becomes tired and it functions at peak efficiency all the time. Its only limitation is a limited field-of-view.

Surveillance is a qualitative measurement. There must be an apparent temperature differential between the target and its background. This may be due to an emissivity difference or an actual temperature difference. Table 18-2 lists representative targets encountered in surveillance activities.

Table 18-2
TYPICAL TARGETS

Activity	**Representative targets**
Automobile safety	People, animals, obstacles
Law enforcement	People, vehicles, boats, small planes
Animal counts	Animals
Search and rescue	People
Air/space surveillance	Fires, geological phenomenon, pollution, environmental changes
Military	Tanks, trucks, aircraft

General Motors offers an optional thermal imaging system on its premium automobile, Cadillac. The uncooled pyroelectric detector provides range performance that is 3 to 5 times further than normal headlights. This allows the driver to "see" animals and people crossing the road at longer distances. Glare from oncoming headlights may prevent the driver from seeing obstacles, people, or animals. The thermal imaging system is not affected by glare and therefore offers an image that could not otherwise be seen by the driver. Since LWIR system performance is minimally degraded in haze and light fog, the imaging system offers a significant range advantage during poor weather.

The only effective way of defeating a surveillance system is to hide behind an opaque object. This includes extremely dense vegetation, buildings, vehicles, and natural objects (hills and rocks). Methods to reduce the apparent temperature have had limited success. The apparent temperature differential can be reduced with low emissivity paint or by adding thermal insulation.

18.1.1. LAW ENFORCEMENT

Law enforcement activities include catching thieves (Figure 18-1), fugitives (Figure 18-2), and illegal aliens (Figure 18-3). It is often important to determine is a vehicle has been recently driven. Although Figure 18-4 illustrates a moving vehicle, a recently driven vehicle will provide nearly the same thermogram with the exception of the heated taillights. Since engines have a high heat capacity, they will provide a thermal image for at least 4 hours. A fleeing fugitive discarded a recently fired gun (Figure 18-5). This gun was not visually discernable in the thick brush but was easily found with a thermal imaging system. Additional law enforcement activities include detecting forged documents and counterfeited money (see Figures 4-17 and 4-18).

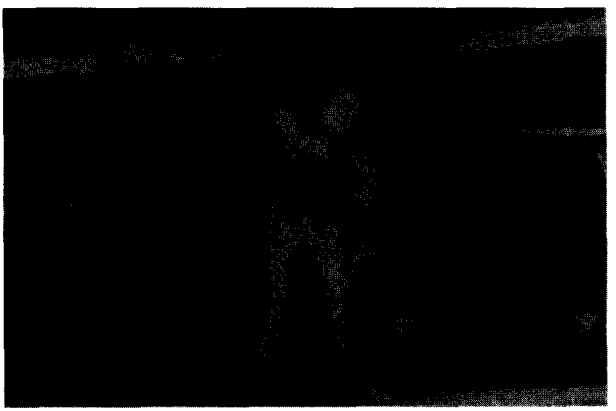


Figure 18-1. This car thief thought that, by operating at night, no one would be able see him. Although this image is saturated, it does not affect its usefulness as a surveillance tool. (By courtesy of the Academy of Infrared Thermography).

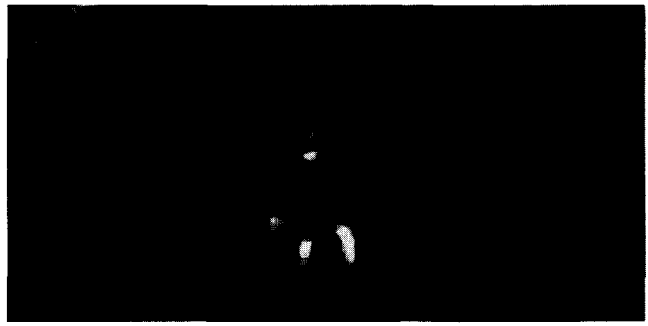


Figure 18-2. A fleeing fugitive climbing a fence. (By courtesy of IRcameras.com).

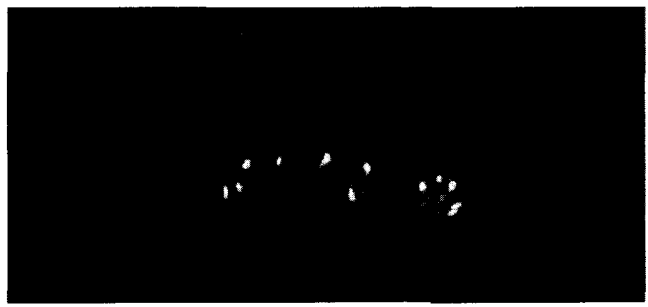


Figure 18-3. Nighttime border crossing by illegal aliens. High resolution is not required for all surveillance activities. (By courtesy of IRcameras.com).

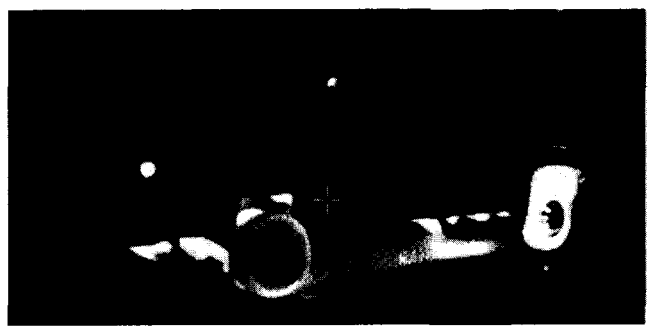


Figure 18-4. Moving pickup truck. Friction between the road and tires will always heat up the tires. At grazing angles, a paved road becomes reflective and reflects the heat from the underside of the truck. The engine also heats the front wheels. Figure 11-20 illustrated a dump truck (By courtesy of IRcameras.com).

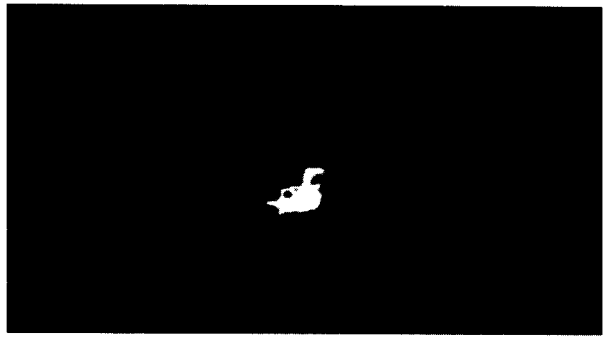


Figure 18-5. A recently fired discarded gun. The heavy brush prevented visual discovery. (By courtesy of Indigo Systems).

Drug interdiction includes locating individuals as illustrated in Figures 18-2 and 18-3, locating small aircraft, and surveying dwellings. The thermogram illustrated in Figure 18-6 was previously presented in Figure 13-2. In that caption, it was stated that the excess heat was due to a broken window seal. However, if the window was intact and the owner was suspected of growing drugs, an alternate interpretation is possible. Cannabis requires a high temperature to grow (about 90°F or 32°C). Excessive temperature in a dwelling accompanied with high utility bills may indicate drug production. Image interpretability depends upon numerous facts.

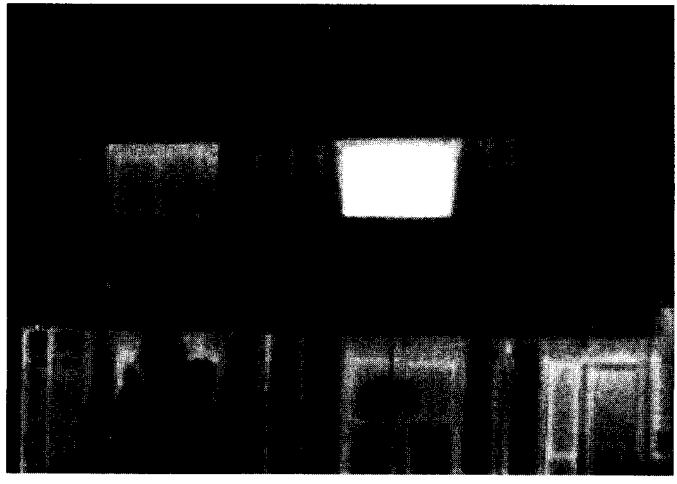


Figure 18-6. A room that may have been heated to grow cannabis. (By courtesy of the Academy of Infrared Thermography).

18.1.2. SEARCH AND RESCUE

Sea rescue usually comes to mind when discussing search and rescue missions. The human body (98.6°F or 37°C) provides a large ΔT against a water background. Unfortunately, only a small portion is above water. While this small target is easily discernible at close distances, it becomes more difficult to locate at long ranges. It is similar to looking for a needle in a haystack. With a limited field-of-view system, a large distance is required to view a large area. But then the target becomes very small and may be hard to find. Shorter distances mean that a smaller area is viewed and overall search time is significantly increased.

Smoke provides tremendous obscuration in the visible region of the spectrum but tends to be fairly transparent in the infrared region. The reason is further described in the next section. Firefighters use thermal imaging systems to locate fires and people (Figure 18-7).

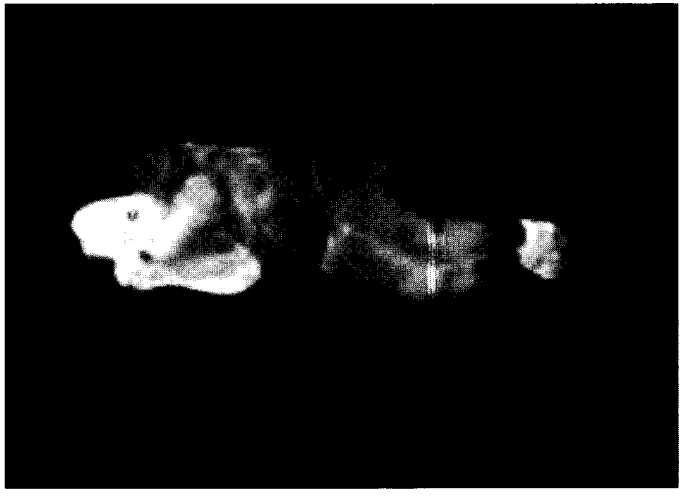


Figure 18-7. A sleeping woman in a smoked filled room. The dense smoke did not permit visual location. (By courtesy of Indigo Systems).

18.1.3. AIR/SPACE SURVEILLANCE

The U.S. Forest Service makes extensive use of thermal imaging systems to locate and track fires (see Figure 2-14). This is difficult in the visible region since the smoke obscures the actual fire. We cannot eliminate the smoke without eliminating the fire. It is therefore necessary to locate the fire and direct fire-

fighting personnel to the correct location. Since smokes do not attenuate LWIR radiation as much as MWIR radiation (See Figure 5-7), a LWIR system is desirable.

Subsurface fires can exist in both natural (e.g., peat[1]) and man-made (e.g., landfill) materials. With subsurface fires, there is often little smoke. However, they produce a thermal signature. Since natural objects are heated by the sun and can produce solar reflections, it is recommended that subsurface fires be evaluated at nighttime.

Shorelines can be monitored for illegal dumping or spillage of waste material. If the water is used for cooling industrial processes, then the heated discharged water may create thermal pollution (see Figure 2-16). Figure 18-8 depicts an aerial view of a stream. Thermograms can locate cool water supplied by underground springs and heated water caused by man-made pollution. Both situations affect the local ecosystem. Oil spills can be located, tracked, and monitored. Since the emissivity of oil ($\varepsilon = 0.97$) is different from water ($\varepsilon = 0.98$), a thermal signature exists even though the temperatures are the same.



Figure 18-8. Aerial view of a stream. (By courtesy of IRcameras.com)

The National Oceanic and Atmospheric Administration (NOAA) operates numerous satellites to collect global environmental data. The current satellites are the Advanced Very High Resolution Radiometer (AVHRR) and the Geostationary Operational Environmental Satellite (GOES). These systems have a multi-spectral capability (Table 18-3).

Table 18-3
AVHRR and GOES SPECTRAL BANDS (μm)

Channel	AVHRR		GOES Satellites I-M
	Satellites 6, 8, 10	Satellites 7, 9, 11, 12, 14	
1	0.58 to 0.68	0.58 to 0.68	0.55 to 0.75
2	0.725 to 1.00	0.725 to 1.00	3.8 to 4.0
3	3.55 to 3.93	3.55 to 3.93	6.5 to 7.0
4	10.5 to 11.5	10.3 to 11.3	10.2 to 11.2
5	10.5 to 11.5	11.5 to 12.5	11.5 to 12.5

The various channels are used to identify crops and environmental changes (visible and near IR channels). GOES' channel 3 is used to locate water vapor. This is the image seen during many television weather reports. The LWIR bands are used to locate thermal differences. For many applications, the images supplied by NOAA are composites of two or more channels (i.e., imagery from channel 1 may be subtracted from the imagery obtained in channel 2) to highlight spectral differences. Figures 18-9 through 18-11 were obtained from NOAA's website.[2] Geological surveys include volcanic activity and geothermal activity.[3]

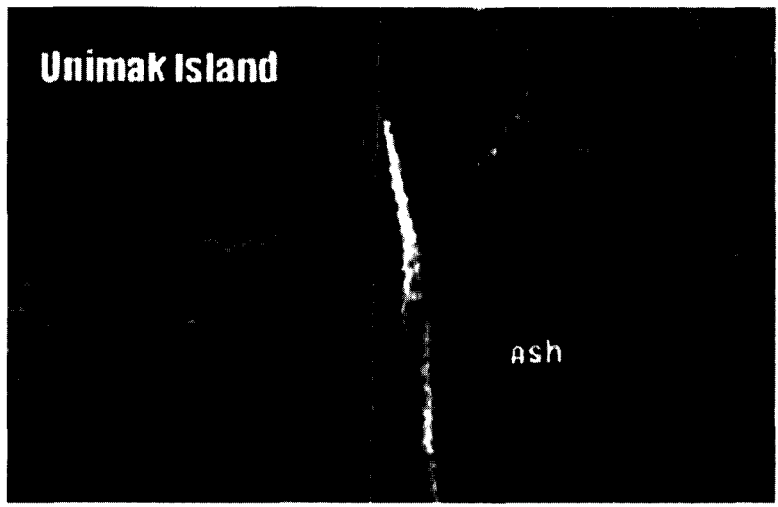


Figure 18-9. Ash plume from the Shishaldin Volcano on the Aleutian island of Unimak taken with AVHRR channels 4 and 5. (By courtesy of NOAA[2])



Figure 18-10. Heated water caused by the Gulf Stream off the eastern United Stated. The landmass is the Mid-Atlantic States and the major waterway is the Chesapeake Bay taken with AVHRR channels 4 and 5. The dark water on the bottom right is the warm Gulf stream. (By courtesy of NOAA[2]).

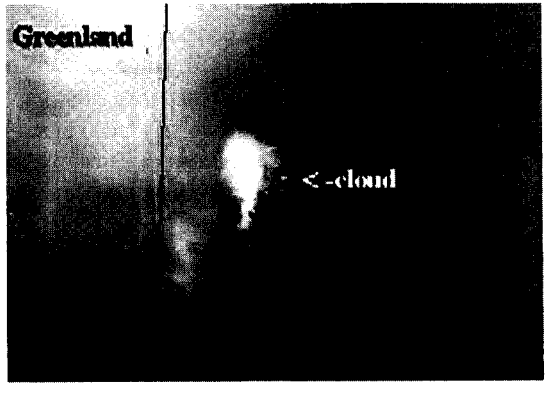


Figure 18-11. Unidentified heated cloud in Greenland that may have been caused by a meteorite strike taken by AVHRR channel 4. (By courtesy of NOAA[2]).

18.1.4. ANIMAL MONITORING

Accurate animal counting is extremely difficult. As an aerial evaluation, topology, vegetation, and weather conditions hamper it. Animal activity varies with the time of day and season. Sufficient resolution is needed to identify the specific species. This suggests that you must be relatively close. However, if too

close, they may be disturbed simply by your presence or the sounds emanating from the aircraft.

Note that by using a higher resolution imaging system (small IFOV), you can view the animals at a longer distance. However, smaller IFOV systems will have a smaller overall field-of-view. As the FOV decreases, it becomes more difficult to survey large areas. For accurate counting you must consider the IFOV, FOV, and speed of the aircraft. Counting cannot be performed in real time if there are numerous animals scattered over a large region. Here the imagery is captured on videotape and evaluated later.

18.1.5. MILITARY

The battlefield is often labeled as the "dirty" battlefield to indicate that there may be soot and smoke from burning materiel, tactical screening smoke, and dust kicked up by bomb blasts and vehicular traffic. These airborne materials substantially reduce atmospheric transmittance. Since these materials do not affect LWIR radiation as much as MWIR radiation, the LWIR system is the system of choice for land-based operations. Tactical screening smokes such as phosphorus completely block view of the target in the visible region. These smokes are fairly transparent in the LWIR region (Figure 18-12). Muzzle blasts produce hot gases that are easily detected (Figure 18-13). As illustrated in Figure 18-14, a nonuniform background hampers target detection. This nonuniformity is often labeled as *thermal clutter*. Fortunately, another target cue is available: most objects are moving during surveillance activities. Aircraft engines are always detectable (Figure 18-15).



Figure 18-12. Typical battlefield scene. The hot spots are pieces of burning phosphorus. Visually, you would see an incredibly large cloud of white smoke. (By courtesy of IRcameras.com).



Figure 18-13. Firing of a 20-mm cannon. (By courtesy of IRcameras .com).



Figure 18-14. A tank on a road. The varying background alters the thermal signature of the tank. (By courtesy of IRcameras.com).

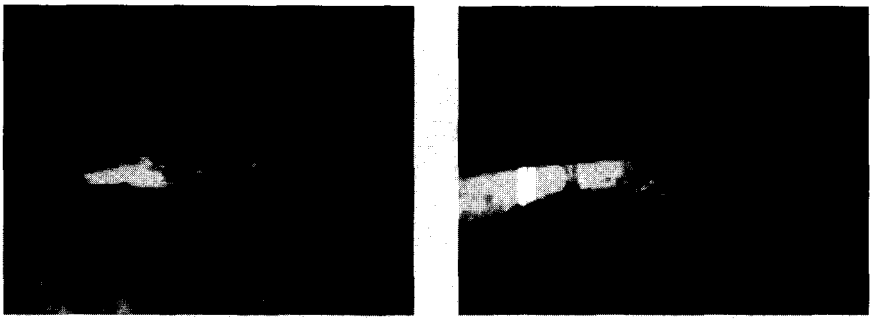


Figure 18-15. The hot engine and exhaust gases are easily discernible in the infrared region. (By courtesy of IRcameras.com).

18.2. MINIMUM RESOLVABLE TEMPERATURE (MRT)

The Johnson criteria link the MRT to range performance. The 1975 NVL model was used for scanning systems. To quantify all the noise sources that exist in staring arrays, the three-dimensional noise model was created and it is an integral part of FLIR92. Detailed descriptions of these models can be found in References 4 through 7. This section highlights FLIR92 performance modeling methodology. The MRT was previously discussed In Section 7.4. *Observer response* and Section 7.5. *MRT and MDT.*

18.2.1. PERCEIVED SIGNAL-TO-NOISE RATIO

The displayed SNR, for a very large target, is

$$SNR = \frac{\tau_A^R \Delta T}{NEDT} = \frac{\Delta T_{APPARENT}}{NEDT} \quad . \tag{18-1}$$

The MTF of the camera reduces the signal created by small targets. Further, the eye/brain "filters" enhance the displayed ***SNR***. Thus, the perceived signal-to-noise ratio becomes

$$SNR_P = k \frac{MTF_{SYS} \Delta T_{APPARENT}}{NEDT} \frac{1}{(eye\ spatial\ filter)\ (eye\ temporal\ filter)}, \tag{18-2}$$

where k is a constant and MTF_{SYS} includes both the camera MTF and the eye MTF. Selecting a threshold value that is required to just perceive a target and inverting Equation 18-2 provides a minimum detectable ΔT which is called the MRT:

$$MRT = SNR_{TH} \frac{NEDT}{MTF_{SYS}} \beta_1 \quad , \tag{18-3}$$

where β_1 is the eye/brain filter that provides both temporal and spatial filtering. This equation is in the same functional form as the 1975 NVL model. FLIR92 incorporates the three-dimensional model (described in the next section). When the eight "noise" components are included, the FLIR92 MRT model becomes

$$MRT = SNR_{TH} \frac{NEDT}{MTF_{SYS}} \sqrt{\beta_1^2 + ... + \beta_8^2 \frac{\sigma_8^2}{NEDT}} \quad , \tag{18-4}$$

where each β_i is the "filter" that interprets noise value σ_i. Since the NEDT is a function of the background temperature, the MRT is also a function of the same background (See Figure 7-13).

A word of clarification is necessary here. The constant, SNR_{TH}, is approximately the SNR enhancement provided by the eye/brain filter. It includes, in part, both temporal and spatial integration effects. It is *not* the signal-to-noise ratio of the video signal or the SNR of the luminance on the display. Depending on the noise characteristics and the target characteristics, the eye can detect[8] signals whose video SNR is as low as 0.05 (see Figure 7-11). To perceive these low SNRs, the target must be a well-known geometrical shape such as a bar, star, letter, or number. Small unrecognizable targets (a blob) require higher SNRs.

The ability to perceive targets embedded in noise depends on the target spatial extent with respect to the noise spatial frequencies. Large bars are easier to perceive compared to small targets that "disappear" into the noise. Figure 7-11 only illustrates the spatial integration capabilities of the eye. With live video, the random noise is changing from frame-to-frame and the eye's temporal integration provides an additional enhancement by a factor of three to six.

18.2.2. THREE-DIMENSIONAL NOISE MODEL

The noise is divided into a set of eight components[9] that relate temporal and spatial noise to a three-dimensional coordinate system (Figure 18-16). This approach allows full characterization of all noise sources including random noise, fixed pattern noise, streaks, rain, 1/f noise, and any other artifact. Analyzing the noise in this manner has the advantage of simplifying the understanding of complex phenomena by breaking it down into a manageable set of components. The method simplifies the incorporation of complex noise factors into model formulations.

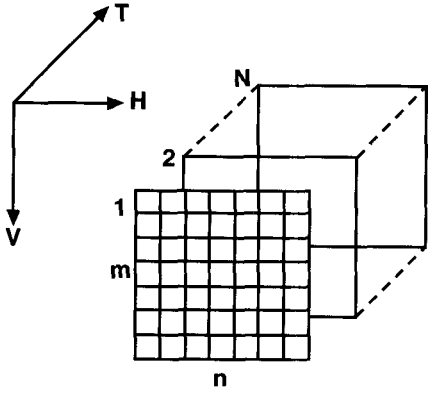


Figure 18-16. Three-dimensional noise model coordinate system illustrating data set N_{TVH}.

The T-dimension is the temporal dimension representing the video framing sequence. The other two dimensions (horizontal and vertical) provide spatial information. For a staring array, ***n*** and ***m*** indicate detector element locations in the horizontal and vertical directions, respectively.

Table 18-4 describes the three-dimensional noise components. The subscripts describe the noise "direction." The value σ_{TVH} represents the rms noise value of the three-dimensional data set $\boldsymbol{m} \times \boldsymbol{n} \times \boldsymbol{N}$. σ_{VH} is the rms noise value after averaging in the T-direction. Its data set contains $\boldsymbol{m} \times \boldsymbol{n}$ elements, and so on.

Depending on the system design and operation, any one of these noise components can dominate. The origins of these components are significantly different and the existence and manifestation depend on the specific design of the imaging system. Not all of the noise components may be present in every imaging system.

Table 18-4
THREE-DIMENSIONAL NOISE DESCRIPTORS

3-D noise component	Description
σ_{TVH}	Random 3-D noise
σ_{VH}	Spatial noise that does not change from frame-to-frame
σ_{TH}	Variations in column averages that change from frame-to-frame (rain)
σ_{TV}	Variations in row averages that change from frame-to-frame (streaking)
σ_{V}	Variations in row averages that are fixed in time (horizontal lines or bands)
σ_{H}	Variations in column averages that are fixed in time (vertical lines)
σ_{T}	Frame-to-frame intensity variations (flicker)

Fixed pattern noise is incorporated though σ_{VH}, σ_{V}, and σ_{H}. Currently, only σ_{TVH} is predicted (it is the NEDT) and the remaining noise components must be determined from measurements or estimates. Figures 18-17 through 18-19, generated by the System Image Analyzer (SIA) software,[10] illustrate the effect of these noise sources. Figure 18-17 is the basic image. In Figure 18-18, fixed pattern and random noise appear similar in a single frame. Random noise changes from frame-to-frame whereas fixed pattern noise does not. Figure 18-19 illustrates how σ_{TV} or σ_{V} affects the visibility of horizontal bars. Scanning systems often exhibit this type of noise.



Figure 18-17. Ideal image (no noise). Generated by SIA software.[10]

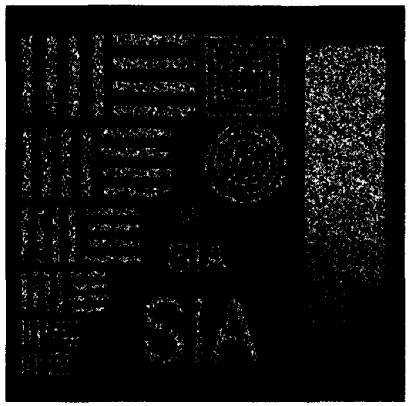


Figure 18-18. Image with random and fixed pattern noise.

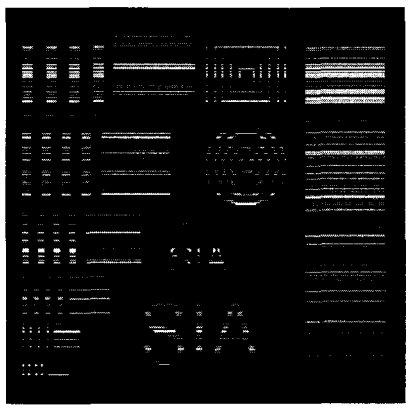


Figure 18-19. Image with dominant horizontal banding (high σ_{TV} or σ_V).

18.2.3. TWO-DIMENSIONAL MRT

Although FLIR92 is called two-*dimensional*, it is a two-*directional* model. That is, the threshold is predicted in the vertical and horizontal directions. With unequal MTFs, the predicted MRT will be different in the two directions. The two directional values are brought together with a two-dimensional spatial frequency that approximates the response of an equivalent radially symmetric system.

The two-dimensional MRT is created by taking the geometric average of the horizontal and vertical MRT frequencies at each contrast value (Figure 18-20):

$$f_{2D} = \sqrt{f_V f_H} = \sqrt{f_x f_y} \quad . \tag{18-5}$$

The two-dimensional MRT is a mathematical construct that is used for range performance predictions. It cannot be measured because f_{2D} is perceptual and therefore is not real.

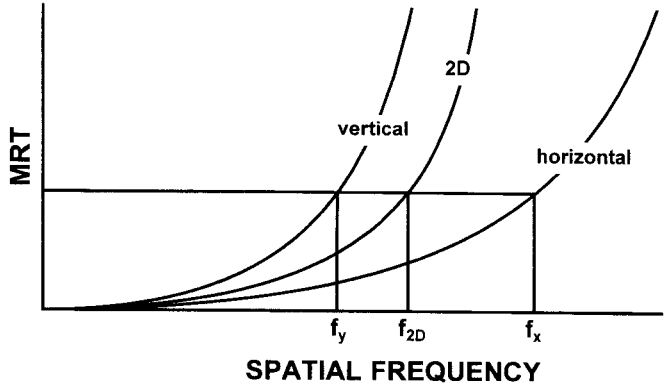


Figure 18-20. The two-dimensional MRT is mathematically created from the horizontal and vertical MRTs. It is really a two-*directional* MRT.

18.3. RANGE PREDICTIONS

The Johnson criterion provides the link between the target-angular-subtense and the spatial frequency scale on the MRT graph. The signature of the target is modified by the atmospheric attenuation. When the target's apparent ΔT is reduced to the MRT curve, the performance range is obtained. Depending on the Johnson criterion selected, this intersection is the detection, recognition, or identification range.

A word of clarification. Detection, as used with the Johnson criteria, means location of an object that we want to view with more detail. This is not "hot spot detection" which simply means location of a target. An object, if hot enough, can be detected. For example, we can see stars in the sky even though we cannot see any detail. Hot spot detection would be used in location of fires and infrared search and track (IRST) activities. The range to a "hot spot" object uses the minimum detectable temperature (MDT).

Within the real world, there is a probability associated with every parameter. The target signature is not one number but a range of values that follow a diurnal cycle. The atmospheric transmittance is not fixed but can change in minutes. There appears to be an overwhelming set of combinations and permutations. Therefore, only a few representative target contrasts and a few representative atmospheric conditions are selected and the performance range is calculated for these conditions.

18.3.1. TARGET ΔT

Because of the wide variation in target signatures, Ratches et. al. stated[11] *One of the main problems in performance modeling is to obtain an exact target signature. ... The problem is further complicated by the fact that one target can have many different signatures under various operational and environmental conditions. .... We cannot easily describe all the complex target characteristics corresponding to the real-world IR signature ... . Therefore we utilize only the overall general features of the target such as size and average temperature difference from the background. The resulting predictions then correspond to the results of a large ensemble of experiments. However, the results of any specific experiment with its unique target signature will not necessarily come close to the predictions for the general ensemble.*

An average ΔT is assigned to each target. Table 18-5 provides some common values. These values assume that the background is near 293K. If the background is substantially different, then the target ΔT must be appropriately modified.

Table 18-5
REPRESENTATIVE ΔTs

Target	ΔT (°C)	Minimum dimension (m)
Tank	1.25	2.3 (front view)
Jeep	1.5	1.75 (front view)
Human	2.0	0.75 (depends upon clothing)
Animal (deer)	0.5	0.5 (top view)

18.3.2. JOHNSON CRITERIA

The Johnson[12] methodology has become known as the equivalent bar pattern approach. Observers viewed military targets through image intensifiers and were asked to detect, decide the orientation, recognize, and identify the targets. Air Force tri-bar charts whose bars had the same contrast as the scaled models were also viewed and the maximum resolvable bar pattern frequency was determined. The number of bars per critical object dimension was increased until the bars could just be individually resolved. In this way, detectability was correlated with the sensor's threshold bar pattern resolution. These results became the foundation for the discrimination methodology used today. *Critical* dimension refers to the target dimension that must be discerned for detection, recognition, or identification. In the early literature, the minimum dimension was called the critical dimension.

18.3.3. DISCRIMINATION

Johnson used the *minimum* dimension in his work, whereas the *critical* dimension is equal to the square root of the target area. The critical dimension is

$$h_c = \sqrt{A_{target}} \cdot \tag{18-6}$$

For rectangular targets, $h_c = (HW)^{1/2}$ where H and W are the target's height and width respectively. The two-dimensional FLIR92 model uses the critical dimension approach the same way that the 1975 NVL model uses the minimum dimension.

Converting to a two-dimensional model requires removing the directional bias imposed by the one-dimensional model. This is achieved[13] by reducing all values by 25%, or equivalently, multiplying all discrimination values by 0.75. This adjustment then provides the same range performance predictions whether predicted by the one-dimensional 1975 NVL or two-dimensional FLIR92 model. Table 18-6 provides the commonly used discrimination levels. By convention, each 50% probability is labeled as N_{50} (e.g., in one-dimension, N_{50} is 1, 4, or 8 cycles for detection, recognition, or identification, respectively). A cycle is one bar plus one space. Figure 18-21 illustrates the expected imagery for detection, recognition, and identification.

Table 18-6
COMMON DISCRIMINATION LEVELS

Task	Description	One-dimension N_{50}	Two-dimension N_{50}
Detection	The blob has a reasonable probability of being an object being sought.	1.0	0.75
Classical recognition	Object discerned with sufficient clarity that its specific class can be differentiated.	4.0	3.0
Identification	Object discerned with sufficient clarity to specify the type within the class.	8.0	6.0

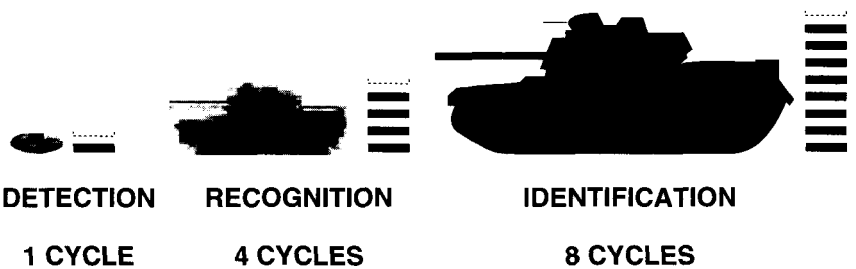


Figure 18-21. One-dimensional Johnson criteria interpretation. The equivalent bar target is shown next to the minimum dimension of the tank. We can detect the tank when its size is equal to one cycle ($N_{50} = 1$). If the atmosphere is transparent ($T_A = 1$), then the range for recognition is 1/4 of the detection range and the identification range is 1/8 of the detection range.

18.3.4. TARGET TRANSFER PROBABILITY FUNCTION

The results of threshold experiments such as Johnson's provide an approximate measure of the 50% probability of discrimination level. Results of several field tests[14] provided the cumulative probability of discrimination or target transfer probability function (TTPF) (Table 18-7). The TTPF can be used for all discrimination tasks by simply multiplying the 50% probability of performing the task by the TTPF multiplier. For example, from Table 18-7, the probability of 95% recognition (in one dimension) is $2N_{50} = 2(4) = 8$ cycles across the target's minimum dimension.

Table 18-7
DISCRIMINATION CUMULATIVE PROBABILITY

Probability of discrimination	Multiplier
1.00	3.00
0.95	2.00
0.80	1.50
0.50	1.00
0.30	0.75
0.10	0.50
0.02	0.25
0.00	0.00

An empirical fit[15] to the data provides

$$P(N) = \frac{\left(\frac{N}{N_{50}}\right)^{E}}{1 + \left(\frac{N}{N_{50}}\right)^{E}} , \qquad (18\text{-}7)$$

where

$$E = 2.7 + 0.7\left(\frac{N}{N_{50}}\right) . \qquad (18\text{-}8)$$

Figure 18-22 illustrates the full TTPF for the three levels of discrimination as identified by Johnson.

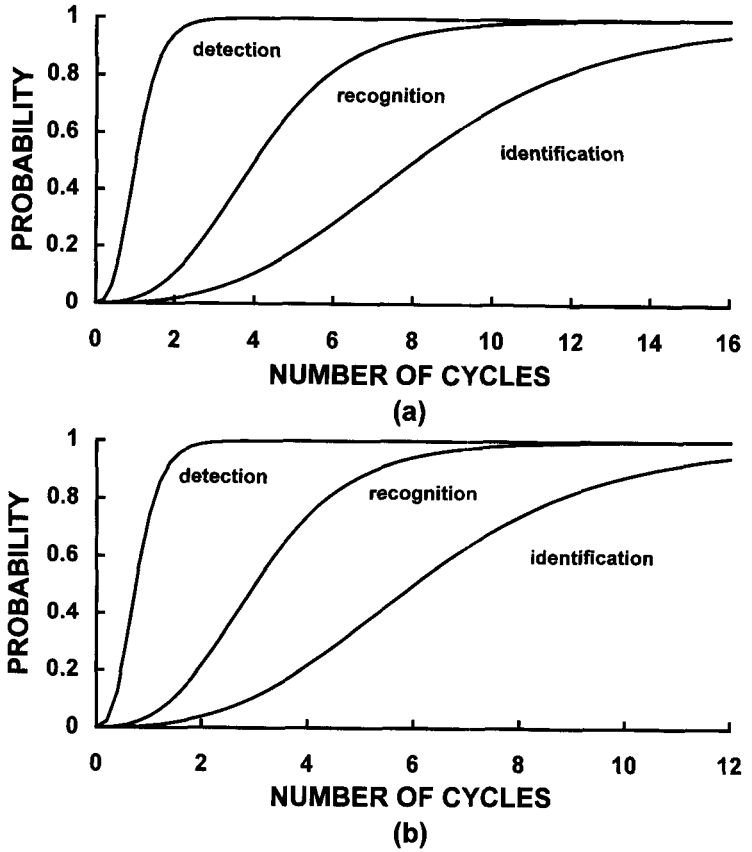


Figure 18-22. Target transfer probability function for detection, recognition, and identification. (a) One-dimensional, and (b) two-dimensional. Note differences in the scale.

18.3.5. RANGE PREDICTION METHODOLOGY

The MRT abscissa is converted into a range scale using a target discrimination value. When using the one-dimensional 1975 NVL model, the number of cycles that appear across the target is

$$N_x = \frac{h}{R} f_x \ , \qquad (18\text{-}9)$$

where h is the minimum dimension and h/R is the target-angular-tense at range R. Since f_x has units of cycles/mrad, h should be in meters and R in kilometers.

The apparent temperature differential, $\Delta T_{APPARENT}$ at the system's entrance aperture is

$$\Delta T_{APPARENT} = \tau_A^R \Delta T \quad . \tag{18-10}$$

Consider, for example, a target whose minimum dimension is 3 m and we want to recognize it ($N_{50} = 4$). Then the conversion from spatial frequency to range is

$$R = \frac{3}{4} f \quad . \tag{18-11}$$

Thus, the frequency axis is multiplied by 3/4 to obtain kilometers (Figure 18-23).

With the two-dimensional model, the critical dimension, h_c, is the square root of the target area, A_{TARGET}. The number of equivalent cycles across the target is

$$N_T = \frac{\sqrt{A}}{R} f_{2D} = \frac{h_c}{R} f_{2D} \, . \tag{18-12}$$

The target transfer probability function is used to predict the probability of range performance. Here, a range is selected and the $\Delta T_{APPARENT}$ is calculated. This value intersects the MRT curve at what is called the critical frequency. Multiplying the target-angular-subtense by the critical frequency provides the number of cycles across the target. Referring to the TTPF (Figure 18-22), the probability is determined for that particular range. Then a new range is selected and the process is repeated until the entire probability function is determined (Figure 18-24).

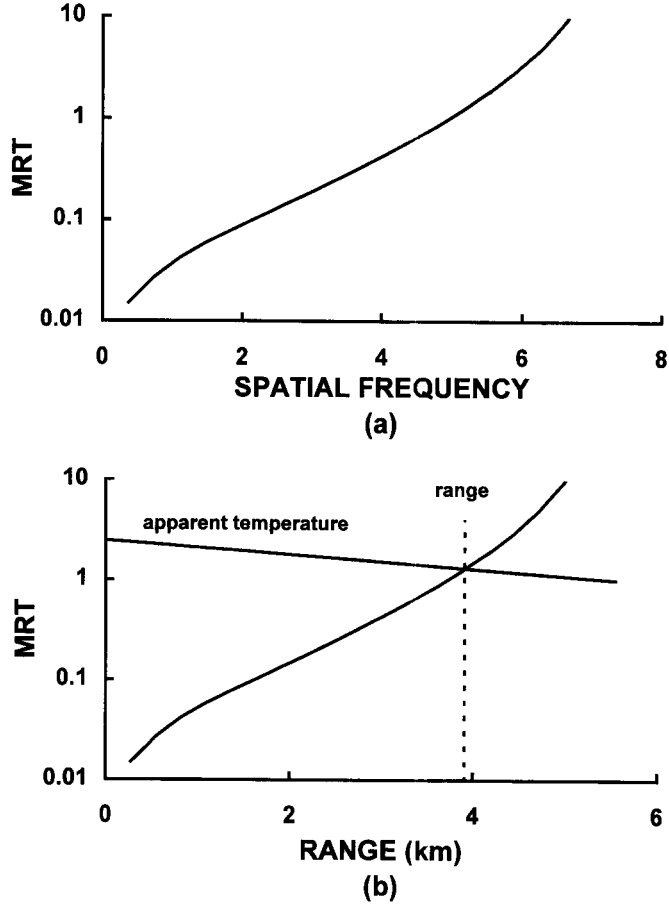


Figure 18-23. Recognition range for a typical common module system (one-dimensional). (a) MRT and (b) conversion of spatial frequency into range. $N_{50}=4$, $h=3$ m, and $\Delta T=2.5°$C. If $\tau(\lambda)\approx\tau$, then $\Delta T_{APPARENT}$ is a straight line when plotted in semi-logarithmic coordinates. When the average atmospheric attenuation is 0.85/km, the recognition range is approximately 3.9 km for this example.

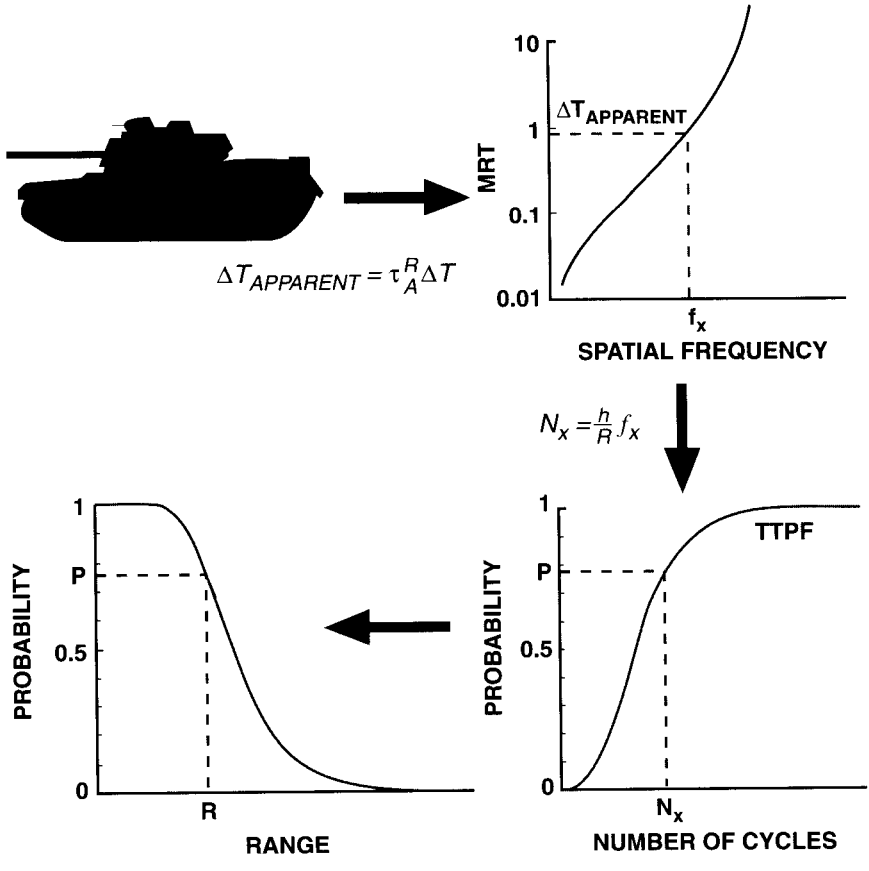


Figure 18-24. Methodology to determine range performance probability.

18.4. REFERENCES

1. M. Tervo, "Supervision of Self-heating in Peat Stockpiles by Aerial Thermography," in *Thermosense XIII*, G. S. Baird, ed., SPIE Proceedings Vol. 1467, pp. 161-168 (1991).
2. These images were downloaded from NOAA's website at http://www.noaa.gov.
3. S. Björnsson and K. Árnason, "State of the Art of Aerial Thermography in Iceland - Thermography of Geothermal Areas during the past 20 Years," in *Thermosense XVII*, S. A. Semanovich, ed., SPIE Proceedings Vol. 2473, pp. 2-14 (1995).
4. *The Infrared and Electro-Optical Systems Handbook*, J. S. Accetta and D. L. Shumaker, eds., copublished by Environmental Research Institute of Michigan, Ann Arbor, MI and SPIE Press, Bellingham, WA (1993).
5. G. C. Holst, *Electro-optical Imaging System Performance*, JCD Publishing, Winter Park, FL (1995).
6. J. A. Ratches, W. R. Lawson, L. P. Obert, R. J. Bergemann, T. W. Cassidy, and J. M. Swenson, "Night Vision laboratory Static Performance Model for Thermal Viewing Systems," ECOM Report ECOM-7043, Fort Monmouth, NJ (1975).
7. *FLIR92 Thermal Imaging Systems Performance Model, User's Guide*, NVESD document UG5008993, Fort Belvoir, VA (1993).
8. F. A. Rosell, "Psychophysical Experimentation," in *The Fundamentals of Thermal Imaging Systems*, F. Rosell and G. Harvey, eds., NRL Report # 8311, pg. 225. Naval Research Laboratory, Washington, D.C. (1979).
9. J. D'Agostino and C. Webb, "3-D Analysis Framework and Measurement Methodology for Imaging System Noise," in *Infrared Imaging Systems: Design, Analysis, Modeling and Testing II*, G. C. Holst, ed., SPIE Proceedings Vol. 1488, pp. 110-121 (1991).
10. System Image Analyzer (SIA) software is available from JCD Publishing, 2932 Cove Trail, Winter Park, FL 32789.
11. J. A. Ratches, W. R. Lawson, L. P. Obert, R. J. Bergemann, T. W. Cassidy, and J. M. Swenson, "Night Vision laboratory Static Performance Model for Thermal Viewing Systems," ECOM Report ECOM-7043, pg. 2, Fort Monmouth, NJ (1975).
12. J. Johnson, "Analysis of Imaging Forming Systems," in *Proceedings of the Image Intensifier Symposium*, pp. 249-273, Warfare Electrical Engineering Dept., US Army Engineering Research and Development Laboratories, Ft. Belvoir, VA (1958). This article is reprinted in *Selected Papers on Infrared Design*, R. B. Johnson and W. L. Wolfe, eds., SPIE Proceedings Vol. 513, pp. 761-781 (1985).
13. L. Scott and R. Tomkinson, "An Update on the C^2NVEO FLIR90 and ACQUIRE Sensor Performance Model," in *Infrared Imaging Systems: Design, Analysis, Modeling and Testing II*, G. C. Holst, ed., SPIE Proceedings Vol. 1488, pp. 99-109 (1991).
14. J. A. Ratches, W. R. Lawson, L. P. Obert, R. J. Bergemann, T. W. Cassidy, and J. M. Swenson, "Night Vision Laboratory Static Performance Model for Thermal Viewing Systems," ECOM Report ECOM-7043, pg. 56, Fort Monmouth, NJ (1975).
15. J. D. Howe, "Electro-Optical Imaging System Performance Prediction," in *Electro-Optical Systems Design, Analysis, and Testing*, M. C. Dudzik, ed., pg. 92. This is Volume 4 of the *Infrared and Electro-Optical Systems Handbook*, J. S. Accetta and D. L. Shumaker, eds., copublished by Environmental Research Institute of Michigan, Ann Arbor, MI and SPIE Press, Bellingham, WA (1993).

19
NONDESTRUCTIVE TESTING

Nondestructive testing (NDT) may be called active infrared thermography since it combines thermal imaging and controlled heat injection. Although called "heat injection," it is actually flooding the surface for a brief amount of time with radiation. The heat may be injected as a flash pulse (impulse), wide pulse, or a series of periodic pulses. The radiation (heat) may be applied by high intensity xenon flash lamps, lasers, incandescent lamps, or heat guns. If the surface reflectivity is low (high emissivity), the surface will heat up and then the heat will propagate (via conduction) through the material.

Consider a single pulse of heat injected onto a surface. The surface temperature may briefly reach 450K. As the heat travels through the material, the surface will cool. If a subsurface barrier is encountered, propagation is altered. A portion of the heat wave will reflect back to the surface and reheat the surface. The time from heat deposition to reheating is related to the defect depth (Figure 19-1). The surface temperature is illustrated in Figure 19-2. The defect can also be detected by monitoring the rear surface. Thermal signatures from buried defects or other sub-surface features appear, peak, and fade at different times depending on the thermal properties of the material and defect, and defect size and depth.

NDT requires a method to rapidly change the surface temperature of an object. Heat can be carefully injected by using a controllable light source. However, NDT methods also apply if there is a controllable method to reduce surface temperature. This could be by flooding the surface with cold water, liquid nitrogen, or any other liquid that evaporates quickly.

NDT is similar to locating buried objects (see Chapter 17, *Buried objects*). The surface temperature is a function of the heat load (solar for buried objects and applied for NDT). Appropriate data analysis will separate the buried object signal from other signals (flaw versus normal image).

A sampling of the rather extensive literature indicates the widespread application of this technique, including the detection of debonding in adhesive joints and honeycomb structures, voids in ceramics, hot spots in printed circuit boards, and delaminations or cracking in composites. NDT is still in its infancy. Emerging techniques will improve defect detection capability.

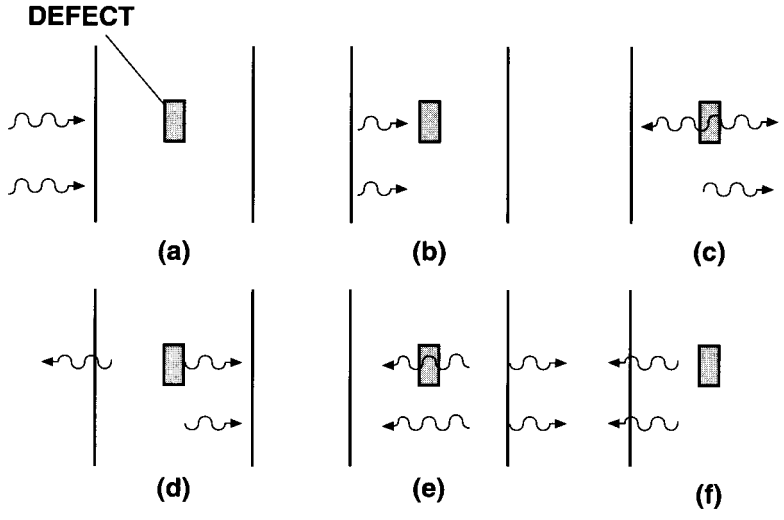


Figure 19-1. Idealized propagation of a single heat pulse through a thin material, (a) An impulse of energy is applied to the surface. (b) The heat pulse travels through the material and encounters a defect. (c) The defect partially reflects and partially transmits the pulse. (d) When the reflected pulse reaches the surface, it radiates its energy. (e) The transmitted pulse reaches the rear surface and is reflected. The rear surface also radiates some of the energy. (f) The pulse reflected from the rear surface finally reaches the front surface and radiates. Diffusion (neglected here) significantly affects the surface temperature distribution.

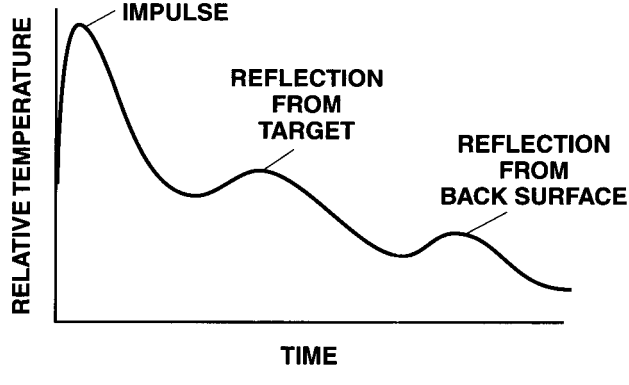


Figure 19-2. Exaggerated surface temperature as a function of time to illustrate the phenomenology. The heat is injected as an impulse.

Although Vavilov[1] proposed standardized terminology, no industry-wide uniformity exists. Terms such as pulsed infrared imaging (PII), nondestructive inspection (NDI), nondestructive evaluation (NDE), thermal nondestructive testing (TNDT), thermal wave imaging (TWI), time-resolved radiometry (TRR), thermal/infrared nondestructive testing (T/I NDT), dynamic thermal tomography, pulse phase thermography, and modulated thermography are used almost interchangeably. These terms are used according to the way the energy is injected, experimental procedure, and data analysis technique.

The number of papers is too numerous to reference. Appendix C, *Thermal Sensing and Imaging 1980-1999,* contains over 140 papers devoted to NDT. These papers were presented at SPIE's conference *Thermosense*. It represents a fraction of papers that are published each year. References 2 and 3 provide additional theory and applications.

19.1. APPLICATIONS

In general, a good structural bond is a good thermal bond. Therefore, any deviation from structural integrity tends to modify heat flow. Voids, disbonds, delaminations, foreign matter (inclusions), badly cured areas, and surface cracks can be detected. Since thermal diffusion can completely obliterate the signal from a defect, the NDT method tends to be limited to thin materials. One major advantage is that the item under test does not have to be disassembled.

Much work has been performed on the newer composites. These composites are lighter, stronger, and more corrosion resistant compared to existing materials. Composites are used in automobiles, aircraft, boats, and many other components such as printed circuit boards. These materials include carbon fiber reinforced plastics (CFRP), continuous fiber ceramic matrix composites (CFCC), and glass-reinforced plastics (GRP).

Unfortunately, while composites are stronger and lighter than conventional materials, they may not have the same impact strength. For example, glass reinforced plastics are used extensively on recreational and small commercial boats. GRPs do not rust (compared to steel) and will not oxidize (compared to aluminum). However, repeated bumps against a dock can cause fractures and cracks. The hull can become waterlogged if there is a crack and the internal water can destroy the internal hull components.

With our aging aircraft fleet, it is necessary to check for flaws, fatigue cracks, corroded lap joints, bonding, and corroded rivets. Corroded or loose rivets

will not make good thermal contact with the aircraft skin. After heat injection, the skin and rivets should cool at approximately the same rate. If a rivet is corroded, it will stay hotter for a longer period of time. If the skin is within good thermal contact with the ribs, then the ribs will conduct heat away from the skin. With disbonding, the skin remains hot longer after heat injection.

Figure 19-3 illustrates some defects that can be detected by NDT methods. NDT can measure the size and depth of various defects. It can also monitor wall thickness on pipes and conduits.

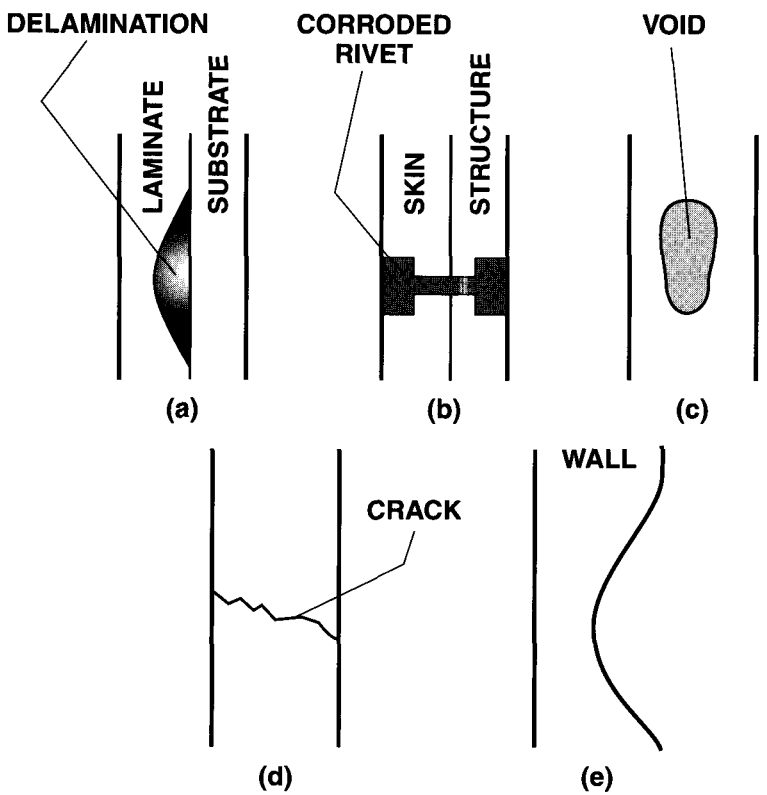


Figure 19-3. Various defects sensed by NDT. (a) Delamination, (b) corroded rivet, (c) void, (d) crack, and (d) wall thinning.

19.2. HEAT TRANSFER

The differences between various thermal NDT techniques is primarily by the way in which energy is injected[4] into the specimen: flash pulse (impulse or Dirac pulse), step, square pulse, and source modulation (Figure 19-4). In keeping with the thermal *wave* concept, the impulse function contains all frequencies. A train of pulses can be described by the time between pulses (period). By varying the period, T, each frequency ($f = 1/T$) is separately applied.

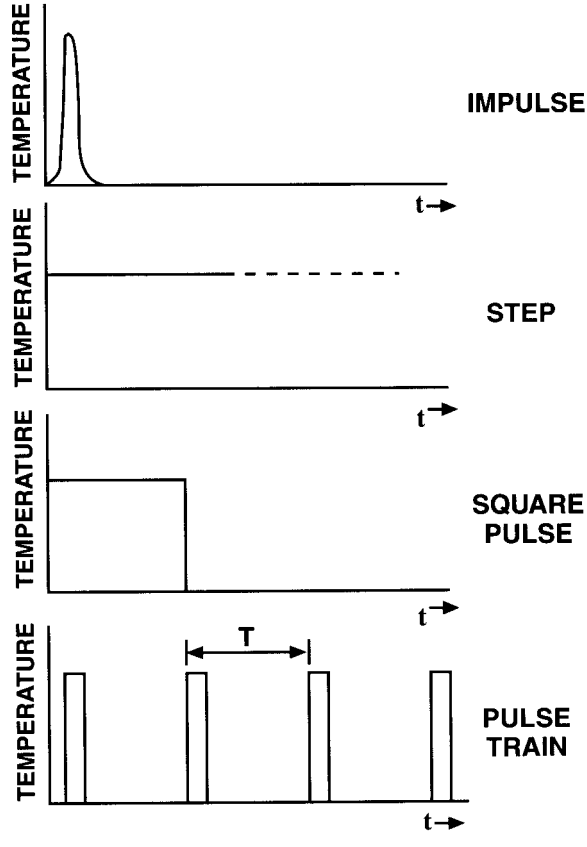


Figure 19-4. Various energy sources. A sinusoidal pulse is difficult to generate. It is approximated by a periodic series of pulses (pulse train). The period of the pulse train is T.

The selection of energy deposition depends upon the material properties, type of defect, and anticipated thermal contrast. The thermal contrast is defined as[5]

$$C = \frac{T_{DEFECT}(t) - T_{DEFECT}(t=0)}{T_{SOUND}(t) - T_{SOUND}(t=0)} = \frac{\Delta T_{DEFECT}}{\Delta T_{SOUND}} \quad , \qquad (19\text{-}1)$$

where the subscript ***SOUND*** is a part of the sound material (no defects). Note that ΔT represents the surface temperature increase above the ambient temperature (which is the initial temperature at $t = 0$). The maximum value of the contrast depends upon the heating technique and the defect depth. Since the depth is unknown, it is necessary to store a series of images (time sequence) to find the maximum contrast. While the minimum detectable value of the contrast is not specified, it is clear that the temperature difference between the good and defective part must be well above the noise level of the thermal imaging system:

$$\Delta T_{DEFECT} - \Delta T_{SOUND} >> NEDT \quad . \qquad (19\text{-}2)$$

Equivalently, the contrast must provide a good signal-to-noise ratio. Because of diffusion, defects must be relatively large. The general rule[6] is that a defect can be detected if its radius-to-depth is greater than one.

19.2.1. FLASH PULSE (IMPULSE or DIRAC PULSE)

The flash pulse technique is useful for testing high thermal conductivity material (e.g., aluminum and steel) that are less than six millimeters thick. For an impulse that irradiates a large area (negligible radial flow), the time-depth dependence of temperature is[7]

$$T(z,t) - T_{AMBIENT} = \frac{Q}{\sqrt{4\pi\alpha t}} e^{-\frac{z^2}{4\alpha t}} \quad , \qquad (19\text{-}3)$$

where z is the depth, Q is the amount of heat deposited, α is the thermal diffusivity and $T_{AMBIENT}$ is the ambient temperature. The object is assumed to be of uniform temperature prior to the heat injection: $T(0,0) = T_{AMBIENT}$. The injected heat raises the object's temperature above its equilibrium value. The exponent indicates that the heat is rapidly attenuated. The value, α, depends upon material properties:

$$\alpha = \frac{k}{\rho c} \quad , \tag{19-4}$$

where k is the thermal conductivity, ρ is the material density (not to be confused with reflectivity), and c is the specific heat. The time of the peak temperature at a depth z (Figure 19-5) is

$$t_{PEAK} = \frac{z^2}{2\alpha} \quad . \tag{19-5}$$

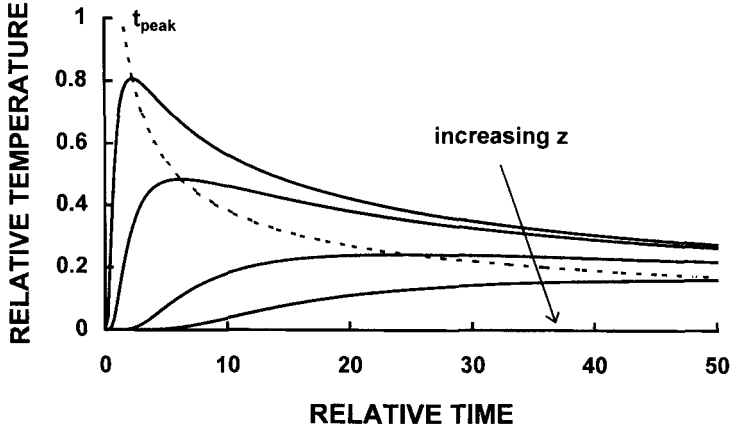


Figure 19-5. The internal temperature as a function of the depth and time. After a long period of time, the internal temperature tends to reach a constant value that is independent of depth. This means that it is difficult to locate very deep defects by the impulse method.

If the wave reflects off a flaw at depth L, the heat pulse must travel $2L$ to reflect back to surface. The surface temperature is

$$T(0,t) - T_{AMBIENT} = \frac{QR_{THERMAL}}{\sqrt{4\pi\alpha t}} e^{-\frac{(2L)^2}{4\alpha t}} \quad , \tag{19-6}$$

where $R_{THERMAL}$ is the thermal reflection coefficient. It is

$$R_{THERMAL} = \frac{e_M - e_F}{e_M + e_F} \quad , \tag{19-7}$$

where the subscripts M and F referring to the material and flaw, respectively. The two thermal effusivities are

$$e_M = \sqrt{k_M \rho_M c_M} \tag{19-8}$$

and

$$e_F = \sqrt{k_F \rho_F c_F} \quad . \tag{19-9}$$

The effusivity is inversely related to the thermal resistance (See Equation 2-6). With high thermal conductivity materials (large k), heat travels quickly (low thermal resistance and high effusivity). As the effusivity of the flaw increases, the thermal reflection decreases and resultant surface temperature decreases. Equivalently, as the flaw's effusivity increases, it becomes more difficult to measure the flaw. If a defect is at depth L, the time to reach the defect and reflect back to the surface is

$$t_{DEFECT} = \frac{(2L)^2}{2\alpha} = \frac{2(L)^2}{\alpha} \quad . \tag{19-10}$$

Analytical and experimental techniques have been developed to determine qualitatively[8] the depth of the defects in metals and composite materials. Deeper defects will be observed at a later time (Equation 19-10). Simultaneously the surface temperature decreases for deeper defects (Equation 19-6). More energy is necessary to detect very deep defects. This limits the flash pulse method to relatively thin materials.

19.2.2. STEP and SQUARE PULSE IRRADIATION

The controlled square pulse enables an object to achieve a predetermined temperature. It is preferable over the flash pulse technique when inspecting thick and low thermal conductive materials. It is also useful to determine the integrity of thin coatings. The flash and square wave step techniques are different in the heating stage. However the cooling stages tend to be similar, if not identical, especially for longer observation times (much greater then the step time).

If heat is applied continuously, the time-depth temperature dependence is[8,9]

$$T(z,t) - T_{AMBIENT} = 2Q\sqrt{\frac{t}{\pi k \rho c}}\, e^{-\frac{z^2}{4\alpha t}} - \frac{z}{2k}\, erfc\left(\frac{z}{\sqrt{4\alpha t}}\right) \quad . \tag{19-11}$$

The surface temperature, in absence of any reflection is

$$T(0,t) - T_{AMBIENT} = 2Q\sqrt{\frac{t}{\pi k \rho c}} \quad . \tag{19-12}$$

As illustrated in Figure 19-6, the surface temperature of a thin coating depends upon the coating thickness. For an infinitely thick coating, the temperature will increase linearly with $t^{1/2}$. For thin coatings, the temperature starts to roll off as the heat pulse enters the higher thermal conductivity substrate (metal). Thus, the time history of the temperature provides a measure of the coating thickness. Figure 19-7 illustrates the coating surface temperature when the substrate is air and metal. The air substrate would simulate a separation between the coating and substrate. The increase in temperature is due to the low thermal conductivity of air. Thus, disbonding can be identified. Since the temperature rolls off before one second, the heat pulse only need be one second long. For this measurement, a one-second pulse provides the same information as a step response.

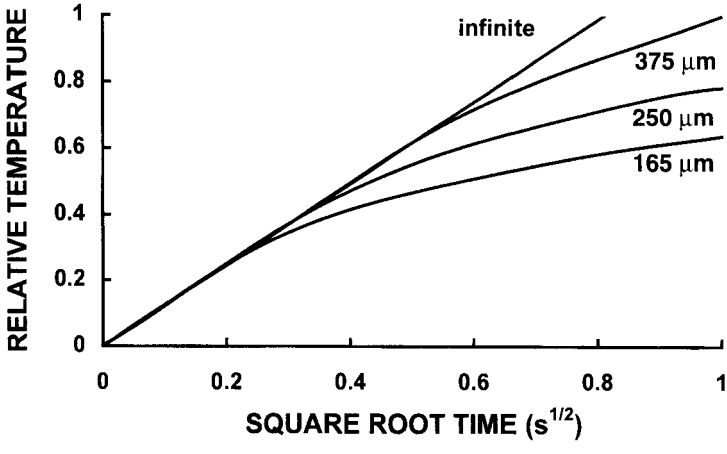


Figure 19-6. Surface temperature as a function of $t^{1/2}$ for a zirconia coating on a metal substrate for three different coating thicknesses. The roll-off time is a measure of coating thickness. (From reference 9).

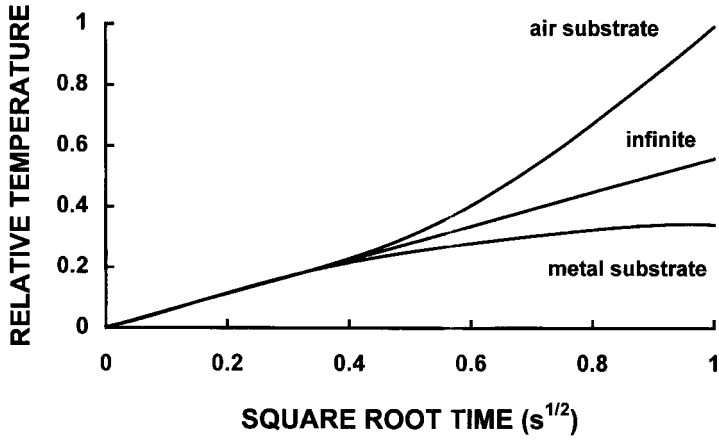


Figure 19-7. Surface temperature as a function of $t^{1/2}$ for a zirconia coating with metal and air substrates subjected to step heating. (From reference 9).

19.2.3. MODULATED IRRADIATION

Injecting a series of heat pulses can increase the signal-to-noise ratio. The result is the launching of "thermal waves" (waves of temperature) into the object. If a modulated heat source is applied to the surface of a sample, a temperature modulation starts to propagate into the material. After a transient time lasting several cycles, a stationary condition is reached: Every point in the sample undergoes an oscillating temperature whose amplitude decreases rapidly with depth. This technique is useful when testing composite materials or very thick metals.

If the input is sinusoidal, then the temperature[10] at a depth z is

$$T(z,t) = T_{AMBIENT} e^{-\sigma z} \cos\left(\sigma z - \omega t\right) \quad , \tag{19-13}$$

where

$$\sigma = \sqrt{\frac{\omega}{2\alpha}} \quad . \tag{19-14}$$

This is a traveling wave whose velocity is

$$v = \sqrt{2\alpha\omega} \quad . \tag{19-15}$$

The damping term, $e^{-\sigma z}$, provides a thermal diffusion length (where the amplitude is 1/e) of

$$\mu = \sqrt{\frac{2\alpha}{\omega}} \quad . \tag{19-16}$$

These two factors cause the waves to decay very rapidly. For a semi-infinite coating of thickness L, the surface temperature ($z = 0$) is[6]

$$T(0,t) = \frac{(1-R)I_o}{k\sigma}\left[\frac{1+Re^{-2\sigma L}}{1-Re^{-2\sigma L}}\right]\cos(\omega t) \quad . \tag{19-17}$$

The thermal reflection coefficient, $R_{THERMAL}$, is

$$R_{THERMAL} = \frac{e_C - e_S}{e_C + e_S} \quad , \tag{19-18}$$

where the subscripts C and S referring to the coating and substrate, respectively.

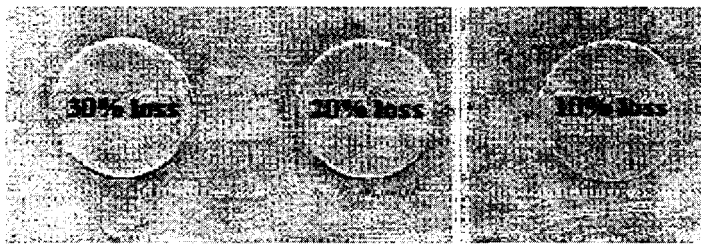
19.3. TEST METHODOLOGY

Low emissivity materials such as aluminum must be painted to improve heat transfer from the source. Paint could be the primer coat or water based that can be removed with high-pressure water jets. It must be recognized that highly absorbent paint is generally highly emissive at the infrared wavelengths. The paint may alter the natural thermal response of the material (see Section 12.3.4, *Increasing the emissivity*).

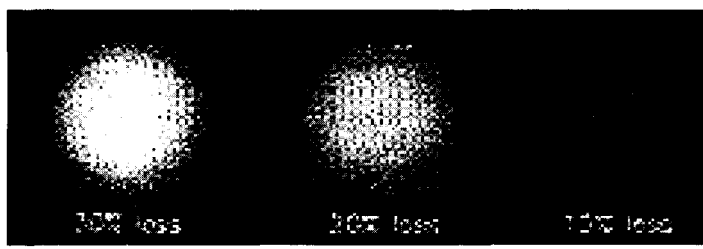
Because heat propagation occurs in a relatively short period of time, it may be necessary to have a thermal imaging system capable that can operate at several hundred frames per second. This also requires a computer capable of storing large amount of data. However, if qualitative results are adequate, then storing every other, every 5th or every 10th frame may be satisfactory.

Before evaluating material for defects, it is prudent to run several experiments with a simulant that has well-characterized "flaws" (Figure 19-8). Data analysis will determine flaw detectability as a function of size and depth. Based upon these initial studies, heat source arrangement, pixels on target, frame rate, and data analysis methodologies are selected for optimum detectability. Once the test configuration is established, it is necessary to obtain images of good components as a measure of

acceptability. Once allowable deviations are determined, then it is possible to determine unacceptable components.



(a)
ALUMINUM PLATE



(b)
THERMOGRAM

Figure 19-8. Simulated corrosion in 1-mm thickness aluminum. The front surface was painted black to increase its emissivity. (a) Each 25.4-mm diameter hole is flat-bottomed and is at a different depth from the front surface. They represent 10%, 20%, and 30% material loss due to corrosion. (b) Thermogram of the front surface after irradiation with a single pulse of heat. (From reference 8, by permission of Arnold Daniels).

19.3.1. HEAT INJECTION METHODS

Figure 19-9 illustrates reflection-mode imaging: The camera and heat source(s) are positioned on the same side of the specimen surface. Reflection-mode imaging tends to provide more quantitative information. It is the only method available for fully assembled components (e.g., where the opposite side is not accessible as with an aircraft skin).

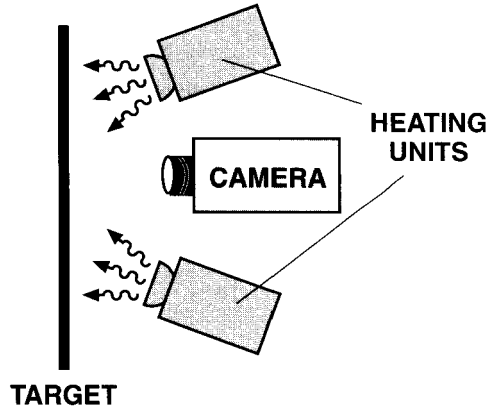


Figure 19-9. Generic arrangement for reflection-mode imaging.

Figure 19-10 illustrates transmission-mode imaging: The camera and heat source are positioned on opposite sides of the material. The appearance and maximum contrast times are less dependent on flaw depth for transmission mode imaging, allowing simultaneous observation of defects over a relatively large depth range. Additionally, better contrast can be achieved for deep defects in relatively thick materials, assuming the thermal wave has sufficient energy to propagate through the target and the defect signature is not obscured by lateral diffusion.

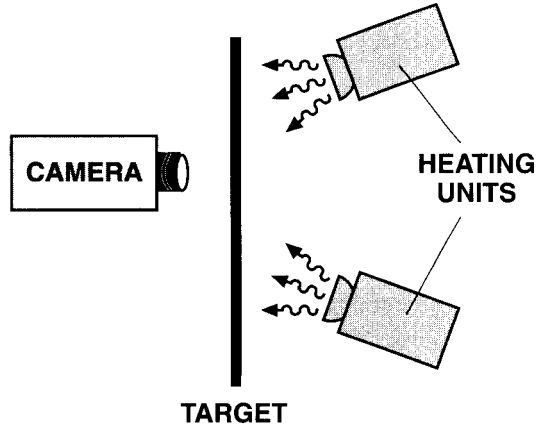


Figure 19-10. Generic arrangement for transmission-mode imaging.

Heat can be supplied by heat guns, lasers, incandescent lamps, or flash lamps. Xenon flashlamps (Figure 19-11) can provide a large amount of energy (tens of kilojoules) over short times (less than 1 ms) and thereby approximate an impulse. Depending upon the electrical circuitry they can provide in excess of 30 flashes per second. Line sources are appropriate for continuous monitoring of large objects. Either the object moves (Figure 19-12) or the setup can move to scan large areas.

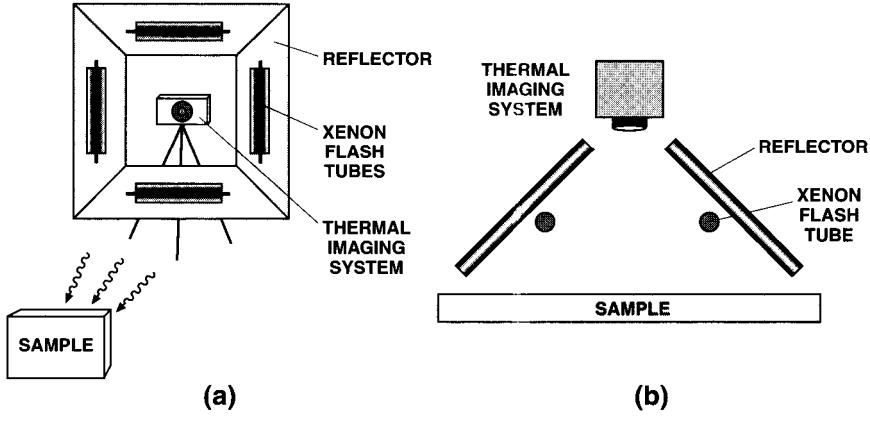


Figure 19-11. Area illumination with four xenon lamps and a reflective housing to direct the energy into the material. (a) Front view and (b) cross sectional view.

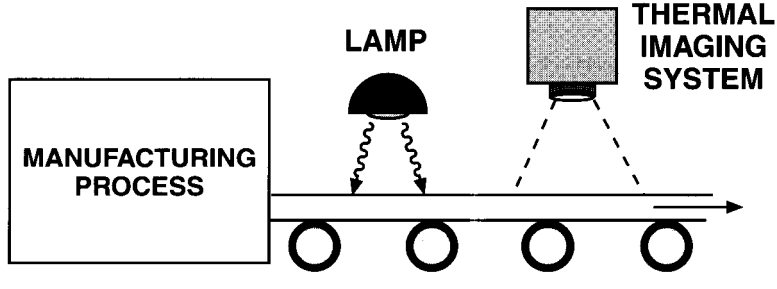


Figure 19-12. Line source illumination used for quality control. (Also see Figure 12-12).

19.3.2. DATA ANALYSIS

Figure 19-13 illustrates some generic time/temperature profiles. These curves are typically obtained with reflection-mode heating when excited by an impulse. The bottom curve of Figure 19-13 is for a very thick (assumed semi-infinite) slab of material. The time/contrast curves are created by a point-by-point subtraction of each individual curve from the bottom (no defect) curve. It is easier to discern defects when the data is plotted in log-log coordinates. Subtraction yields the curves given in Figure 19-5 (a linear scale).

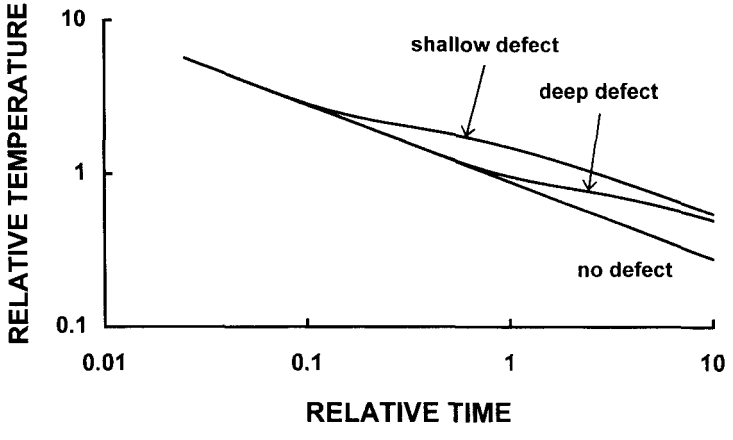


Figure 19-13. Surface time/temperature profile for an infinitely thick material with a variety of defects. Embedded materials (e.g., corrosion) and voids have different thermal properties. When encountered, the slope of the profile changes.

Thermal imaging systems can only provide a snapshot of the surface temperature distribution. In order to obtain a time history, it is necessary to collect a large number of images (Figure 19-14). Each pixel is followed in time to create the curves in Figure 19-13. Although the curves appear continuous, they are actually a series of discrete points connected by a continuous line. Each discrete point represents a single datum from one frame. Since each pixel is followed in time, it is straightforward to develop a two-dimensional time history. This allows the creation of a two-dimensional representation of the defects (called a tomogram).

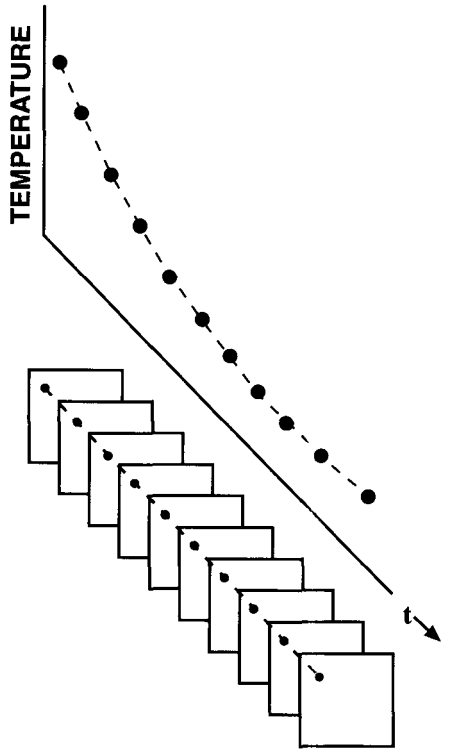


Figure 19-14. Methodology to obtain the time/temperature profile.

As the frame rate increases, the time available to capture an image decreases. This reduces the signal-to-noise ratio and defects will be lost in the noise. To overcome the reduction in defect detectability, a boxcar integration scheme is used to average many frames. As illustrated in Figure 19-15, the material is irradiated with an impulse. At a fixed time after the impulse, an image is collected. The material is allowed to reach thermal equilibrium and the process is repeated. If N frames are averaged together, then the signal-to-noise ratio increases by the square root of N. Different delay times are selected to provide an enhanced version of Figure 19-14. Boxcar integration provides a large number of frames and the maximum number that can be collected may be limited by the storage capability of the computer.

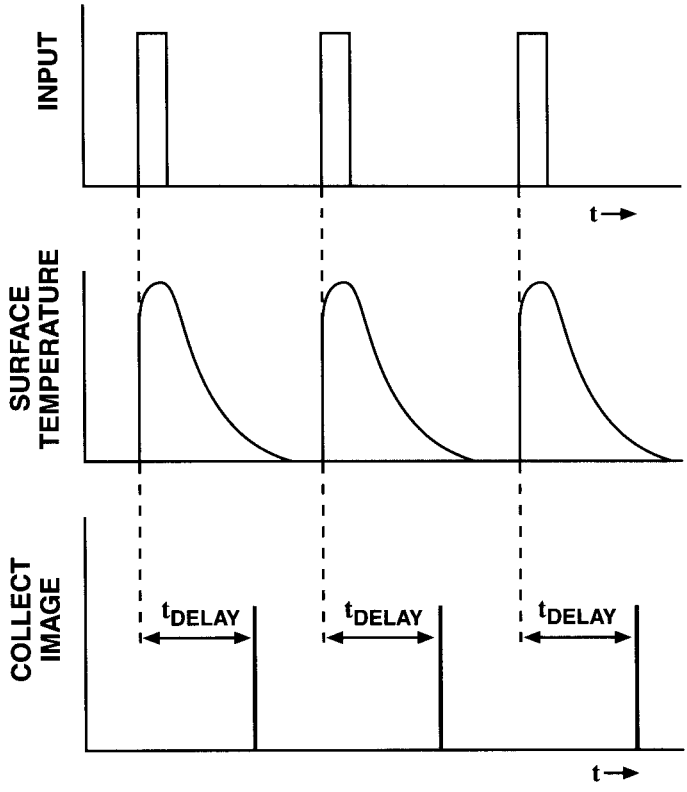


Figure 19-15. Boxcar integration methodology. For each delay time t_{DELAY}, the frames are averaged together to increase the SNR.

19.3.3. TEMPERATURE/TIME GUIDELINES

The resultant thermal contrast depends upon the initial surface temperature increase. For relatively thin laminates, a small temperature difference is adequate whereas thick laminates or sandwich construction panels require a larger temperature difference to produce an adequate thermal contrast. Equivalently, as the material thickness increases, the heat source must supply more energy.

The required initial surface temperature depends upon the material's thermal properties, thickness, and the defect's size and depth. This varies with application. Table 19-1 provides typical temperature increases for differences necessary to detect defects in marine structures composed of glass fiber composites. The time to reach

the back surface depends upon the material's thermal properties and thickness. Table 19-2 provides some estimates for glass fiber composites.

Table 19-1
TYPICAL TEMPERATURE DIFFERENCES
for GLASS FIBER COMPOSITES
(From reference 11)

Structure Thickness (cm)	**Minimum temperature difference**	
	°C	**°F**
up to 1.0	5	9
1.0 to 2.0	10	18
2.0 to 5.0	15	27
5.0 to 8.0	20	36

Table 19-2
TRANSIT TIME in GLASS FIBER COMPOSITES
(From reference 11)

Structure thickness (cm)	**Minimum transit**
Laminate Up to 1.5	1 minute
Laminate 1.5 to 3.0	4 minutes
Laminate 3.0 to 5.0	15 minutes
Balsa Core 2.5 cm with 0.15 cm skins	10 minutes
Balsa Core 5 cm with 1 cm skins	40 minutes

19.4. REFERENCES

1. V. P. Vavilov, "Subjective Remarks on the Terminology used in Thermal/Infrared Nondestructive Testing," in *Thermosense XVIII*, D. D. Burleigh and J. W. Spicer, eds., SPIE Proceedings Vol. 2766, pp. 276-281 (1996).
2. X. P. V. Maldague, *Nondestructive Evaluation of Materials by Infrared Thermography*, Springer-Verlag, New York (1992).
3. L. D. Favro, P. K. Kuo and R. L. Thomas, "Real-time Thermal Wave Imaging," In *Non-destructive Evaluation*, A. Mandelis, ed., pp. 24-47, PTR Prentice Hall, Englewood Cliffs, NJ (1994).
4. A. Daniels, "Optimization of Pulsed Temporal Stimulation for Thermal Nondestructive Testing," in *Thermosense XX*, J. R. Snell and R. N. Wurzbach, eds., SPIE Proceedings Vol. 3361, pp. 254-265 (1998).
5. X. P. V. Maldague, *Nondestructive Evaluation of Materials by Infrared Thermography*, page 123, Springer-Verlag, New York (1992).
6. X. P. V. Maldague, *Nondestructive Evaluation of Materials by Infrared Thermography*, page 7, Springer-Verlag, New York (1992).
7. H. S. Carlsaw and J. C. Jaeger, *Conduction of Heat in Solids,* second edition, page 259, University Press, Oxford, U.K. (1959).
8. A. Daniels, "Nondestructive Pulsed Infrared Quantitative Evaluation of Metals," in *Thermosense XVIII*, D. D. Burleigh and J. W. Spicer, eds., SPIE Proceedings Vol. 2766, pp. 185-201 (1996).
9. J. W. Maclachan Spicer, W. D. Kerns, L. C. Aamodt, and J. C. Murphy, "Time-Resolved Infrared Radiometry (TRIR) of Multilayer Organic Coatings using Surface and Subsurface Heating," in *Thermosense XIII*, G. S. Baird, ed., SPIE Proceedings Vol. 1467, pp. 311-321 (1991).
10. D. Wu, A. Salerno, B. Schönbach, H. Hallin, and G. Busse, "Phase Sensitive Modulation Thermography and its Applications for NDE" in *Thermosense XIX*, R. N. Wurzbach and D. D. Burleigh, eds., SPIE Proceedings Vol. 3056, pp. 176-182 (1997).
11. T. S. Jones, "Field Condition Limitations for Thermography of Marine Composites," in *Thermosense XVIII*, D. D. Burleigh and J. W. Spicer, eds., SPIE Proceedings SPIE Vol. 2766, pp. 164-173 (1996).

20
PROCESS/QUALITY CONTROL

Thermograms of various applications were presented in previous chapters to illustrate various physical concepts such as thermal conductivity, heat capacity, frictional losses, and electrical energy dissipation. Tables 10-2 through 10-5 listed a myriad of applications and Chapters 13 through 19 (Table 20-1) discussed the more common applications.

Thermal imaging is also used to inspect pressure vessels, heat exchangers, chillers, tanks, and piping systems. Inspection of finished products for flaws and quality control is expanding into many industries. With the ability to perform image processing in real time, many industries now perform 100% inspection of their products. Each industry and each company within an industry seem to have a different approach to process/quality control. Applications differ from facility to facility depending upon the process equipment and the material being manufactured. This chapter briefly discusses applications in six industries. Addition information on industrial applications can be found in Appendix C, *Thermal Sensing and Imaging 1980-1999.*

Table 20-1
CHAPTER TOPICS

Chapter	Topics	Typical test
Chapter 13 Building envelope inspection	Building science, windows, and insulation	Qualitative
Chapter 14 Roof inspection	Water ingress and insulation	Qualitative
Chapter 15 Power distribution	Power lines and transformers	Quantitative
Chapter 16 Electrical/mechanical inspection	Electrical distribution, fuses, circuit breakers, motors, and gears	Quantitative
Chapter 17 Buried objects	Underground storage tanks and pipe lines	Qualitative
Chapter 18 Surveillance	Military requirements and search and rescue	Qualitative
Chapter 19 Nondestructive testing	Detection of voids and delaminations	Quantitative

20.1 AUTOMOTIVE

Automobiles are complex machines containing gears, pulleys, heat exchangers, low voltage and high voltage components, and storage tanks. Thermograms of these generic components were previous illustrated. Vehicles are made from a variety of materials including rubber, plastic, metal, glass, and composites. Welding holds the frame together and numerous methods to verify good welds are available.[1-4] Figure 2-13 illustrated the cooling efficiency of the fins on an air-cooled engine. Figures 2-18 and 2-19 illustrated overheating of brake rotors. Figure 20-1 shows the heating pattern of a windshield defroster. In all these cases, thermography helped in the design of the components and was able to locate potential defects or hazardous conditions.

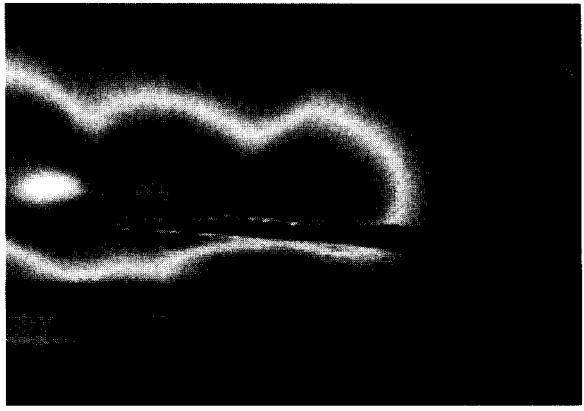


Figure 20-1. Automobile windshield defroster. The heating pattern can clearly be seen. It is desirable to uniformly heat the windshield. (By courtesy of IRcameras.com)

20.2. PETROCHEMICAL

Crude oil flows through process heater tubes inside a furnace. If the oil gets too hot, it cracks: hydrogen is separated from the carbon. The carbon remains in the tube and is called coke. The coke insulates the tube wall from the cooling effect of the crude oil and that causes the tube temperature to increase further. Heater tubes fail[5] more frequently than any other component at a refinery.

Infrared radiation from the furnace flame provides significant path radiance that obscures the tubes. Fortunately, gas flames have spectral features in the infrared. A flame filter centered at 3.9 μm allows you to see though the flame and measure the

temperature of the tubes (See Figure 4-14). Since oil is flowing through the tubes, they will be cooler than the walls of the furnace. If coke is present, the tube temperature will increase since the coke prevents the oil from cooling the tubes.

Oil flames are more difficult to penetrate. They contain solid particles (usually carbon) that tend to scatter the infrared radiation from the tubes. Further, these heated particles also emit broad band (nearly blackbody) radiation. Although a filter can suppress the radiation from the flame, the particles "fog" the infrared image and the tubes are difficult to see.

Refractory generally refers to any material with a very low thermal conductivity. Refractory materials are used to line the inside of furnaces to keep the heat inside. It lowers heating costs and protects the exterior shell. In a well-designed furnace, the exterior temperature will be fairly uniform. A low temperature could mean that there is a buildup of scale. High temperatures suggest defects in the refractory (Figures 20-2 and 20-3). The lining can crack and separate from the exterior shell. In both cases, the hot gases will affect the integrity of the exterior shell.

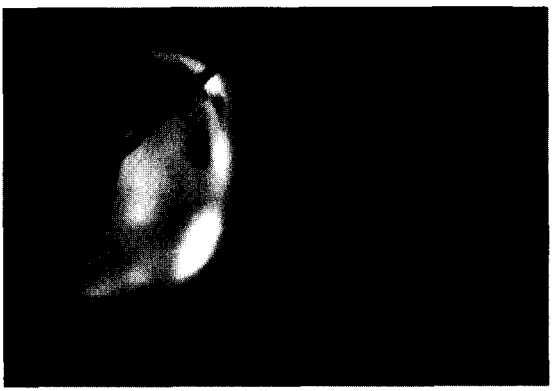


Figure 20-2. Refractory breakdown. (By courtesy of the Academy of Infrared Thermography).



Figure 20-3. Refractory breakdown. Breakdown occurs more frequently on sharply curved surfaces. (By courtesy of IRcameras.com).

20.3. DIE CASTINGS AND MOLDING

With injection molding and blow molding of plastics,[6] quality depends upon effective heat transfer from the part to the mold. Dimensional precision and surface finish are maintained when there is a minimal temperature gradient in the part. Large complex parts can vary in thickness by a factor of 10 over a few centimeters of distance. Thermal gradients and hot spots on the part and mold create residual stresses in the part that lead to warpage.

Figure 20-4 shows an automobile fan that has thick walls in the center and thin blades. Uniform cooling is required to prevent the part from warping and becoming unbalanced. Thermographic analysis easily locates thermal gradients. With this knowledge, the process can be changed to minimize gradients and thereby improve product quality.

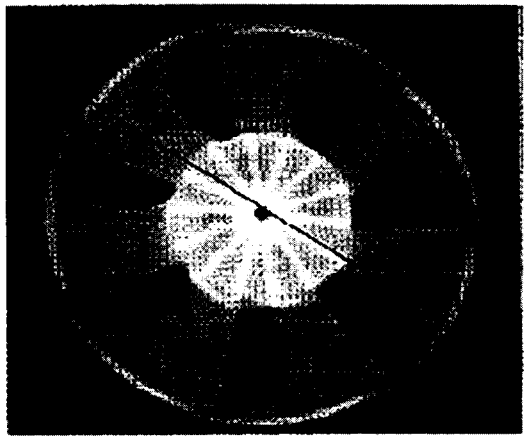


Figure 20-4. Recently molded automobile fan. A temperature profile (dark line running from 10 o'clock to 4 o'clock) across the part shows temperatures as high as 290°F (143°C) at the center and as low as 150°F (66°C) on the blades. (From Reference 6).

20.4. PRINTED CIRCUIT BOARDS

Printed circuit boards can be extremely complex thermally. Closely mounted, power-consuming components can easily create localized hot spots (Figures 20-5 and 20-6). During research and development, the optimum distribution of components

can be determined to avoid these hot spots. Thermography can assess the effective of heat sinks and component cooling.

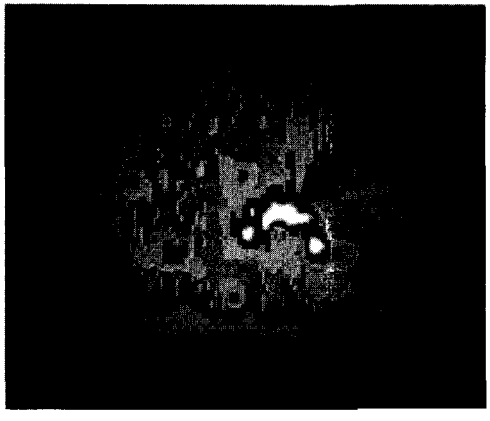


Figure 20-5. Overheated component on a printed circuit board. The edges of the board are at room temperature and cannot be seen in this thermogram. That is, there is no ΔT between the board edge and the background. (By courtesy of Gary J. Weil, president, EnTech Engineering).

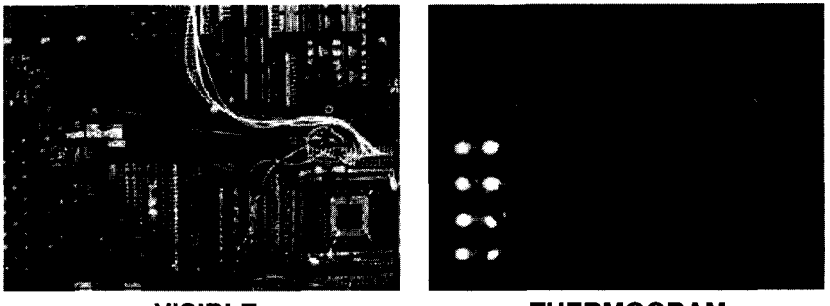


Figure 20-6. Overheated components on a printed circuit board. (By courtesy of Indigo Systems).

The difficulty with measuring printed circuit boards is that they are usually placed in close proximity to other boards. When close together, they cannot be viewed by an imaging system. The closeness affects the heat dissipation. As the space between the boards decreases, the board temperature increases. Further, the

boards are usually placed within a closed box. Components cannot be measured in a closed box or if close to other boards. Nevertheless, potential thermal anomalies can be discovered by looking at a single separated board.

For some applications, qualitative measurements are adequate; for example, Figure 20-7 illustrates bad solder joints. For quantitative measurements, it is necessary to know the emissivity of each component. Then, an image processing software program (in an ancillary computer) can provide the emissivity corrections and provide accurate temperature measurements.

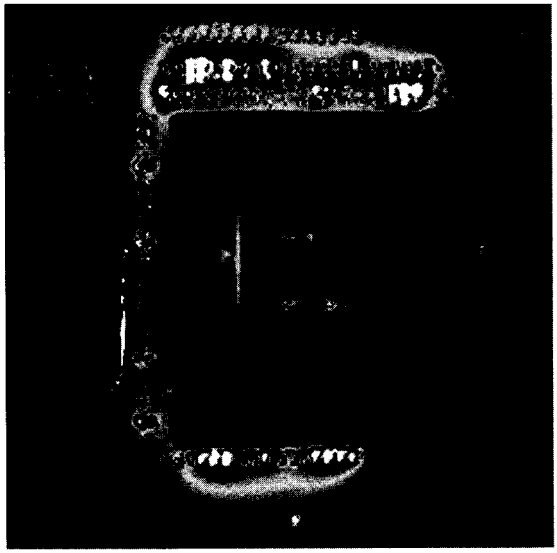


Figure 20-7. Overheated solder joints on a printer circuit board (By courtesy of IRcameras.com).

20.5. METALS

Most metals have a low emissivity when manufactured. The emissivity increases when the surface is stained, oxidized, or scratched. The difference in emissivity creates a difference in detected radiation. As a qualitative measurement, the precise value of the emissivity is not necessary. This is actually an advantage. The emissivity of the manufactured material is often not known precisely and can vary slowly. The detected radiation from the "normal" material also changes slowly. This slow change can be ignored. However, a flaw or defect creates an abrupt change in emissivity with a corresponding abrupt change in detected radiation, which is a condition that is easily recorded.

On the other hand, for process control it is necessary to monitor the temperature. In this case the emissivity must be known. Low emissivity materials reflect significant radiation. Since manufacturing facilities have numerous furnaces it is desirable to shield these sources in order to make accurate measurements (see Figure 12-9). Oxidation and scale further complicate temperature measurements.

20.5.1. ALUMINUM

In hot rolling, aluminum ingots, typically 20 to 30 inches thick (0.5 to 0.8 m) are reduced through a sequence of rolling operations to approximately 0.1 inch (~2.5 mm) in thickness.[7] Temperatures depend on the particular alloy, but generally start out at about 550°C (~1000°F) decreasing to about 175°C (~350°F) at the strip gauge. The temperature of the aluminum bar is controlled by the speed of the mill and by coolant applied to the rolls and to the bar.

Aluminum has a low emissivity and it is strongly alloy dependent. Surface roughness and surface oxidation also influence emissivity values. Since surface roughness and oxidation are process specific, different rolling conditions and their corresponding emissivities must be well characterized in order to measure the temperature accurately.

There are three flaws[8] of general concern that occur in flat rolled aluminum: surface discolorations, broken surfaces, and voids or inclusions. The severity, quantity, and distribution of the flaws will provide critical information regarding process malfunction. Streaks or stains on the aluminum surface increase the emissivity. As a result, surface discolorations are easily detectable.

Scratches, small indentations exemplify broken surfaces, and foreign material rolled into the sheet. Within the scratch or indentation, the slight increase in surface area permits formation of more aluminum oxide, which has an emissivity of 0.22 to 0.40 compared with less than 0.1 for bare aluminum. Furthermore, the walls of the scratch form a tiny cavity. Emitted radiation experiences multiple reflections between the cavity walls before exiting the sheet. In this manner, the broken surface simulates a microscopic blackbody.

Aluminum is widely used as beverage container.[9] The aluminum is coated with a clear organic coating to prevent chemical attack by the contents of the container. The coating varies in thickness from 0.0001 to 0.0007 inches (2.5 to 18 μm) depending on what product will eventually go into the container. The emissivity from the coated aluminum sheet ranges from 0.25 for the thin coating to 0.75 for the thicker coating. The coating takes place on a continuous process line that may be moving up

to 10 ft/s (3 m/s). Bare aluminum has an emissivity of less than 0.1. If there is a hole in the coating, there is an abrupt change in emissivity and an abrupt change in detected radiation. Real time image processing can easily detect flaws (missing coating).

20.5.2. STEEL

Temperatures are monitored[10] during melting, pouring, and rolling of steel. After the liquid steel is cast into solid form, it goes through[11] casting, reheating, hot rolling, cold rolling, annealing, temper rolling, and coating. These processes are characterized by a wide span of processing temperatures from about 1300°C (~2300°F) in reheating, down to about 70°C (~160°F) in temper rolling.

It is difficult to accurately measure the temperature of hot slabs exiting a reheat furnace. Both loose oxide and scale can partially obscure the hot steel. Most mills rely on a downstream measurement and then use a computer model to estimate the exit temperature.

20.6. PAPER INDUSTRY

Paper[12] is made from a slurry of wood pulp and other materials. This slurry is compressed and dried. A critical aspect for the final paper quality and strength lie in the uniformity of the drying process. It easy to see wet spots on paper since evaporative cooling creates a temperature differential.

Kodak[13] is a major manufacturer of photographic paper and film. Each product may have a different coating and there are hundreds of types of coatings. By using thermography, the coating application can be monitored to evaluate its "lay down" uniformity.

If a problem is encountered, each process factor is evaluated. The factor control setting is increased or decreased while simultaneously monitoring the product with infrared thermography. This procedure quickly identifies the exact band of heaters that are outside the control limits. Real time thermography analysis enables the process to be brought within the control limits.

20.7. REFERENCES

1. P. Banerjee and B. A. Chin, "Infrared Sensor-based On-line Weld Penetration Control," in *Thermosense XV*, L. R. Allen, ed., SPIE Proceedings Vol. 1933, pp. 83-92 (1993).
2. S. Raghavan, H. C. Wikle, and B. A. Chin, "Adaptive Control of Arc Welding using Infrared Sensing," in *Thermosense XV*, L. R. Allen, ed., SPIE Proceedings Vol. 1933, pp. 76-82 (1993).
3. E. A. Fuchs, K. W. Mahin, A. H. Ortega, L. A. Bertram, D. R. Williams, and A. R. Pomplum, "Thermal Diagnostics for Monitoring Welding Parameters in Real Time," in *Thermosense XIII*, G. S. Baird, ed., SPIE Proceedings Vol. 1467, pp. 136-149 (1991).
4. M. A. Khan, N. H. Madsen, and B. A. Chin, "Infrared Thermography as a Control for the Welding Process," in *Thermosense VI*, G. J. Burrer, ed., SPIE Proceedings Vol. 446, pp. 154-163 (1983).
5. A. G. Imgram, J. B. McCandless, "Infrared Thermal Imaging of Refinery Equipment," in *Thermosense V*, G. E. Courville, ed., SPIE Proceedings Vol. 371, pp. 47-54 (1982).
6. M. Prystay, H. Wang and A. Garcia-Rejon, "Application of Thermographic Temperature Measurements in Injection Moulding and Blow Moulding of Plastics," in *Thermosense XVIII*, D. D. Burleigh and J. W. Spicer, eds., SPIE Proceedings Vol. 2766, pp. 5-14 (1996).
7. M. Fairlie, W. Fraser, B. Farahbakhsh, R. Lamb, and O. Meijer, "On-line Temperature Measurement in Hot Rolling of Aluminum using Infrared Imaging Systems," in *Thermosense XI*, G. B. McIntosh, ed., SPIE Proceedings Vol. 1094, pp. 84-92 (1989).
8. J. B. Setzer, Jr. and M. Thangavelu, "Infrared Sensor for Automated Inspection of Hot Metal Surfaces," in *Thermosense XII*, S. A. Semanovich, ed., SPIE Proceedings Vol. 1313, pp. 200-206 (1990).
9. M. J. Haugh, D. P. Stone, and M. Thangavelu, "Paint Skip Detector," in *Thermosense XII*, S. A. Semanovich, ed., SPIE Proceedings Vol. 1313, pp. 190-199 (1990).
10. S.-A. Ljungberg, "The Information Potential using IR-Technology for Condition Monitoring of Reheating Furnaces within the Steel and Iron Industry," in *Thermosense XIX*, R. N. Wurzbach and D. D. Burleigh, eds., SPIE Proceedings Vol. 3056, pp. 133-145 (1997).
11. G. R. Peacock, "A Review of Non-Contact Process Temperature Measurements in Steel Manufacturing," in *Thermosense XXI*, D. H. LeMieux and J. R. Snell, Jr., eds., SPIE Proceedings Vol. 3700, pp. 171-189 (1999).
12. J.-M. Karjanmaa, "Thermal Imaging and Paper Finishing Machines," in *Thermosense XV*, L. R. Allen, ed., SPIE Proceedings Vol. 1933, pp. 110-117 (1993).
13. S. Stern, "Infrared Thermography Imaging System Multi-Applications for Manufacturing," in *Thermosense XII*, S. A. Semanovich, ed., SPIE Proceedings Vol. 1313, pp. 53-63 (1990).

21
INSPECTION PROCEDURES

Infrared monitoring is not an exact science. The calculated surface temperature depends upon the object's temperature, emissivity, and surrounding temperature. A well-trained thermographer can estimate the emissivity and surrounding temperature and thereby obtain a reasonable value for the object's true surface temperature. Given the material's conductivity, convection, and heat capacity, a well-trained thermographer can estimate the location of the subsurface defect and the severity of the defect.

The customer, who often has little or no thermography training, will not understand all the principles involved. You must explain the differences between qualitative and quantitative measurements and which one will be used and why. Your approach will be convincing if you show representative thermograms of similar problems you have encountered in the past. It is extremely useful to also provide photos. These could be taken with a 35-mm, Polaroid®, or (preferably) a digital camera. A digital camera provides a real time image, stores a large number of images, and the electronic format allows easy transfer into the final report. Further you must explain what may be found on this inspection – both positive and negative results.

The customer is requesting only one product and that is your interpretation of the thermal anomaly. Unless licensed in other areas, you should not state categorically what the precise problem is. You can only state that a thermal anomaly has been found and, from previous experience, what you believe the problem to be. When available, the thermal anomaly should be compared to published standards and guidelines. Note that the customer usually wants a yes/no answer in terms of deleterious defects. You must resist the temptation to provide that simple answer. Generally speaking, auxiliary tests are require to confirm your thermal observation. For example, a roof cannot be determined to be defective until a roof core is taken. Buried objects cannot be identified until unearthed.

Determine whether the requested inspection is possible or even necessary. If this type of inspection is new to you, survey the literature to see if a similar problem been solved before. For example, review the papers listed in Appendix C, *Thermal Sensing and Imaging 1980-1999.*

The preliminary work before an inspection is as important as the inspection itself. No inspection is complete without a final report. Be sure to tell the customer that you will offer preliminary findings at an exit interview (at the

conclusion of the inspection). Emphasize that the findings are preliminary. However, you must point out those areas that need immediate attention for safety reasons. Also state when the final report will be available (preferably less than 5 days). The final report will contain full data analysis.

While this chapter appears to apply only to inspections (roof, power distribution, electrical, or mechanical), it is appropriate for all testing. Test plans are vital for laboratory tests as well as field tests. Every test, no matter how small (or apparently trivial) should have a test plan. Without a plan, important data is often overlooked and not collected. It is often impossible to repeat the test at a later date. Special equipment may no longer be available, required personnel may have been assigned to other jobs, or the appropriate test conditions may not be present. It is extremely embarrassing to tell your customer that you missed some data.

21.1. PRELIMINARY WORK

The preliminary activities are who, what, where, why, and how. By answering all these questions, it is relatively simple to write a test plan and to conduct the inspection.

21.1.1. WHO

There are four "whos." As the thermographer, you are primary "who." You must establish credibility with the customer. You need evidence of valid certification (e.g., ASNT Level I, II, or III certification). You may need professional/business licenses with appropriate registrations that are required by local codes. Provide a list of previous (satisfied) customers (with their permission) as references. Provide a copy of a sample report (with permission to use).

The second "who" is an expert supplied by the customer. This individual must be knowledgeable in identifying materials, components, structures, previous repairs, previously noted problems, as well as ensuring that the firm's safety regulations are observed. Only a licensed electrician should remove electrical panels and measure current.

The third "who" are all the people that may be involved in the inspection. Factory workers may have to modify their work procedure while you are there. Foremen need notification of the inspection. Interior inspection of an office building may require permission of the tenants. Some installations require approval by security.

The final "who" is the person who receives the results. Who must be satisfied that the inspection is well executed and complete? This is the person you must really satisfy.

21.1.2. WHAT

The customer must state the goal of the inspection. Before undertaking an inspection, the following questions must be answered: What must be detected (e.g., delamination, disbond, cracks, porosity, casting voids, or water infiltration)? What is the depth of the flaw? What is the minimum flaw size to be detected? Will the entire structure be inspected or only limited to critical areas? What is the type of materials and construction of the object to be inspected?

If the object is reflective, can it be painted to increase the emissivity? The surface quality dramatically affects the infrared radiation that is measured. Each inspection has its own unique problems. For example, for buried object detection, shrubs should be removed, grass mowed, and debris removed.

Here, you decide if the inspection can be fruitful based upon your knowledge and capability. Be sure the customer knows the limitations of the inspection such as areas that are uninspectable or inaccessible. Safety shrouds and enclosures prevent direct viewing of electrical components, and moving components, or rotating machinery. Recall that the smallest target that you can measured is limited by the MIFOV and the smallest temperature differential by the NEDT. The atmospheric transmittance often limits the maximum range at which a target can be detected.

21.1.3. WHEN

Based upon your experience, you decide how long the inspection will take. The customer, to some degree determines when it should start. He will pick times that do not impact his schedule. But it is desirable to perform electrical and mechanical inspections when the system is under full load. For example, if evaluating a school's electrical distribution, the inspection should not be during the summer or semester breaks.

Weather is the dominant factor in scheduling outdoor inspections. The list of environmental limitations is extensive. For example, you need high significant solar loading, no rain, no dew or frost, and minimal wind. Surveys can normally begin 1 hour after sunset and can be conducted until sunrise. But environ-

mental conditions can vary dramatically. It may be necessary to cancel an inspection or to stop an inspection if significant fog occurs or cloud cover occurs. The inspection must stop if it rains. Weather reports provide a 5-day forecast. Call the customer 5 days, 3 days and 1 day before the inspection to discuss weather conditions.

21.1.4. WHERE

This seems self-explanatory. "Where" generally means the physical address and the specific place (e.g., building number and room number). A site survey will reveal access limitations for personnel and equipment. Lines-of-sight may be limited by walls and mechanical fixtures.

More important is the environmental condition at the location. "Where" is also used to determine if any condition exists that may adversely affect results. For example high temperatures around boilers may affect camera operation. Dust, dirt, and other particulates act as insulators and may have emissivities that affect the accuracy of your temperature measurements.

21.1.5. WHY

"Why" is self-explanatory: To find defects in components, to improve process quality control, determine the operating condition of components, and to predict when marginally defective components should be replaced. Nothing convinces a customer more than representative thermograms of similar objects with known defects coupled with an estimate of cost savings.[1-5]

21.1.6. HOW

The "how" is really the test plan. It includes both the necessary equipment as well as any special requirements to perform the inspection experiment. For outdoor inspections, you may need an airplane, special all- terrain vehicle, or power cart. For indoor inspections you may need a power cart to move from location to location if the facility is very large. Is a man-lift needed to raise equipment or personnel to the inspection area? The need for special equipment must be identified during the preliminary site inspection.

21.2. SAFETY

Safety cannot be overstated. The thermographer may be subjected to a variety of conditions that require safety procedures. Slippery floors, uneven footing, and low hanging pipes are obvious problems.

Energized electrical circuitry, rotating shafts, and moving mechanical assemblies can be extremely dangerous. These devices usually have mechanical guards (shrouds) or are enclosed in a box. In most situations, the guard must be removed or the housing opened to view the suspect components. This exposes the thermographer to an extremely dangerous situation.

Ideally, the power is removed before any panel or safety guard is removed. This occurs automatically for those panels that have safety lockouts. The power must then be restored prior to making any measurements. The power must be removed again to reassemble the safety panels or guards. Only a trained expert knowledgeable in the safe operation of those devices should remove panels and safety guards. The thermographer must abide by all safety regulations and procedures.

It is dangerous to go on a roof at nighttime, especially if alone. Not all roofs have safety rails. If flight tests are desired for aerial viewing, then two flights are usually required. The daytime flight is used to obtain photos and familiarize the personnel with the overall landscape and location of buildings. The infrared survey is conducted after dark. Nighttime flying can be dangerous when tall buildings, power lines, radio towers, and smokestacks are present. These structures may limit the closest distance to the structure being evaluated. In large commercial parks, it may be hard to locate the correct roof at nighttime. Strobe lights can be placed on the roof corners. The pilot and thermographer can see these but an infrared camera generally does not detect them if the duty cycle is low. If several images are needed to create a mosaic of the roof, the camera (and plane) must be correctly aligned with the roof.

21.3. STANDARDS AND GUIDELINES

Standards and guidelines list the maximum allowable temperatures. Rectification of thermal anomaly is not included in these guidelines. Only the customer can decide when to repair the component. Unfortunately, to date only a few standards exist. As a result, when you find a thermal anomaly, you make an educated guess of the probable cause.

21.4. TEST PROCEDURE

Ask your customer if the test procedure must be written and approved before testing can begin. Even if not required, a written test plan becomes a checklist. Any qualified thermographer can follow a well-written test plan. The key here is "well-written."

21.4.1. TEST PLAN

The following elements should be included in a comprehensive test plan. Since many of the headings are self-evident, they are often omitted. Generally, a generic test procedure is written and many sections may be used as "boiler plate." That is the same sections become generic to all tests. This is generally true for the equipment, safety, method of collecting data, and data analysis technique sections. The remaining sections are modified according to the specific task.

Modifications to the test plan may be necessary during the course of an inspection. As data is collected, it may lead you to measure additional nearby components or to examine some areas in more detail.

OBJECTIVE

This is the "why" and "what."

TEST LOCATION

This is the "where."

NAMES OF RESPONSIBLE INDIVIDUALS

This is the "who." You will need the name, phone number, and instructions where to meet your contact and customer's expert. Be sure to have a list of emergency phone numbers.

EQUIPMENT NEEDED

There are two sets of equipment: Those supplied by the customer and that which you bring along. It is very important to clearly state the customer's responsibility. The thermal imaging system and its associated equipment are obvious. Below is a list of equipment often forgotten.

MISCELLANEOUS

- Spare batteries
- AC adapters
- Clipboard, worksheets, note pad and pencil
- Ink, paint, or tape to increase emissivity,

Tool kit
Polaroid®, 35-mm, or (preferably) digital camera
Flashlight
Paint or marking pen (to indicate thermal anomalies)
Battery powered strobe lights for locating a roof
Portable phone (cell phone)

SAFETY (as required)
Hard hat
Safety glasses
Safety shoes
Ear plugs
Face mask
Respirator

ENVIRONMENTAL
Coveralls
Warm clothing if outdoors
Protective tarp for equipment in case of unexpected weather
Protective enclosures for the equipment if operating in a harsh environment

CUSTOMER SATISFACTION
Clipboard, worksheets, note pad, and pencil for customer
Copy of test plan

PRELIMINARY SITE SURVEY

The preliminary site survey will identify any problems such as limited line-of-sight or inaccessible areas. It will identify those areas where added safety is an issue such as open energized electrical cabinets and roofs without guardrails. Note all stairs, steps, warning signs, items suspended from the ceiling, small items on the floor, and low ceilings. Note water, dirt, or chemicals on the floor that may be slippery or contribute to uneven footing. Excessive dust, particulates, aromas, or gases may affect you. Even if not required by the customer's safety regulations, you may want to use a facemask. Verify if there are any radiation hazards (e.g., surveying a nuclear power plant) or hazardous chemicals (e.g., manufacturing facility).

If a large area is to be inspected, an efficient route is identified at this time. Usually, the preliminary site survey is performed before the test plan is written. The results of the survey are included in the plan.

DATES and REQUIRED CONDITIONS

This is the "when." Required conditions for outdoor measurements focus on the weather. For electrical and mechanical measurements, select times when the system is operating at or near full load.

SAFETY

As a result of safety considerations, you may need additional equipment such as that listed above. Although you have performed a preliminary site survey to identify potential safety problems, never forget that you lose your depth perception when looking at a camera monitor. With a narrow FOV lens, it is like looking through a soda straw. Have someone else guiding you when walking and using the camera.

SECURITY

Security includes the method to enter the facility (badges may be needed) and equipment check-in. Verify the security of equipment when not in use to avoid theft.

DETAILED PROCEDURE

This section would precisely list the components to be inspected. It includes the lens required to achieve the field-of-view and MIFOV for the test. The length of this section depends upon who is performing the inspection. If someone other than you performed the preliminary survey, it tends to be longer.

DATA COLLECTION

Gathering of accurate data is critical to the success of an inspection program. For the thermal imagery, the primary concern is image storage. If a thermal anomaly is discovered, how will it documented and marked? Methods include grease pencils, tape, and paint. It is often useful to have imagery taken with a standard Polaroid®, 35-mm or (preferably) digital camera (e.g., Figures 8-1, 13-5, 16-6, and 20-6). The repairman will probably not be knowledgeable in thermal imagery and may have difficulty in locating components based solely upon a thermogram.

DATA ANALYSIS TECHNIQUES

Develop standard, systematic methods of collecting, recording and accumulating data. An efficient system allows basic record keeping to be done by an experienced secretary rather than by the thermographer. Once the data is recorded, either on a form or in a computer, it becomes the basis for the final report. The test plan should outline the data analysis technique.

While the analysis must be based upon sound scientific principles, note that the customer is probably not trained in thermography or physics. The data must be presented in a form that the customer can understand. Use the terminology of his industry for a "real world" answer.

Decide what mode of data storage will be used. In the simplest of systems, a good paper form with some means of feedback and, possibly, a means of cataloguing it historically can be elegantly efficient. A simple sketch of the problem or a photo (Polaroid®, 35-mm, digital) conveys the visual information powerfully. A videotaped record of all inspected equipment may also be desirable. Tape indices are essential for retrieving information. Most companies seem to favor a system that keeps videotapes on file, but relies on videoprint for working records.

VERIFICATION

Thermal imaging can only measure the surface temperature. If the temperature is above or below preset guidelines, then a thermal anomaly has been discovered. A thermogram cannot precisely determine the cause of the problem. A thermographer can make an educated guess based upon his knowledge of similar problems and the physics of heat transfer. If a thermal anomaly is found, auxiliary equipment is necessary to verify the problem. For example to verify that a roof is defective, it is necessary to take core samples or use moisture meter probes.

Beware of the possibility of false or missed defect findings caused by reflections and emissivity variations. Interpretation is more difficult if the surface is curved. Environmental factors such as wind speed and the presence of moisture confound outdoor measurements.

21.4.2. GOOD ENGINEERING PRACTICES

Good engineering practices are simply common sense. If a thermal anomaly is discovered, question the customer's expert about possible causes. Questions to ask include: Has the component been repaired or replaced? If repaired, do we know what materials were used? Are there known heat sources in the general area? Is the equipment overloaded? Is the component damaged? Have any problems previously been noticed?

Verify that you are at the right place at the right time. Specifically, you want to perform the inspection when the equipment cycles or during full load. Arrive 15 minutes early to set up. Do not overestimate your physical capabilities with the equipment -

particularly if the inspection will take all day. If working at night, remember that it is interrupting your normal sleep habits. Take breaks at regular intervals.

Do not get too close to equipment. Never make contact with electrical equipment, even if you are told that it is de-energized. Never have loose fitting clothing near rotating equipment. Be particularly careful with camera cords, wires, and straps.

If using a vehicle, use seat belts, do not lean outside vehicle while it is moving, and as necessary, have all equipment attached with safety lines (in case you lose your grip).

21.5. EXIT CONFERENCE

An exit conference takes place at the conclusion of many inspections. Here, preliminary data interpretation is presented. Fully ascertain the thermal anomaly before telling your customer. As appropriate, solicit opinions from the customer's expert. Use auxiliary equipment as necessary.

An exit conference with the customer is valuable for several reasons: You minimize surprises by communicating important findings at this time rather than having them arrive in a written report several days after an inspection. Serious problems, which may need immediate corrective action, can be discussed. For non-serious problems, only provide a provisional evaluation. Full data analysis is required for a full evaluation.

21.6. FINAL REPORT

If the test plan is well written, then the final report is straightforward. It follows the test plan with the addition of analyzed data with recommendations. The information given in the final report must support the data interpretation. The "boilerplate" used for the test plan can simply be copied into the final report. To maximize customer satisfaction, provide the report within 5 days of the inspection. The headings for a comprehensive final report follows. Depending upon the customer and task, some elements may be omitted.

EXECUTIVE SUMMARY

Brief description what installations have been examined and which installations were not possible to examine and why. Briefly list the number and severity of thermal anomalies encountered.

TEST LOCATION, DATE, and TIME

This section contains the description of the installations inspected. For outdoor measurements, it would also contain weather data. As appropriate, it may contain building, roof, or equipment information and construction details.

NAMES OF RESPONSIBLE INDIVIDUALS

Same list as that used in the test plan

EQUIPMENT USED

Description of the thermal imaging system used along with lens information (f-number and field-of-view) and system resolution. If the customer supplied any equipment, it would be listed in this section.

TEST PROCEDURE

The information provided here assists in data analysis and interpretation.

DATA ANALYSIS TECHNIQUES

A brief explanation about the physics of thermography with emphasis on the theory that applies to this particular inspection. This assists the customer in interpreting the thermograms.

DATA

This section contains all the data and representative thermograms. Provide the emissivity used and whether tabulated values or measured values were used. Discuss the data collection limitations such as how an error in emissivity affects the calculated temperature.

RESULTS

When available, use guidelines to list the severity of the thermal anomaly. List auxiliary equipment used to verify the cause of the thermal anomaly.

CONCLUSIONS

A summary containing identification and fault class for all faults found.

RECOMMENDATIONS

A thermographer should not make definitive recommendations unless he has the appropriate certifications. The thermographer only notes thermal anomalies and offers possible causes. He does not make recommendations of what is to be replaced or repaired.

21.7. REFERENCES

1. R. P. Madding and N. McNamara, "Steam Leak Cost Estimation using Thermographically Acquired Pipe Temperature Data." In *Thermosense XIX*, R. N. Wurzbach and D. D. Burleigh, eds., SPIE Proceedings Vol. 3056, pp. 146-152 (1997).
2. J. P. Evans and R. N. Wurzbach, "Study of Cost Benefits of Identification of Non-Problems with Infrared Thermography," in *Thermosense XVI*, J. R. Snell, ed., SPIE Proceedings Vol. 2245, pp. 14-21 (1994).
3. P. P. Johnson, "Is It Worth It? Statistics of Corporate-Based IR Program Results," in *Thermosense XIII*, G. S. Baird, ed., SPIE Proceedings Vol. 1467, pp. 47-50 (1991).
4. J. M. Garner, "IRS - Infrared Research Services vs $$$ - The Bottom Line," in *Thermosense XIV*, J. K. Eklund, ed., SPIE Proceedings Vol. 1682, pp. 23-29 (1992).
5. J. R. Wallace, "A Case Study of Applying Infrared Thermography to Identify a Coolant Leak in a Municipal Ice Skating Rink," in *Thermosense XI*, G. B. McIntosh, ed., SPIE Proceedings Vol. 1094, pp. 112-118 (1989).

APPENDIX A
TEMPERATURE CONVERSION

The conversion from Celsius to Fahrenheit (or reverse) is straightforward:

$$T_{CELSIUS} = \frac{5}{9}(T_{FAHRENHEIT} - 32),$$

and

$$T_{FAHRENHEIT} = \frac{9}{5} T_{CELSIUS} + 32.$$

The other conversions are

$$T_{KELVIN} = T_{CELSIUS} + 273.15 \quad ,$$

and

$$T_{RANKINE} = T_{FAHRENHEIT} + 459.7 .$$

Although simple, it is difficult to make the conversion quickly and without a calculator. Table A-1 tabulates the conversion for easy reference. Select the current temperature in the center column. If the current temperature is in °C, then the **left** column converts °C to °F. If the current temperature is in °F, then the **right** column converts °F to °C.

Table A-1
TEMPERATURE CONVERSION

To °F	From T	To °C
-22.0	-30	-34.4
-20.2	-29	-33.9
-18.4	-28	-33.3
-16.6	-27	-32.8
-14.8	-26	-32.2
-13.0	-25	-31.7
-11.2	-24	-31.1
-9.4	-23	-30.6
-7.6	-22	-30.0
-5.8	-21	-29.4
-4.0	-20	-28.9

To °F	From T	To °C
-4.0	-20	-28.9
-2.2	-19	-28.3
-0.4	-18	-27.8
1.4	-17	-27.2
3.2	-16	-26.7
5.0	-15	-26.1
6.8	-14	-25.6
8.6	-13	-25.0
10.4	-12	-24.4
12.2	-11	-23.9
14.0	-10	-23.3

To °F	From T	To °C
14.0	-10	-23.3
15.8	-9	-22.8
17.6	-8	-22.2
19.4	-7	-21.7
21.2	-6	-21.1
23.0	-5	-20.6
24.8	-4	-20.0
26.6	-3	-19.4
28.4	-2	-18.9
30.2	-1	-18.3
32.0	0	-17.8

Table A-1 (Continued)

To °F	From T	To °C
32.0	0	-17.8
33.8	1	-17.2
35.6	2	-16.7
37.4	3	-16.1
39.2	4	-15.6
41.0	5	-15.0
42.8	6	-14.4
44.6	7	-13.9
46.4	8	-13.3
48.2	9	-12.8
50.0	10	-12.2
51.8	11	-11.7
53.6	12	-11.1
55.4	13	-10.6
57.2	14	-10.0
59.0	15	-9.4
60.8	16	-8.9
62.6	17	-8.3
64.4	18	-7.8
66.2	19	-7.2
68.0	20	-6.7
69.8	21	-6.1
71.6	22	-5.6
73.4	23	-5.0
75.2	24	-4.4
77.0	25	-3.9
78.8	26	-3.3
80.6	27	-2.8
82.4	28	-2.2
84.2	29	-1.7
86.0	30	-1.1
87.8	31	-0.6
89.6	32	0.0
91.4	33	0.6
93.2	34	1.1
95.0	35	1.7

To °F	From T	To °C
95.0	35	1.7
96.8	36	2.2
98.6	37	2.8
100.4	38	3.3
102.2	39	3.9
104.0	40	4.4
105.8	41	5.0
107.6	42	5.6
109.4	43	6.1
111.2	44	6.7
113.0	45	7.2
114.8	46	7.8
116.6	47	8.3
118.4	48	8.9
120.2	49	9.4
122.0	50	10.0
123.8	51	10.6
125.6	52	11.1
127.4	53	11.7
129.2	54	12.2
131.0	55	12.8
132.8	56	13.3
134.6	57	13.9
136.4	58	14.4
138.2	59	15.0
140.0	60	15.6
141.8	61	16.1
143.6	62	16.7
145.4	63	17.2
147.2	64	17.8
149.0	65	18.3
150.8	66	18.9
152.6	67	19.4
154.4	68	20.0
156.2	69	20.6
158.0	70	21.1

To °F	From T	To °C
158.0	70	21.1
159.8	71	21.7
161.6	72	22.2
163.4	73	22.8
165.2	74	23.3
167.0	75	23.9
168.8	76	24.4
170.6	77	25.0
172.4	78	25.6
174.2	79	26.1
176.0	80	26.7
177.8	81	27.2
179.6	82	27.8
181.4	83	28.3
183.2	84	28.9
185.0	85	29.4
186.8	86	30.0
188.6	87	30.6
190.4	88	31.1
192.2	89	31.7
194.0	90	32.2
195.8	91	32.8
197.6	92	33.3
199.4	93	33.9
201.2	94	34.4
203.0	95	35.0
204.8	96	35.6
206.6	97	36.1
208.4	98	36.7
210.2	99	37.2
212.0	100	37.8
213.8	101	38.3
215.6	102	38.9
217.4	103	39.4
219.2	104	40.0
221.0	105	40.6

Table A-1 (Continued)

To °F	From T	To °C
221.0	105	40.6
222.8	106	41.1
224.6	107	41.7
226.4	108	42.2
228.2	109	42.8
230.0	110	43.3
231.8	111	43.9
233.6	112	44.4
235.4	113	45.0
237.2	114	45.6
239.0	115	46.1
240.8	116	46.7
242.6	117	47.2
244.4	118	47.8
246.2	119	48.3
248.0	120	48.9
249.8	121	49.4
251.6	122	50.0
253.4	123	50.6
255.2	124	51.1
257.0	125	51.7
258.8	126	52.2
260.6	127	52.8
262.4	128	53.3
264.2	129	53.9
266.0	130	54.4
267.8	131	55.0
269.6	132	55.6
271.4	133	56.1
273.2	134	56.7
275.0	135	57.2
276.8	136	57.8
278.6	137	58.3
280.4	138	58.9
282.2	139	59.4
284.0	140	60.0

To °F	From T	To °C
284.0	140	60.0
285.8	141	60.6
287.6	142	61.1
289.4	143	61.7
291.2	144	62.2
293.0	145	62.8
294.8	146	63.3
296.6	147	63.9
298.4	148	64.4
300.2	149	65.0
302.0	150	65.6
303.8	151	66.1
305.6	152	66.7
307.4	153	67.2
309.2	154	67.8
311.0	155	68.3
312.8	156	68.9
314.6	157	69.4
316.4	158	70.0
318.2	159	70.6
320.0	160	71.1
321.8	161	71.7
323.6	162	72.2
325.4	163	72.8
327.2	164	73.3
329.0	165	73.9
330.8	166	74.4
332.6	167	75.0
334.4	168	75.6
336.2	169	76.1
338.0	170	76.7
339.8	171	77.2
341.6	172	77.8
343.4	173	78.3
345.2	174	78.9
347.0	175	79.4

To °F	From T	To °C
347.0	175	79.4
348.8	176	80.0
350.6	177	80.6
352.4	178	81.1
354.2	179	81.7
356.0	180	82.2
357.8	181	82.8
359.6	182	83.3
361.4	183	83.9
363.2	184	84.4
365.0	185	85.0
366.8	186	85.6
368.6	187	86.1
370.4	188	86.7
372.2	189	87.2
374.0	190	87.8
375.8	191	88.3
377.6	192	88.9
379.4	193	89.4
381.2	194	90.0
383.0	195	90.6
384.8	196	91.1
386.6	197	91.7
388.4	198	92.2
390.2	199	92.8
392.0	200	93.3
393.8	201	93.9
395.6	202	94.4
397.4	203	95.0
399.2	204	95.6
401.0	205	96.1
402.8	206	96.7
404.6	207	97.2
406.4	208	97.8
408.2	209	98.3
410.0	210	98.9

Table A-1 (Continued)

To °F	From T	To °C
392	200	93
401	205	96
410	210	99
419	215	102
428	220	104
437	225	107
446	230	110
455	235	113
464	240	116
473	245	118
482	250	121
491	255	124
500	260	127
509	265	129
518	270	132
527	275	135
536	280	138
545	285	141
554	290	143
563	295	146
572	300	149
581	305	152
590	310	154
599	315	157
608	320	160
617	325	163
626	330	166
635	335	168
644	340	171
653	345	174
662	350	177
671	355	179
680	360	182
689	365	185
698	370	188
707	375	191

To °F	From T	To °C
707	375	191
716	380	193
725	385	196
734	390	199
743	395	202
752	400	204
761	405	207
770	410	210
779	415	213
788	420	216
797	425	218
806	430	221
815	435	224
824	440	227
833	445	229
842	450	232
851	455	235
860	460	238
869	465	241
878	470	243
887	475	246
896	480	249
905	485	252
914	490	254
923	495	257
932	500	260
941	505	263
950	510	266
959	515	268
968	520	271
977	525	274
986	530	277
995	535	279
1004	540	282
1013	545	285
1022	550	288

To °F	From T	To °C
1022	550	288
1040	560	293
1058	570	299
1076	580	304
1094	590	310
1112	600	316
1130	610	321
1148	620	327
1166	630	332
1184	640	338
1202	650	343
1220	660	349
1238	670	354
1256	680	360
1274	690	366
1292	700	371
1310	710	377
1328	720	382
1346	730	388
1364	740	393
1382	750	399
1400	760	404
1418	770	410
1436	780	416
1454	790	421
1472	800	427
1490	810	432
1508	820	438
1526	830	443
1544	840	449
1562	850	454
1580	860	460
1598	870	466
1616	880	471
1634	890	477
1652	900	482

Table A-1 (Continued)

To °F	From T	To °C
1652	900	482
1670	910	488
1688	920	493
1706	930	499
1724	940	504
1742	950	510
1760	960	516
1778	970	521
1796	980	527
1814	990	532
1832	1000	538
1850	1010	543
1868	1020	549
1886	1030	554
1904	1040	560
1922	1050	566
1940	1060	571
1958	1070	577
1976	1080	582
1994	1090	588
2012	1100	593
2030	1110	599
2048	1120	604
2066	1130	610
2084	1140	616
2102	1150	621
2120	1160	627
2138	1170	632
2156	1180	638
2174	1190	643
2192	1200	649
2210	1210	654
2228	1220	660
2246	1230	666
2264	1240	671
2282	1250	677

To °F	From T	To °C
2282	1250	677
2372	1300	704
2462	1350	732
2552	1400	760
2642	1450	788
2732	1500	816
2822	1550	843
2912	1600	871
3002	1650	899
3092	1700	927
3182	1750	954
3272	1800	982
3362	1850	1010
3452	1900	1038
3542	1950	1066
3632	2000	1093
3722	2050	1121
3812	2100	1149
3902	2150	1177
3992	2200	1204
4082	2250	1232
4172	2300	1260
4262	2350	1288
4352	2400	1316
4442	2450	1343
4532	2500	1371
4622	2550	1399
4712	2600	1427
4802	2650	1454
4892	2700	1482
4982	2750	1510
5072	2800	1538
5162	2850	1566
5252	2900	1593
5342	2950	1621
5432	3000	1649

To °F	From T	To °C
5432	3000	1649
5522	3050	1677
5612	3100	1704
5702	3150	1732
5792	3200	1760
5882	3250	1788
5972	3300	1816
6062	3350	1843
6152	3400	1871
6242	3450	1899
6332	3500	1927
6422	3550	1954
6512	3600	1982
6602	3650	2010
6692	3700	2038
6782	3750	2066
6872	3800	2093
6962	3850	2121
7052	3900	2149
7142	3950	2177
7232	4000	2204
7322	4050	2232
7412	4100	2260
7502	4150	2288
7592	4200	2316
7682	4250	2343
7772	4300	2371
7862	4350	2399
7952	4400	2427
8042	4450	2454
8132	4500	2482
8222	4550	2510
8312	4600	2538
8402	4650	2566
8492	4700	2593
8582	4750	2621

APPENDIX B
EMISSIVITY

Emissivity depends upon the material, its surface condition, and temperature. Surfaces may be polished, oxidized, or coated. The thickness of the oxidation or coating affects the emissivity. Emissivity also varies with age of the paint, dust, dirt, and condensation. The variation with temperature must be known to accurately measure the temperature during manufacturing.

Unfortunately, the emissivity is a function of viewing angle. In general, as the viewing angle increases from normality, the emissivity decreases (see Figure 4-4). For opaque objects ($\tau = 0$), as the emissivity decreases, the reflectivity increases:

$$\varepsilon + \rho = 1 \quad .$$

The values in Table B-1 should be considered as representative. It provides the emissivity for normal incidence. When the wavelength is not specified, then the emissivity values can be used for both the mid-wave and long-wave infrared regions. If the temperature is not given, assume that the values are for ambient conditions (77°F or 25°C). Since the values depend upon surface condition and material composition, values published elsewhere may differ from those given in Table B-1. To obtain accurate emissivities it is recommended that the thermographer perform emissivity tests on the specific material being evaluated.

Table B-1
REPRESENTATIVE EMISSIVITIES
(Courtesy of the Academy of Infrared Thermography)

Material	Temp. (°C)	Wavelength (μm)	Emissivity
Alloys			
20-Ni, 24-Cr, 55-Fe, oxidized	200		0.90
20-Ni, 24-Cr, 55-Fe, oxidized	500		0.97
60-Ni, 12-Cr, 28-Fe, oxidized	270		0.89
60-Ni, 12-Cr, 28-Fe, oxidized	560		0.82
80-Ni, 20-Cr, oxidized	100		0.87
80-Ni, 20-Cr, oxidized	600		0.87
80-Ni, 20-Cr, oxidized	1300		0.89

Table B-1 (continued)

Material	Temp. (°C)	Wavelength (μm)	Emissivity
Aluminum			
Disk, roughened	26	3	0.28
Disk, roughened	26	10	0.18
Foil	26	3	0.09
Foil	26	10	0.04
Heavily weathered	17		0.83-0.94
Polished		2-5.6	0.05
Polished	100	8-14	0.09
Commercial sheet	100		0.09
Lightly oxidized	25-600		0.10-0.20
Heavily oxidized	25-600		0.20-0.40
Unoxidized	25		0.02
Unoxidized	500		0.06
Asbestos			
Board	20		0.96
Slate	20		0.96
Brass			
Matte	20		0.07
Polished	28		0.03
Oxidized	100-600		0.61-0.59
Brick			
Common	17	2-5.6	0.81-0.86
Firebrick	17	2-5.6	0.68
Fireclay	1000		0.75
Masonry	0	5	0.94
Red Rough	21		0.93
Carbon			
Candle soot	20		0.95
Graphite, filed surface	20		0.98
Cast Iron			
Polished	200	3-14	0.21
Finished	20		0.44
Light oxidation	199		0.64
Heavy oxidation	104		0.95
Cement		8-14	0.54
Chromium			
Polished	40-1090		0.08-0.26
Clay, fired		8-14	0.91

Table B-1 (continued)

Material	Temp. (°C)	Wavelength (μm)	Emissivity
Concrete			
Concrete	20		0.92
Concrete: dry	36	5	0.95
Concrete: rough	17	2-5.6	0.92-0.97
Mortar	17	2-5.6	0.87
Mortar: dry	38-260	2-5.6	0.94
Copper			
Lght oxidation		8-14	0.65
Heavy oxidation	25		0.78
Cuprous oxide	800-1100		0.66-0.54
Cuprous oxide	38		0.87
Molten copper	1080-1280		0.16-0.13
Polished	20	3	0.03
Polished	20	10	0.02
Fiber board, porous, untreated	20	2-5.6	0.85
Fiberglass	20		0.75
Glass			
Standard		8-14	0.92
Polished plate	20		0.94
Gold, polished	38-260	3-14	0.02
Granite			
Natural Surface	36	5	0.96
Smooth	21		0.45
Gypsum	20	3-14	0.80-0.90
Ice		3-14	0.97
Iron			
Tempered iron, polished	40-250		0.28
Steel casting, polished	770-1040		0.52-0.56
Ground seal steel	945-1100		0.55-0.61
Hot rolled		8-14	0.77
Oxidized		8-14	0.74
Rusted surface	20		0.70
Foundry iron (oxidized at 600°C)	198-600		0.64-0.78
Iron oxide	500-1200		0.85-0.89
Ingot	925-1120		0.87-0.95
Sheet iron	25		0.80

Table B-1 (continued)

Material	Temp. (°C)	Wavelength (μm)	Emissivity
Lead			
Pure (unoxidized)	125-225	3-14	0.06-0.08
Lightly oxidized	25-300		0.43
Heavy oxidation		8-14	0.63
Limestone	38		0.95
Magnesium			
Oxidized	275-825		0.20-0.55
Oxidized	900-1670		0.20
Marble			
White	38		0.95
Smooth, white	38		0.56
Polished, gray	38		0.75
Mica	38		0.75
Molybdenum	38		0.06
Oxidized at 1000°F	316		0.80
Nickel			
Polished	25	3-14	0.05
Not polished	20		0.11
Plate (oxidized)	198-600		0.37-0.48
Nickel oxide	650-1255		0.59-0.86
Oil			
Lubricating, thin film on nickel			
Nickel base alone	20		0.05
Film thickness = 0.001"	20		0.27
Film thickness = 0.002"	20		0.46
Film thickness = 0.005"	20		0.72
Thick coating	20		0.82

Table B-1 (continued)

Material	Temp. (°C)	Wavelength (μm)	Emissivity
PAINTS:			
Aluminum	38		0.27-0.67
Acrylic, blue (Cu_2O_3)	24		0.94
Acrylic, black (CuO)	24		0.96
Acrylic, green (Cu_2O_3)	24		0.92
Acrylic, yellow (PbO)	24		0.90
Acrylic, yellow (PbO)	24	3	0.93
Acrylic, white ($A1_2O_3$)	24		0.94
Acrylic, white (Y_2O_3)	24		0.90
Krylon, flat black	50	10	0.95
Krylon, flat black	50	3	0.96
Krylon, flat white #1502	40	8-14	0.99
Lacquer, dull, black		8-14	0.97
Lacquer, white			0.87
Lacquer, white	100		0.92
Lacquer, white	200		0.95
Lacquer, matte black	100		0.97
Lacquer, shiny black, on metal			0.87
Oil, average of 16 colors		2-5.6	0.94
Oil, flat black	100	2-5.6	0.94
Oil, gloss black	20	2-5.6	0.94
Oil, flat gray	20	2-5.6	0.92
Oil, gloss gray	20	8-14	0.97
Shellac, dull black	100		0.84
Shellac, shiny black on tin	20	2-5.6	0.91
Varnish, flat	20		0.82
Radiator Paint			
White	100		0.79
Cream	100		0.77
Plaster, rough coat	20		0.91
Plasterboard, untreated	20	2-5.6	0.90
Plastic			
Black		2-5.6	0.95
White		2-5.6	0.84
Plexiglas	17	2-5.6	0.86
Polypropylene	17	2-5.6	0.97

Table B-1 (continued)

Material	Temp. (°C)	Wavelength (μm)	Emissivity
Porcelain, glazed		8-14	0.92
PVC	17	2-5.6	0.91-0.93
Rubber		8-14	0.95
Black stopper	35	5	0.97
Sand	20		0.76-0.90
Silk Cloth	20		0.78
Silver			
Plate (0.5 mil thickness on Ni)	93-371		0.06-0.07
Polished	38		0.01
Skin, human	32		0.98
Soil		6.5-20	
Dry	20		0.92
Frozen			0.93
Saturated with water	20		0.95
Stainless Steel			
18-8	25	8-14	0.16
18-8 buffed	20		0.16
18-8 oxidized at 800°C	60	8-14	0.85
18-8 sandblasted	20	5	0.44
304 (8 Cr, 18 Ni)	215-490		0.44-0.36
310 (25 Cr, 20 Ni	215-520	5	0.90-0.97
Steel		5	
Cold Rolled	93		0.75-0.85
Galvanized			0.28
Polished Sheet	38	5	0.07
Rough Surface		2-5.6	0.96
Oxidized	25		0.80
Unoxidized	100		0.08
Styrofoam, insulation	37		0.60
Tape			
Electrical, black insulating	35		0.97
Masking	36		0.92
Textile (all colors)			0.95
Tile			
Floor, asbestos	35		0.94
Glazed	17		0.94

Table B-1 (continued)

Material	Temp. (°C)	Wavelength (μm)	Emissivity
Tin			
Tin-plated sheet iron	100		0.07
Heavily oxidized	0-200		0.60
Water			0.98
Distilled	20	8-14	0.96
Ice, smooth	-10		0.96
Frost crystals	-10		0.98
Snow	-10	3-5	0.85
Snow		8-14	0.80
Wood			
Chipboard, untreated	20	2-5.6	0.90
Oak, planed	20		0.90
Paneling, light finish	36	5	0.87
Planed		8-14	0.85
Plywood	17	2-5.6	0.83-0.98
Plywood, smooth finish	36	5	0.82
Plywood, untreated	20	2-5.6	0.83
Spruce, polished	36	5	0.86
Zinc, bright galvanized	38		0.23

APPENDIX C

Thermal Sensing and Imaging 1980-1999

Selected SPIE papers on CD-ROM, Volume 7.
John Snell and Douglas Burleigh, Editors (1999)

This appendix provides the Table of Contents and Introduction to *Thermal Sensing and Imaging, 1980-1999*. This CD-ROM is available from SPIE, PO Box 10, Bellingham, WA 9898227-0010, telephone 360-676-3290.

Although several thousand papers appeared in the SPIE Proceedings, *Thermosense*, this CD-ROM contains only 384 papers that represent the best in nondestructive testing and predictive maintenance. The Introduction is included so that you may understand the editorial philosophy of why the specific papers were selected. The Table of Contents lists the papers by SPIE Proceedings volume number and manuscript number. This CD-ROM is fully searchable by title, author, keyword, and phrase. No conference was held in 1986.

INTRODUCTION

On this CD-ROM, you will find a collection of high-quality papers we have selected from past Proceedings of Thermosense. The Proceedings of SPIE represent an immense body of knowledge gathered over the past 21 years by some of the best thermographers in the world. On my bookshelf, the row of yellow bound Proceedings is nearly two feet long. The pages are familiar and well worn from frequent use. Until this electronic collection there has been no other single source of information anywhere for thermographers that is even half as valuable. Now we can not only read the papers (without broken bindings!) but search them, and view them digitally.

Support and sponsorship of the early conferences was broad, including DOE and the American Society for Photogrammetry and Remote Sensing. We were unable to get permission to include papers from the first two conferences, but selections have been made from all others (1980-1999). Although we have taken our jobs as editors very seriously, early on it became clear that neither of us was qualified to edit all of the papers. We therefore decided to do the job jointly. You should also know that, in the interests of space and value, we have chosen to include only select papers that are in the two subjects of NDT and predictive maintenance. We trust that time will not prove this to have been a mistake. The titles of the papers that were not selected are also listed and are available directly from SPIE.

It has been a privilege to review the Proceedings for this edition. Our professional "attic" held a wide variety of works. Time proved some to be visionary, while others simply recorded the hard work accomplished over the years. A few are simply gems! There were numerous papers we reread with the same fascination that gripped us the first time, as well as some that were of historic value only.

While the papers are separated into the two categories of NDT and PM, the reader is encouraged to browse through both sections, as the line between these two categories is not always a sharp line, but occasionally a fuzzy one. It was not always easy to decide where to put a paper.

For example, there are several papers on the detection of water in aerospace structures. And there are others on the detection of the loss of metal from corrosion in metallic aircraft skins. These papers would be found in the NDT section.

But there are also papers on the detection of water in building walls and frescos (art works). And there are papers on the detection of the thinning of the walls of steel pipes. These papers are found in the PM section. These papers use NDT principles, but the application is PM.

Much can still be learned from reading these papers. They will continue to guide us to new and better uses for the technology. While our interest originally was to select only papers relating to buildings, maintenance, and NDT, others have tempted us (such as brown bats and buried treasure.) and we think the collection is the better for the seasoning.

Editing this CD was also a history lesson. This conference, and much of commercial infrared as well, had its beginnings in the "energy crisis" of the late 1970s. Although we were not present at the earliest conferences, the lists of early authors clearly indicate the incredible knowledge that was being filtered here. Building diagnostics was the hot topic (along with inspection of solar heating systems), and this technology proved to be an invaluable tool for those who were coping with rising fuel costs. From the outset the conference has focused on applied thermography—a fact that helps assure that this collection of papers still has value today.

We were unable to read these Proceedings without thinking ahead to the future time when someone else will be viewing our Proceedings as history. Humor helps soften the sting. Thus, it was hard not to smile while reading of early thermographers struggling to make accurate measurements and dreaming of lighter, cheaper equipment. Physics and human nature have not changed. Also fascinating is the use of the term "active thermography" so many years ago, and the more recent "quickening" of the focal plane array technologies that have lately taken us so far so fast.

From the beginning there has been strong international involvement in Thermosense. The Scandinavians and the Canadians, in particular, have been con-

sistently strong supporters. The lists of authors and steering committee members are remarkable. Some, like Andy Kantsios, are no longer with us. Others, including Herb Kaplan, Bob Madding, Greg McIntosh, Tony Colantonio, Gary Orlove, and Doug Burleigh, still have vital, leading roles in Thermosense today. Many of the others are no doubt still active but have merely chosen new settings and roles in which to act. The Steering Committees have always been responsible for organizing the conferences. It is largely through the relationships that members have with their profession colleagues that this happens. For that reason, as well as for posterity, we have chosen to include a listing of the steering committee members for each conference. These people are so obviously important to where we are presently.

It is also clear that throughout our history the manufacturers of equipment have had a critical role in growing this industry and helping accumulate this body of knowledge. Although the players have changed teams and the teams have changed colors many times over the years, to each and all of them we express deepest appreciation for their efforts.

We are proud to have been associated with Thermosense all these years. Many fine people at SPIE have contributed to the success of the meeting and also worked with us to realize the CD-ROM collection of Thermosense papers. Without the support of SPIE, this body of knowledge, both the original yellow books and this CD-ROM, might never have existed.

Thermosense, of course, continues even as you read this. The 1999 conference promises to be the largest ever with a continued, strong international presence; it is positively overflowing with exciting papers and the enthusiasm and energy of our Chair Dennis LeMieux of the General Motors Mesa Desert Proving Ground. Because of that strength, we made the decision to include a selection of these papers from the 1999 meeting in this collection . We highly recommend you contact SPIE to find out how you can be involved in future conferences.

This collection represents the only record of good, solid knowledge that is readily accessible to all of us. It is impossible to imagine what the next 21 years will bring to thermography. How exciting it is, however, that each of us can have a role in shaping the future of our industry and in the shaping of our world through technological advances. Global needs are greater than ever, certainly dwarfing those we faced when Thermosense first began. We are confident that, armed with the knowledge we have gained in these past 21 years, our profession will continue to help find new solutions to these problems, both old and new. That will have a dramatic, positive impact on people everywhere over the next two decades and more.

John Snell
Douglas Burleigh

NONDESTRUCTIVE TESTING

Papers from Thermosense III, October 1980, No papers selected

Papers from Thermosense IV, October 1981, No papers selected

Papers from Thermosense V, October 1982

Thermography-applications to the manufacture and nondestructive characterization of composites by E. G. Henneke, K. L. Reifsnider, R. J. Shuford, Y. L. Hinton, B. R. Markert [0371-20]

Papers from Thermosense VI, October 1983, No papers selected

Papers from Thermosense VII, November 1984

Test of jet engine turbine blades by thermography, by K. Ding [0520-11]

Thermographic evaluation of bond lines and material consistency of composites by J. B. Chambers [0520-16]

Materials characterization by thermographic imaging by W. J. Rowe [0520-17]

Applications of real-time thermography for nondestructive testing of composites by Y. L. Hinton, R. J. Shuford, C. G. Pergantis [0520-20]

Evaluation of photovoltaic panels with IR thermography by R. Tscharner, K. H. S. Rao, R. Schwarz, A. V. Shah [0520-34]

The non-destructive evaluation of composites and other materials by thermal pulse video thermography by J. M. Milne, W. N. Reynolds [0520-42]

Papers from Thermosense VIII, September 1985

Void detection in metals using heat flow parallel to the target surface by G. L. Orlove, R. P .Madding, C. P. Burger, B. Raj [0581-06]

Papers from Thermosense IX, May 1987

Thermal testing methods as new tool in NDT by C. Florin [0780-44]

Papers from Thermosense X, April 1988

Thermographic inspection of superplastically formed diffusion bonded titanium panels by D. L. Haavig, D. C. King [0934-18]

Papers from Thermosense XI, March 1989

Subsurface flaw detection in reflective materials by thermal-transfer imaging by X. Maldague, J. C. Krapez, P. G. Cielo [1094-27]

Thermographic NDT of graphite epoxy filament-wound structures by D. D. Burleigh [1094-28]

Flash lamp heat flux requirements for thermographic inspection of fiber composite laminates by S. D. Cowell, D. D. Burleigh, T. J. Murray [1094-29]

Papers from Thermosense XII, April 1990

Material property measurements with post-processed thermal image data by C. S. Welch, W. P. Winfree, D. M. Heath, E. Cramer, P. Howell [1313-19]

Recent advances in digital thermography for nondestructive evaluation by R. A. Buchanan, P. E. Condon, L. M. Klynn [1313-20]

Numerical modeling of thermographic nondestructive testing for graphite epoxy laminates by S. D. Cowell, D. D. Burleigh [1313-21]

Transient thermographic NDE of turbine blades by X. Maldague, P. G. Cielo, D. Poussart, D. Craig, R. Bourret [1313-24]

Dynamic thermal tomography by V. P. Vavilov [1313-27]

Papers from Thermosense XIII, April 1991

Thermally stimulated infrared thermography for composite, ceramic and metallic materials inspection by H. Tretout, D. .David, J. Y. Marin, R. De Mol [1467-200]

Applications of tridimensional heat calibration to a thermographic nondestructive evaluation station by X. Maldague, L. Fortin, J. Picard [1467-28]

Qualitative and quantitative evaluation of moisture in thermal insulation by using thermography (Invited Paper) by V. P. Vavilov, A. I. Ivanov, A. A. Sengulye [1467-29]

Flaw dynamics and vibrothermographic-thermoelastic nondestructive evaluation of advance composite materials by L. H. Tenek, E. G. Henneke II [1467-30]

Quantitative measurement of thermal parameters over large areas using pulse-video thermography by C. P. Hobbs, D. Kenway-Jackson, J.M. Milne [1467-31]

Corrosion evaluation of coated sheet metal by means of thermography and image analysis by P. Jernberg [1467-33]

Thermographic analysis of the anisotropy in the thermal conductivity of composite materials by D. D. Burleigh, W. De La Torre [1467-35]

Time-resolved infrared radiometry of multilayer organic coatings using surface and subsurface heating by J. W. Maclachlan Spicer, W. D. Kerns, L. C. Aamodt, J. C. Murphy [1467-36]

Infrared thermal-wave studies of coatings and composites by L. D. Favro, T. Ahmed, D. Crowther, H. J. Jin, P. K. Kuo, R. L. Thomas, X. Wang [1467-37]

Papers from Thermosense XIV, April 1992

Thermographic imaging of cracks in thin metal sheets by K. E. Cramer, W. P. Winfree, P. A. Howell, H. I. Syed, K. A. Renouard [1682-24]

Processing infrared images of aircraft lapjoints by H. I. Syed, W. P. Winfree, K. E. Cramer [1682-25]

Inversion of pulsed thermal-wave images for defect sizing and shape recovery by L. D. Favro, D. J. Crowther, P. K. Kuo, R. L. Thomas [1682-26]

Automatic defects recognition in composite aerospace structures from experimental and theoretical analysis as part of an intelligent infrared thermographic inspection system by D. G. David, J. Y. Marin, H. R. Tretout [1682-27]

Detection of failures in plastic composites using thermography by A. Laine [1682-29]

Evaluation of moisture content in porous material by dynamic energy balance by E. G. Grinzato, C. Bressan, P. G. Bison, P. Baggio, C. Bnacina [1682-30]

Infrared thermography of fatigue in metals by M. P. Luong, [1682-34]

Thermography evaluation of metal bonding materials by M. Safai [1682-35]

Source patterning in time-resolved infrared radiometry of composite structures by J. W. Maclachlan Spicer, W. D. Kerns, L. C. Aamot, J. C. Murphy [1682-37]

Papers from Thermosense XV, April 1993

Inversion of pulse-echo thermal wave images by L. D. Favro, D. J. Crowther, P. K. Kuo, R. L. Thomas [1933-15]

Comparison of scanning and focal-plane-array cameras for IR thermal wave imaging by S. M. Shepard, T. Ahmed, L. D. Favro, P. K. Kuo [1933-16]

Time-resolved infrared radiometry (TRIR) using a focal-plane array for characterization of hidden corrosion by J. W, M. Spicer, W. D. Kerns, L. C. Aamodt, R. Osiander, J. C. Murphy [1933-18]

Corrosion detection in aircraft skin by H. I. Syed, K. E. Cramer [1933-19]

Adaptive thermal tomography algorithm by V. P. Vavilov, X. Maldague, B. Dufort, A. I. Ivanov [1933-20]

Infrared thermographic inspection of superplastically formed/diffusion-bonded titanium structures by D. A. Theilen, R. J. Christofersen, B. G. Dods, D. C. Emahiser, B. H. Robles [1933-21]

Evaluation of a prototype thermal wave imaging system for nondestructive evaluation of composite and aluminum aerospace structures by J. J. Selman, J. T. Miller [1933-22]

Quantitative thermal depth imaging of subsurface damage in insulating materials by K. E. Cramer, P. A. Howell, W. P. Winfree [1933-24]

Large-area thermographic inspection of GRP composite marine vessel hulls by T. S. Jones, H. Berger, E. Weaver [1933-25]

Active thermal testing of moisture in bricks by P. G. Bison, C. Bressan, E. G. Grinzato, S. Marinetti, V. P. Vavilov [1933-26]

Remote sensing study of detecting of flaws in structural material by Y Okamoto, F. Kaminaga, T. Inagaki, T. Numao, K. Fukuzawa, H. Ichikawa [1933-27]

Papers from Thermosense XVI, April 1994

Thermographic NDT based on transient temperature field under joule effect heating by T. Sakagami, K. Ogura [2245-17]

Thermal-wave imaging of composites and polymers by L. D. Favro, P. K. Kuo, R. L. Thomas [2245-18]

Optimization of thermographic NDT using finite element analysis by K. E. Llay, M. Safai [2245-19]

Thermographic inspection of marine composite structures by T. S. Jones, E. A. Lindgren [2245-20]

Nondestructive testing (NDT) of satellite structures during their assembly by infrared stimulated thermography by D. G. David, H. R. Tretout, J. Y. Marin, A. Perez, A. Delpet, J. M. Desmarres [2245-23]

Thermographic nondestructive testing (TNDT) of honeycomb composite structural parts of Atlas space launch vehicles by D. D. Burleigh, D. R. Kuhns, J. E. Engel [2245-24]

New results for prediction of cutting tools wearing resistance using one- and two-side transient thermal NDT method by V. Vavilov, V. A. Pushnykh, V. Tsipilev, A. V. Shipulin, E. G. Grinzato [2245-26]

Moisture evaluation by dynamic thermography data modeling by P. G. Bison, E. G. Grinzato, S. Marinetti [2245-28]

Object shape determination from a single infrared thermal image by E. Barker, X. Maldague, D. Laurendeau [2245-29]

Infrared thermography standards for nondestructive testing by R. J. Bruening, L. Mordfin [2245-32]

Dual-band infrared imaging to detect corrosion damage within airframes and concrete structures by N. K. Del Grande, P. F. Durbin [2245-43]

Defect detection in multilayered, plasma-sprayed zirconia by time-resolved infrared radiometry: a comparison between analytical and experimental methods by P. G. Happoldt, W. A. Ellingson, T. P. Gardiner, J. A. Krueger [2245-49]

Papers from Thermosense XVII, April 1995

State of the art of aerial thermography in Iceland: thermography of geothermal areas during the past 20 years by S. Bjornsson, K. Arnason [2473-01]

TX model: a quantitative heat-loss analysis of district heating pipes by means of IR surface-temperature measurements by H. Zinko, B. Perers [2473-02]

Air-leakage effects on stone cladding panels by A. Colantonio [2473-04]

Infrared survey of 50 buildings constructed during 100 years: thermal performances and damage conditions by S.-A. Ljungberg [2473-05]

Crawling spot thermal nondestructive testing (NDT) for plaster inspection and comparison with dynamic thermography with extended heating by P. G. Bison, A. Braggiotti, C. Bressan, E. G. Grinzato, S. Marinetti, V. Vavilov [2473-07]

Imaging the early time behavior of reflected thermal wave pulses by L. D. Favro, X. Han, P. K. Kuo, R. L. Thomas [2473-19]

Methodology of processing experimental data in transient thermal nondestructive testing (NDT) by E. G. Grinzato, V. Vavilov, P. G. Bison, S. Marinetti, C. Bressan [2473-20]

Differential thermography applied to structural integrity assessment by J. R. Lesniak, B. R. Boyce [2473-21]

Thermal wave nondestructive testing (NDT) of ceramic coatings by S. M. Shepard, L. D. Favro, R. L. Thomas [2473-22]

Microwave-source time-resolved infrared radiometry for monitoring of curing and deposition processes by R. Osiander, J. M. Spicer, J. C. Murphy [2473-23]

Full-field characterization of thermal diffusivity in continuous-fiber ceramic composite materials and components by J. S. Steckenrider, S. A. Rothermel [2473-24]

Infrared inspection of advanced army composites by T. S. Jones, E. A. Lingren, C. G. Pergantis [2473-26]

Thermographic nondestructive testing (NDT) technique for delaminated defects in composite structures by Y. W. Qin, N. Bao [2473-27]

Quantitative thermal imaging of aircraft structures by K. E. Cramer, P. A. Howell, H. I. Syed [2473-28]

Transient thermal nondestructive testing (NDT) of defects in aluminum panels by X. Maldague, V. V. Shiryaev, E. Boisvert, V. Vavilov [2473-29]

Flash infrared thermography for nondestructive testing (NDT) I/E of naval aircraft by P. J. Kulowitch, I. M. Perez, D. M. Granata [2473-31]

Inspection of low-density polyethylene using near-infrared imaging by M. W. Jones, J. M. Chandler, S. Bernstein [2473-33]

Thermal image study of detecting near-underground structures by means of infrared radiometer by Y. Okamoto, Z. Fan, C. Liu, T. Inagaki [2473-34]

Novel applications of thermal imaging in the steel industry by J. Chen, R. Barow [2473-35]

Corrosion/erosion detection in steel storage vessels using pulsed infrared imaging by M. J. Bales, C. C. Bishop [2473-36]

Nondestructive investigation by thermal waves of new aeroengine components by L. J.-P. Guazzone, R. Danjoux [2473-50]

Papers from Thermosense XVIII, April 1996

Field condition limitations for thermography of marine composites by T. S. Jones [2766-20]

Practical aspects of thermal nondestructive testing by D. D. Burleigh [2766-21]

Nondestructive pulsed infrared quantitative evaluation of metals by A. Daniels [2766-23]

Thermal characterization of defects in aircraft structures via spatially controlled heat application by K. E. Cramer, W. P. Winfree [2766-24]

Forced-diffusion thermography technique and projector design by J. R. Lesniak, D. J. Bazile [2766-25]

Analysis methods for full-field time-resolved infrared radiometry by R. Sander, J. W. M. Spicer, J. C. Murphy [2766-26]

Computational pulse shaping for thermographic inspections by W. P. Winfree, K. E. Cramer [2766-27]

Measuring defect depths by thermal-wave imaging by L. D. Favro, X. Han, P. K. Kuo, R. L. Thomas [2766-28]

Estimation of depth, width, and magnitude of material inhomogeneities from photothermal measurements by U. Seidel, H.-G. Walther [2766-29]

Determining thermal diffusivity and defect attributes in ceramic matrix composites by infrared imaging by S. Ahuja, W. A. Ellingson, J. Stuckey, E. R. Koehl [2766-30]

Infrared thermography: nonplanar inspection by J. -F. Pelletier, X. Maldague [2766-32]

Damage inspection of CFRP using resistive-heating thermographic NDT by T. Sakagami, K. Ogura, S. Kubo [2766-40]

Statistical evaluation of thermographic NDT performance applied to CFRP by V. P. Vavilov, P. G. Bison, E. G. Grinzato [2766-45]

Papers from Thermosense XIX, April 1997

Remote-sensing visible and infrared method of locating underground objects using thermal image technique by Y. Okamoto, C. Liu, H. Agu, T. Inagaki [3056-06]

Energy assessment of building envelopes through NDT methods by I. Meroni, V. Esposti [3056-09]

Pulsed phase thermography of aluminum specimens by J.-P. Courturier, X. Maldague [3056-30]

Phase-sensitive modulation thermography and its applications for NDE by D. Wu, A. Salerno, B. Schonbach, H. Hallin, G. Busse [3056-32]

Infrared video lock-in imaging at high frequencies by L. D. Favro, Z. Ouyang, L. Wang, X. Wang, F. Zhang, R. L. Thomas [3056-33]

Infrared scanning of damage in leather by M. P. Luong, D. Parganin [3056-34]

Application of infrared thermography to fracture mechanics by N. Ogasawara, M. Shiratori [3056-35]

NDE of composite materials by thermal method and shearography by P. G. Bison, C. Bressan, G. Cavaccini, A. Ciliberto, E. G. Grinzato [3056-38]

Lock-in thermographic inspection of wood particle boards by D. Wu, A. Salerno, J. Sembach, X. Maldague, J. Rantala, G. Busse [3056-39]

Coating-tolerant thermography for the detection of cracks in structures by J. R. Lesniak, D. J. Bazile, M. J. Zickel [3056-40]

IR technique for detection of wall thinning in service water piping by P. A. Zayicek, S. M. Shepard [3056-41]

Papers from Thermosense XX, April 1998

Pulsed thermographic inspection of spot welds by S. M. Shepard, B. B. Chaudhry, R. L. Predmesky, M. J. Zaluzec [3361-15]

Nondestructive testing of the concrete roof shell at the Seattle Kingdome by G. J. Weil [3361-28]

Fast infrared measurements of the thermal diffusivities of anisotropic materials by L. D. Favro, Z. Ouyang, L. Wang, F. Zhang, R. L. Thomas [3361-36]

Optimization of pulsed temporal stimulation for thermal nondestructive testing by A. Daniels [3361-37]

Cooling down thermography: principle and results for NDE by S. Danesi, A. Salerno, D. Wu, G. Busse [3361-38]

Thermal tomography characterization and pulse-phase thermography of impact by damage in CFRP, or why end users are still reluctant about practical use of transient IR thermography by V. P. Vavilov, S. Marinetti, E. G. Grinzato, P. G. Bison [3361-39]

Thermal diffusivity imaging of aerospace materials and structures by W. P. Winfree, D. M. Heath [3361-41]

Thermographic detection and quantitative characterization of corrosion by application of thermal line source by K. E. Cramer, W. P. Winfree [3361-43]

Inspection of metallic thermal protection systems for the X-33 launch vehicle using pulsed infrared thermography by J. O. Taylor, H. M Dupont [3361-44]

Applications for thermal NDT on advance composites in aerospace structures by S. R. Baughman [3361-46]

Theory and application of coating tolerant thermography by J. R. Lesniak, D. J. Bazile, M. J. Zickel [3361-47]

Advanced image processing for defect visualization in infrared thermography by Yu.A.Plotnikov,W.P.Winfree [3361-49]

Thermal inspection of SiC/SiC ceramic matrix composites by R. Osiander, J. W. M. Spicer, J. M. Amos [3361-51]

Papers from Thermosense XXI, April 1999

Finite element analysis as a tool for thermography by J. M. Kleinfeld [3700-01]

Accuracy of thermal NDE numerical simulation and referential signal evolutions by V. P. Vavilov [3700-02]

Pulsed phase thermography processing with a neural network by X. P. Maldague, S. Vallerand, Y. Largouet [3700-03]

Visualization of subsurface defects in composites using a focal plane array infrared camera by Y. A. Plotnikov, W. P. Winfree [3700-04]

Thermographic modeling of water entrapment by I. M. Perez, P. J. Kulowitch, M. F. Dersch [3700-05]

Evaluation of high thermal conductivity graphite fibers for thermal management in electronics applications by J. W. M. Spicer,D.W. Wilson, R. Osiander,J.Thomas, B. O. Oni [3700-06]

Fast infrared imaging of static and dynamic crush tests of composite tubes by X. Han, L. D. Favro, R. L. Thomas, M. Chadwick. A. Caliskan, N. Griffith, [3700-07]

Imaging the geometry and location of defects in adhesive-bonded and spot-welded lap joints using steady state thermographic techniques by D. Turler [3700-09]

Quality control of heat pipelines and sleeve connections by infrared measurements by W. Gross, T. Hierl, H. Scheuerpflug, U. Schirl, M. J. Schulz [3700-12]

Defect localization in solar modules by thermal infrared microscopy by W. Gross, T. Hierl, H. Scheuerpflug, J. Zettner, M. J. Schulz [3700-13]

Pulsed thermographic inspection application in commercial aircraft repair by R. Ducar [3700-14]

Thermographic testing for the X-33 launch vehicle by vD. D. Burleigh [3700-15]

Thermal inspection of solder quality of electronic components by J. Varis, R. Vuohelainen, R. K. Lehtiniemi [3700-18]

New thermographic nondestructive testing technique using microwave heating by T. Sakagami, S. Kubo [3700-61]

Minimum radiation temperature difference and detection limit of flaws by means of infrared radiometer by Y. Okamoto, A. Kamoi, O. Makishi [3700-62]

PREDICTIVE MAINTENANCE

Papers from Thermosense III, September 1980

Heat flow in structures by G. J. Burrer [0254-02]

Meteorology and infrared measurements by James B. Evans [0254-03]

Isolating the building thermal envelope by D. T. Harrje, K. J. Gadsby [0254-11]

Thermographic study of transient heat-flow in residential dwellings by Dag. Holmsten [0254-13]

Detecting moisture in buildings using infrared thermography by Stephen J. Marshall [0254-18]

Canadian experience in certification and training of thermography personnel by Peter A. D. Mill [0254-30]

Buying thermography by Robert P. Madding [0254-31]

Papers from Thermosense IV, September 1981

Interpolating R-values from thermograms by S. N. Flanders, S. J. Marshall [0313-19]

Detection of moisture in commercial and industrial built-up roofing systems by Victor Sopko [0313-21]

We need to know more about infrared emissivity by Stephen J. Marshall [0313-22]

Recent advances in the quantification of industrial heat loss using thermography by G. B. McIntosh [0313-35]

Uses of infrared thermography in the Low-Cost Solar Array Program by Stuart D. Glazer [0313-38]

Practical methods for improving thermal measurements by Claes Ohman [0313-43]

Papers from Thermosense V, October 1982

Science behind thermography by Robert P. Madding [0371-01]

What's out there: state-of-the-art survey of thermal infrared instrumentation by Richard H. Munis, Herbert Kaplan [0371-02]

Overview of industrial applications of thermal sensing by Herbert Kaplan [0371-03]

Roof moisture surveys: current state of the technology by Wayne Tobiasson [0371-04]

Monitoring of generator stator core lamination repairs using thermographic techniques by D. C. Stevens [0371-06]

Infrared thermal imaging of refinery equipment by A. G. Imgram, J. B. McCandless [0371-07]

Thermographic aspects of industrial predictive maintenance by G. S. Baird [0371-09]

Thermographic inspection of mechanical systems by Jay G. Vanier, D. E. Gay [0371-10]

Infrared scanning for electrical maintenance by Steven E. Eisenbath [0371-12]

Practical thermal measurement techniques by Gary L. Orlove [0371-16]

Use of thermography to establish a maintenance program for a pelletizing mill by Terry L. Loomis [0371-17]

Steel mill infrared surveillance: a case study by Edward R. Schaufler [0371-18]

Temperature measurements on semi-permanent mold surfaces using infrared thermography by Ronald G. Hurley [0371-19]

Thermography: a diagnostic tool for locating wet insulation in built-up roofing systems by Al H. Knehans, Paul E. Styer [0371-29]

Locating wet cellular plastic insulation in recently constructed roofs by Charles Korhonen, Wayne Tobiasson [0371-30]

Thermographic inspections and the residential conservation service program (RCS) by Ronald J. Ward [0371-41]

Glass temperature measurement for the glass industry by Gabor B. Kalos [0371-42]

Design analysis of rotating machinery using infrared thermography by Charles C. Roberts, Jr. [0371-43]

Quantitative analysis of sludge incinerators by Stephen A. Seeber [0371-45]

Papers from Thermosense VI, October 1983

Infrared sensors and process control by R. P. Madding [0446-03]

Heat loss due to thermal bridges in buildings by J. B. Fang, R. A. Grot, K. W. Childs, G. E. Courville [0446-06]

Use of thermography in the diagnostics of energy use in multifamily dwellings by K. J. Gadsby, D. T. Harrje [0446-07]

The role of thermography in the assessment of the thermal integrity of federal office buildings by Y.-M.L.Chang, R. A. Grot [0446-08]

Use of infrared thermography for the identification of design and construction faults in buildings by S. A. Seeber [0446-09]

Thermographic inspection of high-rise building envelopes by J. R. Wallace [0446-10]

Thermal signatures associated with different types of moisture-damaged roofing insulation by D. J. Templeton, D. E. Gay [0446-11]

An investigation of factors influencing infrared roof moisture surveys using a mathematical model by K. W. Childs, G. E. Courville, P. W. Childs [0446-12]

Comparison of aerial to on-the-roof infrared moisture surveys by C. Korhonen, W. Tobiasson, A. Greatorex [0446-13]

Application of airborne thermal infrared moisture surveys by H. W. MacKay, G. R. Lawrence [0446-14]

Industrial applications of qualitative thermography by L. D. Arrington [0446-15]

Infrared thermal sensing of sewer voids by G. J. Weil [0446-16]

Appraising process furnace tubes with imaging radiometers by R. P. Bruno, G. J. Burrer [0446-17]

Thermographic inspection of operating pumping units in Permian Basin oil fields by R. E. Witte [0446-21]

Infrared thermography as a control for the welding process by M. A. Khan, N. H. Madsen, B. A. Chin [0446-22]

The infrared emittance of semi-transparent materials measured at cold temperatures by S. J. Marshall [0446-26]

Thermovision used for nondestructive testing of solar panels by J. A. Baldo [0446-27]

Infrared evaluation of electrical machinery by R. Brown [0446-28]

Assessment of thermography as a means for determining steam trap performance by G. L. Orlove [0446-29]

Inferring temperature from optical radiation measurements by D. P. DeWitt [0446-32]

A comparison of infrared flyover, infrared walkover, and visual inspection techniques for detecting roof moisture anomalies by K. B. Ouzts, J. Vanier, D. E. Brotherson [0446-36]

Using high-resolution hand-held radiometers to measure in-situ thermal resistance by D. M. Burch, D. F. Krintz [0446-40]

Papers from Thermosense VII, November 1984

Principles of calibration for radiometric temperature measurements by D. P. DeWitt [0520-01]

The technologist as an expert witness by R. E. K. Morrill [0520-02]

Infrared thermography and the expert witness by C. C. Roberts, Jr. [0520-03]

Infrared (IR) transmitting materials by W. L. Truett [0520-05]

A proposed model for thermal image scene analysis by S. J. Marshall, R. H. Munis [0520-08]

Aerial thermography and spot radiometer applications for detecting thermal anomalies of office buildings by Y. M. Chang, L. S. Galowin [0520-25]

Residential thermal anomalies and their origins by S. Allen, L. R. Allen [0520-26]

Economics of thermographic predictive maintenance inspections by G. Baird [0520-28]

Location of reinforcement by induction-thermography by B. Hillemeier [0520-35]

Thermography as a diagnostic tool in building engineering by C. Florin [0520-36]

Papers from Thermosense VIII, September 1985

The misuse of infrared thermography by C. C. Roberts, Jr. [0581-03]

Questions of quality in thermographic services by G. S. Baird [0581-04]

Utility infrared program justification and development by D. Brooks II [0581-18]

Quality aspects of electric utility inspections by G. S. Baird [0581-19]

The use of infrared thermography in evaluating substation transformers by R. A. Faccinto [0581-20]

Electric motor care using infrared diagnostics by R. Brown [0581-21]

Infrared thermography as a predictive maintenance tool by R. D. Lucier [0581-23]

Thermal imaging for the nuclear power industry by F. T. Caruso [0581-26]

Thermographic applications for industrial/utilities predictive maintenance by J. G. Clark [0581-27]

Determining condenser air infiltration using thermographic methods by T. G. Harter [0581-28]

Infrared testing: the least cost approach to effective electrical maintenance by S. A. Seeber [0581-29]

Fraud in the energy conservation field: what's the real cost by K. L. Reinke, Jr. [0581-30]

Thermographic imaging and computer image processing of defects in building materials by J. W. Martin, M. E. McKnight, D. P. Bentz [0581-31]

Development of infrared thermographic standards for New Jersey state buildings by S. Allen, L. R. Allen [0581-32]

Thermographic observation of mechanical power transmission belt drives by T. Carmody [0581-34]

Papers from Thermosense IX, May 1987

Nondestructive methods for inspection of seams of single-ply roofing membranes by W. J. Rossiter, Jr. [0780-01]

Investigation into the factors affecting infrared temperature measurements for building applications by Y. M. Chang [0780-03]

Infrared thermographic quality control for newly constructed office buildings prior to closing by S. Allen [0780-04]

Combination of thermography and pressure tests to combat air leakage problems inbuilding enclosures by W. G. Spruin [0780-05]

Measurement of temperature distribution of glass plate using infrared thermography by Y. W. Lin [0780-07]

Regional implementation of Public Works Canada developments in thermography for building diagnostic purposes by A. Colantonio [0780-08]

Infrared evaluation of an underground stream distribution system by D, J. Templeton, M. B. Palmer [0780-09]

Effect of circuit loading on electrical problem temperature by G. S. Baird [0780-12]

Nonproblems in power plants: a primer on correct diagnosis by R. D. Lucier [0780-14]

High speed real time quantification of thermal data for process and industrial control by G. B. McIntosh [0780-19]

Industrial applications of fiber optics in infrared thermal monitoring by J. Bedrossian, Jr. [0780-20]

Temperature measurement of a friction surface in brake testing by G. Manghi [0780-34]

Analysis of thermal patterns on a motorized ski deck by C. C. Roberts, Jr. [0780-35]

Proposed code of ethics for infrared thermographic professionals by C. C. Roberts, Jr. [0780-40]

Status of the American Society for Testing and Materials (ASTM) efforts to provide a standard practice for infrared roof moisture surveys by V. Sopko [0780-41]

Bibliography of nondestructive testing (NDT) of composite materials performed with infrared thermography and liquid crystals by D. D. Burleigh [0780-42]

Aerial thermography: a tool for detecting heat losses and defective insulation in building attics and district heating networks by S.-A Ljungberg, M. Rosengren [0780-43]

Infrared thermography study and digital thermal image processing for solar collectors in irrigation by G. Destobbleire [0780-48]

Papers from Thermosense X, April 1988

Application of infrared thermography in fire and explosion investigation by C. C. Roberts, Jr. [0934-01]

Certification, qualification, and certificate of completion: what is the difference? by G.S. Baird [0934-02]

Mobile infrared thermographic surveys of building within a community by S. Allen [0934-05]

Experimental and theoretical evaluation of infrared thermography for surveying the condition of bridge decks by T. Masliwec [0934-06]

Roof diagnostics: the scanning window by D. B. Barry, J. C. Wong [0934-07]

Development of a diagnostic testing and calibration system for infrared imaging equipment used in building diagnostics by A. Colantonio, G. B. McIntosh [0934-08]

Stress affected livestock as seen by thermography by G. B. Desroches [0934-20]

Remote infrared thermal sensing of sewer voids: four-year update by G. Weil [0934-26]

Method for conducting airborne infrared roof moisture surveys by W. Tobiasson [0934-40]

Roof moisture survey: a case history by R. A. Malone, A. R. Ash [0934-41]

Thermography for district heating network applications: operational advantages and limitations by S.-A. Ljungberg [0934-42]

Conditions for detecting malfunctions of buried heat distribution systems by thermographic methods by M. D. Lyberg [0934-43]

Papers from Thermosense XI, March 1989

Survey of the use of IR thermography in the Department of Energy's Weatherization Assistance Program by J. R. Snell Jr. [1094-01]

Aerial thermography: cartographic presentation of thermographic data for building applications by S. A. Ljungberg [1094-02]

Pressurization effects on thermal images of building envelopes by A. Colantonio [1094-03]

Review of the ASTM standard on IR testing of concrete bridge decks by G. J. Weil [1094-04]

Update on New Jersey's use of IR testing of concrete bridge decks by S. M. Semanovich, L. R. Allen [1094-05]

Infrared thermography as quality control for foamed in-place insulation by J. A. Schwartz [1094-06]

Temperature patterns on roof systems with ventilated air cavities by M. D. Lyberg [1094-07]

Thermography in commercial nuclear power plants by J. E. Black, Jr. [1094-08]

Analysis of electrical arcs using infrared thermography by C. C. Roberts [1094-10]

On-line temperature measurement in hot rolling of aluminum using IR imaging

systems by M. J. Fairlie, W. C. Fraser, B. Farahbakhsh, R. Lamb, O. Meijer [1094-13]

Case study of applying infrared thermography to identify a coolant leak in a municipal ice skating rink by J. R. Wallace [1094-16]

Papers from Thermosense XII, April 1990

Department of National Defense's use of thermography for facilities maintenance by J. E. Kittson [1313-01]

Infrared qualitative and quantitative inspections for electric utilities by T. L. Hurley [1313-02]

Status report on the Electric Power Research Institute IR guidelines project by R. D. Lucier [1313-03]

Estimation of hardware-failure rates using IR thermography by A. Madrid [1313-04]

Steel plant predictive-maintenance programs utilizing IR NDT by R. J. Graf, G..J.Weil [1313-05]

Infrared-thermography imaging system multiapplications for manufacturing by S. A. Stern [1313-06]

Rational approach to nuclear power station IR surveys by F. G. Bryson [1313-07]

Manufacturers' recommended body of knowledge for thermographic diagnostics by R. P. Madding [1313-09]

High-resolution thermal scanning for hot-strip mills by D. Holmsten, R. Houis [1313-29]

Paint skip detector by M. J. Haugh, D. P. Stone, M. Thangavelu [1313-31]

Infrared sensor for automated inspection of hot metal surface by J. B. Setzer, Jr., M, Thagavelu [1313-32]

Papers from Thermosense XIII, April 1991

Surveying the elements of successful infrared predictive maintenance programs by J. R. Snell, Jr., R. W. Spring [1467-01]

Buried-steam-line temperature and heat loss calculation by J. H. McDavid [1467-02]

Infrared-thermography-based pipeline leak detection systems by G. J. Weil, R. J. Graf [1467-03]

Utility gains through infrared predictive maintenance by J. E. Black, Jr. [1467-04]

Thermographic monitoring of lubricated couplings by R. N. Wurzbach [1467-05]

Is it worth it? Statistics of corporate-based IR program results by P. Johnson [1467-06]

So now what? Things to do if your IR program stops producing results by R. D. Lucier [1467-07]

Integrating thermography into the Palisades Nuclear Plant's electrical predictive maintenance program by W. C. Ridley [1467-08]

Field documentation and client presentation of infrared inspections on new masonry structures by P. C. McMullan [1467-10]

Infrared detection of moist areas in monumental buildings based on thermal inertia analysis by E. Grinzato, A. Mazzoldi [1467-11]

Discussion of the standard practice for the location of wet insulation in roofing systems using infrared imaging (ASTM C1153-90) by V. Sopko III [1467-12]

Applications and development of IR techniques for building research in Finland by H. I. Kaasinen, A. Kauppi, E. Nykanen [1467-13]

Thermal analysis of masonry block buildings during construction by L. R. Allen, S. A. Semanovich [1467-15]

Thermography and complementary methods: a tool for cost-effective measures in retrofitting buildings by M. D. Lyberg, S. Ljungberg [1467-16]

Infrared thermographic analysis of snow ski tracks by C. C. Roberts, Jr. [1467-24]

Behavioral observations in thermal imaging of the big brown bat: Eptesicus fuscus by J. J. Kirkwood, A. Cartwright [1467-39]

Detection of citrus freeze damage with natural color and color infrared video systems by C. H. Blazquez [1467-43]

Accurate temperature measurement in thermography: an overview of relevant features, parameters, and definitions by T. Hamrelius [1467-52]

Thermal analysis of the bottle forming process by J. S. Wilson [1467-62]

Papers from Thermosense XIV, April 1992

Role of comparative and qualitative thermography in predictive maintenance by R. N. Wurzbach, R. G. Hammaker [1682-01]

Developing operational protocol for thermographic inspection programs by J. R. Snell, Jr., R. W. Spring [1682-02]

Infrared Research Services versus $$$: the bottom line by J. M. Garner [1682-03]

Development of a comprehensive IR inspection program at a large commercial nuclear utility by N. A. MacNamara, A. E. Hammett [1682-04]

Predictive maintenance for the 90's: an overview by R. D. Lucier [1682-05]

Thermographic inspection and heat flow simulation of midspan joints by M. I. Forssander [1682-06]

Renovation concepts for private houses: the use of thermography as a supporting method by T. Kauppinen, A. Hakkila, M. Hekkanen [1682-09]

Metal cladding envelope problems, retrofit solutions, and quality control investigations by A. Colantonio [1682-10]

Case study of commercial building envelope air leakage detection using infrared imaging by P. C. McMullan [1682-11]

Thermographic inspections of air distribution systems by W. T. Morgan [1682-12]

Predictive maintenance of district heating networks by infrared measurement by L. Koskelainen [1682-13]

Infrared thermographic detection of buried grave sites by G. J. Weil, R. J. Graf [1682-50]

Papers from Thermosense XV, April 1993

Database system for managing thermography files of district heating networks by L. Koskelainen [1933-01]

Integration of infrared thermography into various maintenance methodologies by W. T. Morgan [1933-02]

Increasing maintainability and operability of emergency diesel generators with thermographic inspections by R. N. Wurzbach, J. E. Hart [1933-03]

Masonry building envelope analysis by P. C. McMullan [1933-06]

Infrared thermography for assessing the quality of waterproofing of bridges under construction by H. I. Kaasinen [1933-07]

Use of thermography to register air temperatures in cross sections of rooms and to visualize the airflow from air-supply diffusers by J. Sundberg [1933-08]

Impact of aerial infrared roof moisture scans on the U.S. Army's ROOFER program by A. Knehans, J. Ledford [1933-10]

Applications of aerial thermography in peat production in Finland by M. Tervo, E. Kiukaanniemi, T. Kauppinen [1933-14]

Pulsed thermal nondestructive testing of layered materials by O. Troitsky [1933-28]

Nondestructive remote sensing of hazardous waste sites by G. J. Weil, R. J. Graf, L. M. Forister [1933-31]

Thermal imaging and paper-finishing machines by J.-M. Karjanmaa [1933-36]

Verification of plugged nozzles in reactor-building spray systems by L. Carter [1933-38]

Papers from Thermosense XVI, April 1994

Guidelines to thermographic inspection of electrical installations by T. Perch-Nielsen, J. C. Sorensen [2245-03]

Study of cost benefits of identification of non-problems with infrared thermography by J. P. Evans, R. N. Wurzbach [2245-04]

Advanced leak location-research evaluation demonstration (ALL-RED) project by R. G. Hammaker, R. J. Colsher [2245-05]

Detection of problems in high-power voltage transmission and distribution lines with an infrared scanner/ video system by C. H. Blazquez [2245-06]

How to prepare a written practice for infrared/ thermal nondestructive examination method by H. M. Sadek [2245-07]

Use of an infrared scanner and a nuclear meter to find wet insulation in a ballasted roof by W. Tobiasson, A. Greatorex [2245-12]

Thermographic inspection of a tennis court building with modern steel construction: constructional mistakes and bad craftsmanship by S.-A. Ljungberg [2245-13]

Use of infrared thermography in aiding and monitoring weatherization work: lessons learned by R. Gerardi [2245-14]

Application of thermal imaging to electronic fault diagnosis by L. G. Allred, T. R. Howard [2245-33]

Temperature measurement on and inside lamps by B. Wallin [2245-36]

Papers from Thermosense XVII, April 1995

Nondestructive testing: use of IR and acoustic methods in buildings pathology by W. Esposti [2473-06]

Application of differential infrared thermography in power generation facilities by H. Kaplan, P. A. Zayicek [2473-10]

Problems inherent to quantitative thermographic electrical inspections by J. R. Snell, Jr. [2473-11]

Increasing predictive program effectiveness by integrating thermography and lubricant analysis by J. P. Evans, T. J. Jarc, R. N. Wurzbach [2473-12]

Thermal instability observation in power transistors by radiometric detection of temperature maps by S. Pica, G. Scarpetta [2473-13]

Electrical fault location for surface-mounted feeders in metallic conduit by S. Finneson [2473-14]

Use of an infrared sensing technique in the regular monitoring of incinerators and a kiln by J. Varrio, S. Kesanto, T. Heikkinen [2473-15]

American Society for Nondestructive Testing (ASNT) certification of thermographers by R. W. Spring [2473-18]

Infrared scanning of failure processes in wood by P. M. Luong [2473-37]

Papers from Thermosense XVIII, April 1996

Application of thermographic temperature measurements in injection molding and blow molding of plastics by M. Prystay, H. Wang, A. Garcia-Rejon [2766-05]

Optimization of cooling channel design and spray patterns in aluminum die casting using infrared thermography by M. Prystay, C. A. Loong, K. Nguyen [2766-06]

Thermographic inspection of hydraulic systems by T. E. Green, J. R. Snell, Jr.[2766-07]

ASNT certification of thermographers at DuPont Company by L. G. Eads, R. W. Spring [2766-08]

Developing written inspection procedures for thermal/infrared thermography by J. R. Snell, Jr. [2766-10]

Infrared thermography as a diagnostic tool to indicate sick-house syndrome: a case study by S.-A. Ljungberg [2766-11]

Improvements in new residential construction using infrared thermography and blower door by D. McCleary, R. Harvey, S. A. Semanovich [2766-12]

Evaluation of internal boiler components and gases using a high-temperature infrared (IR) lens by R. G. Hammaker, R. J. Colsher, J. J. Miles, R. P. Madding [2766-16]

Infrared thermography at EDF: a common technique for high-voltage lines but new in monitoring and diagnosis of PWR plant components by D. Provost [2766-17]

Using thermography to detect misalignment in coupled equipment by C. K. Kelch, P. E. Grover [2766-18]

Usefulness of high-resolution thermography in fault diagnosis of fluid power components and systems by M. Pietola, J. P. Varrio [2766-19]

Remote temperature sensing as a means of maintaining ski lift towers by C. C. Roberts, Jr. [2766-43]

Papers from Thermosense XIX, April 1997

Analysis of thermal radiation in coal-fired furnaces by J. J. Miles, R. G. Hammaker, R. P. Madding, J. E. Sunderland [3056-03]

Thermal performance of prefabricated multistory houses in Tallinn, Estonia, based on IR survey by T. T. Kauppinen, J. Hyartt, L. Sasi [3056-10]

Quantitative evaluation of building thermal performance by IR thermography inspection data by V. P. Vavilov, I. A. Anoshkin, D. G. Kourtenkov, C. D. Trofimaov, T. T. Kauppinen [3056-11]

Infrared in automotive applications (Invited Paper) by R. L. Predmesky, M. J. Zaluzec [3056-21]

Some automotive applications of infrared thermography for quality improvements by (Invited Paper) by G. B. Champman II [3056-23]

Infrared electrical inspection myths by R. Newport [3056-24]

Information potential using IR technology for condition monitoring of reheating furnaces within steel and iron industry by S.-A Ljungberg [3056-25]

Steam-leak cost estimation using thermographically acquired pipe temperature data by R. P. Madding, N. A. MacNamara [3056-26]

Substation component identification for infrared thermographers by J. L. Giesecke [3056-27]

Improving thermographic analysis using image histories by S. Johnson, R. Neff [3056-28]

Papers from Thermosense XX, April 1998

Diagnostic monitoring by infrared imaging of avian embryos by R. N. Wurzbach [3361-11]

High-voltage switchyard thermography case study by R. P. Madding [3361-17]

Imaging of sealant injection into a main steam valve by D. N. Fogarty [3361-18]

Radiometric imaging of internal boiler components inside a gas-fired commercial boiler by J. J. Miles, R. G. Hammaker, R. P. Madding, J. E. Sunderland [3361-19]

Infrared thermography of fan and compressor systems in a predictive maintenance program by R. N. Wurzbach [3361-20]

Evaluation of thermal cracker operation by use of an infrared camera by E. H. Edwin, T. Arnesen, G. I. Hugosson [3361-22]

Infrared thermography and ultrasound for both testing and analyzing valves by A. E. Rozlosnik [3361-24]

Amplitude-sensitive modulation thermography to measure moisture in building materials by W. Wild, K. A. Buscher, H. Wiggenhauser [3361-25]

Infrared thermographic surveying of building debris: Tomsk High Military School of Communication Engineering catastrophe case study by V. P. Vavilov [3361-26]

Optimal environment conditions to detect moisture in ancient buildings: case studies in Northern Italy by E. Rosina, N. Ludwig, L. Rosi [3361-29]

Thermographic inspection and quality assurance of energy conservation procedures for electric buses by H. C. Fennell [3361-30]

Tracking rotating components for complete construction of simulated images by D. T. Sass, J. D. White, T. G. Gonda, J. C. Jones [3361-31]

Online industrial thermography of die casting tooling using dual-wavelength IR imaging by H. E. Kourous, B. N. Shabestari, S. D. Luster, J. P. Sacha [3361-33]

Infrared thermography for examination of paper structure by H. T. Kiiskinen, P. I. Pakarinen [3361-34]

Full-field IR measurement of subsurface grinding temperatures by T. Sakagami, V. Madhavan, G. Harish, K. Krishnamurthy, Y. Ju, T. N. Farris, S. Chandrasekar [3361-35]

IR-camera methods for automotive brake system studies by R. B. Dinwiddie, K. Lee [3361-48]

Infrared technology in automotive components research and development by W. H. El-Ratal, D. C. Bee [3361-50]

Papers from Thermosense XXI, April 1999

Non-contact process temperature measurements in steel manufacturing by G. R. Peacock [3700-22]

Thermal imaging of railroad cars used for molten iron transport by C.A. Sahr [3700-24]

Thermography in the condition monitoring of refractory lining by T. T. Kauppinen, K. Ruotsalainen, P. Alamaki, J. Lilja [3700-26]

Recommendations for strengthening the infrared technology component of any condition-monitoring program by J. R. Nicholas, Jr. R. K. Young [3700-27]

Assessment of cooling tower thermal performance using infrared thermography by N. A. MacNamara, P.A. Zayicek [3700-30]

Infrared thermography locates overloaded neutral conductors by J. McComb, H. E. Niebla [3700-31]

Thermographic study of an electrical distribution station by E.H. Castro, E. Leone, M. Costanzo, R. Luca [3700-33]

Nondestructive evaluation of steam traps by G. L. Orlove [3700-34]

Non-contact IR thermometers in modern maintenance by V. S. Ribeiro [3700-36]

Transfer of infrared thermography by predictive maintenance technologies to Russian and Ukrainian nuclear power plants by R. Pugh, R. Huff [3700-38]

Emissivity measurement and temperature correction accuracy considerations by R. P. Madding [3700-45]

Infrared thermographic investigation procedures for four types of generic exterior wall assemblies by A. Colantonio [3700-53]

Moisture entrapment in buildings with EFIS and stucco facades in the state of Florida by K. M Barker, M. G. Knettel [3700-54]

Moisture monitoring of historical buildings by long-period temperature measurements by E.G. Grinzato, F. Peron, M. Strada [3700-55]

Using infrared thermography to determine the presence and correct placement of grouted cells in single-width concrete masonry unit (CMU) walls by G. R. Stockton, L. R. Allen [3700-56]

Quantitative infrared thermography in fire tests by H. Heinrich, K. H. Dahlem [3700-57]

Identification of convective heat loss on exterior cavity wall assemblies by A. Colantonio [3700-59]

Index

Absolute humidity, 80
Absorber, 62
Absorptance, 60
AC coupling, 102
Active infrared thermography, 291
Active target, 176
Advanced Very High Resolution Radiometer, 271
Adverse weather, 171
Aerodynamic heating, 132, 178
Aerosols, 79, 81
Air leakage, 201
Aircraft, 174, 179, 293
Airy disk, 117
Aluminum, 204, 296, 302, 316
Aluminum processing plant, 232
Aluminum wire, 227
Ambient temperature, 74, 133
American Society for Nondestructive Testing, 148
American Society for Testing and Materials, 224
American Wire Gauge, 228
Animal counting, 273
Annealing furnace, 194
Anomaly, 157
Apparent emissivity, 67
Apparent temperature, 64, 183, 191
Applications, 151
Art forgery, 72
Ash plume, 272
ASNT, 148
Asphalt shingle, 163
ASTM, 224
Atmospheric correction, 197
Atmospheric transmittance, 13, 74
Attenuation coefficient, 75
Automobile, 311
Automobile fan, 313
Average weather conditions, 86
AVHRR, 271
AWG, 228

Back surface mirror, 181
Background, 49, 58
Ball mill, 246
Bandgap engineered photodetectors, 98
Banding, 280
Baseline thermogram, 185, 240
Battlefield, 274
Bearings, 244
Beaufort scale, 168
Beer-Lambert law, 75
Belt, 248
Beverage container, 316
Black hot, 90
Black paint, 194
Black tape, 194
Blackbody, 52, 66
Blow molding, 313
Bolometer, 98
Boost, 105
Border crossing, 268
Boxcar integration, 307
Brake rotor, 41
Brakes, 177
Bridge deck, 171, 256
British thermal unit, 21
BTU, 21
Building construction, 201
Building envelope, 200
Building/structure inspection, 154
Buried objects, 256, 291
Bus bar, 232

Cadillac, 266
Calibration, 145, 185
Calibration points, 106

Calibration source, 66
Calorie, 22
Camera formula, 92
Cannabis, 269
Cannon, 275
Car, 163
Car thief, 267
Carbon fiber reinforced plastics, 293
Ceiling insulation, 209
Celsius, 10
Cemetery, 256
Center-to-center spacing, 119
Centigrade, 10
Certification, 148, 320
CFCC, 293
CFRP, 293
Church, 202
Circuit breaker, 43, 131, 234, 243
Circular mil, 227
Classical semiconductors, 98
Clouds, 168, 219
Clutter, 259, 274
Coating thickness, 299
Coke, 311
Cold spike, 132
Color, 8, 43, 52
Color temperature, 52
Combustion, 36
Common module, 93, 95
Comparison, 157
Compressor, 42
Concrete block, 203, 204
Condensation, 201, 207
Condition monitoring, 151
Conduction, 27
Conductor, 226
Cone angle, 66
Consistent observer, 150
Contacts, 254
Continuous fiber ceramic matrix composites, 293
Continuous sheet, 194
Continuous strip annealing furnace, 194
Contrast, 296
Convection, 32, 233
Convective cooling, 230
Cooled detectors, 97
Cooling fins, 237
Copper loss, 229
Copper wire, 227
Corrosion, 302
Counterfeiting, 72
Coupling, 246
Cracks, 293
Crimp connection., 44
Crude oil, 311
Customer, 319

Dampness, 201
DAS, 118
Data analysis, 326
Data storage, 327
DC restoration, 102
Dee-star, 100, 115
Defect, 291
Deficiency, 152
Defroster, 311
Delta-T, 50
Depressurization, 211
Detection, 283
Detectivity, 100
Detector, 48
Detector-angular-subtense, 118
Dewar, 34
Differential infrared thermography, 144
Diffuse surface, 174
Digitization, 104
Dirac pulse, 296
Dirty battlefield, 274
Disbonding, 299
Discrimination, 283
Distribution panel, 240
Diurnal cycle, 165, 217
Double-glazed window, 30

Drug interdiction, 269
Dual band measurement, 197
Dynamic range, 44, 139
Dynamic thermal tomography, 293

Earthshine, 174
Ecosystem, 271
Effusivity, 298
Electrical connection, 44, 225, 236, 240
Electrical inspection, 153
Electrical insulation, 227
Electrical power, 239
Electrical repair priority, 252
Electromagnetic radiation, 11
Electromotive force, 7
Emissivity, 60, 173, 187, 250, 301
Emissivity correction, 187
Emissivity improver, 194
Emissivity uncertainty, 190
EMUX, 93
Energy conversion, 157
Engine, 39
Engine compartment, 177
Engineering practices, 327
Environment, 63, 132, 159, 216
EOMUX, 93
Equivalent bar pattern, 283
Error analysis, 190
Evaporation, 209
Evaporative cooling, 25, 210
Exception, 152
Exfiltrate, 210
Exhaust gas, 40, 276
Exit conference, 328
Exterior walls, 200
Extinction, 75

Fahrenheit, 10
False color, 8
Fan, 249, 313
Far infrared, 14
Fatigue, 293
Fault, 152
Filament, 69
Fill factor, 103, 119
Final report, 328
FIR, 14
Fire, 37, 82, 270
Firefighters, 270
Fixed pattern noise, 102, 105
Flame filter, 71
Flash pulse, 296
Flexible coupling, 246
FLIR, 93
FLIR92, 276
F-number, 92
Footprint, 134
Forced convection, 233
Forensics, 72
Forest fire, 37
Forgery, 72
Forward looking infrared, 93
Frame rate, 143
Freeze-thaw cycle, 201, 213
Friction, 4
Frictional heat, 40, 177
Front surface mirror, 181
Fugitive, 268

Gain/level normalization, 102, 106
Gearbox, 249
General Motors, 266
Geometric factors, 65
Geostationary Operational Environmental Satellite, 271
Germanium, 68, 94
Glass, 31, 69, 174
Glass building, 175
Glass fiber composite, 307
Glass-reinforced plastics, 293
GOES, 271
Gold cup, 195
Golden thermogram, 185, 240
Good engineering practices, 327

Goose down, 29
Gram-calorie, 21
Graves, 256
Gray body, 68
GRP, 293
Guidelines, 251, 323
Gulf stream, 273
Gun, 269

Harrah's Casino, 138
Harsh environment, 132
Haze, 82
Heat, 3, 21
Heat capacity, 23
Heat injection, 291
Heat leakage, 207
Heater tubes, 311
Historic buildings, 201
Household bulb, 69
Humidity, 79

Identification., 283
IFOV, 118
Illegal aliens, 268
Image processing, 105, 144
Image quality, 105, 110, 127
Image transfer, 195
Imaging resolution, 120
Impulse pulse, 296
Incandescence, 53
Incandescent bulb, 54
Inclusions, 293
Indium antimonide, 99
Induced current, 44
Inductive loop, 243
Industry, 156
Infiltrate, 210
Infiltration, 45
Injection molding, 313
Inspection procedures, 319
Instantaneous-field-of-view, 118
Insulation, 29, 213
Integration time, 143

Jaggies, 104
Jet engine, 40, 72
Johnson criteria, 283
Joule-Thompson effect, 40

Kelvin, 10
Keystone footprint, 134
Knife switch, 241
Kodak, 317

Land mine, 259
Lap joints, 293
Law enforcement, 72, 267
Legs, 38
Level I, II, and III certification, 148
Light bulb, 69
Limited Access, 181
Line scanner, 93
Line source, 304
Liquid nitrogen, 97
Liquid-in-glass, 5
Liquid-in-glass thermometer, 5
LN2, 97
Lobby entrance, 206
Long wavelength infrared, 14
LOWTRAN, 84
LWIR, 14

Magnesium, 94
Maintenance industry, 2
Masonry-cladded building, 211
Mass transport, 45, 157, 211
MDT, 127
Measurement resolution, 120
Measuring IFOV, 121
Mechanical, 97
Mechanical inspection, 154
Mechanical power, 239
Mechanical repair priority, 255
Mercury cadmium telluride, 99

Metals, 315
Meteorite, 273
Meteorological range, 79, 81, 85
Mid-wavelength infrared, 14
MIFOV, 121
Mildew, 201
Military signature, 162
Military tank, 165
Military users, 149
Mine, 259
Minimum detectable temperature, 127
Minimum resolvable temperature, 127, 276
Mirror, 181
MODTRAN, 84
Modulated irradiation, 300
Modulated thermography, 293
MoirÈ pattern, 104
Moisture, 213
Monitor, 108
Mosaic, 137
Motion, 177
Motion sensor, 7
Motorcycle, 37
MRT, 127, 276
MRT observers, 149
Multi-belt pulley, 249
Multiflex, 194
MWIR, 14
MWIR versus LWIR, 76, 79, 82, 93, 108
Mylar, 70

Narcissus, 132
National Electrical Code, 227
National Oceanic and Atmospheric Administration, 271
NDE, 293
NDI, 293
NDT, 291
NEDT, 59, 111, 114
NET, 111
NETD, 111
Nitrogen, 97
NOAA, 271
Noise equivalent differential temperature, 111
Noise equivalent power, 100
Noise equivalent temperature, 111
Noise equivalent temperature difference, 59, 111
Nondestructive evaluation, 293
Nondestructive inspection, 293
Nondestructive testing, 291
Nonuniformity correction, 106
NUC, 106
Nuclear power plant, 38
NVL model, 276
Nyquist frequency, 122

Oblique viewing, 134
Observer response, 125
Observer training, 147
Oil pipeline, 262
Oil spills, 271
Oil-filled circuit breaker, 234
Oil-filled transformer, 237
Optical pyrometer, 8, 53
Overloaded wires, 241

Paint, 163, 194
Paper, 317
PAS, 119
Passive target, 163
Path radiance, 74, 83
PCMCIA card, 145
Peat, 271
Petrochemical, 311
Phase change, 24, 203, 221
Phosphorus, 274
Photoconductive, 98
Photoconductive detector, 98
Photoemissive device, 98
Photovoltaic, 98

Photovoltaic detector, 98
Physical attributes, 139
Pickup truck, 268
PII, 293
Pinion gear shaf, 246
Pipeline, 257, 260
Pitch, 119
Pixel-angular-subtense, 119
Planck's blackbody law, 52
Plastics, 313
Platinum silicide, 99
Pollution, 271
Polyester film, 70
Polyethylene, 70
Power distribution, 225
Power line, 161
Power loss, 229
Predictive maintenance, 2, 151
Pressurization, 211
Preventive maintenance, 2
Printed circuit board, 313
Process control/quality control, 156
Pseudo color, 8, 43
Pulley, 248
Pulse phase thermography, 293
Pulsed infrared imaging, 293
Pyroelectric, 98
Pyroelectric detector, 98
Pyrometer, 8, 53

Qualified observer, 150
Qualitative, 151
Qualitative measurement, 2
Quantitative, 151
Quantitative measurement, 2
Quantum well, 98
Quantum well detector, 98
Quartz, 94

Radiation, 34, 48
Rain, 169
Range prediction, 87, 281, 286
Rankine, 10
Raster scan, 95
Razor blades, 67
Recognition, 283
Reconstruction, 107
Refinery, 311
Reflectance, 60, 221
Reflection, 297
Reflection-mode imaging, 302
Refractory, 312
Relative humidity, 220
Repair priority, 252, 255
Resistance, 6, 226
Resistance thermometer, 6
Resolution, 111, 117
Responsivity, 48, 100
Rivets, 293
Rock wool, 30
Roller, 194
Roof, 36, 163, 213
Roof construction, 215
Rotating shaft, 244
R-value, 30, 216

Safety, 323, 326
Safety shroud, 247
Salt Lake City, 263
Salts, 203
Sampling, 104
Sapphire, 94
Scanner, 95
Scanning window, 169, 178
Scene based correction, 107
Schottky barrier photodiode, 98
Second generation, 94
Seeing, 147
Selective radiator, 68
Self-emission, 83
Sensitivity, 111, 114
Short wavelength infrared, 14
Sick-house syndrome, 204
Signal averaging, 198

Signal processing in the element, 99
Signal transfer function, 114
Signal-to-noise ratio, 276
Silicon, 94
Site survey, 325
SiTF, 114
Sky, 162
Skyshine, 174
Slit response function, 119, 120
Sluice gate, 39
Smoke, 82, 270
Smoke pencil, 211
Snow, 169
Solar absorption, 163
Solar glint, 175, 176
Solar heated, 161
Solar loading, 216, 260
Solder joint, 315
Spatial frequency, 113
Spatial resolution, 117
Specific heat capacity, 23
Specular surface, 174
SPRITE, 95, 99
Square pulse, 298
SRF, 119
St. Louis Gateway Arch, 83
Stack effect, 211
Standards, 323
Standing water, 220
Steady state, 159
Steam line, 260
Steel, 296, 317
Stefan-Boltzmann law, 48, 63, 183
Step pulse, 298
Stop-action, 143
Storage tank, 164, 258
Strip annealing furnace, 194
Strobe light, 323
Studs, 205
Styrofoam, 29
Sun, 35
Sun filter, 108
Sun glint, 94
Sunshine, 174
Surface moisture, 220
Surface temperature, 292
Surveillance, 265
Survey, 325
Sweat glands, 27
SWIR, 14
Symmetry, 157
Synchronization, 143

T/I NDT, 293
Tactical screening smoke, 82, 274
Tank, 165, 275
Tape player, 145
Target, 49, 58
Target signature, 157
Target transfer probability function, 284
Target visibility, 126
TDI, 95
Temperature, 230
Temperature calibration, 186
Temperature guidelines, 251
Temperature references, 106
Test plan, 324
Test procedure, 324
Thermal, 98
Thermal anomaly, 152, 157
Thermal bridge, 201
Thermal capacity, 157
Thermal clutter, 259, 274
Thermal conductivity, 28, 216, 231
Thermal contrast, 296
Thermal crossover, 165
Thermal derivative, 58, 115
Thermal detector, 98
Thermal equilibrium, 61, 159
Thermal imaging band, 14
Thermal imaging system, 8
Thermal inertia, 164
Thermal nondestructive testing, 293
Thermal reflection, 297

Thermal wave, 300
Thermal wave imaging, 293
Thermal/infrared nondestructive testing, 293
Thermocouple, 7
Thermoelectric, 97
Thermoelectric cooler, 97
Thermometer, 5
Thermos, 34
Thief, 267
Three-dimensional noise model, 278
Threshold, 147
Time-resolved radiometry, 293
TNDT, 293
T-number, 92
Tomogram, 305
Tracer gas, 211
Training program, 148
Transformer, 44
Transformer bushing, 236
Transmission lines, 235
Transmission-mode imaging, 303
Transmittance, 60
TRR, 293
Truck, 268
TTPF, 284
TWI, 293
Two-dimensional, 280
Two-dimensional MRT, 280

Uncertainty, 114, 198
Uncertainty analysis, 190
Uncooled detectors, 97
Underground storage tank, 258
Units, 19
Universal joint, 246
UST, 258
Utility pole, 161

Vapor barrier, 215
Varicose veins, 38
Vehicle, 177
Verification, 327
Very long wave infrared, 14
Video standards, 145
VLWIR, 14
Voids, 259, 293
Volcano, 272

Washed out, 169
Water, 216
Water ingress, 201
Water vapor, 76, 79, 80, 272
Weather, 86, 171
Wedge method, 194
Welding, 311
White hot, 90
Wien's law, 52
Wind, 168, 220, 233, 261
Window, 30, 132, 138, 204
Windshield defroster, 311
Wire, 227
Wood, 26
Wood pulp, 317
Wool, 29

Xenon flashlamp, 304

Zinc selenide, 94
Zinc sulfide, 94
Zoom, 123